Targeted mutagenesis in medaka using targetable nuclease systems

（ゲノム編集ツールを用いたメダカにおける標的遺伝子破壊）

Satoshi Ansai

2016

Contents

Chapter 1

General Introduction

Genetics is the study to know the relationships between genes and phenotypic traits in living organisms. Genetic analysis is generally classified into two approaches; forward genetics that determines the genetic basis responsible for a phenotypic trait and reverse genetics that analyzes the phenotypic effects of altered DNA sequences. Recent advances in DNA sequencing technologies have facilitated whole-genome and transcriptome sequencing in a wide range of organisms and therefore have increased the importance of reverse genetics for understanding of functions of individual genes found in the sequenced genome. Targeted gene knockout by homologous recombination (HR) using targeting vector is a powerful approach for showing gene function and understanding of complex biological processes [1]. However, because occurrence frequency of HR events varied among species and/or cell types, gene targeting by effective HR in eukaryotes has been generally limited to yeast, chicken DT40 cell, and mouse embryonic stem (ES) cells. Even though gene targeting in ES cells is a useful approach for analysis in multicellular organisms, the application of this approach is still not a feasible option in most organisms because of the difficulty in establishing germline-competent ES cell lines.

Of course, a number of genomes have been sequenced in teleost fish species including models for basic research fields, such as zebrafish (*Danio rerio*) [2], medaka (*Oryzias latipes*) [3], threespine stickleback (*Gasterosteus aculeatus*) [4], platyfish (*Xiphophorus maculatus*) [5], and cichlid fishes [6], and fishes for aquaculture and fishing industry like tiger pufferfish (fugu) (*Takifugu rebripes*) [7], Atlantic cod (*Gadus morhua*) [8], rainbow trout (*Oncorhynchus mykiss*) [9], Atlantic salmon (*Salmo salar*) [10], tongue sole (*Cynoglossus semilaevis*) [11], and Pacific bluefin tuna (*Thunnus orientalis*) [12]. On the other hand, available techniques for genetic manipulation in teleost fishes, especially loss-of-function approaches, has been restricted to two methods: RNA knockdown using chemichally modified antisense oligonucleotide, e.g. morpholinos and peptide nucleic acids (PNAs) [13], and gene knockout by targeting-induced local lesions in genome (TILLING) [14, 15]. These techniques have some drawbacks; RNA knockdown by antisense oligonucleotides injection into fertilized eggs yields transient results and only in the embryonic stages, and TILLING requires a library of chemically mutagenized fish that is difficult to construct and therefore available only in three species, zebrafish [14, 15], medaka [16], and fugu [17]. This fact has hindered understanding of each gene function identified in the genome sequencing projects by the reverse genetics approach in teleost fishes.

Genome editing using targetable nuclease systems is an emerging technology that has overcome these shortcomings in targeted gene knockout. Targetable nuclease systems including engineered endonucleases (EENs) and RNA-guided endonucleases (RGENs) are developed to induce DNA double strand breaks (DSBs) at specific genomic loci [18, 19]. The DSBs in eukaryotic cells are generally repaired by non-homologous end joining (NHEJ) or homology-directed repair (HDR) pathways, resulting in genomic modification at the target loci such as targeted gene disruption by small deletions and insertions, large deletion, gene correction with donor DNA, and targeted integration of a transgene fragment [20]. At the beginning of this Ph.D. work, targeted gene disruption using targetable nucle-

ases had been reported in a number of animal models including *Drosophila* [21, 22], sea urchin [23], *Xenopus* [24], and rat [25–27]. However, there had been few reports of targeted mutagenesis with the nucleases in teleost fishes, except some studies in zebrafish [28–30].

Here, I intended to establish the efficient analytical techniques for gene functions by the reverse genetics approach, which could be easily applied to a wide range of teleost fish species. In this study, medaka was used as a model species because of its advantageous characteristics for genetics, such as short generation time (2–3 months), large numbers of transparent eggs (10–40/day), availability of genomic information and highly polymorphic inbred strains, and smaller genome size (800 Mb) compared to zebrafish [31]. Additionally, medaka is the first fish species that an exogenous DNA fragment was introduced to generate transgenic fish [32], and therefore efficient protocols for microinjection into the fertilized eggs has been established [33]. At first, I demonstrated successful targeted mutagenesis in medaka by microinjection of three classes of targetable nuclease systems: zinc-finger nucleases (ZFNs), transcription activator-like effector nucleases (TALENs), and clustered regularly interspaced short palindromic repeats (CRISPR)/CRISPR-associated (Cas) system-based RGEN into the fertilized eggs. Subsequently, to assess the usefulness of targeted mutagenesis using the nucleases in loss-of-function analysis, I also demonstrated targeted disruption of medaka *tph2* gene that is involved in serotonin synthesis in the brain stem and examined the neurobehavioral phenotypes in the homozygous mutant by a newly developed behavioral testing system for medaka.

Chapter 2

Targeted mutagenesis using zinc-finger nucleases

2.1 Introduction

The first targetable nuclease applied for targeted genome editing was the zinc-finger nuclease (ZFN), an artificial nuclease consisting of engineered zinc fingers (ZFs) fused to the nuclease domain of a type IIS restriction enzyme FokI [34]. The DNA binding domain of ZFNs generally contain between three and six individual Cys_2His_2 ZF repeats and can recognize between 9 and 18 bp. The α-helix of each domain can determine the base-specificity, indicating that modification of residues constituting the helix allows for engineering ZFs to bind desired sequences [35]. Targeted genome editing using ZFNs, such as induction of small insertions and deletions (indels) with NHEJ or targeted integration of homologous donor vectors with HDR, has been demonstrated in not only various types of cultured cells but also a wide range of model organisms [20].

In medaka, however, targeted gene disruption using ZFNs has not yet been reported. Hence, it is unclear whether medaka cells are in circumstances where ZFNs can work. To address this question, EGFP-ZFNs that has already been confirmed to efficiently cleave the *EGFP* gene in transgenic crickets [36] and other transgenic animals were used. Then, I demonstrated successful targeted disruption of the exogenous *EGFP* gene in transgenic medaka strains using ZFNs. I investigated whether ZFNs could introduce mutations at the target sites in somatic and germ cells of medaka.

2.2 Materials and Methods

Transgenic medaka

The d-rR-Tg(actb2k-EGFP) strain was generated as follows: The medaka *β-actin* (*actb*) promoter region (ca. 2.4-kb) was amplified with PCR using the primers b-actFWMCS and b-act-RVcommon17bp (Table 2.1) from the pbact-RG vector [37]. The resulting amplicon was fused to an *EGFP* gene fragment, which contains an SV40 early polyA signal, from the pEGFP-1 vector (Clontech) using overlap PCR. This fragment was inserted into the pPBact-GFPMK vector at the XhoI-SalI site of pPB-UbC [38]. This vector construct was introduced into fertilized eggs of the d-rR strain by a microinjection method [39].

The Tg(olvas-EGFP) strain contains the olvas-green fluorescent protein (GFP) transgenic vector, (which includes the 5.1-kb of the promoter region of the medaka vasa gene (*olvas*), the *EGFP* gene, and 0.64-kb of the 3′ region of *(olvas*) and was generated previously [40]. This strain has been maintained at the NBRP Medaka (Strain ID: TG870; http://www.shigen.nig.ac.jp/medaka/).

Table 2.1. Oligonucleotide sequences used in this chapter

Name	Sequence [5′–3′]
b-actFWMCS	GACCTTAATTAACTCGAGAAGCTTGAATTCATATG-AGAGCGAGGAAGAGGA
b-act-RVcommon17bp	CTTGCTCACCATGGTGGCTAAACTGGAAAAGAACA
olvas3′UTRFW-XhoI	TAGACTCGAGCAACTGAGCGCCGGTCGCTA
olvas3′UTRRV-HpaINheI	ATGCGCTAGCGTTAACGTGCACTCTCAGTACAATCT
EGFP-start	CCATGGTGAGCAAGGGCGAGGA
CGYFP-RV	GACTGCGGCCGCTTACTTGTACAGCTCGTCCAT
pEGFP vec 4FW	GGCCTTTTGCTGGCCTTTTG
vasa5′RV2	GTCGATGGCGACCATTGACTG
Sal-GFP-start	ACGTGTCGACCCATGGTGAGCAAGGGCGAG
Chr9-FW	GAAGCAACTGCTGCATACTC
Chr9-RV	AGTTCAGCGCCTGCATGACA
Chr12-FW	TGTACCACTCTCCTCCAGGT
Chr12-RV	TCTGCAGTTCAGTGCTGCTC
EGFP_ZFN_Target_2F	GCGACACCCTGGTGAA
EGFP_ZFN_Target_2R	TGGCTGTTGTAGTTGTACTC

Construction of ZFNs targeting *EGFP* gene

Zinc finger arrays recognizing the coding sequence of *EGFP* gene were selected from zinc-finger randomized libraries by bacterial one-hybrid selection and single-strand annealing assay as described previously [23]. Each ZF array was subcloned into a transcription vector containing a T7 promoter, a nuclear localization signal, a SV40 late polyA signal [23], and one of two enhanced heterodimeric FokI domain variants, *Sharkey*-based DS and RR versions [41]. The vector pNSe2-eGFP2L-DS or pNSe2-eGFP2R-RR was constructed to target EGFP-R or EGFP-R site, respectively.

To construct the pNSe2-eGFP2L-DS-vas3 and pNSe2-eGFP2R-RR-vas3 vectors, which contain 3′UTR of *olvas*, the 3′UTR region was amplified from the olvas-EGFP transgenic vector [40] with primers olvas3′UTRFW-XhoI and olvas3′UTRRV-HpaINheI (Table 2.1). Subsequently, the amplicon was cloned into the pNSe2-eGFP2L-DS and pNSe2-eGFP2R-RR vectors and used XhoI and NheI as a substitute for the SV40 late polyA signal.

***In vitro* RNA synthesis and microinjection**

The vectors containing the ZFNs coding sequences were linearized by NheI digestion. Next, capped RNA sequences were synthesized using the mMessage mMachine T7 Ultra Kit (Ambion). The capped RNA sequences were diluted and injected into fertilized eggs of the *EGFP* transgenic strains as described above.

Microscopic observation

The fish were observed with fluorescence stereomicroscope MZFLIII with GFP2 filter set (Leica Microsystems), and captured the images with a digital, color, cooled, charge-coupled camera device, a VB-7010 (KEYENCE).

Genomic DNA preparation, genotyping, and sequence analysis
Genomic DNA was extracted using either the Blood and Tissue Genomic DNA Extraction Miniprep System (Viogene) or a conventional phenol-chloroform method.

The full-length *EGFP* gene was amplified from genomic DNA by performing PCR using the following pair of primers: EGFP-start and CGYFP-RV (Table 2.1) and used to genotype the fish. To genotype the F1 fish from founder #V38, the upstream region of the olvas-GFP transgenic vector was amplified using PCR primers pEGFP-4FW and vasa5′RV2 (Table 2.1).

To investigate induced mutations, amplified full-length *EGFP* fragments that were purified using Wizard SV Gel and PCR Clean-Up System (Promega) were directly sequenced. For single clone analysis, the full-length *EGFP* gene was amplified using the primers Sal-GFP-start and CGFP-RV (Table 2.1), and the resulting PCR products were subcloned into the SalI-NotI site of pBluescript II KS (+) (Stratagene). The nucleotide sequences of the fragments or clones were analyzed with either EGFP-start primer or the M13-reverse primer.

Off-target analysis
Potential off-target sites in the medaka genome (matched 16- or 17-bp of 18-bp EGFP-ZFN recognition sites) were searched using a "Pattern Match" tool in New Medaka Map (beta) (http://viewer.shigen.info/medakavw/patternmatch/).

The genomic regions that contained potential off-target sites were amplified with the primer set Chr9-FW and Chr9-RV, or Chr12-FW and Chr12-RV (Table 2.1). The PCR products were subcloned into the pGEM-T Easy vector (Promega) and sequenced using the M13-reverse primer.

Melting curve analysis
I performed PCR amplifications and detected fluorescence using DNA Engine Opticon System (MJ Research) and KAPA SYBR FAST qPCR kit (KAPA Biosystems) with primers EGFP_ZFN_Target_2F and EGFP_ZFN_Target_2R .(Table 2.1) The reaction contained 1 μL genomic DNA (approximately 100 ng/μL) (which had been extracted from each of the F1 larvae by the conventional phenol-chloroform method), 5 μL Master Mix (2×) Universal, and 0.2 μmol/L of each primer in a total volume of 10 μL. The cycling conditions were as follows: one cycle at 95 ℃ for 2 min and 40 cycles of 95 ℃ for 2 s followed by 60 ℃ for 20 s. Next, the mixture was heated from 60 to 95 ℃ and fluorescence intensities were measured at every 0.2 ℃ increment.

2.3 Results

ZFNs introduce targeted mutations in somatic cells of the injected medaka embryos
The EGFP coding sequence (5′-GGGCATCGACnnnnnnGAGGACGGCA-3′) was selected as the target site for ZFN (Fig. 2.1), and therefore 2 ZF arrays — eGFPL for the EGFP-L site (5′-GTCGATGCCC-3′) and eGFPR for the EGFP-R site (5′-GAGGACGGCA-3′) — were selected. Table 2.2 shows the amino acid sequences of the recognition helices obtained from the selected ZF arrays.

Various concentrations of RNA that codes for EGFP-ZFNs were injected into d-rR-Tg(actb2k-EGFP) heterozygotic fertilized eggs. Most embryos that were injected with 10 ng/μL or more of ZFN RNA showed morphological abnormalities within 1 day postfertilization (dpf), for example, abnormally aggregated blast disc (Fig. 2.2A), shortened embryonic body (Fig. 2.2B), or lethality (Table 2.3). On the other hand, 48 of the 50 embryos that were injected with 5 ng/μL of ZFN RNA developed normally at 1 dpf (Table 2.3).

The d-rR-Tg(actb2k-EGFP) strain expresses EGFP fluorescent strongly in skeletal muscles and eyes

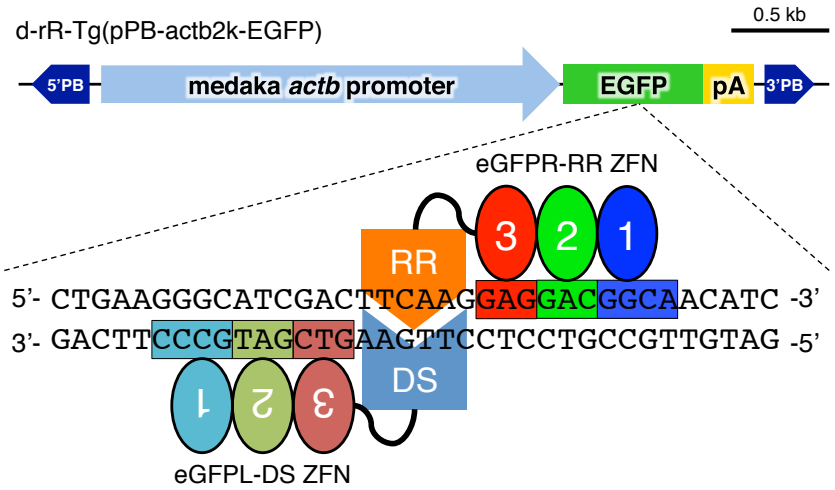

Figure 2.1. Structure of the transgene of d-rR-Tg(actb2k-EGFP) and a target site of EGFP-zinc-finger nucleases (ZFNs). The d-rR-Tg(actb2k-EGFP) strain carries the transgene including *piggybac* transposon sequences, medaka β-actin (*actb*) promoter, *EGFP* gene, and SV40 early polyA signal. The target sequence of EGFP-ZFNs is shown below. Colored boxes indicate the recognition sequences for each zinc finger of the ZFNs.

Table 2.2. Amino acid sequences of selected zinc fingers (ZFs) in EGFP-ZFNs

Finger	Target site	Recognition helix amino acid sequence[a]
eGFPL ZFN		
ZF1	GCC(C)	RQRELLR
ZF2	GAT	VTFNLTR
ZF3	GTC	DQSALVR
eGFPL ZFN		
ZF1	GGC(A)	TSGHLVR
ZF2	GAC	DLANLNR
ZF3	GAG	RPDNLAK

[a] Residues $-$ 1 to+6 in the recognition sequences are shown.

Table 2.3. Survival of embryos injected with RNAs of EGFP-ZFNs at 1 day postfertilization (dpf)

RNA concentration (ng/μl)	Injected eggs[a]	Normal embryos at 1 dpf
0	66	64
5	50	48
10	11	0
20	17	0
40	18	0

[a] Injected eggs were obtained by crossing d-rR-Tg(actb-EGFP) with d-rR wild-type.

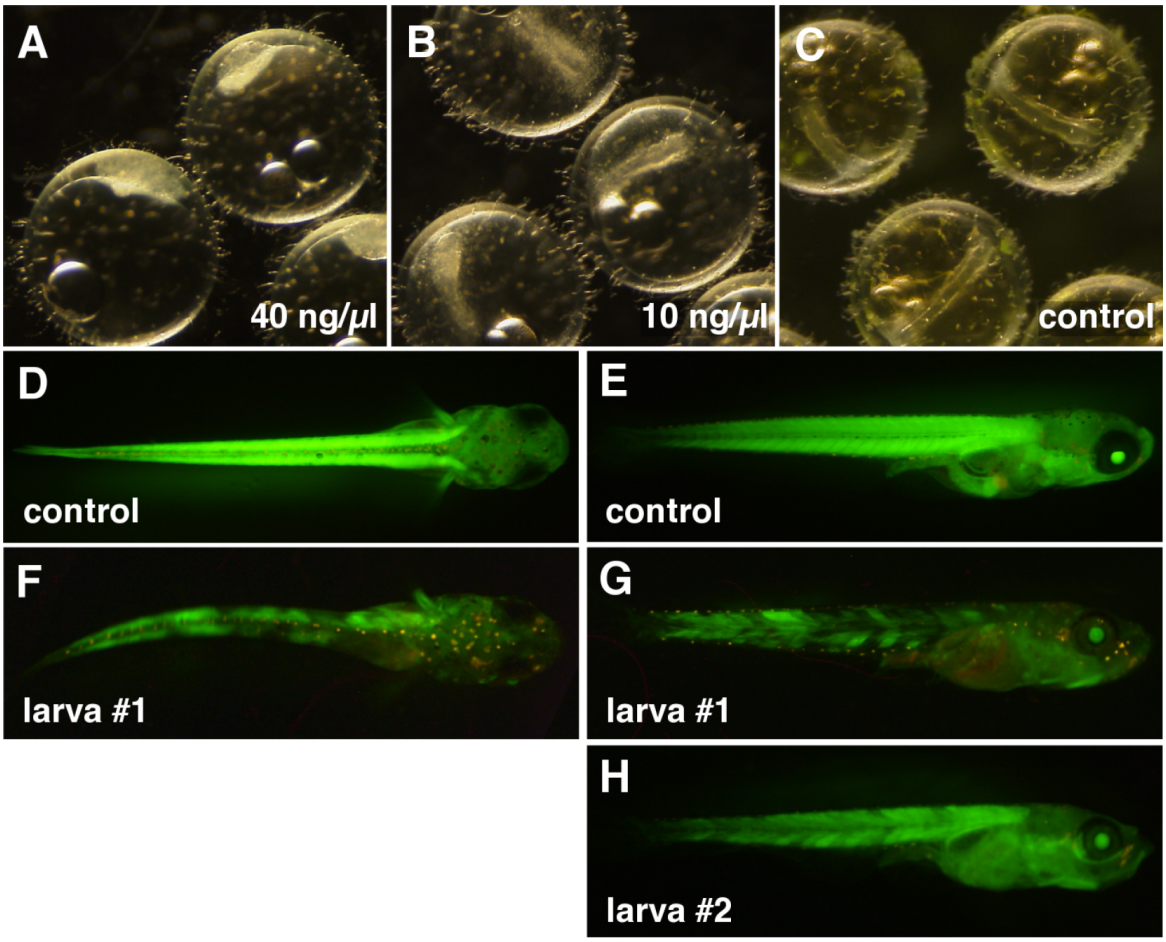

Figure 2.2. Morphological abnormality and loss of green fluorescent protein (GFP) fluorescence in embryos and larvae from the d-rR-Tg(actb2k-EGFP) strain that had been injected with EGFP-zinc-finger nucleases (ZFN) RNA. (A, B) Morphological abnormality of 1 dpf embryos injected with (A) 40 ng/μL or (B) 10 ng/μL the ZFN RNA. (C) Control embryos that were not injected with ZFNs developed normally at 1 day postfertilization (dpf). (D–H) Fluorescent images of hatching larvae. (D, E) Dorsal and lateral views of a control larva without ZFNs injection, respectively. Particularly strong expression of GFP fluorescence was observed in the skeletal muscles and eyes. (F, G) Lateral and dorsal views, respectively, of larva #1, which had been injected with 5 ng/μL of ZFN RNA. Mosaic loss of the GFP fluorescence was observed. (H) A lateral view of larva #2 that had been injected with 5 ng/μL ZFN RNA. Minimal loss of fluorescence was observed.

(Fig. 2.2D, E). Therefore, I assumed that the somatic cell EGFP gene lesions in embryos that were injected with ZFNs would be detected easily in this transgenic strain. To validate targeted genome cleavage and the formation of lesions in the EGFP gene with EGFP-ZFNs, I examined the skeletal muscle of hatching fish (that had been injected with ZFNs as embryos) for GFP fluorescence. Some larvae showed mosaic loss of GFP fluorescence (Fig. 2.2F–H). Larva #1 showed diminished fluorescence in a large portion of the skeletal muscle on the right side of the trunk (Fig. 2.2F, G). Whereas, larva #2 (Fig. 2.2H) showed minimal loss of fluorescence in the skeletal muscle.

To investigate if loss of GFP fluorescence was caused by ZFN-induced mutations in somatic cells, I closely investigated 10 of the 48 normally developed embryos that had been injected with 5 ng/μL ZFN RNA. Significant loss of GFP fluorescence was observed in two of the 10 embryos, (#3 and 4; Fig. 2.3A). The *EGFP* gene in each embryo was amplified by PCR and subcloned, and each clone was

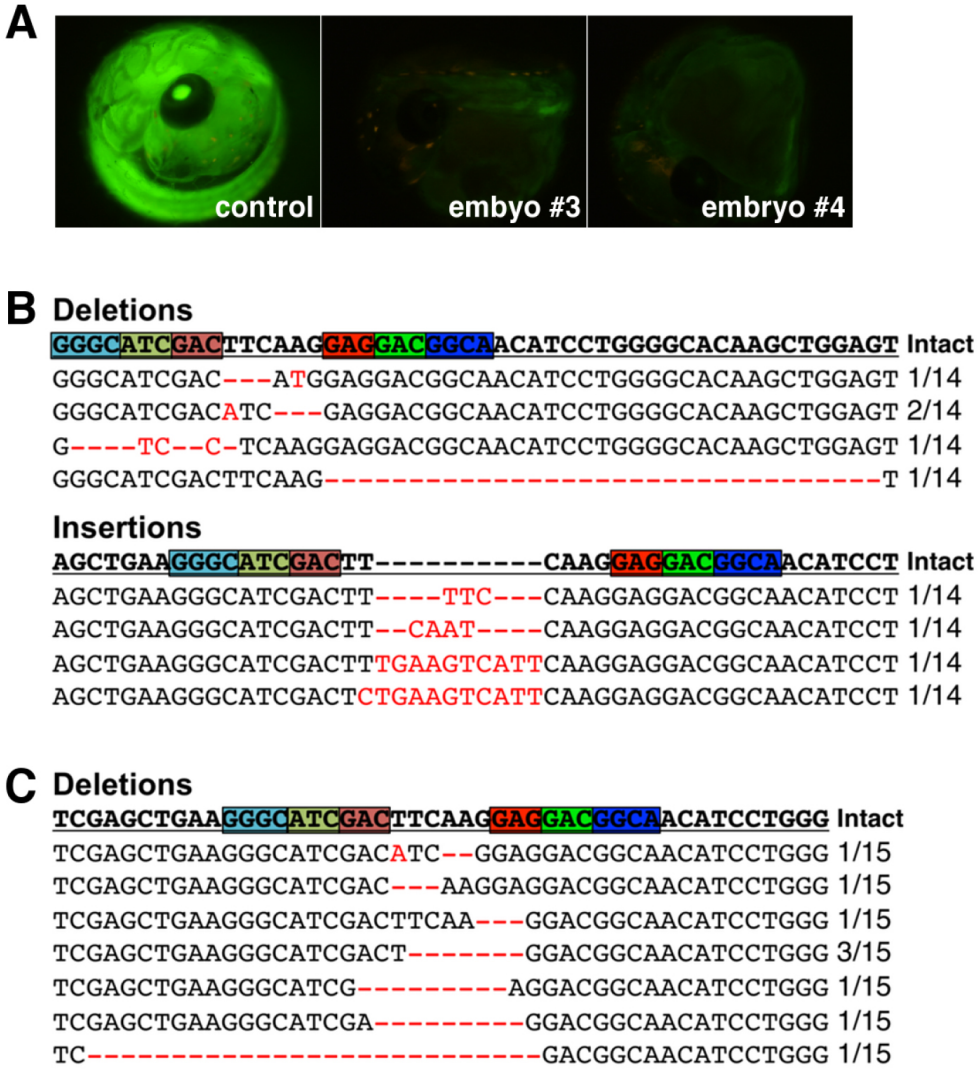

Figure 2.3. Sequence analysis of two embryos from the d-rR-Tg(actb2k-EGFP) strain injected with EGFP-zinc-finger nucleases (ZFNs). (A) Fluorescent images of the analyzed embryos. "Control" shows an embryo that was not injected with the ZFNs. (B, C) Sequences observed in embryos #3 and #4, respectively. Red letters or dashes indicate the mutations found. Colored boxes indicate recognition sequences of EGFP-ZFNs. Numbers on the right indicate the numbers of mutated clones detected out of all analyzed clones.

subjected to sequence analysis. In embryo #3, the target site contained deletions (five out of 14 clones, 35.7%; four types) and insertions (four out of 14 clones, 28.6%; four types) (Fig. 2.3B). The target site of embryo #4 contained deletions (nine out of 15 clones, 60%; seven types) (Fig. 2.3C). The results indicate that these ZFNs are able to disrupt the gene by cleaving the target site in medaka somatic cells. In addition, these results indicate that ZFN-induced mutations occurred during relatively late stages of early embryogenesis. More than eight patterns of mutations were discovered in each embryo, which suggests that these mutations occurred during the 8-cell stage or later in the ZFN-injected embryos.

Heritable mutations introduced by EGFP-ZFNs

To validate that ZFN-induced mutations are introduced into germ cells and transmitted to subsequent generations, I experimented further on embryos that had been injected with EGFP-ZFNs and raised

Table 2.4. Results of microinjection with RNAs of EGFP-ZFNs

Strain	RNA (ng/μl)	Injected	Hatched	Sexually matured	Germ-line transmission rate
d-rR-Tg(pPB-actb2k-EGFP)	7.5	161[a]	62 (39%)[a]	12[b]	50% (6/12)
Tg(olvas-EGFP)	5	71	59 (83%)	48	6.25% (3/48)

[a] These numbers include fish without transgenes.

[b] This number excludes fish that lacked GFP fluorescence.

until they reached sexual maturity. In this experiment, modified EGFP-ZFNs that were fused to *olvas* 3′UTR as a substitute for an SV40 polyA signal were used. It is known that an RNA sequence fused to *vasa* 3′UTR is stable and has enhanced expression in the germ cells [42, 43].

EGFP-ZFNs fused to *olvas* 3′UTR were injected into fertilized eggs of the d-rR-Tg(actb2k-EGFP) strain (Table 2.4 summarizes this screening process). At present, homozygous fish of this transgenic strain have not been obtained for unknown reasons. Therefore, RNA sequences were injected into fertilized eggs that had been obtained by crossing heterozygotic fish [d-rR-Tg(actb2k-EGFP) strain] with d-rR wild-type fish. Thus, the population of injected eggs included both GFP-transgenic and non-transgenic individuals. Of the 161 embryos injected with 7.5 ng/μL ZFN RNA, 62 (39%) hatched normally and 49 (30%) survived at 2 months post-hatch. Of the 49 adult fish, I identified 17 as transgenic by GFP observation, and 12 of the 17 transgenic fish were raised to sexual maturity. Some of the transgenic fish displayed mosaic loss of GFP fluorescence, thus I classified these 12 fish into four groups by fluorescent microscopic observation (Fig. 2.4). Fish #A35 demonstrated significant fluorescence loss in more than half of its skeletal muscles (“++” in Fig. 2.4). Three fish (#A4, #A21, and #A47) exhibited loss of the fluorescence in approximately 10–50% of the skeletal muscle (“+” in Fig. 2.4). Four fish (#A18, #A22, #A37, and #A38) showed loss of fluorescence in <10% of the skeletal muscle (“±” in Fig. 2.4). However, four fish (#A24, #A39, #A44, and #A48) showed no apparent loss of GFP fluorescence in skeletal muscles (“−” in Fig. 2.4). These 12 mature fish were crossed with d-rR wild-type fish. I collected more than 40 F1 eggs from each pair, genotyped the embryos that lacked GFP fluorescence by PCR amplifying the *EGFP* region, and determined the nucleotide sequences of each PCR amplicon by direct sequencing analysis. Six fish (#A4, #A18, #A22, #A35, #A37, and #A38) were identified as founders harboring mutations at the target of EGFP-ZFNs in their germ cells (Table 2.5). Each founder possessed at least one mutant allele that included a 5- to 36-bp deletion and a 4-bp insertion (Fig. 2.5A). To measure the frequency of mutation events in the germ cells of each founder, I genotyped each founder’s F1 embryo. The germ-line transmission rate of mutations in these founders ranged from 8.1% (3 of 37; #A22) to 100% (13 of 13; #A35) (Table 2.5). In founder #A35, *EGFP* genes were disrupted in most of the somatic (Fig. 2.4) and germ cells (Table 2.5), which indicates that the ZFN-induced lesion in this founder occurred during early developmental stages. However, no mutations were found in the germ-line of founder #A21, although, a significant loss of fluorescence was evident in the skeletal muscle (Fig. 2.4). In founder #A18, the majority of germ cells (65%) carried ZFN-induced mutations; however, the loss of fluorescence was observed in a small proportion of skeletal muscle (Fig. 2.4). These indicate that the degrees of germ cell lesions do not necessarily correlate with those of somatic cell lesions.

In addition, I investigated mutation variations in somatic and germ-line cells from the two founders (#A18 and #A38). Genomic DNA was extracted from each founder fish and its F1 larvae. The EGFP gene region of each founder was amplified by PCR and subcloned, and the nucleotide sequence of each

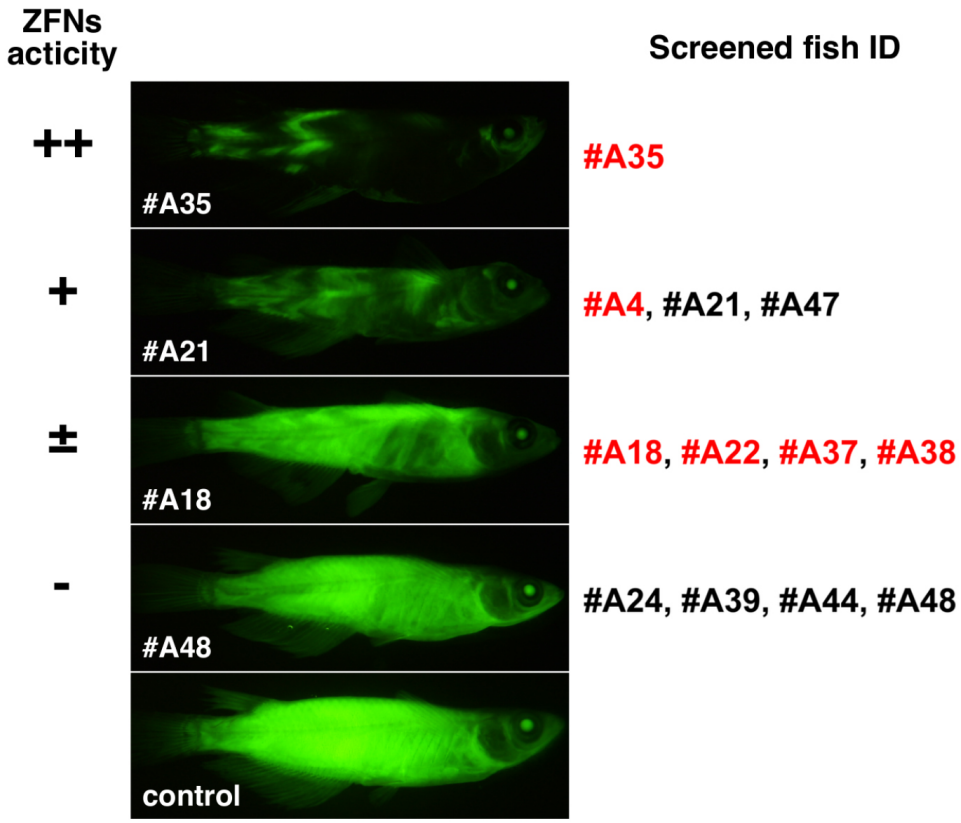

Figure 2.4. Twelve screened fish of the d-rR-Tg(actb2k-EGFP) strain were classified into four groups according to level of mosaic loss of green fluorescent protein (GFP) fluorescence with EGFP-zinc-finger nucleases (ZFNs). For "ZFNs activity", "++", "+", and "±" indicate loss of GFP fluorescence in more than half, 10–50%, and <10% of skeletal muscles, respectively. The "−" indicates no apparent loss of fluorescence. Fluorescent images of a representative fish in each group are shown. "Control" shows a fish that was not injected with the ZFNs. "Screened fish ID" indicates the IDs of screened fish included in each group. Red ID numbers indicate the founders that carry mutant alleles.

clone was determined. Six or two types of mutations in the founder #A18 or #A38, respectively (Fig. 2.6). For F1 larvae, the *EGFP* gene region of each F1 fish that lacked GFP fluorescence was amplified by PCR, and the nucleotide sequence of each amplicon was determined by direct sequencing. Two or one type(s) of mutations were found in F1 larvae of #A18 or #A38, respectively (Fig. 2.5A). The nucleotide sequences of germ cell mutations were not necessarily identical to the mutations in somatic cells. This suggests that the ZFN-induced lesions in these founders were introduced after germ cell differentiation and proliferation.

Furthermore, I investigated EGFP-ZFNs for the ability to introduce off-target lesions in the injected fish genome. Two potential off-target sites matched 16 out of the 18 bp in the ZFN target site. Off-target 1 (Chr.9: 5,471,017-5,470,994; 5′-GGCATCG**GG**gatgaaGAGGACGGC-3′) and off-target 2 (Chr. 12: 9,872,378-9,872,401; 5′-**A**GCATCGACttcaac**A**AGGACGGC-3′), were identified in the medaka genome using a "Pattern Match" tool. Genomic regions, which included the off-target sites, were PCR-amplified from the 2 founders (#A18 and #A38; described above, respectively). These PCR amplicons were subcloned and the nucleotide sequences of 20 clones from each embryo were

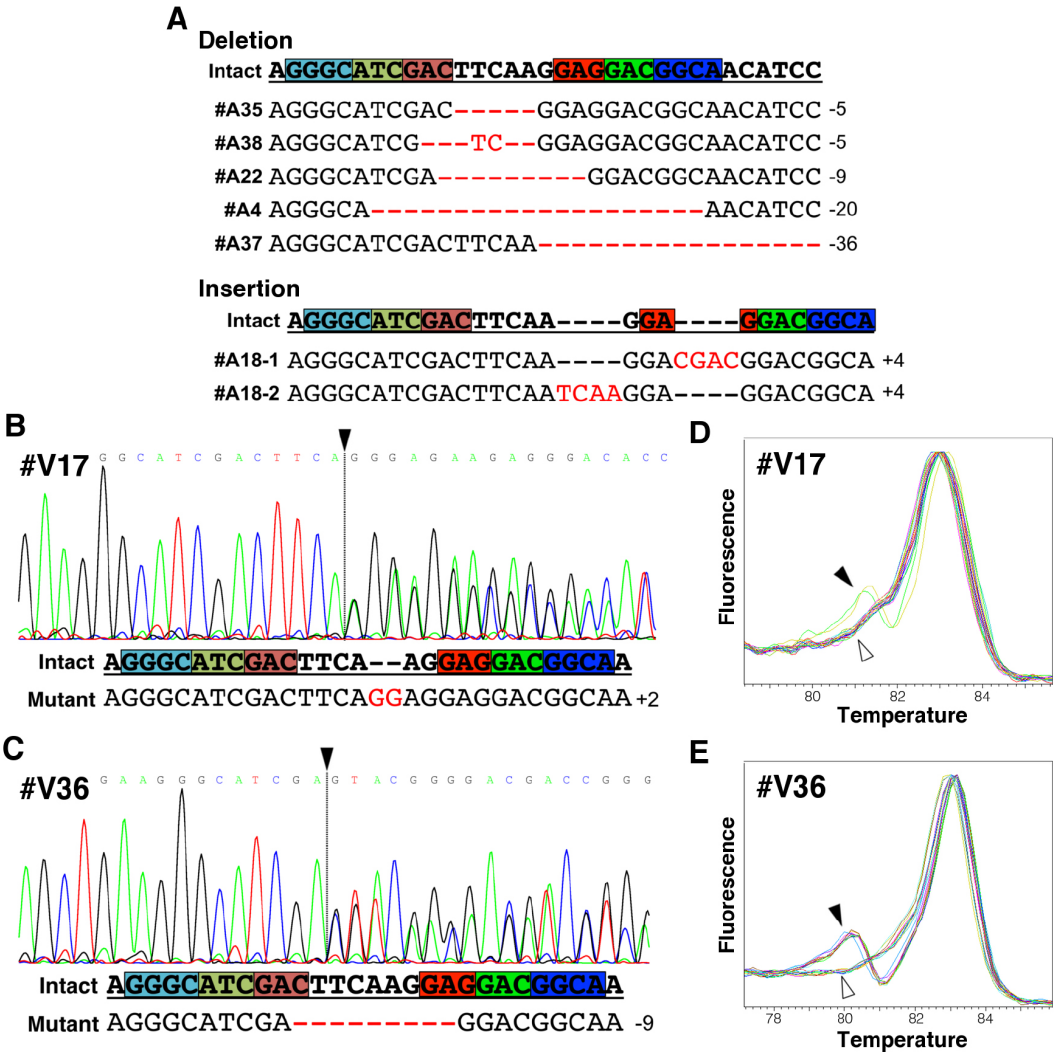

Figure 2.5. Zinc-finger nucleases (ZFN)-induced mutations found in F1 progeny from six founders of d-rR-Tg(actb2k-EGFP) and two founders of Tg(olvas-EGFP). Red dashes or letters indicate patterns of deletions or insertions, respectively, found in their progeny. Colored boxes indicate EGFP-ZFNs recognition sequences used in this study. Numbers on the right side indicate the numbers of deletions or insertions. (A) Deletions or insertions were identified by direct sequence analysis in heterozygotic F1 embryos from the d-rR-Tg(actb2k-EGFP) founders. (B, C) Mutations were indentified in each heterozygotic F1 larva from the Tg(olvas-EGFP) founders #V17 and #V36, respectively. From the direct sequence analysis of each F1 larva, an overlap of two sequences is indicated by the positions of black arrowheads and broken lines. Both intact and mutant sequences were indentified from these two sequences by single clone analysis (shown on the downside of the each panel). (D, E) Melting curves of amplicons from EGFP gene of each F1 larva for detection of mutations in germ cells of #V17 and #V36, respectively. These graphs display negative first derivatives of the measured fluorescence plotted against temperatures. Open arrowheads indicate melting curves of intact sequences, and black arrowheads indicate melting curves of mutant sequences.

Table 2.5. ZFN-induced mutant alleles and frequencies of mutation event in germ cells of founders

Founder	Mutation allele	Frequency[a]
d-rR-Tg(pPB-actb2k-EGFP)		
#A4	20 bp deletion	n/a[b]
#A18	4 bp deletions[c]	65.2% (30/46)
#A22	9 bp deletion	8.1% (3/37)
#A35	5 bp deletion	100% (13/13)
#A37	36 bp deletion	8.8% (5/57)
#A38	5 bp deletion	34.1% (15/44)
Tg(olvas-EGFP)		
#V17	2 bp insertion	6.4% (3/47)
#V36	9 bp deletion	52.4% (11/21)
#V38	Large deletion	100% (11/11)

[a] These values are shown as percentages of identified mutant F1 embryos and numbers of mutant F1 embryos/numbers of F1 embryos carrying the transgene (in parentheses).

[b] Founder died before the frequency of mutation event was determined.

[c] Founder carried two types of 4-bp insertion in germ cells.

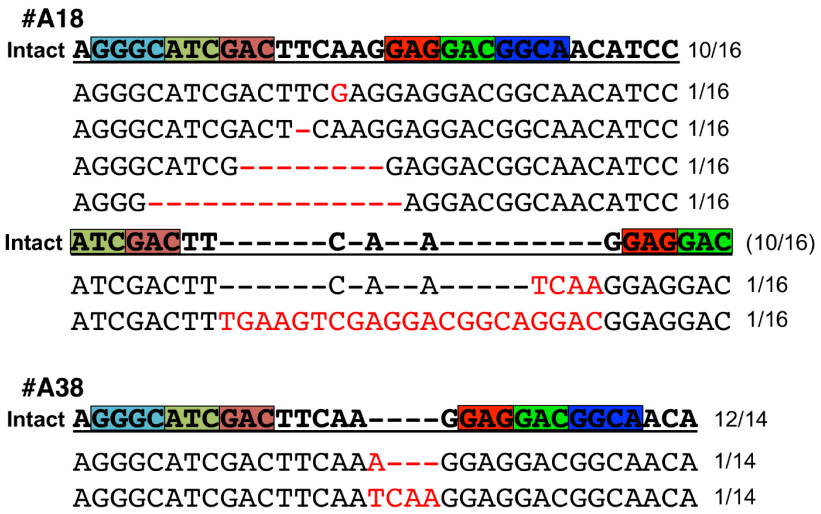

Figure 2.6. Mutations in two founders from the d-rR-Tg(actb2k-EGFP) strain, #A18 and #A38. In founder #A18, six types of mutations were identified, and included both deletions and insertions. In #A38, two types of insertions were identified. Red dashes or letters indicate patterns of deletions or insertions detected in each founder. Colored boxes indicate recognition sequences of the EGFP-ZFNs used in this study. Numbers on the right side indicate the numbers of mutated clones from all of the analyzed clones.

analyzed. No mutations were observed at two potential off-target sites in the two founders, which suggests that ZFNs could induce mutations at their target sequences specifically.

In transgenic strains established via random integration, such as conventional microinjection methods, the transgenes may be integrated into a different position in the chromosome and laid under different positional effects in each transgenic strain. Therefore, it is preferable to validate the availability of ZFNs with other transgenic strains. I selected a Tg(olvas-EGFP) strain harboring relatively low copy numbers of the transgene, olvas-GFP (in my preliminary study). 5 ng/μL of EGFP-ZFNs fused to *olvas* 3′UTR RNA were injected into fertilized eggs that had been obtained by crossing homozygotic fish [Tg(olvas-EGFP) strain] with d-rR wild-type fish (Table 2.4 summarizes this screening process). Of the 71 embryos injected with ZFN RNA, 59 (83%) hatched normally and 48 (68%) were raised to sexual maturity. I investigated the mature fish for mutations in germ cells by the same procedure described for the germ-line transmission screening of d-rR-Tg(actb2k-EGFP), and I identified three founders with mutations at the ZFN target sites (#V17, #V36, and #V38) (Table 2.5). From direct sequencing of each F1 larva of #V17 and #V36, I found overlaps between two different sequences, although, their *EGFP* gene region genotypes were heterozygous (Fig. 2.5B, C). This result indicates that this transgenic strain carries more than two copies of exogenous *EGFP* gene per haploid. To confirm the presence of the mutant allele, I subcloned PCR amplicons of *EGFP* gene region and analyzed the nucleotide sequences. In addition to intact sequences, a 2-bp insertion or a 9-bp deletionin in #V17 (Fig. 2.5B) or #V36 (Fig. 2.5C), respectively. The reason why the non-fluorescing F1 larvae carried both intact and mutant *EGFP* genes remains unknown. I assume that some fish with ZFN-induced mutations express GFP fluorescence because they possess the other intact *EGFP* gene as well. This suggests that some mutant founder fish may be labeled as "no mutation" because the F1 larvae were negatively screened for GFP fluorescence.

Melting curve analysis is popular to identify specific fragments and to assess the homogeneity of a sample in real-time PCR systems. Briefly, in plots of negative first derivatives of the fluorescence versus temperatures of PCR product, homogenous PCR amplicons show a single peak (for example, open arrowheads in Fig. 2.5D, E), whereas heterogenous amplicons show extra peaks. Melting curve analysis was conducted in each F1 progeny of founders #V17 and #V36, and found that the melting curve from each mutant larva amplicon displayed an added peak (black arrowheads in Fig. 2.5D, E). The frequency of mutation events in germ cells by counting the numbers of F1 larvae that exhibited the different curves, which indicated the mutation frequency was 6.4% (3 of 47) in #V17 and 52.4% (11 of 21) in #V36 (Table 2.5).

Founder #V38 contained the *EGFP* gene in somatic cells, but its F1 larva was not PCR-positive using EGFP-start and CGYFP-RV primers. However, for 11 (58%) of the 19 F1 larvae, the region upstream of the transgenic vector, including portions of the *olvas* promoter and the vector's bacterial backbone, was PCR-amplified with primers pEGFP-4FW and vasa5′RV2. These indicate that a broad region of the transgene, including whole *EGFP* gene CDS and some part of the vector's bacterial backbone, was deleted in founder #V38 germ cells. It is likely that ZFNs induce large deletions in medaka as described in rat previously [26].

2.4 Discussion

In this chapter, I demonstrated targeted gene disruption in medaka using ZFNs. Functional ZFN RNA sequences for the *EGFP* gene were injected into embryos from transgenic medaka strains and caused various mutations that included both insertions and deletions around the ZFN target site. I also discovered that these mutations in germ cells were transmitted to progeny. This is the first report to describe targeted gene disruption by ZFNs in medaka.

The embryos that were injected with EGFP-ZFN RNA in high concentrations (more than 10 ng/μL

of ZFN fused to the SV40 late polyA signal RNA) exhibited morphological abnormalities or lethality during early developmental stages. In zebrafish, it was reported that increasing amount of ZFNs caused nonspecific developmental abnormalities and that lesions in off-target sites occurred with greater frequency in morphologically abnormal embryos (relative to normal embryos) [29]. In addition, extra DSBs have been correlated to increased dose-dependent cytotoxicity in primary human cells [44]. These various lines of evidence support the hypothesis that the morphological abnormalities and lethality observed in the medaka embryos that had received high doses of ZFNs were caused by nonspecific cleavage at off-target sites. The threshold RNA dose that causes this cytotoxicity varies depending on the architectures of the nuclease domain or the lots of synthesized RNA (data not shown). Therefore, I recognized the need to choose appropriate RNA doses for each ZFN. Based on my own experience, EGFP-ZFN RNA doses that result in abnormalities or lethality for approximately half of the injected embryos at 1 dpf will be appropriate for efficient disruption at the target gene.

I assumed that the timing of mutation formation resulted in mosaic *EGFP* gene lesions in the germ cells of ZFN-injected fish. The experimet using the d-rR-Tg(actb2k-EGFP) strain showed that ZFN-induced mutations were transmitted through the germ line with high frequency (50%; six of 12 screened fish) and the frequency of mutation events in founder germ cells varied (8.1–100%). These frequencies are equal or superior to those determined in previous ZFN-mediated gene disruption studies in zebrafish [28–30] and previous studies that established transgenic strains in my laboratory [40, 45, 46]. In this experiment, it is likely that I missed in-frame deletions or insertions that had no effect on GFP fluorescence because I analyzed the nucleotide sequences of *EGFP* gene in F1 fish that lacked GFP fluorescence. This suggests that the frequency of mutation events may actually be higher than those determined in this study.

In the experiment to validate germ-line transmission of ZFN-induced mutations, EGFP-ZFNs were fused to *olvas* 3′UTR that are known to stabilize RNA and enhance translation of RNA in germ cells [42,43]. Given the result of genotyping in F1 progeny, all of the germ cells in two founders (#A35 and #V38) and more than 50% of the germ cells in two founders (#A18 and #V36) were mutated (Table 2.5). It is likely that these higher frequencies of mutation events in their germ cells were caused by enhanced expression of the ZFN proteins in the germ cells. In this study, only the ZFNs fused to *olvas* 3′UTR were subjected to the germ-line transmission analysis. Thus, further experiments that compared germ-line mutation frequencies with the ZFN fused to a SV40 polyA signal will be required to evaluate the effects of *olvas* 3′UTR. In addition, optimizations of the expression system of ZFN proteins in medaka early embryonic stages, including 5′ and 3′ UTR of injected RNA sequences, will be required to facilitate genome cleavage by ZFN.

To measure the frequency of germ cell mutation events in founders #V17 and #V36, a melting curve analysis was conducted with a standard Real-Time PCR system. I successfully detected mutant embryos by analyzing the genomic DNA extracted from each F1 larva (Fig. 2.5D, E). This method is more simple and cost-effective than other mutation detection methods, including direct sequencing and Surveyor nuclease assay [47, 48]. However, this method was insufficiently sensitive to detect mosaic mutations in somatic cells of ZFN-injected embryos and, slight mutations in bulk genomic DNA that was extracted from a number of F1 larvae (data not shown). These results suggest that more effective methods for detecting ZFN-induced mutations are required to evaluate genome cleavage activities of newly designed ZFNs and to identify the founders that carry mutations in germ cells easily.

In normally developed medaka embryos that had been injected with ZFN RNA, the two potential off-target sites (2-bp mismatched) in the genome showed no lesions. Furthermore, no developmental abnormalities were observed in the progeny of founders carrying ZFN-induced mutations (data not shown). Although all off-target mutations were not identified in my survey, these results indicate that effects of off-target mutations resulting from appropriate doses of ZFN RNA are small enough for removal by a simple backcross. The use of ZFNs potentially enables us to establish knockout medaka strains rapidly, whereas more time is required for repeated backcrossing to reduce background

mutations during the establishment of knockout strains in the TILLING approach [33].

Chapter 3

Targeted mutagenesis using custom-designed transcription activator-like effector nucleases

3.1 Introduction

Successful targeted mutagenesis in medaka using zinc-finger nuclease (ZFN) technology was demonstrated in the chapter 2. This system can induce site-specific DNA double-strand breaks that can be repaired by nonhomologous end joining or homology-directed repair, resulting in targeted gene disruptions by insertions and deletions (indels) or in targeted integrations by homologous recombination, respectively [20]. Because of its widespread applicability, this approach has been an alternative approach for effective reverse genetics in medaka, in addition to RNA knockdown using antisense oligonucleotides [49, 50] and gene knockout by targeting-induced local lesions in genome (TILLING) [16]. However, there are some limitations to generating a zinc finger domain that binds specifically to a certain genomic target sequence; therefore, the widespread adoption of this technology has been hindered [51].

Transcription activator-like effector nucleases (TALENs) have been reported as an alternative engineered nuclease for genome editing [51–53]. These enzymes consist of a fusion between a FokI nuclease domain and a transcription activator-like (TAL) effector DNA recognition domain found in plant pathogenic bacteria of the genus *Xanthomonas* [52]. The TAL effector domain is composed of 33–35 amino acid repeats, each of which interacts with a single target nucleotide; a polymorphic pair of residues at positions 12 and 13 in each repeat, known as repeat variable di-residues (RVDs), determines its base specificity [54, 55]. This modularity of DNA recognition allows customization of the TAL effector domain to successfully target the sequence of interest by efficient modular assembly methods [56–58]. The TALEN technology has become a powerful approach for genome editing in a number of animal models [36, 59–64].

Here, I demonstrate successful targeted mutagenesis in medaka using TALENs. In this chapter, I designed and constructed TALENs that target the second exon of the medaka *DJ-1* gene, a homolog of the human *DJ-1* (*PARK7*) gene, mutations in which cause autosomal recessive early-onset Parkinson ' s disease [65]. Using these TALENs, both somatic and germ-line mutations in the target sequence were specifically induced with high efficiency. I also showed that the DJ-1 protein was lost in homozygous null mutants generated by these TALENs. Moreover, to establish a more effective scaffold of TALENs in medaka, I investigated the effect of the N- and C-terminal regions of the TAL effector domain on the gene-disrupting activity of DJ1-TALENs.

3.2 Materials and Methods

Fish

The wild-type medaka used in this study was a d-rR strain [66]. Fish were handled in accordance with the Animal Research Guidelines at Kyoto University. Fish were maintained in an aquarium with recirculating water in a 14-/10-h day/night cycle at 26 ℃.

Design and construction of TALENs for the *DJ-1* gene

The genomic sequence of the *DJ-1* locus was identified from the Ensembl medaka genome browser (http://www.ensembl.org/Oryzias_latipes). Potential TALEN target sites in the locus were searched using the TALEN Targeter program (https://tale-nt.cac.cornell.edu/node/add/talen) [67] with the following parameters: (1) spacer length of 14–17, (2) repeat array length of 16–18, and (3) upstream base of T only.

TAL repeats were assembled by the Golden Gate assembly method [56] with slight modifications [68]. Each module containing an RVD was excised from each module plasmid (pNI, pHD, pNN, and pNG vectors) using BsaI-HF (New England Biolabs), and then the fragment was purified using NucleoSpin Gel and PCR Clean-up kit (MACHEREY-NAGEL). To generate repeat arrays, the modules were cloned into the dephosphorylated array plasmid (pFUS vectors) using Ligation high Ver.2 (TOYOBO). Both the assembled repeat arrays and a last repeat module were excised with Esp3I (Thermo Scientific). The fragments were purified using the NucleoSpin Gel and PCR clean-up kit (MACHEREY-NAGEL) and then cloned into expression vectors pCS2TAL3DD or pCS2TAL3RR that contain the SP6 promoter, the truncated N- and C-terminal regions of the TAL effector domain (136 and 63 amino acids, respectively), and either the DD or RR heterodimeric FokI domain [69].

Construction of truncated TALEN backbone vector

For the addition of a BglII and NheI site at the 3′ end of the SV40 late poly(A) signal in pCS2TAL3DD and pCS2TAL3RR vectors, a fragment containing the polyA signal was amplified by PCR from the pCS2TAL3DD vector using the primers FokI-FW and latepA-RV-MCS (Table 3.1) and was cloned into the XbaI/NotI site of the pCSTAL3DD and pCS2TAL3RR vectors.

To generate deletion variants of the TALENs, the TAL effector domain was PCR-amplified from the pTAL3 vector [56]. Each N-terminal region of the domain was PCR-amplified using the primer N287FW or N153FW with TAL_R2 (Table 3.1) and cloned into two Asp718 sites of pCS2TAL3DD and pCS2TAL3RR. The C-terminal region of each domain was amplified using the primer C230RV or C47RV with M13-FW (Table 3.1) and cloned into the XhoI/BamHI sites of pCS2TAL3DD and pCS2TAL3RR.

RNA preparation and microinjection

The expression vectors for the TALENs were linearized by digestion with either NotI or BglII. Capped RNAs were synthesized using the mMessage mMachine SP6 Kit (Life Technologies, Gaithersburg, MD) and purified using the RNeasy Mini Kit (QIAGEN). Pairs of RNA for the TALENs were injected into fertilized eggs of the d-rR strain by a microinjection method [39].

Somatic mutation analysis in TALEN-injected embryos

Each embryo that was injected with RNA coding for DJ1-TALENs was incubated for 1 hr at 55 ℃ in 100 μl lysis buffer containing 150 mM sodium chloride, 0.5% sodium dodecyl sulfate (SDS), 25 mM ethylenediaminetetraacetic acid (EDTA) (pH 8.0), 10 mM Tris–HCl (pH 8.0), and 200 μg/ml of proteinase K. The lysate was extracted with phenol:chloroform and precipitated with ethanol. The

Table 3.1. Oligonucleotide sequences used in this chapter

Name	Sequence [5′–3′]
FokI-FW	GTCAAAAGTGAACTGGAGGAG
latepA-RV-MCS	GCGCCGCGGCCGCTAGCAGATCTTAAAAAACCTCCCACACCTC
N287FW	AGATTACGCTGCTCATGGTACCGATCCCATTCGTCCGCGCAG
N153FW	TCATGGTACCGCCCCGCGACGGCGTGCT
TAL_R2	GGCGACGAGGTGGTCGTTGG
M13-FW	GTAAAACGACGGCCAGT
C230RV	CACTTTTGACTAGTTGGGATCCATCCGGGAGGCCGCCCCA
C47RV	TTGGGATCCGATCAATTCCGGCGCGTGCGG
DJ1-FW2	TGTGACTGTAGCGGGTCTGA
DJ1-RV1	GTGTGAACAACGCTGCATTT
M13-RV	GGAAACAGCTATGACCATG
DJ1-off1-FW	GCATGCCAGAATGTGCTTT
DJ1-off1-RV	GTTGCAAAGCAGTTGCAGAA

DNA precipitate was dissolved in 30 μl deionized water. The genomic region including the target site of the TALENs was amplified using the primers DJ1-FW2 and DJ1-RV1 (Table 3.1). This reaction contained 2 μl of genomic DNA template, 3 μl of 10× reaction buffer, 0.8 mM of each dNTP, 1.5 mM of $MgCl_2$, 0.2 μM of each primer, and 0.75 unit of HybriPol DNA Polymerase (Bioline) in a total volume of 30 μl. The cycling conditions were as follows: one cycle at 95 生 for 2 min, followed by 30 cycles of 95 生 for 20 sec, 58 生 for 30 sec, and 72 生 for 30 sec. The resulting PCR product was precipitated with ethanol for buffer exchange and was digested at 37 生 overnight in 10 μl HaeIII digestion solution that contained 1× M buffer and 2.5 unit of HaeIII (Takara Bio). These reactions were analyzed using a microchip electrophoresis system (MCE-202 MultiNA; Shimadzu) with the DNA-500 Reagent Kit. The molar concentrations of both digested and undigested fragments were quantified using the MultiNA Viewer software.

For sequence analysis in the injected embryos, the *DJ-1* locus was amplified with TaKaRa Ex Taq (Takara Bio) using the primers DJ1-FW2 and DJ1-RV1 (Table 3.1). The PCR conditions were as follows: one cycle at 94 生 for 2 min, followed by 35 cycles of 98 生 for 10 sec, 56 生 for 30 sec, and 72 生 for 30 sec. The PCR amplicons were subcloned into the pGEM-T Easy vector (Promega) and sequenced using the primer M13-RV (Table 3.1). The sequencing was performed by Operon Biotechnologies.

Founder screening

TALEN-injected fish were crossed with wild-type fish of the d-rR strain. Their F1 larvae were lysed individually in 25 μl of alkaline lysis buffer containing 25 mM NaOH and 0.2 mM EDTA (pH 8.0) and incubated at 95 生 for 10 min. Subsequently, the reaction was neutralized using 25 μl of 40 mM Tris–HCl (pH 8.0). These reactions were centrifuged at 20,000 × g for 3 min, and the supernatants were used as genomic DNA samples. Mutations in the *DJ-1* region in each genomic DNA sequence were analyzed by PCR amplification and subsequent HaeIII digestion as described above. Mutant alleles in each mutant F1 fish were determined by direct sequencing of the *DJ-1* region that was PCR-amplified using the primers DJ1-FW2 and DJ1-RV1 (Table 3.1) and purified using the Wizard SV Gel and PCR Clean-Up System (Promega).

Off-target analysis
Potential off-target sites were identified in the medaka genome using the e-PCR program (http://www.ncbi.nlm.nih.gov/projects/e-pcr/) as described previously [62]. In this study, the criteria for determining off-target sites were that up to five non-identical bases and 1-bp gaps can occur in each recognition sequence, and the spacer between two putative recognition regions should be <100 bp.

The genomic region containing the potential off-target site was PCR-amplified from the F1 larvae of TALEN-injected fish using the primers DJ1-off1-FW and DJ1-off1-RV (Table 3.1). Each amplified product was purified using the Wizard SV Gel and PCR Clean-Up System and directly sequenced using the primer DJ1-off1-FW (Table 3.1).

Western blot analysis
The head regions from adult medaka were homogenized in cooled phosphate-buffered saline (PBS), pH 7.4, and centrifuged at 20,000 × g for 5 min. The supernatants were boiled in SDS sample buffer containing 50 mM Tris–HCl (pH 6.8), 2% SDS, and 6% 2-mercaptoethanol. Protein samples were separated on a 15% polyacrylamide gel containing SDS and transferred to a polyvinyl difluoride membrane. The membrane was blocked in PBST (PBS with 0.1% Tween-20) containing 1% Block Ace (DS Pharma Biomedical) and was probed with rabbit anti-meDJ-1 [70] diluted 1:1000. The secondary antibody used was anti-rabbit IgG, alkaline phosphatase (AP)-linked antibody (Cell Signaling Technology) diluted 1:2000, and signals were developed using nitroblue tetrazolium and 5-bromo-4-chloro-3-indolyl phosphate in AP buffer containing 100 mM Tris–HCl (pH 9.5), 100 mM NaCl, and 50 mM $MgCl_2$.

Statistical analysis
Disruption activities of the truncated TALENs were analyzed with one-way analysis of variance (ANOVA) followed by Tukey's honestly significant difference (HSD) test using the R statistical software (https://www.r-project.org).

3.3 Results

Design and construction of TALENs for the medaka *DJ-1* gene
The medaka *DJ-1* gene (Ensembl gene no. ENSORLG00000004285), an ortholog of the human *DJ-1* (*PARK7*) gene in medaka, has six exons and encodes 189 amino acids [70]. I scanned potential TALEN target sites in the second exon of the *DJ-1* gene using the TALEN Targeter program [67] and identified a target site that consisted of 18 bp of the left binding site (5′-CTGTCCCGATACTAGCTT-3′), 16 bp of the right site (5′-GCAGAGACTCACCTGT-3′), and a 15-bp spacer sequence containing a HaeIII cleavage site (5′-GGAAGAGGCCAGCAA-3′) (Fig. 3.1). This target site also meets all five previously described design guidelines [56]. To construct a pair of TALENs cleaving this target site, I assembled RVD modules by the Golden Gate assembly method [56] with slight modifications. All the assembled RVD modules in each site are described in Fig. 3.1.

Efficient mutagenesis with DJ1-TALENs in somatic medaka cells
To evaluate whether DJ1-TALENs can induce mutations in the target sequence, 300 ng/μl of RNA coding for the TALENs was injected into fertilized eggs of the d-rR strain. To detect induced mutations, genomic DNA was extracted from each injected embryo at 3 days post fertilization (dpf). The 285-bp long genomic region containing the TALEN target site was PCR-amplified from each genomic DNA, and the amplified product was digested with HaeIII (Fig. 3.2A). Control embryos without the

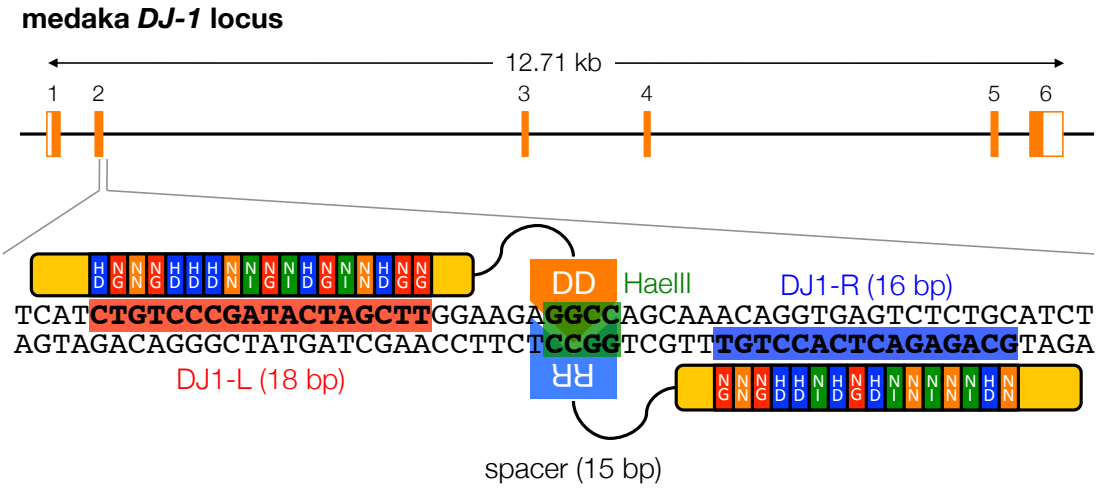

Figure 3.1. Genomic structure of the medaka *DJ-1* gene (Ensembl gene no. ENSORLG0000004285) and design of DJ1-TALENs. *DJ-1* gene has six exons that code 189 amino acids of the DJ-1 protein. DJ1-TALENs were designed to target the second exon of the gene. Red and blue boxes indicate the left and right recognition sequences of the TALENs, respectively. The RVDs of the TAL effector domain for each binding site are shown with the recognition sequences. The large green box in the center of the sequence indicates a cleavage site with HaeIII for mutation analysis.

TALENs showed two fragments (199 and 86 bp, a and b, respectively, in Fig. 3.2A) produced by complete digestion with HaeIII. On the contrary, in all 20 TALEN-injected embryos, these two fragments disappeared and one undigested fragment (285 bp, a+b in Fig. 3.2B) distinctly emerged instead, indicating that the HaeIII recognition site in the TALEN target sequence had been mutated. To investigate mutation patterns at the target site, a part of the *DJ-1* gene region containing the target site was PCR-amplified from two TALEN-injected embryos (#1 and #2) and was subcloned, and then each clone was sequenced. All 26 clones sequenced had mutated sequences that contained four types of indels (15/15) in embryo #1 (Fig. 3.2C) and six types of indels (11/11) in embryo #2 (Fig. 3.2D), indicating that DJ1-TALENs induced indel mutations around the target site with extremely high efficiency. As shown in Fig. 3.2D, the HaeIII recognition site was newly generated in the mutated allele, and, as a result, two digested fragments of slightly different sizes were observed (Fig. 3.2B, #2).

DJ1-TALENs can induce mutations in a dose-dependent manner

To evaluate the dose dependence of TALEN-mediated gene disruption efficiency, various concentrations (10–300 ng/μl) of RNA coding for the TALENs were injected. Most embryos injected with the TALENs showed no obvious developmental defects at 5 dpf (Table 3.2). This suggested that TALENs exhibit lower toxicity in the injected medaka embryos than do ZFNs, which induced significant developmental defects or lethality by injection with >10 ng/μl of RNA, although the *Sharkey*-based DS and RR type of nuclease domains were used in these nucleases [71]. Genomic DNA was extracted from each surviving embryo at 5 dpf, and then the HaeIII digestion pattern of the PCR-amplified fragment containing the TALEN target site was analyzed using the MultiNA system. I determined that all TALEN-injected embryos carried mutations at the TALEN-targeted site based on the appearance of the undigested fragment (Fig. 3.3A, a+b). To quantify the disrupting activity at each concentration of TALENs, I calculated the "mutation rate" as the molar concentration of the HaeIII-undigested fragment (Fig. 3.3A, a+b) as a percentage of the sum of the molar concentrations of the undigested fragment (Fig. 3.3A, a+b) and the larger digested fragment (Fig. 3.3A, a). As shown in Fig. 3.3B, I

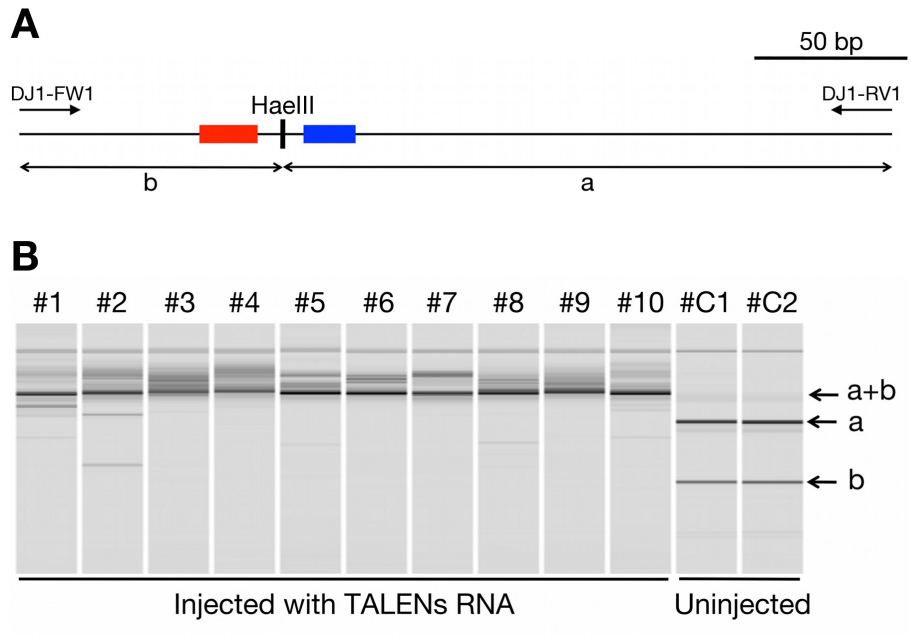

C

```
TCTGTCCCGATACTAGCTTGGAAGAGGCCAGCAAACAGGTGAGTCTCTGCA WT  0/15
TCTGTCCCGATACTAGCTTGGAAG-------CAAACAGGTGAGTCTCTGCA -7  4/15
TCTGTCCCGATACTAGCTTGGAAG-------CTAACAGGTGAGTCTCTGCA -7  9/15
-----------CTAGTGCAGCAGAAACGTGGCAAACAGGTGAGTCTCTGCA -17 1/15
------------CTAG--TG--------CAGCAGA---------------- -57 1/15
```

D

```
TCTGTCCCGATACTAGCTTGGAAGAGGCCAGCAAACAGGTGAGTCTCTGCA WT  0/11
TCTGTCCCGATACTAGCTTGGAAG-------CAAACAGGTGAGTCTCTGCA -7  6/11
TCTGTCCCGATACTAGCTTGGAAGA----------CAGGTGAGTCTCTGCA -10 1/11
TCTGTCCCGATAC---------------CAGCAAACAGGTGAGTCTCTGCA -15 1/11

GATACTAGCTTGGAAGAG----------------GCCAGCAAACAGGTGAG WT  0/11
GATACTAGCTTGGAAGGCCAAGCTCA---------CCAGCAAACAGGTGAG +7  1/11
GATACTAGCTTGGAAGACTTGGAAGACTCACCT-----GCAAACAGGTGAG +11 1/11
GATACTAGCTTGGAAGAGCATGGAGGCTTGGAAGGCCAGCAAACAGGTGAG +16 1/11
```

Figure 3.2. Somatic mutations in embryos injected with 300 ng/μl RNA for DJ1-TALENs. (A) In the wild type, a 285-bp amplified fragment obtained using primers DJ1-FW2 and DJ1-RV1 is digested into 199-bp (a) and 86-bp (b) fragments by HaeIII. Red or blue boxes indicate the left or right recognition sites of the TALENs, respectively. (B) Gel images of HaeIII-digested fragments analyzed in MultiNA. The TALEN-injected embryos (#1–#10) showed an undigested fragment (a+b), while control embryos that were not injected with TALEN (#C1 and #C2) showed that the intact fragment (a+b) was completely digested into two fragments (a and b). (C and D) Subcloned sequences observed in TALEN-injected embryos #1 and #2, respectively. Red letters or dashes indicate the identified mutations. Red and blue boxes in wild-type (WT) sequences indicate the left and right recognition sites of the TALENs, respectively. Green boxes indicate the HaeIII cleavage site. The sizes of the insertions and deletions are shown to the right of each mutated sequence (−, deletions; +, insertions). Numbers on the right edge indicate the numbers of mutated clones identified from all analyzed clones from each embryo.

Table 3.2. Survival of embryos injected with various concentrations of RNAs for DJ1-TALENs

RNA concentration (ng/μl)	Injected	Survival at 1 dpf	Survival at 5 dpf
0	20	20	20
10	20	19	19
50	20	20	19
100	23	23	23
200	20	20	20
300	22	20	20

Table 3.3. Germ-line transmission of TALEN-mediated mutations in each G0 fish

G0 Founder			
ID	Sex	F1 larvae analyzed	Mutants (%)[a]
1M	Male	28	24 (85.7%)
1F	Female	37	21 (56.8%)
8M	Male	39	39 (100%)
8F	Female	34	25 (73.5%)
10M	Male	28	17 (60.7%)
11M	Male	32	19 (59.4%)
11F	Female	32	14 (43.8%)

[a] The values shown are the numbers of mutant F1 larvae as determined by PCR amplification and subsequent HaeIII digestion.

found that 10 ng/μl of TALEN RNA induced mutations with low efficiency (38.5% ± 13.6), whereas >50 ng/μl of RNA induced mutations with extremely high efficiency (almost 100%). These results indicate that the DJ1-TALENs dose-dependently induced mutations at the target site.

Heritable mutations are induced with DJ1-TALENs

To investigate whether TALEN-mediated mutations are also induced in germ cells and transmitted into subsequent generations, the injected fish were raised to sexual maturity and then their progeny was analyzed. Of the 125 eggs injected with 200 ng/μl of TALEN RNA, 95 (76%) hatched normally and 86 (69%) reached adulthood. Seven of the 86 adult G0 fish were crossed with wild-type fish of the d-rR strain, and their F1 progeny were genotyped by PCR amplification and subsequent HaeIII digestion using genomic DNA extracted from each F1 larva. I found that all 7 G0 fish screened transmitted TALEN-induced mutations to their F1 progeny. The germ-line transmission rates of the mutations in each G0 founder ranged from 43.8% (14 of 32; #11F) to 100% (39 of 39; #8M) (Table 3.3). There was no apparent difference in these rates between the sexes of the G0 founders (Table 3.3). Subsequently, the target region of the TALENs was sequenced in all F1 mutant larvae identified by HaeIII genotyping. While 2 of the 7 G0 founders (#8F and #11F) carried only one type of mutation in their germ cells, the others (#1M, #1F, #8M, #10M, and #11M) carried from three to five types of mutations in their germ cells (Table 3.3). All mutations identified from the F1 larvae are shown in Fig. 3.4. These results indicate that DJ1-TALENs induced heritable mutations in injected fish with high efficiency.

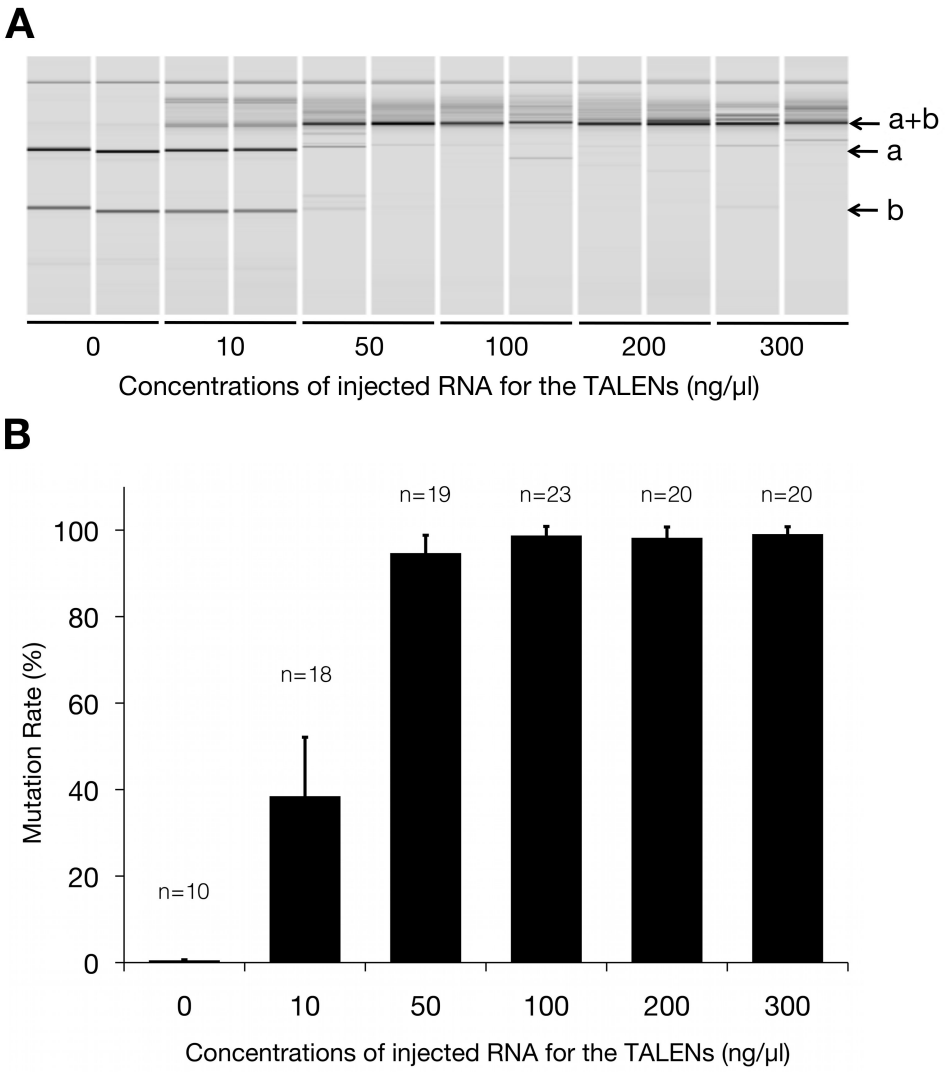

Figure 3.3. Dose-dependent mutagenesis by DJ1-TALENs. (A) MultiNA gel images of HaeIII digestion. A PCR fragment containing the TALEN target site was digested with HaeIII. Gel images from two representative embryos injected with 0–300 ng/μl RNA for the TALENs are shown. (B) Mutation rates at each injected TALEN RNA concentration. The mutation rate was calculated as the molar concentration of the undigested fragment (a+b) with HaeIII as a percentage of the sum of molar concentrations of the undigested fragment (a+b) and the larger digested fragment (a). The molar concentration of each fragment was quantified using the MultiNA Viewer software. Columns and error bars represent mean ± SEM. "n" indicates the numbers of embryos analyzed.

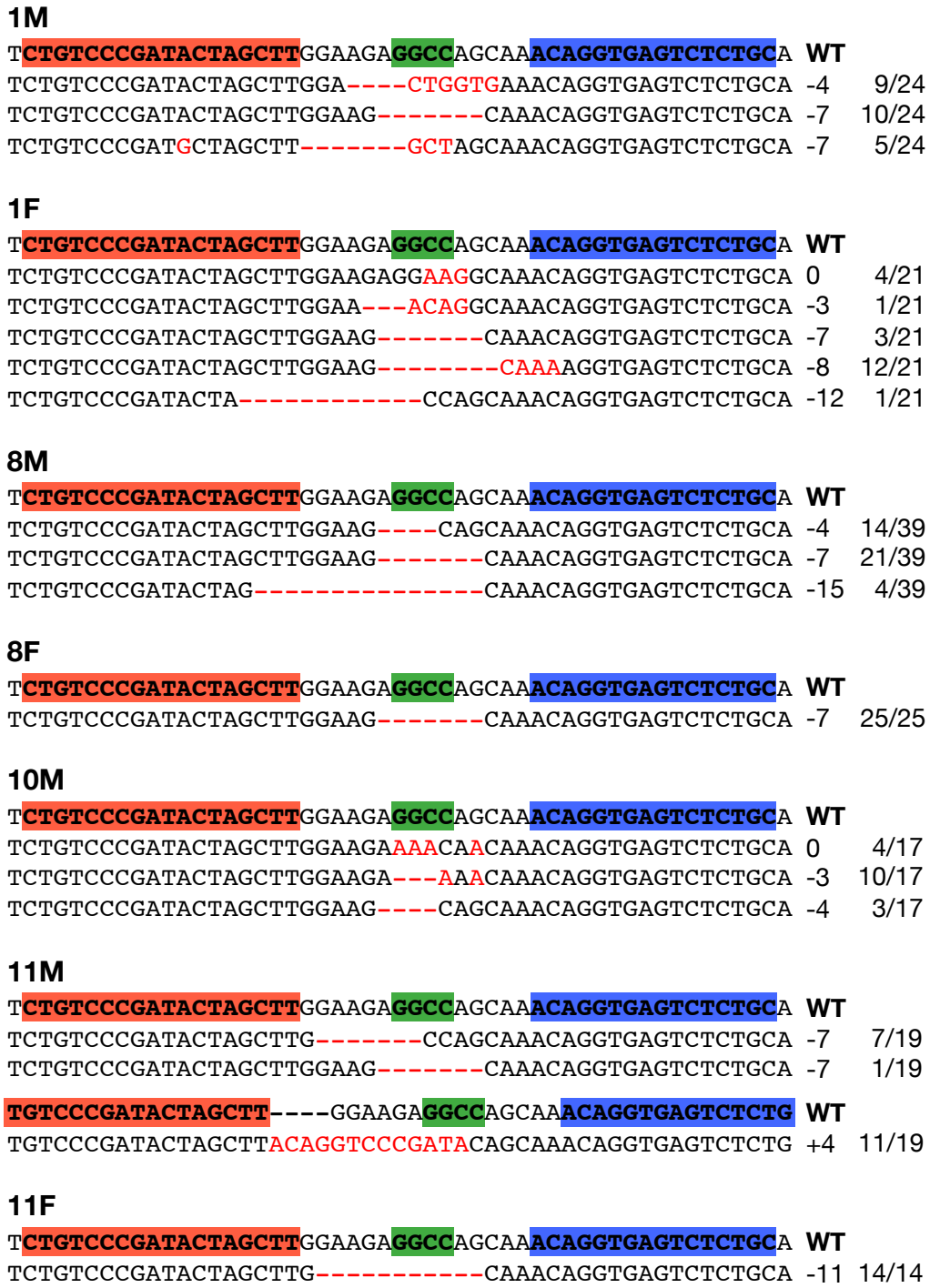

Figure 3.4. TALEN-induced mutations observed in F1 larvae from seven G0 founders. Red letters or dashes indicate the identified mutations. Red and blue boxes in the wild-type (WT) sequences indicate the left and right recognition sites of the TALENs, respectively. Green boxes indicate the HaeIII cleavage site. The sizes of the insertions and deletions are shown to the right of each mutated sequence (−, deletions; +, insertions). The numbers on the right edge indicate the numbers of larvae carrying each mutated sequence among all sequenced larvae.

Table 3.4. Potential off-target site of DJ1-TALENs identified with the e-PCR program. This list shows candidate off-target sites identified as follow three conditions; (1) up to five non-identical bases (mismatches) in each recognition sequence, (2) up to one base pair gap in each recognition sequence, (3) <500 bp spacer length between the two putative recognition regions. Red letters shows the target site of DJ1-TALENs. Blue letters shows a potential off-target region analyzed in this study.

Chromosome	Strand	From	To	Mismatch	Gap	Spacer
chr5	+	7477585	7477635	0	0	15
chr5	+	28112014	28112249	10	2	198
chr7	−	17711418	17711581	10	1	127
chr9	−	15931407	15931476	10	2	32
chr12	+	5685843	5685985	7	2	105
chr12	−	19269294	19269518	10	2	187
chr13	−	23653665	23654214	7	2	512
chr16	+	21165226	21165700	10	2	437
scaffold693	+	42746	43178	9	2	395
scaffold791	−	31456	31899	10	2	406
ultracontig149	−	166188	166675	6	2	450
ultracontig62	+	293467	293699	9	1	196
ultracontig72	−	2589715	2589917	10	1	166
ultracontig88	−	226571	227065	7	2	457

Specificity of mutations induced by DJ1-TALENs

For accurate genome editing, it is important to induce mutations site-specifically with TALENs. I searched for potential off-target sites of DJ1-TALENs using the e-PCR program and identified 13 candidates for potential off-target sites in the medaka genome (Table 3.4). It has been reported that the scaffold of my TALENs had less disrupting activity when the spacers between two binding sites were >24 bp long [53]. Since 12 of 13 candidates have >100 bp in their spacers (Table 3.4), it is unlikely that the TALENs induce mutations at these sites. I analyzed a candidate site (chromosome 9: 15,931,407–15,931,476) that had 10-bp mismatches and 2-bp gaps in the recognition sequences and the shortest 32-bp spacer among the 13 candidates. The genomic region containing the off-target candidate site was PCR-amplified from 12 F1 larvae of four founders (#1M, #1F, #8M, and #8F) that carried independent mutations in their *DJ-1* regions (Fig. 3.4), and then the amplified product was subjected to direct sequencing. As a result, no mutation was identified at the off-target site, indicating that DJ1-TALENs have no potential off-target site with significant similarity to their target site in medaka genome.

Homozygous *DJ-1* mutants generated with DJ1-TALENs lacked DJ-1 protein

Next, I investigated whether genomic mutations with DJ1-TALENs affect the production of the DJ-1 protein. Interestingly, a frameshift mutation with the same 7-bp deletions (5′-AGGCCAG-3′ in the spacer region) was identified in F1 larvae from five G0 founders (Fig. 3.4; Fig. 3.5A). This frameshifted mutant allele (named *DJ-1*$^{\Delta 7}$) yields a truncated DJ-1 protein due to an additional region of altered translation (Fig. 3.5B). Therefore, null mutants that carried *DJ-1*$^{\Delta 7}$ in both alleles were generated by crossing the founders #8M and #8F. To analyze the production of the DJ-1 protein, extracts from the head region of this F1 null mutant, a G0 fish injected with 200 ng/μl TALEN RNA and a wild-type fish of the d-rR strain were subjected to Western blot analysis with the anti-medaka DJ-1 antibody produced previously [70]. An immunoreactive band with a molecular mass of 23 kDa

was detected in the wild-type fish, while no signals were detected in the F1 *DJ-1*$^{\Delta 7/\Delta 7}$ fish (Fig. 3.5C). This result indicated that loss-of-function mutations were induced by the TALENs. It is noteworthy that even the G0 fish injected with the TALENs completely lacked DJ-1 protein (Fig. 3.5D). It is reasonable to assume that, in the G0 fish, the *DJ-1* gene was completely disrupted by TALEN injection (Fig. 3.3).

Disrupting activity of DJ1-TALENs largely depends on the length of the N- and C-terminal regions of the TAL effector domain

The length of fully assembled TAL effectors (>800 amino acids) makes it difficult to handle their DNA constructs and RNA transcripts. Therefore, there have been several efforts to identify the minimal N- and C-terminal regions of the TAL effector domain for efficient DNA cleavage [53, 72]. Here, the pCS2TAL3DD and pCSTAL3RR vectors were used for TALEN RNA synthesis, both of which harbor 136 or 63 amino acids in the N- or C-terminal regions of the TAL effector domain. The TALENs generated from these vectors induced site-specific mutation with high efficiency not only in the medaka (in this study) but also in the zebrafish [69].

To identify more efficient scaffolds of TALENs for *in vivo* genome cleavage, six types of deletion variants of DJ1-TALENs were constructed (Fig. 3.6A). N287 and C230 scaffolds were comparable to the original scaffold of TALENs [52,56], while N153 and C47 were comparable to one of the effective deletion variants (named "NC" type) [72]. Each pair of RNA sequences for these TALENs was injected into fertilized eggs and did not show significant toxicity to the embryo (summarized in Table 3.5). From each 5-dpf embryo, the genomic DNA fragment containing the target site of the DJ1-TALENs was PCR-amplified and was subjected to subsequent HaeIII digestion to assess the "mutation rate" as described previously (Fig. 3.6B). As shown in Fig. 3.6B, with higher concentrations of TALEN-RNA (180 nM), N287C230 and N136C230 induced mutations in about 50% of the injected embryos. On the other hand, other constructs (N287C63, N136C63, N153C47, and N136C47) induced higher mutation rates (over 75%). This trend was more remarkable in the case of lower amounts of TALEN-RNA (9 nM). Among the N136 scaffolds (N136C230, N136C63, and N136C47 in Fig. 3.6A), I found that 63 amino acids of the C-terminal region of the domain showed the highest disrupting activity (38.5 ± 13.6%). In addition, among the C63 scaffolds, N287C63 showed a higher disruption rate (69.6 ± 11.7%) than did N136C63 (38.5 ± 13.6%). This tendency was also observed in the C47 scaffolds: N153C47 showed a higher disruption rate (22.7 ± 9.9%) than did N136C47 (9.7 ± 4.1%). As above, in my experiments, the longer N-terminal regions showed more disruption activity.

3.4 Discussion

I demonstrated successful targeted mutagenesis in medaka using TALENs: that is, TALENs targeted to the medaka *DJ-1* gene could induce mutations in both the somatic and the germ cells of the injected fish with extremely high efficiency. In addition, I also showed that the DJ-1 protein was lost in null mutant fish that carried the TALEN-induced frameshifted mutation in both alleles. These results revealed that the TALEN technology is an available and effective tool for reverse genetics in medaka. This is the first report to describe targeted disruption of an endogenous gene in medaka using engineered TALENs.

TALENs can simply and efficiently produce gene knockout strains with RNA introduction by conventional microinjection methods. In this study, all the screened G0 founders that were injected with the TALENs (7/7; 100%) carried mutations in their germ cells, and these mutation events were induced in their germ cells with high frequency (68.6% on average; Table 3.3). This frequency was equal or superior to those in my mutagenesis study using ZFNs in medaka (46.9% on average) [71] and in previous studies using TALENs in zebrafish (8.3–66.0% on average) [69, 73, 74].

Detailed investigation of the mutations in F1 larvae revealed that up to five types of mutations were

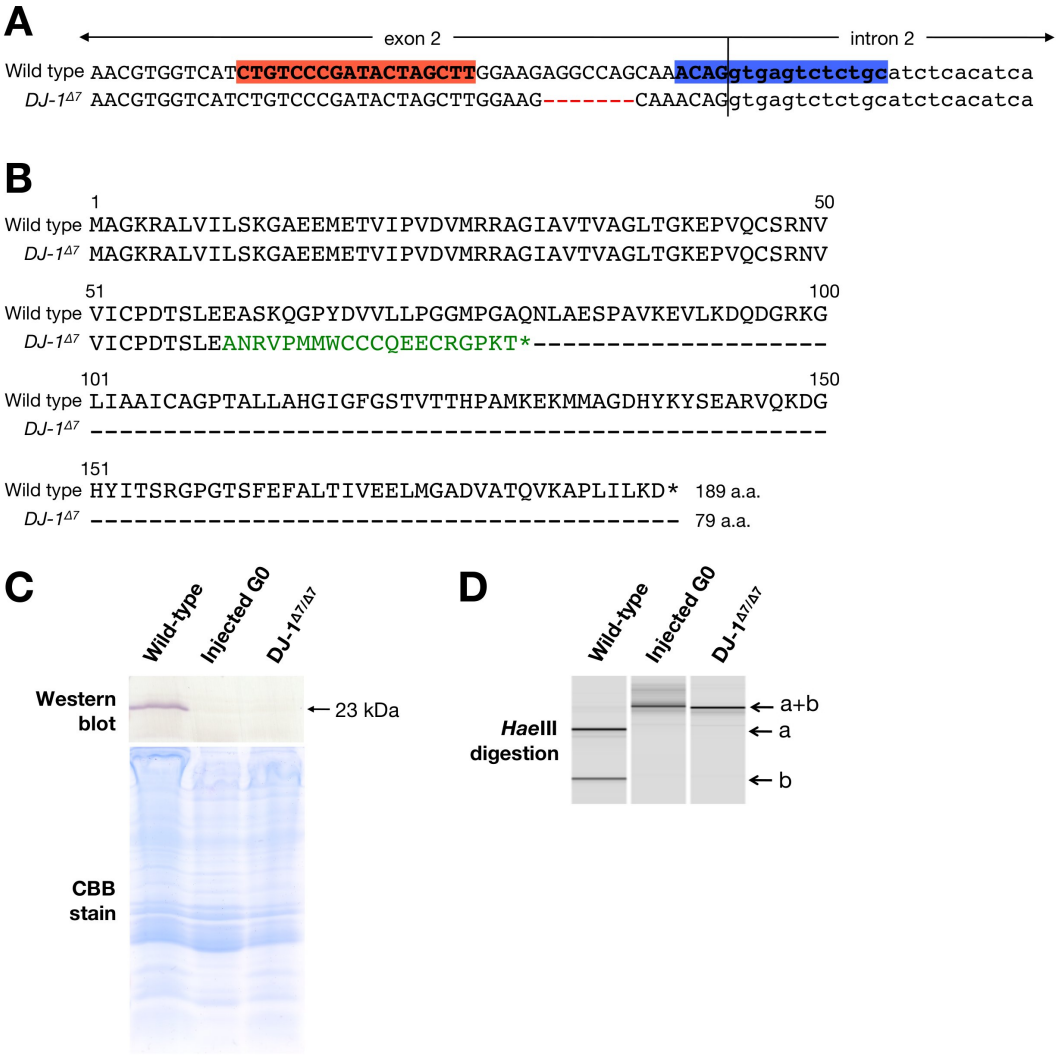

Figure 3.5. Expression of the DJ-1 protein in homozygous mutant fish. (A) Nucleotide sequences from the wild-type and mutant *DJ-1*$^{\Delta 7}$ alleles. Red dashes indicate the TALEN-induced deletion. Red and blue boxes indicate the left and right recognition sites of DJ1-TALENs, respectively. Uppercase and lowercase letters in the sequences indicate the second exon and second intron sequences of the *DJ-1* gene, respectively. (B) Alignment of the amino acid sequences of wild-type (accession no. AB193829) and truncated medaka DJ-1 proteins led by the *DJ-1*$^{\Delta 7}$ frameshifted mutation. The *DJ-1*$^{\Delta 7}$ product has an additional region of altered translation, which is indicated by green letters. (C) Western blot analysis using anti-medaka DJ-1 antibody. Homogenates prepared using the head regions of each fish were used (see Materials and Methods for details). The predicted signal (23 kDa) was detected in the wild-type lysate. No signals were detected in both injected G0 and *DJ-1*$^{\Delta 7/\Delta 7}$ lysates, although the Coomassie Brilliant Blue (CBB)-stained gel showed evenly extracted protein bands among the three samples (bottom). (D) MultiNA gel images of HaeIII digestion. Genomic DNA was extracted from the posterior part of each fish whose head region was analyzed with Western blot in C. PCR fragments containing the target site of DJ1-TALENs were digested with HaeIII. In the wild type, the intact band (a+b) was completely digested into two fragments (a and b), whereas both the injected G0 fish and the *DJ-1*$^{\Delta 7/\Delta 7}$ mutant exhibited an undigested fragment (a+b). (C and D) "Wild-type": without TALEN-injection; "injected G0 fish": injected with 200 ng/μl RNA for the TALENs; "*DJ-1*$^{\Delta 7/\Delta 7}$": F1 fish harboring a 7-bp deletion (*DJ-1*$^{\Delta 7}$) in both alleles.

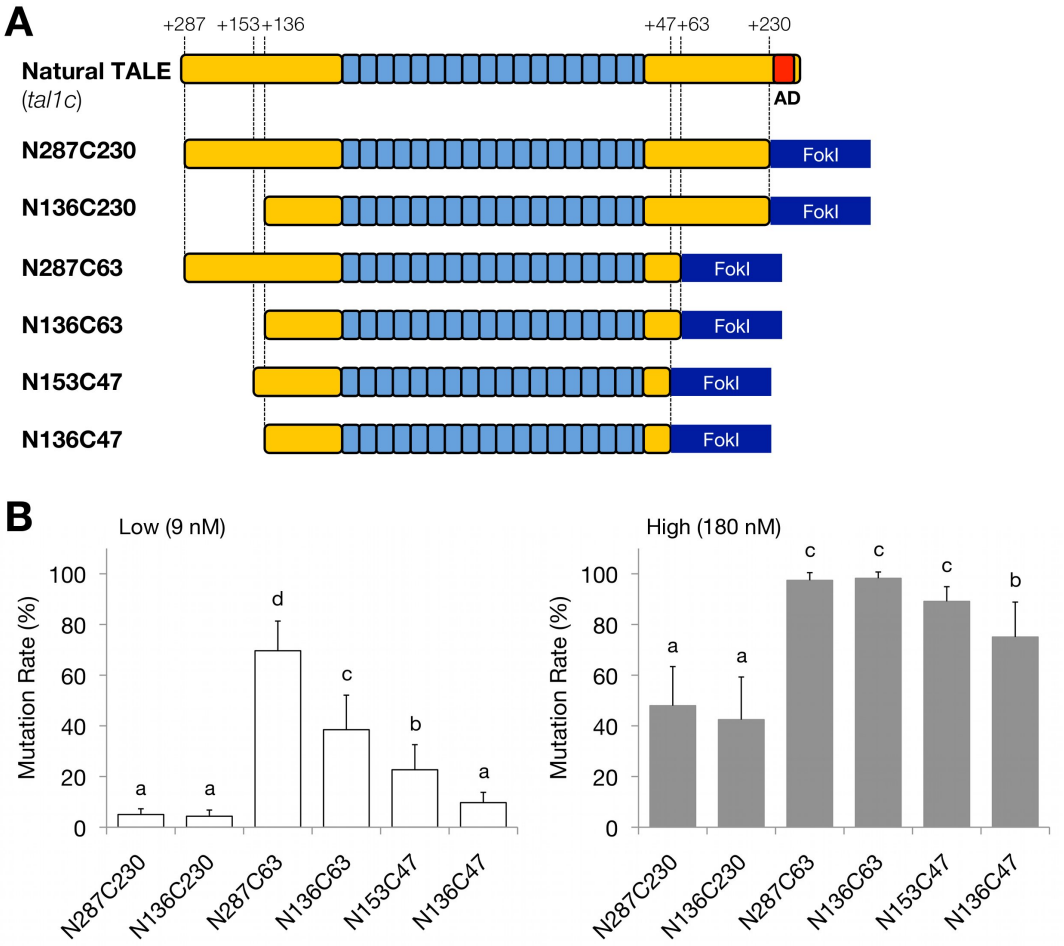

Figure 3.6. Effects of the N and C termini of the TAL effector domain on the gene-disrupting activities of deletion variants of DJ1-TALENs. (A) Schematic of deletion variants in the TAL effector domain. A natural TALE (*tal1c*) has 287 and 278 amino acids in the N- and C-terminal regions of the TAL effector domain, respectively. The transcriptional activation domain (AD) in the C-terminal region is highlighted in red. The names of the deletion variants generated by PCR amplification are indicated on the left side. The numbers of remaining amino acids of the N- and C-terminal regions relative to the position of the repeat modules are shown above. (B) Disruption activities of the truncated TALENs, shown as the mutation rate in the injected embryos. (Left) Mutation rates in the embryos injected with "low" concentrations of RNAs (9 nM) containing a mole ratio equal to 10 ng/μl of RNA for the N136C63 scaffold of the TALENs. (Right) Mutation rates in the embryos injected with "high" concentrations of RNAs (180 nM) containing a mole ratio equal to 200 ng/μl of the N136C63 scaffold. Mutation rate was calculated as the molar concentration of the undigested fragment with HaeIII as a percentage of the sum of the molar concentrations of the undigested fragment and the larger digested fragment. The molar concentration of each fragment was quantified using the MultiNA Viewer software. Columns and error bars represent mean ± SD (n = 12). The differnt letters at the top of the columns indicate significant differences ($P < 0.05$; one-way ANOVA and Tukey's HSD test).

Table 3.5. Results of microinjection with the deletion series of DJ1-TALENs RNA

Scaffold	RNA concentration (nM)		Injected	Survival at 1 dpf
N287C230	Low	9	24	24
	High	180	24	16
N136C230	Low	9	23	23
	High	180	24	24
N287C63	Low	9	24	23
	High	180	24	20
N136C63[a]	Low	9	20	19
	High	180	20	20
N153C47	Low	9	24	21
	High	180	24	22
N136C47	Low	9	24	22
	High	180	22	19

[a] The results from the N136C63 scaffold are the same as shown for 10 and 200 ng/μl in Table 3.2.

induced in the germ cells of each TALEN-injected G0 founder (Fig. 3.4). Taking the high mutation rate mentioned above into consideration, these facts indicate that mutation events occurred independently in a number of embryonic cells in early embryogenesis. From a practical standpoint, this suggests that a number of mutant strains can be obtained from each founder; therefore, determination of mutant alleles by sequencing in each F1 fish is required before mating the F1 fish for the establishment of mutant strains.

Highly efficient induction of mutations by the TALENs also occurred in the somatic cells of injected G0 fish. Interestingly, in a G0 fish injected with 200 ng/μl TALEN RNA, the DJ-1 protein was reduced to undetected levels in Western blot analysis (Fig. 3.5C) in accordance with the fact that lesions were induced at the target site by the TALENs in the G0 fish (Fig. 3.5D). Mosaic patterns of mutations were observed in the RNA-injected fish, as in my previous study using ZFNs [71]; however, in this study, both mutation analysis with HaeIII digestion and sequence analysis suggested that the TALENs induced the complete disruption of the targeted gene in the injected fish (G0) (Figs. 3.2 and 3.3) as well as the complete loss of the protein (Fig. 3.5D). These results strongly suggest that highly effective TALENs can induce complete gene knockout in the TALEN-injected generation as previously reported in zebrafish [73]. This will make it possible to perform gene knockout experiments without mating or the establishment of mutant strains, shortening the duration of experiments. In addition, TALEN-mediated gene lesions and the induced protein losses in the injected fish produced by them are retained throughout their life. This is an additional advantage of using TALEN-injected fish, compared with gene knockdown experiments using antisense oligonucleotides that interfere with gene translation only during the early developmental stages.

On the other hand, when genes whose functions are essential for embryonic development or reproduction were disprupted, the highly efficient induction of mutations that cause complete loss of the targeted gene products is likely to lead to embryonic lethality or sterility in the injected fish. Hence, it may happen that highly effective TALENs make it difficult to obtain heterozygous mutants that exhibit no or weaker defects. However, in this study, I showed that the gene-disrupting activity of DJ1-TALENs was significantly reduced by injecting a low concentration (10 ng/μl) of RNA (39%), whereas >50 ng/μl of RNA efficiently induced mutations (almost 100%) (Fig. 3.3). This result suggests that dilution of the injected RNA enables us to avoid the induction of bi-allelic mutations and thereby

lethality or sterility in the injected fish; therefore, this approach will make it possible to establish gene knockout strains with disruptions in genes with essential functions.

When establishing null mutant strains using random mutagenesis approaches such as the TILLING method, time-consuming and laborious procedures are required to remove unwanted nonspecific mutations, for example, repeated backcrossing, which takes 12 or more months [33]. Meanwhile, because the DNA-binding domain in each TALEN has a sufficiently long binding sequence (recognizing from 16 to 18 bp) that exhibits high DNA-binding specificity, it is likely that there are few off-target effects caused by mutagenesis of potential off-target sites of the TALENs. In fact, I could identify no candidate for an off-target site for DJ1-TALENs using the e-PCR program with the criteria described previously [62]. Upon analyzing a potential off-target site identified with less stringent criteria (allowing up to a 5-bp mismatch and a 1-bp gap in each recognition site) (Table 3.4), no mutations were found at the site in mutated F1 larvae. These results suggest that TALENs induce mutations site-specifically in medaka. Because of this high specificity, backcrossing to reduce off-target defects is not necessarily required when establishing mutant strains using TALENs. In addition to frequently inducing the same mutation, such as *DJ-1*$^{\Delta 7}$ (Fig. 3.5A), this suggests that homozygous null mutants (e.g., *DJ-1*$^{\Delta 7/\Delta 7}$ in this study) can be generated in the F1 generation by crossing between the TALEN-injected G0 founders (Fig. 3.5). This is one of the advantageous characteristics of targeted mutagenesis with the TALEN system: we can obtain and begin to analyze homozygous mutants in the short time period of only 3–4 months.

Despite the high specificity of the TALENs, it was reported that a closely related paralog of the targeted gene was disrupted by TALENs in the zebrafish [69]. As well as the zebrafish, the medaka also has >2000 pairs of paralogs derived from whole-genome duplication in teleosts [3]. This is likely to make it difficult to disrupt and analyze the paralogs independently. Therefore, it is important to search the paralogs of the targeted genes that may carry very similar sequences to the target sequence of the designed TALENs for medaka endogenous genes.

Although Western blot analysis with the anti-medaka DJ-1 antibody indicates that the DJ-1 protein was lacking in both the injected G0 fish and the F1 *DJ-1*$^{\Delta 7/\Delta 7}$ fish (Fig. 3.5C), I did not observe developmental or behavioral defects (data not shown). It was reported that in DJ-1-deficient mice and zebrafish, loss of dopaminergic (DA) neurons is intensely induced by neurotoxins and oxidative stress [75, 76]. These observations suggest that a more detailed investigation of the relationship between the loss of DA neuron and other factors such as external stresses and genetic background is required to explain the functions of DJ-1 in medaka.

In this study, I investigated the effect of the N- and C-terminal regions of the TAL effector domain on the gene-disrupting activity of DJ1-TALENs and found that 287 amino acids of the N-terminal region (N287) and 63 amino acids of the C-terminal region (C63) showed the highest activities among six types of deletion variants of the TALENs (Fig. 3.6). It is likely that the C63 scaffolds efficiently matched the 15-bp spacer sequences used in this study because previous reports suggested that the C-terminal region determines the length of spacer sequences of the TALENs [53, 72]. On the other hand, it remains difficult to explain why both the N287 and the N153 scaffolds had higher activities than the N136 scaffold (Fig. 3.6B) because most previous TALEN studies adopted only the N136 scaffold, in which the deletion of the first 152 amino acids was considered to specifically contribute to transport into plant cells [77]. It is likely that the first 152 amino acids play some role in the DNA cleavage activity of TALENs, such as facilitation of DNA binding and/or stabilization of the proteins. More detailed investigation focused on the functions of the N-terminal region is required to explain my results.

Chapter 4

Design, evaluation, and screening methods for efficient targeted mutagenesis with TALENs

4.1 Introduction

Targeted genome editing with engineered nucleases, such as zinc-finger nucleases (ZFNs) and transcription activator-like (TAL) effector nucleases (TALENs), has become a powerful technology for reverse genetics approaches [78, 79]. Our group and other researchers have previously demonstrated successful targeted mutagenesis in medaka using ZFNs [71, 80] and TALENs [81]. Although it is expensive and labor-intensive to generate zinc finger domain binding specifically to a certain genomic sequence, the modularity of the DNA-recognition domain in TALENs allows researchers to customize TALENs easily using modular assembly methods [56–58, 68]. The TALEN technology has become an effective and robust tool for inducing genomic modifications in a wide range of organisms, including medaka.

Here, I have described efficient detection methods for TALEN-induced mutations at endogenous loci and guidelines for TALEN design for targeted mutagenesis in medaka. I adopted a heteroduplex mobility assay (HMA) using an automated microchip electrophoresis system, which is a simpler and high-throughput method for the detection of TALEN-induced mutations than previously described methods such as restriction fragment length polymorphism (RFLP) analysis [59, 81]; DNA-cleaving assay with mismatch sensitive nucleases, for example, CEL1 endonuclease and T7 endonuclease I [53, 72]; high-resolution melting analysis (HRMA) [69]; the LacZ disruption/recovery assay [82]; and HMA using poly-acrylamide gel electrophoresis (PAGE) [80, 83]. Additionally, in this chapter, I have also proposed design guidelines for efficient targeted mutagenesis using TALENs. First, I found that some pairs of TALENs can dominantly induce specific patterns of mutations, which are thought to be due to short homologous sequences in the target genomic sequences. Second, I also found that a 5′ T adjacent to the half site of each TALEN, which is the only limitation in design of the TALENs [57], is not necessary for genomic DNA cleavage.

4.2 Materials and Methods

Fish

Three strains of medaka were used in this study. The d-rR strain [66] was used for the *DJ-1* experiments. The Cab strain [84] was used for the *snca*, *mc4r*, *notch1b*, and *tbx6* experiments. The *Sakyo*

population, a dark-colored wild-type (*B/B*) fish collected at Sakyo-ku, Kyoto, Japan, was used for the *slc45a2* experiment.

The fish were handled in accordance with The Regulation on Animal Experimentation at Kyoto University. The fish were maintained in an aquarium with recirculating water under a 14/10-h day/night cycle at 26 ℃.

Design and construction of TALENs

Potential TALEN target sites were searched using TALE-NT 2.0 (https://tale-nt.cac.cornell.edu/) [67] with the following parameters: (i) spacer length of 14–17; (ii) repeat array length of 15–18; and (iii) the upstream base of T only. TAL effector repeats were assembled as described previously [81]. Briefly, up to six TAL effector modules (NI for A, HD for C, NN for G, and NG for T) were cloned into the array plasmid pFUS [56, 68], and then the resulting repeat arrays were cloned into the expression vectors pCS2TAL3DD or pCS2TAL3RR [69]. All the assembled RVD modules for each target site have been described in Table 4.2.

RNA preparation and microinjection

The TALEN expression vectors were linearized using digestion with NotI. Capped RNA sequences were synthesized using the mMessage mMachine SP6 kit (Life Technologies). The transcribed RNAs were purified using the RNeasy Mini kit (QIAGEN) according to the RNA clean-up protocol. The RNAs were diluted with Yamamoto's Ringer's Solution (0.75% NaCl, 0.02% KCl, 0.02% $CaCl_2$, and 0.002% $NaHCO_3$, pH 7.3) [33] and then microinjected into fertilized eggs essentially as described [39].

Genomic DNA extraction

Embryos (after breaking the egg envelope [chorion] with fine forceps), larvae, and caudal fin clips from adult fish were lysed individually in 25 μL of alkaline lysis buffer (25 mmol/L NaOH and 0.2 mmol/L ethylenediaminetetraacetic acid [EDTA], pH 8.0) at 95 ℃ for 15 min. After neutralization with 25 μL of 40 mmol/L Tris–HCl (pH 8.0), they were used as genomic DNA samples.

Heteroduplex mobility assay

To detect TALEN-induced mutations, HMA [80, 83] was performed with the following modifications: a short fragment (80–200 bp) containing the target site of TALENs was PCR-amplified from DNA samples (described above) as templates using either KOD FX (TOYOBO) or HybriPol DNA polymerase (Bioline). The primers used are listed in Table 4.1. The resulting amplicons were analyzed using a microchip electrophoresis system (MCE-202 MultiNA; Shimadzu) with the DNA-500 reagent kit or 15% polyacrylamide gel (SuperSep DNA; Wako).

To detect homozygous mutants, 5 μL of a PCR product amplified from each sample was mixed with 5 μL of the PCR product from a wild-type fish. The mixtures were denatured and reannealed at 95 ℃ for 5 min, followed by cooling to room temperature. The resulting samples were analyzed using the MultiNA system.

RFLP analysis

The genomic region that contained the target site of snca-TALENs was amplified using the primers snca-FW1 and snca-RV1 (Table 4.1) with HybriPol DNA polymerase. The resulting PCR product was precipitated with ethanol and was digested at 37 ℃ for overnight in 10 μL of the MseI restriction digestion solution that consisted of NEBuffer 4, 100 μg/mL of bovine serum albumin (BSA), and 2.5 units of MseI (New England Biolabs). The digestion products were analyzed using agarose gel electrophoresis.

Table 4.1. Oligonucleotide sequence used in this chapter

Name	Sequence [5′ – 3′)	Usage
slc45a2-ex1-FW2	cagccctgtctgctgtcagaacctgac	HMA for site #1
slc45a2-ex1-RV2	caaatgccgcttccaccgcatagcag	HMA for site #1
slc45a2-ex5-FW1	ctcctgggctctgagtaccaagtgatc	HMA for site #2
slc45a2-ex5-RV2	ctagtaaacggagcgcactggaagc	HMA for site #2
slc45a2-1FW-EcoRI	cagGAATTCgcctagtttctggactctttgct	Subcloning for site #1
slc45a2-1RV-XhoI	cccCTCGAGatcagccacaccaggctgta	Subcloning for site #1
slc45a2-5FW-EcoRI	cagGAATTCaatggactggggtcactctg	Subcloning for site #2
slc45a2-5RV-XhoI	cccCTCGAGagagttggcttcaccgagag	Subcloning for site #2
DJ1-FW2	tgtgactgtagcgggtctga	HMA, Sequencing
DJ1-RV2	gtcgcaattgccatcacttt	HMA
DJ1-RV1	gtgtgaacaacgctgcattt	Sequencing
snca-FW1	tggtgtggtaataccgatgc	RFLP
snca-RV1	gcactgacagttctggagca	RFLP, Sequencing
snca-FW2	aaggttctgtgcgttctcgt	Sequencing
mc4r-FW	acctccactcccccatgtac	HMA
mc4r-RV	tgctcttgatgagcctgacag	HMA
mc4r-F3	gctacgagcagcttctgatctccactgagg	Sequencing
mc4r-R3	agaagatggtgatgtagcggtcaacggc	Sequencing
notch1b-HMA-FW	attcgcaggtctgagatgct	HMA
notch1b-HMA-RV	ttacttgcactctccgttgc	HMA
tbx6-HMA-FW	ttgtgacatgacccagagga	HMA
tbx6-HMA-RV	ttccctgtgaactgaactgct	HMA
M13-FW	gtaaaacgacggccagt	Sequencing
M13-RV	ggaaacagctatgaccatg	Sequencing
T7 promoter	taatacgactcactataggg	Sequencing

[a] A lower case indicates a thymine at the 5′ end of the targeting sequence of each TALEN.

Microscopic observation

The fish were observed under a fluorescence stereomicroscope MZFLIII (Leica Microsystems), and their images were captured with a digital color cooled charge-coupled camera device (VB-7010, KEYENCE).

Sequence analysis

For somatic mutation analysis of the fish injected with slc45a2-TALENs, those genomic regions that contained the target site of TALENs were amplified from the genomic DNA pools extracted from 12 TALEN-injected embryos using the primers listed in Table 4.1. The amplicons were subcloned into the EcoRI/XhoI site of the pBluescript KS II (+) vector. The fragment containing the cloned genomic sequence was amplified from each colony by using the M13 forward and reverse primers (Table 4.1), and each fragment was sequenced using a T7 promoter primer (Table 4.1).

For direct sequencing analysis of mutant fish generated using TALENs, the genomic region, which includes the target site of the TALENs was PCR-amplified and sequenced using the primers listed in Table 4.1.

Table 4.2. Targeting sequence and amino acid sequence of TALENs used in this chapter

Target Gene	Site	Target genomic DNA sequence[a]	Amino acid sequence of repeat variable di-residues (RVD)
slc45a2 site #1	L	tAAAGAGGACTACATGGAC	NI NI NI NN NI NN NN NI HD NG NI HD NI NG NN NN NI HD
	R	tCCACAGTCCCAAACAC	HD HD NI HD NI NN NG HD HD HD NI NI NI HD NI HD
slc45a2 site #2	L	tCTTTCTCATCGTGCA	HD NG NG NG HD NG HD NI NG HD NN NG NN HD NI
	R	tTTGGCCAGAGGTTTCTCT	NG NG NN NN HD HD NI NN NI NN NN NG NG NG HD NG HD NG
DJ-1	L	tCTGTCCCGATACTAGCTT	HD NG NN NG HD HD HD NN NI NG NI HD NG NI NN HD NG NG
	R	tGCAGAGACTCACCTGT	NN HD NI NN NI NN NI HD NG HD NI HD HD NG NN NG
snca	L	tCCACGCCGCCATGGAC	HD HD NI HD NN HD HD NN HD HD NI NG NN NN NI HD
	R	tCCTTGGCTTTGGAGA	HD HD NG NG NN NN HD NG NG NG NN NN NI NN NI NI
mc4r	L	gTAGCCGATATGTTGGTC	NG NI NN HD HD NN NI NG NI NG NN NG NG NN NN NG HD
	R	cTATGACGATGGTCTCAG	NG NI NG NN NI HD NN NI NG NN NN NG HD NG HD NI NN
notch1b with a 5′-T	L	tGCCCACTGAGTCATGTT	NN HD HD HD NI HD NG NN NI NN NG HD NI NG NN NG NG
	R	tCTGGAGTTGCTTCACA	HD NG NN NN NI NN NG NG NN HD NG NG HD NI HD NI
notch1b without a 5′-T	L	aTGCCCACTGAGTCATGTT	NG NN HD HD HD NI HD NG NN NI NN NG HD NI NG NN NG NG
	R	aTCTGGAGTTGCTTCACA	NG HD NG NN NN NI NN NG NG NN HD NG NG HD NI HD NI
tbx6 with a 5′-T	L	tAAGCTCCACAGAGATGAG	NI NI NN HD NG HD HD NI HD NI NN NI NN NI NG NN NI NN
	R	tTCCACAGAGCCGAGTTCT	NG HD HD NI HD NI NN NI NN HD HD NN NI NN NG NG HD NG
tbx6 without a 5′-T	L	cTCCACAGAGATGAGGTGA	NG HD HD NI HD NI NN NI NN NI NG NN NI NN NN NG NN NI
	R	cTTCCACAGAGCCGAGTT	NG NG HD HD NI HD NI NN NI NN HD HD NN NI NN NG NG

[a] A lower case indicates a 5′ base adjacent to a half site of each TALEN.

4.3 Results

Evaluation of the TALEN activities in the medaka embryos by HMA

As an initial step in creating genome-edited fish by using TALENs, evaluation of each TALEN's activity on an endogenous targeting sequence was required. In my previous study [81], I had evaluated TALEN activity by using an RFLP method, which involves laborious steps such as ethanol precipitation for buffer exchange of PCR amplicon followed by restriction enzyme treatment. To accelerate the production of gene knockout strains by using TALENs, I aimed to develop a more simple and high-throughput evaluation method. Thus, the HMA results were analyzed using the MultiNA system, an automated microchip electrophoresis system with high resolution, in order to detect mutations in medaka target genes of TALEN-injected fish. In this experiment, I designed and constructed two pairs of TALENs (site #1 and site #2) that target the medaka *slc45a2* gene, known as the gene responsible for the oculocutaneous albinism type 4 (*OCA4*), whose mutation is carried by the *b* mutant strain of medaka (also called *himedaka* in Japanese) [85, 86]. A total of 250 ng/μL of each pair of TALENs was injected into fertilized eggs of the *Sakyo* population. Although wild-type fish (*B/B*) show melanin pigmentation in both retinal pigment epithelium and skin melanophores at 5 days postfertilization (dpf) (Fig. 4.1A), some TALEN-injected embryos at 5 dpf displayed mosaic loss of melanin pigmentation. The coverage of melanin-less areas was higher in embryos injected with the TALENs for site #2 (Fig. 4.1C) than for site #1 (Fig. 4.1B). To confirm that this lack of melanin pigmentation was due to lesions in the *slc45a2* gene, 211 or 148 bp genomic fragments including the targeting sequence of the TALENs were PCR-amplified from each 5-dpf embryo injected with slc45a2-TALENs for site #1 or #2, respectively. MultiNA analysis of the PCR amplicons showed that multiple bands with lower mobility were observed in all analyzed TALEN-injected embryos while one dominant amplicon was observed in control embryos that were not injected with TALENs (Fig. 4.1D, E). The number of observed multiple bands is larger in the embryos injected with the TALENs for site #2 than #1. To confirm that these multiple bands are the result of the formation of heteroduplexes, a larger target genomic region (468 and 325 bp for site #1 and #2, respectively) was amplified from genomic DNA pools of 12 TALEN-injected embryos. These PCR products were subcloned into the pBluescript KS II vector, and then each clone was sequenced. Seven of 23 (30%) and nine of 17 (53%) sequenced clones had altered sequences induced by the TALENs for site #1 (Fig. 4.1F) and site #2 (Fig. 4.1G), respectively. These indicated that HMA with the MultiNA system (HMA–MultiNA) can efficiently detect TALEN-induced mutations. The site #2 TALEN showed more mutant PCR products and a higher variety of mutation types than did the site #1 TALEN (Fig. 4.1D–G). These data suggest that the multiplicity of HMA profiles correlates with the TALEN activity as reported in a previous study using PAGE [83]. As mentioned above, I found that combining HMA with the MultiNA system can evaluate the activity of different TALENs *in vivo* in injected medaka embryos.

Genotyping of both heterozygous and homozygous mutants by using HMA

Because the TALEN-injected G0 founders usually generate more than one type of mutant F1 fish, I need to characterize the genotype of each F1 fish. If TALENs induce mutations at low frequency, then many F1 fish would have to be screened to find mutants. Therefore, identification of a successful mutant strain requires a simple and high-throughput method. To confirm that combining HMA with the MultiNA system meets this purpose, I tried to determine genotypes of F1 fish derived from two G0 founders (founder #1F and #8M) injected with DJ1-TALENs [81]. I mated each G0 founder with a wild-type fish, and then the F1 progeny were raised to adulthood. Genomic DNA was extracted from fin clips of each F1 fish, and PCR amplicons containing the target site of the TALENs were subjected to HMA–MultiNA. Two unique HMA profiles were found in 11 of the 20 F1 fish (55%) analyzed from

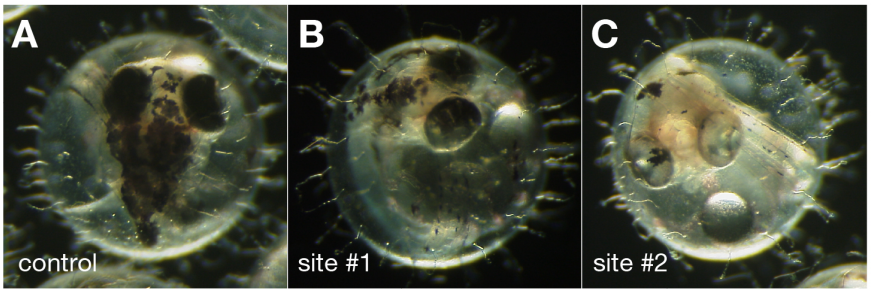

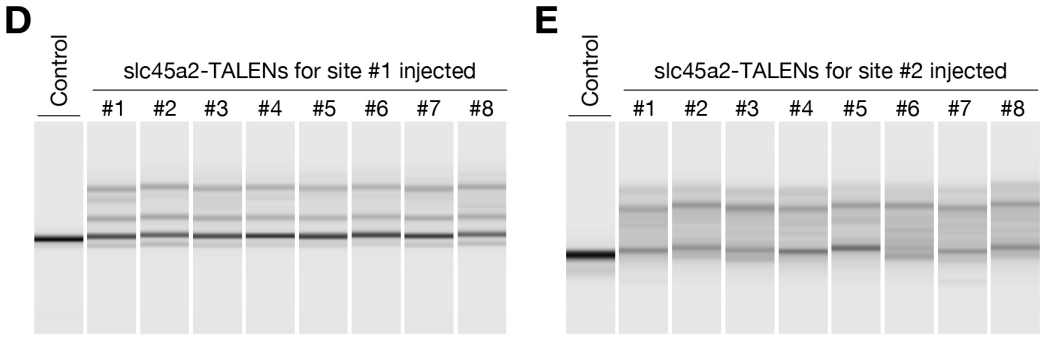

F

slc45a2-TALENs for site #1

```
ACTAAAGAGGACTACATGGACAGTGTGGAGACCTCAGTGTTTGGGACTGTGGAGC   WT   16/23
ACTAAAGAGGACTACATGGACAGTGT--------------TTGGGACTGTGGAGC   Δ14  6/23
ACTAAAGAGGAC----------------------AGTGTTTGGGACTGTGGAGC   Δ23  1/23
```

G

slc45a2-TALENs for site #2

```
CGTCTTTCTCATCGTGCACCTCTTCAGTATTCCAGAGAAACCTCTGGCCAAAGT   WT   8/17
CGTCTTTCTCATCGTGCACCTC--ATGCATTCCAGAGAAACCTCTGGCCAAAGT   Δ2   1/17
CGTCTTTCTCATCGTGCACCTC---AGTATTCCAGAGAAACCTCTGGCCAAAGT   Δ3   1/17
CGTCTTTCTCATCGTGCACCTC------ATTCCAGAGAAACCTCTGGCCAAAGT   Δ6   1/17
CGTCTTTCTCATCGTGCACCTC-------TTCCAGAGAAACCTCTGGCCAAAGT   Δ7   1/17
CGTCTTTCTCATCGTGCACCTCTT-------TCAGAGAAACCTCTGGCCAAAGT   Δ7   1/17
CGTCTTTCTCATCGTGCACC---------TTCCAGAGAAACCTCTGGCCAAAGT   Δ9   1/17
CGTCTTTCTCATCGTGCACCTC----------AGAGAAACCTCTGGCCAAAGT   Δ11  1/17
CGTCTTTCTCATCGTGCACC----------AGAGAAACCTCTGGCCAAAGT   Δ13  1/17
CGTCTTTCTCATCGTGCACCT----------GAGAAACCTCTGGCCAAAGT   Δ13  1/17
```

Figure 4.1. Targeted mutagenesis of the *slc45a2* gene by slc45a2-transcription activator-like effector nucleases (TALENs). (A) Microscopic image of 5-dpf (days postfertilization) embryos of medaka of the *Sakyo* strain without the injection. (B, C) Microscopic images of 5-dpf embryos of the *Sakyo* strain injected with RNA encoding slc45a2-TALENs for site #1 (B) or site #2 (C). Mosaic losses of melanin pigmentation were observed in the retinal pigment epithelium (RPE) and the skin of the TALEN-injected embryos. (D, R) MultiNA gel images of a heteroduplex mobility assay (HMA) in embryos injected with slc45a2-TALENs for site #1 (D) or site #2 (E). Multiple heteroduplex bands were present in PCR products from each TALEN-injected embryo (#1–8), whereas a single band was present with each control embryo (no injection of TALENs). (F, G) Subcloned sequences from a pool of genomic DNA extracted from 12 embryos injected with slc45a2-TALENs for site #1 (F) or site #2 (G). Red dashes and letters indicate the identified mutations. The left and right TALEN-binding sequences are highlighted in red and blue, respectively (top line). Green underlined letters indicate 6-bp homologous sequences in the targeting site. The size of deletions and insertions is shown to the right of each mutated sequence (Δ, deletions; +, insertions). The numbers in the rightmost column indicate the number of mutated clones identified from all the clones analyzed in each embryo.

founder #1F (Fig. 4.2), and three unique HMA profiles were present in all of the 17 fish analyzed (100%) from founder #8M (Fig. 4.2B). Direct sequencing of the PCR amplicons including the target genomic region revealed that the F1 fish from founder #1F had either a 7 bp deletion (Fig. 4.2A, Δ7) or an 8 bp deletion (Fig. 4.2A, Δ8) mutant allele together with the wild-type allele, whereas the F1 fish from the founder #8M had either a 4 bp deletion (Fig. 4.2B, Δ4), or a 7 bp deletion (Fig. 4.2B, Δ7), or a 15 bp deletion (Fig. 4.2B, Δ15) mutant allele together with the wild-type allele. These results indicate that HMA–MultiNA is an effective and rapid method for genotyping of F1 fish harboring TALEN-induced mutations.

Another issue to establish mutant strains is how efficiently homozygotes for a mutation can be distinguished from heterozygotes or wild-type fish. I investigated whether homozygotes can be identified by the HMA–MultiNA method. Heterozygous F1 fish harboring an 8-bp deletion induced by the DJ1-TALENs were mated. Each F2 fish was subjected to HMA–MultiNA, and I identified eight homozygotes (b, e, i, j, k, l, m, and p in Fig. 4.2C), five heterozygotes (a, c, f, h, and o in Fig. 4.2C), and three wild-type fish (d, g, n in Fig. 4.2C) in the 16 analyzed F2 fish. I also showed that comparable results were obtained with HMA using PAGE (Fig. 4.3). However, little difference between the sizes of PCR amplicon from homozygotes and wild-type fish is likely to make it difficult to distinguish between them. I therefore added a slight modification to the HMA–MultiNA method to reliably identify homozygous mutants. The PCR product amplified from a wild-type fish was added to each of the 11 PCR products derived either from the homozygotes for the mutation or wild-type fish. The mixtures were denatured and reannealed and were then analyzed using the MultiNA system again. I found that eight samples (b′, e′, g′, i′, j′, k′, l′, m′, and p′ in Fig. 4.2) showed heteroduplex bands, and I identified them as homozygous mutants carrying an 8-bp deletion in both alleles. These results indicate that HMA is an easy and simple method for the detection of homozygous mutations by using the tandem approach with the PCR products amplified from wild-type fish samples.

Microhomology induces a specific pattern of mutations

The targeting genomic sequences of slc45a2-TALENs for site #1 and #2 includes two stretches of a 6-bp homologous sequence that are located 8 and 16 bp away from each other, respectively (shown in Fig. 4.1F, G as green underlined letters). Sequencing analysis of the embryos injected with slc45a2-TALENs for site #1 showed that six of the seven mutant clones (86%) identified had the same pattern of 14-bp deletions between the 6-bp regions of homologous sequences (Fig. 4.1F). In contrast, no specific pattern of mutations was found in the embryos injected with slc45a2-TALENs for site #2 (Fig. 4.1G). The induction of a specific pattern of mutations by TALENs was also observed in germline mutations of fish injected with snca-TALENs or mc4r-TALENs. Six G0 founder fish injected with snca-TALENs were mated with wild-type fish, and each F1 larva was genotyped using PCR-RFLP analysis with the MseI restriction enzyme and subsequent direct sequencing. All six G0 founders produced F1 progeny harboring an 11-bp deletion between the 3-bp of homologous sequence located 8 bp away from each other (shown as green underlined letters in Fig. 4.4A), with high efficiency (14–59% of the mutated fish; Fig. 4.4A). Similarly, each F1 embryo from seven G0 founders injected with mc4r-TALENs genotyped using HMA and subsequent direct sequencing, showed that all five mutagenized G0 founders produced F1 progeny harboring the same type of an 11-bp deletion between the 6-bp of homologous sequences located 5 bp away from each other (shown as green underlined letters in Fig. 4.4B), with high efficiency (66–100% of the mutated fish; Fig. 4.4B). These results suggest that each pair of TALENs harboring several base pairs of homologous sequences within their targeting genomic sequence has the potential to induce a specific pattern of mutations.

5′ T adjacent to a half site of each TALEN is not required for genomic DNA cleavage

Almost all the engineered TALEN monomers had binding sequences preceded by a 5′ T according to the design guidelines proposed in previous studies [56, 57]. To test whether the 5′ T adjacent to the

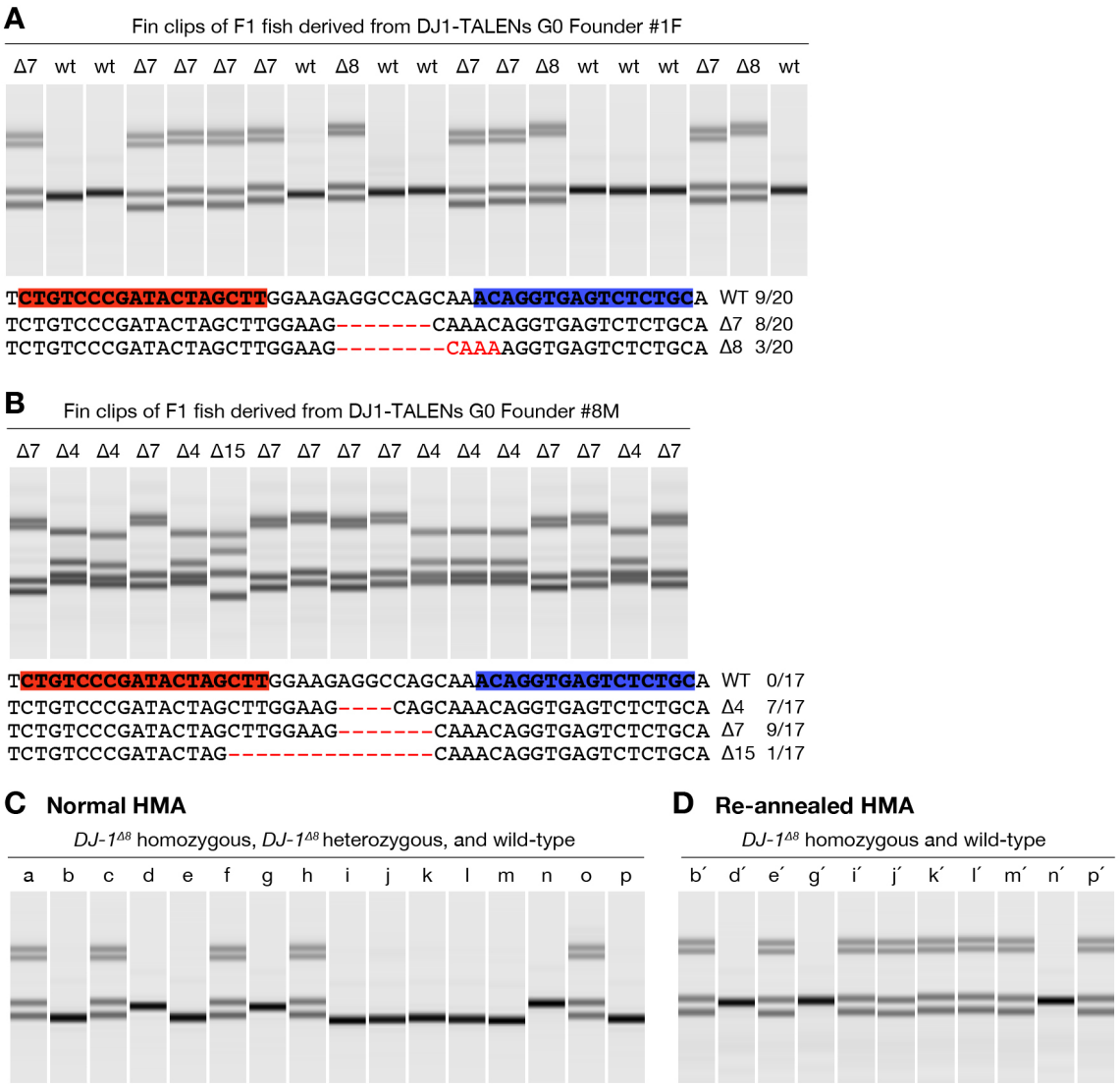

Figure 4.2. Genotyping of F1 and F2 progeny by using a heteroduplex mobility assay (HMA) with the MultiNA system. (A, B) Genotyping of fin clips of F1 fish obtained from DJ1-transcription activator-like effector nuclease (TALEN)-injected founder #1F (A) and #8M (B) mated with wild-type fish. The upper panels show a MultiNA gel image of HMA. Each fish harboring the heterozygous mutation has multiple heteroduplex bands with a unique profile. The lower panels show mutated sequences that were identified in each F1 fish using direct sequencing. Red dashes and letters indicate the mutations identified. The left and right TALEN-binding sequences are highlighted in red and blue, respectively (top line). The size of deletions and insertions is shown to the right of each mutated sequence (Δ, deletions; +, insertions). The numbers in the rightmost column indicate the number of embryos mutated out of all embryos analyzed. (C, D) Genotyping of F2 embryos obtained by intercrossing between heterozygous mutant F1 fish harboring an 8-bp deletion (Δ8 shown in Fig. 4.2A). (B) MultiNA gel images of HMA of the standard procedure (indicated as "normal HMA"). Five heterozygous mutants were identified (a, c, f, h, and o). (D) The MultiNA gel images of HMA of samples reannealed with polymerase chain reaction (PCR) fragments amplified from wild-type genomic DNA. Eight homozygous mutants were identified (b′, e′, g′, i′, j′, k′, l′, m′, and p′).

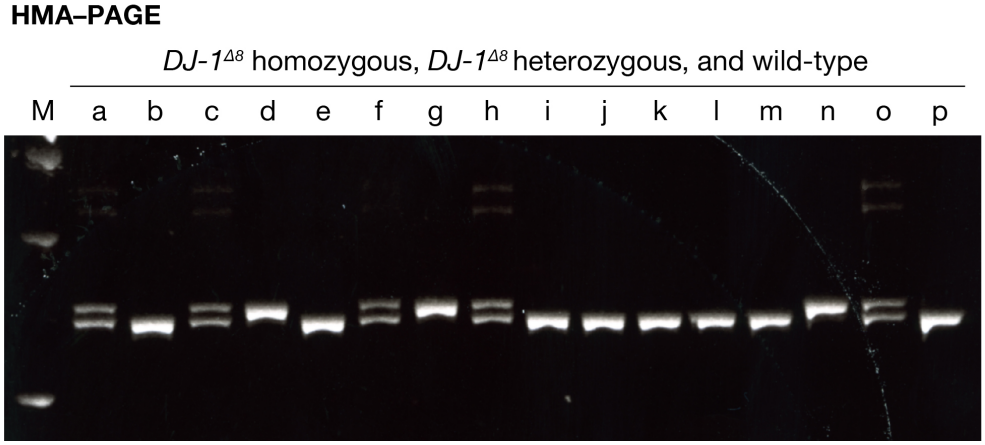

Figure 4.3. Heteroduplex mobility assay (HMA) using polyacrylamide electrophoresis (PAGE) to genotype of F2 embryos obtained by intercrossing between heterozygous mutant F1 fish harboring an 8-bp deletion in the *DJ-1* locus.

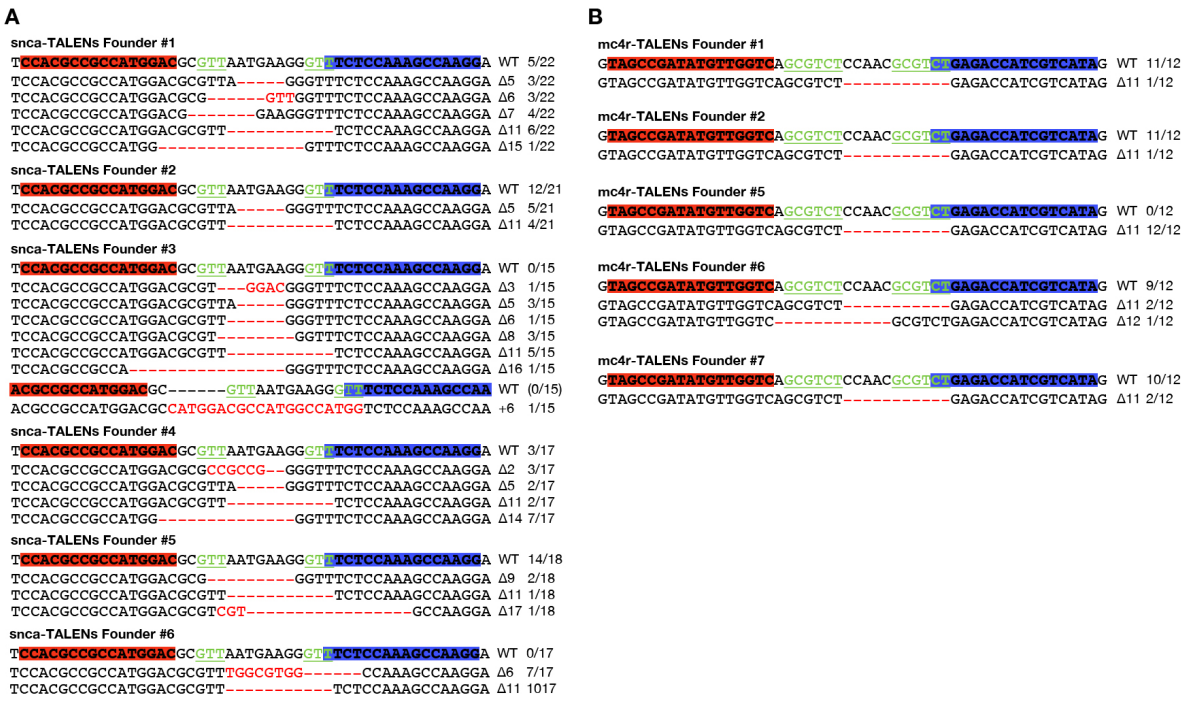

Figure 4.4. Sequences of germline mutations induced by snca- transcription activator-like effector nucleases (TALENs) (A) or mc4r-TALENs (B). Each TALEN-injected G0 founder was mated with a wild-type fish. Mutant sequences identified in each F1 embryo by using direct sequencing are shown. Red dashes and letters indicate the mutations identified. The left and right TALEN-binding sequences are highlighted in red and blue, respectively (top line). Green underlined letters indicate 3-bp and 6-bp homologous sequences in the targeting site of snca-TALENs and mc4r-TALENs, respectively. The size of deletions and insertions is shown to the right of each mutated sequence (Δ, deletions; +, insertions). The numbers in the rightmost column indicate the number of embryos mutated from all the embryos analyzed.

half sites of each TALEN is necessary for genomic DNA cleavage, I examined the activity of two pairs of TALENs at each targeting genomic locus, one having the TALEN binding sequence with a 5′ T and the other without a 5′ T. Two genomic loci, *notch1b* and *tbx6*, were selected as the target sites, and then TALENs with and without the 5′ T specificity (indicated with light blue and orange lines in Fig. 4.5, respectively) were constructed. A total of 160 ng/μL of each pair of TALENs was injected into the fertilized eggs of the *Cab* strain, and genomic DNA was extracted from each 5–7 dpf TALEN-injected embryo. Multiple heteroduplex bands were observed in HMA for all embryos injected with TALENs, indicating that all pairs of TALENs induced mutations in their target sequence (Fig. 4.5). However, embryos injected with tbx6-TALENs without a 5′ T displayed less multiple bands of slow migration (Fig. 4.5B). These results indicate that a 5′ T flanking the half site of each TALEN is not necessary for genomic DNA cleavage.

4.4 Discussion

In this chapter, I describe an efficient method for the detection of TALEN-induced mutations by HMA with the MultiNA system. This approach has some advantages over previously described methods for the detection of TALEN-induced mutations. First, the induction of mutations can be detected at any desired loci without the requirement of a restriction enzyme site for RFLP analysis. Second, this approach consists of a simple procedure that includes PCR amplification of a genomic fragment containing the TALEN targeting sequence and subsequent electrophoretic analysis using the MultiNA system. Third, this approach is more widely applicable to detect mutant alleles in F1 or later generations induced not only by TALENs but also by other engineered nucleases, such as ZFNs and the CRISPR/Cas system. In addition to these characteristics that were similar to those of HMA performed using PAGE [80, 83], this method has an additional advantage on the high-throughput analysis (simultaneous analysis of a maximum of 96 samples) with automated treatment by MultiNA. Thus, HMA–MultiNA is one of the simplest and most high-throughput systems to detect TALEN-induced small insertions and deletions although this system needs a special equipment MCE-202 MultiNA.

I found that some pairs of TALENs can frequently induce a specific pattern of mutation, that is, a deletion between two short (comprising several base pairs) regions of homologous sequence near the spacer region of these TALENs. The DSB repair–mediated deletions are mainly caused by three DSB repair pathways: classical non-homologous end joining (cNHEJ), microhomology-mediated end joining (MMEJ), and single-strand annealing (SSA) [87]. From these pathways, MMEJ uses microhomologous sequences to align the broken ends before joining, thereby causing deletions flanking the original break [87]. This mechanism suggests that the patterns I identified (Δ14 in slc45a2-TALEN site #1, Δ11 in snca-TALENs, and Δ11 in mc4r-TALENs; Fig. 4.1F and 4.4) are likely to be produced by the MMEJ. Although the targeting site of slc45a2-TALENs site #2 has two 6 bp homologous sequences located 16 bp away from each other, an expected specific pattern of 22 bp deletions was not observed in the embryos injected with those TALENs (Fig. 4.1G). This observation indicates that, when a longer deletion is expected (probably >20 bp), the frequency of the expected pattern of deletion induced by the MMEJ is likely to decrease. Additionally, I found that the embryos injected with slc45a2-TALENs site #1 showed fewer bands than those injected with slc45a2-TALENs site #2 in their MultiNA gel images of HMA. This indicates that each HMA profile in the TALEN-injected G0 embryos will be influenced by each frequent pattern of mutation.

From a practical standpoint, my findings suggest that microhomologous sequences in the targeting site of TALENs allow us to predict frequently induced patterns of deletions. In other words, consideration of microhomologies in the targeting site helps induce desired patterns and/or avoid unwanted patterns of mutations. Therefore, a search for homologous sequences can become one of the necessary steps in the protocol for the selection of a targeting site of TALENs. The relevant events can be induced

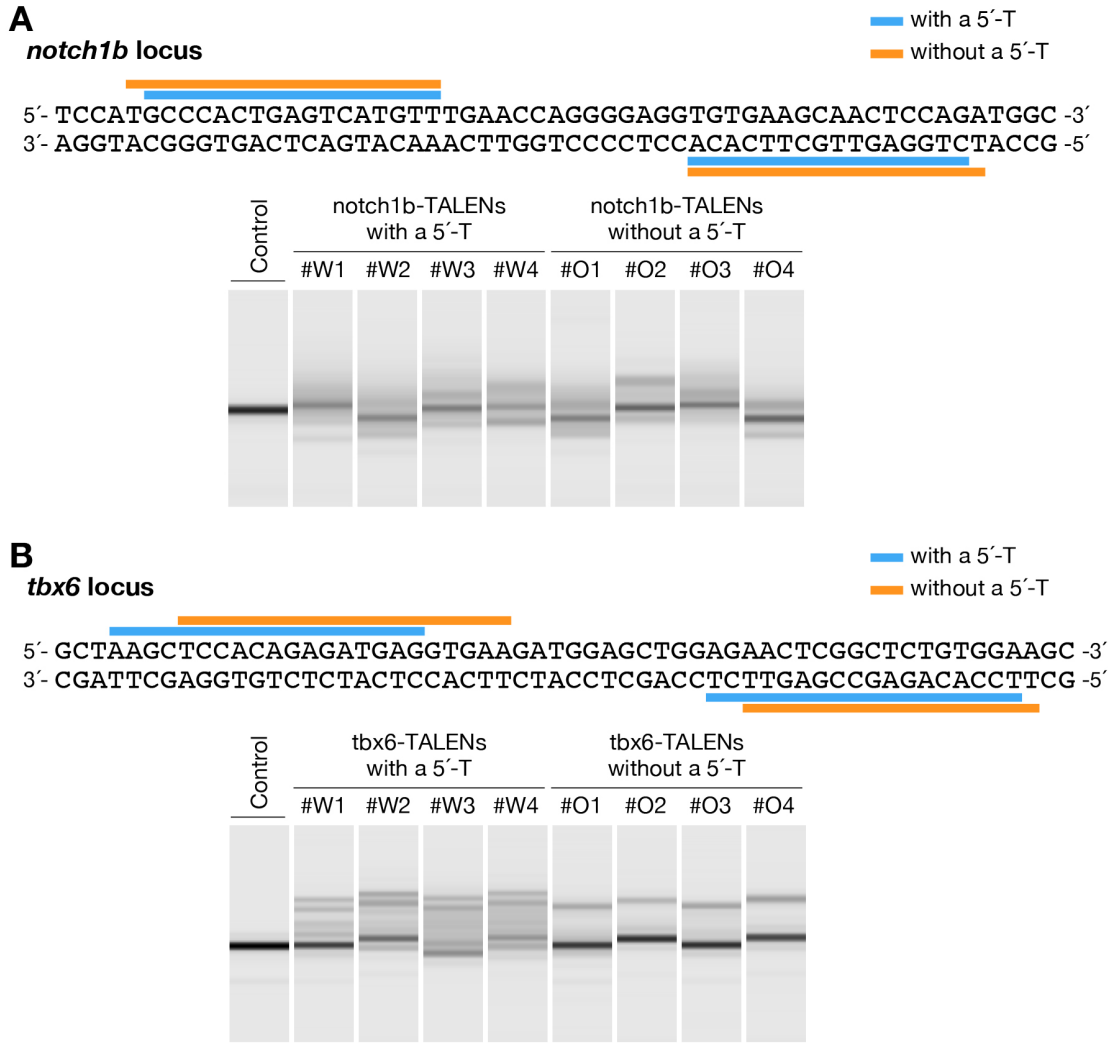

Figure 4.5. Effects of a 5′ T at the ends of each transcription activator-like effector nuclease (TALEN)-binding sequence on the activity of notch1b-TALENs (A) and tbx6-TALENs (B). The upper panels show a schematic illustration of the TALEN design. Light blue and orange lines indicate TALENs recognizing a targeting sequence with and without a 5′ T, respectively. The lower panels show MultiNA gel images of heteroduplex mobility assays (HMAs) of the TALEN-injected embryos. Multiple heteroduplex bands are present in polymerase chain reaction (PCR) products from each embryo injected with TALENs recognizing a targeting sequence with (#W1–4) and without (#O1–4) a 5′ T, whereas a single band is seen with each control embryo (no injection of TALENs).

by DSBs and therefore by their repair pathway, suggesting that this mechanism can be applicable to other engineered nucleases for targeted genome editing.

Previous studies found that nearly all TAL effector binding sites observed in nature are preceded by a 5′ T [54, 55]. Furthermore, the crystal structure of a TAL effector bound to its DNA target suggests that two degenerate repeat folds N-terminal to the canonical repeats associate with a 5′ thymine [88]. In fact, it was reported that a mutation of this thymine reduces TAL effector activity at the target site [54, 89]. However, I find in medaka that TALENs recognizing a targeting sequence without a 5 T′ can induce targeted mutations as effectively as those with a 5′ T (Fig. 4.5). Similarly, mc4r-TALENs induced mutations in a targeting sequence preceded by a G or a C (Fig. 4.4B). This is confirmed by a

report that TALENs can induce mutations at a targeting sequence preceded by a C in human cells [53]. In summary, a T at the 5′ end of TALEN-targeting sites is not required for efficient induction of DNA cleavage. This observation expands the range of sequences targetable by custom-designed TALENs.

Chapter 5

Targeted mutagenesis using CRISPR/Cas system

5.1 Introduction

Genome editing with artificial nucleases such as zinc-finger nucleases (ZFNs) and transcription activator-like effector nucleases (TALENs) has become a powerful tool for approaches involving reverse genetics in a wide range of organisms [78, 79]. These enzymes efficiently induce site-specific DNA double-strand breaks (DSBs), resulting in targeted gene disruptions by insertions and deletions (indels) or targeted gene integrations by homologous recombination. However, since the DNA-binding domain of these nucleases determines their site specificity, re-engineering the binding domain sequence is essential for each new target site.

The type II clustered regularly interspaced short palindromic repeats (CRISPR)/CRISPR-associated (Cas) system has recently emerged as an RNA-guided endonuclease (RGEN) for targeted genome editing. CRISPR and Cas proteins are essential components of the adaptive immune system in bacteria and archaea to detect and silence invading viruses and plasmids [90]. In type II CRISPR system, Cas9 protein, CRISPR RNAs (crRNAs), and trans-activating crRNA (tracrRNA) form ribonucleoprotein complexes that induce site-specific DNA cleavage guided by crRNAs [91, 92]. The recognition specificity of Cas9 endonuclease from *Streptococcus pyogenes* type II CRISPR/Cas system can be programmed only by a synthetic single-guide RNA (sgRNA) consisting of a fusion of crRNA and tracrRNA [92]. Recent studies have shown that Cas9 and engineered sgRNA are the only components necessary and sufficient for targeted DNA cleavage and efficient genome editing in cultured human cells [93–97], mice [98], *Drosophila* [99,100], *Caenorhabditis elegans* [101], and zebrafish [102–106]. Because of its simple customizing process compared to the assembling of TALEN or ZFN modules, the CRISPR/Cas-mediated RGENs have the potential for being developed as a robust and efficient tool for genome editing.

However, RGENs still pose several unanswered questions for research applications [107]. It remains unclear whether the selection of the target sequence is crucial to achieve effective targeted cleavage. Site specificity of DNA cleavage by the Cas9 endonuclease from *S. pyogenes* depends on two factors, one being the base-pair complementarity between the first 20 nucleotides (nts) of a guide RNA and a target DNA sequence, and the other being the sequence "NGG", referred to as the protospacer adjacent motif (PAM), adjacent to the complementary region in the target site [92]. Hwang and colleagues described that sgRNAs transcribed by a T7 RNA polymerase require their target sequence in the form 5′-GG-N_{18}-NGG-3′ because GG is added at the 5′ ends of the transcripts initiated at the T7 promoter [104]. On the other hand, a study in cultured human cells showed that double mismatches at the 5′ ends of the sgRNAs are tolerated [95], and *in vitro* studies showed that the GG required by the T7

Table 5.1. PCR primer sequences used in this chapter

Name	Sequence [5′–3′]	Usage
hSpCas9FW	gcaggatccgccaccatggactataaggac	Cloning of hSpCas9 into the pCS2+ vector
hSpCas9RV	agttctagattactttttctttttgcctggc	Cloning of hSpCas9 into the pCS2+ vector
DJ1-FW2	tgtgactgtagcgggtctga	HMA, RFLP
DJ1-RV1	gtgtgaacaacgctgcattt	RFLP, direct sequencing
DJ1-RV2	gtcgcaattgccatcacttt	HMA
DJ1-FW3	caggaattctttttgtctcttggtggtgct	Subcloning into the pBluescript vector
DJ1-RV3	cccctcgaggtgtgaacaacgctgcattt	Subcloning into the pBluescript vector
M13-FW	gtaaaacgacggccagt	Sequencing
M13-RV	ggaaacagctatgaccatg	Sequencing
T7 promoter	taatacgactcactataggg	Sequencing

promoter do not affect cleaving activities [92, 93]. Furthermore, Ran and colleagues showed that 5′ extension of sgRNA sequences could not contribute to Cas9 targeting specificity in cultured human cells because the 5′ extensions were processed [108]. In fact, Hwang and colleagues. also reported that sgRNAs transcribed by T7 polymerase could target the genomic sequences without the 5′ ends GG in zebrafish [103]. However, there are very few *in vivo* studies that investigate the effects of the 5′-end sequences on the cleaving activities. Second, and more importantly, the relatively short target sequence of 20-bp or fewer for the RGENs raises questions about their specificity. It was reported that potential off-target sites including both a PAM and a perfect match of at least 12-bp at the 3′ end of the 20-bp targeting sequence were not disrupted in mice [98], *Drosophila* [99, 100], and *C. elegans* [101]. However, off-target sites harboring up to five mismatches were mutagenized in cultured human cells [95, 96, 109] and zebrafish [105]. Additionally, a more recent work indicates that the off-target sites that have up to 3-bp mismatches except in the 8-bp sequence adjacent to a PAM can be disrupted by RGENs [110]. These suggest that the RGENs can also induce off-target alterations in other organisms.

5.2 Materials and Methods

Fish

A d-rR strain was used in this study. Fish were maintained in an aquarium with recirculating water in 14/10-h day/night cycle at 26 ℃. The care and use of animals in this study were in accordance with the guidelines of the Animal Experimentation Committee of Kyoto University.

Cas9 nuclease expression vector

A Cas9 expression vector for SP6 *in vitro* transcription, pCS2+hSpCas9, was generated in this study. DNA sequence encoding the human codon-optimized *S. pyogenes* Cas9 nuclease was amplified from the pX330 (Addgene Plasmid #42230) [94] by PCR using the primers: hSpCas9FW and hSpCas9RV (Table 5.1). The resulting PCR product was cloned into the BamHI/XbaI site of pCS2+MT vector [111]. This expression vector is made available as Addgene Plasmid #51815 (http://www.addgene.org).

Table 5.2. Oligonucleotide sequences used for construction of sgRNA recognizing the *DJ-1* locus

sgRNA ID	Direction	Sequence [5′–3′]
No. 1	Sense	TAGGCCTCTTCCAAGCTAGTAT
	Anti-sense	AAACATACTAGCTTGGAAGAGG
No. 2a	Sense	TAGGTCCAGTGCAGCAGAAACG
	Anti-sense	AAACCGTTTCTGCTGCACTGGA
No. 2b	Sense	TAGGCGTCCAGTGCAGCAGAAACG
	Anti-sense	AAACCGTTTCTGCTGCACTGGACG
No. 3a	Sense	TAGGTCTGTCCCGATACTAGCT
	Anti-sense	AAACAGCTAGTATCGGGACAGA
No. 3b	Sense	TAGGCATCTGTCCCGATACTAGCT
	Anti-sense	AAACAGCTAGTATCGGGACAGATG

sgRNA expression vector

The pDR274 vector (Addgene Plasmid #42250), harboring a T7 promoter positioned upstream of a partial guide RNA sequence [104] was used for sgRNA expression. Appropriately designed oligonucleotides were synthesized with oligonucleotide purification cartridge (OPC) purification at Operon Biotechnologies. A pair of oligonucleotides (final concentration: 10 μM each) was annealed in 10 μL of annealing buffer (40 mM Tris–HCl [pH 8.0], 20 mM $MgCl_2$, and 50 mM NaCl) by heating to 95 ℃ for 2 min and then cooling the mixture slowly to 25 ℃ in 1 h. The pDR274 vector was digested with BsaI-HF (New England Biolabs), and the annealed oligonucleotides were ligated into the pDR274 vector. Sequences of the genomic target sites and the annealed oligonucleotides are listed in Table 5.2.

RNA synthesis and microinjection

The Cas9 expression vector was linearized by NotI digestion. Capped RNA was synthesized using the mMessage mMachine SP6 Kit (Life Technologies), and then purified using the RNeasy Mini Kit (QIAGEN). The sgRNA expression vectors were digested by DraI, and the sgRNAs were synthesized using the AmpliScribe T7-Flash Transcription Kit (Epicentre). The synthesized sgRNAs were purified by ammonium acetate precipitation.

These RNA sequences were diluted to appropriate concentrations and injected approximately 2–4 nL of the RNA mixture into fertilized eggs before the first cleavage, as described previously [39].

Genomic DNA extraction

Embryos were lysed individually at 3 days post fertilization (dpf) in 25 μL of alkaline lysis buffer containing 25 mM NaOH and 0.2 mM EDTA (pH 8.0) and incubated at 95 ℃ for 15 min after breaking the egg envelope (chorion) with forceps. Samples were neutralized with 25 μL of 40 mM Tris-HCl (pH 8.0) and used as genomic DNA samples.

Heteroduplex mobility assay

Heteroduplex mobility assay (HMA) was performed to detect RGEN-induced mutations [80, 83, 112]. A 146-bp fragment containing the entire genomic target sequence of the *DJ-1* gene was amplified using primers DJ1-FW2 and DJ1-RV2 (Table 5.1). The reaction mixture contained 1 μL of genomic DNA as template, 1× PCR buffer for KOD FX, 0.4 mM of each dNTP, 0.2 μM of each primer, and 0.05 unit of KOD FX (TOYOBO) in a total volume of 10 μL. The cycling conditions were as follows: one cycle at 94 ℃ for 2 min, followed by 35 cycles of 98 ℃ for 10 sec, 56 ℃ for 20 sec, and 68 ℃ for

20 sec. The resulting amplicons were analyzed using a microchip electrophoresis system (MCE-202 MultiNA; Shimadzu) with the DNA-500 reagent kit.

Sequence analysis for somatic mutations
For sequence analysis at *DJ-1* locus, the genomic region including the target site of sgRNAs was amplified with KOD -plus- Neo DNA polymerase (TOYOBO) using the primers DJ1-FW3 and DJ1-RV3 (Table 5.1). The PCR conditions were as follows: one cycle at 94 生 for 2 min, followed by 35 cycles of 98 生 for 10 sec, 58 生 for 30 sec, and 68 生 for 30 sec. The PCR amplicons were subcloned into the EcoRI/XhoI site of the pBluescript KS II (+) vector. The fragment containing the cloned genomic sequence was amplified from each colony using the M13 forward and reverse primers (Table 5.1). Each fragment was sequenced using a T7 promoter primer (Table 5.1).

Quantification of mutations with restriction fragment length pattern (RFLP)
A 285-bp fragment including the genomic target sequence of the sgRNA was amplified using the primers DJ1-FW2 and DJ1-RV1 (Table 5.1). The reaction mixture contained 2 μL of genomic DNA template, 1× reaction buffer, 0.8 mM of each dNTP, 1.5 mM of $MgCl_2$, 0.2 mM of each primer, and 0.5 unit of HybriPol DNA Polymerase (Bioline) in a total volume of 20 μL. The cycling conditions were as follows: one cycle at 95 生 for 2 min, followed by 30 cycles of 95 生 for 20 sec, 58 生 for 30 sec, and 72 生 for 30 sec. The resulting product was precipitated with ethanol for buffer exchange and was digested at 37 生 for overnight in 10 μL of the solution containing 1× L buffer and 2 units of the AluI restriction enzyme. After inactivation at 80 生 for 10 min, the digested fragments were analyzed using a microchip electrophoresis system (MCE-202 MultiNA; Shimadzu) with the DNA-500 reagent kit. The molar concentrations of both digested and undigested fragments were quantified using the MultiNA Viewer software. The mutation rate was calculated as the ratio of the undigested fragment to the sum of the undigested fragment and the larger digested fragment as described previously [81].

Off-target analysis
Potential off-target sites in the medaka genome were searched using a "Pattern Match" tool in New Medaka Map (beta) at the NBRP medaka web site (http://viewer.shigen.info/medakavw/patternmatch) with 2 criteria: criterion (i) perfect matching in the 12-bp sequence at the 3′ end of the 20-bp target sequence and the NGG PAM sequence; criterion (ii) matching of 16 to 18 bp of the 18 bp sequence at the 3′ end of the target followed by either the NGG or the NAG PAM sequence. All identified potential off-target sites were analyzed by HMA using the primers listed in supplementary material Tables 5.3 and 5.4, as described above. Subsequently, the genomic region containing altered off-target sites was amplified with TaKaRa Ex Taq (Takara Bio) and subcloned into either the pGEM-T vector (Promega) or the T-Vector pMD20 (Takara Bio). The fragment containing the cloned genomic sequence was amplified from each colony with the M13 forward and reverse primers (Table 5.1), and then each fragment was sequenced using a T7 promoter primer or a SP6 promoter primer (Table 5.1).

Founder screening
RGEN-injected fish were mated with wild-type fish of the d-rR strain and genomic DNA was extracted from each F1 embryo. Mutation in each embryo was analyzed by HMA using the primers DJ1-FW2 and DJ1-RV2 (Table 5.1). Mutant alleles in each embryo were determined by direct sequencing of the *DJ-1* gene region, amplified using the primers DJ1-FW2 and DJ1-RV1 (Table 5.1).

Statistical analysis
Mutation rates were analyzed with one-way analysis of variance (ANOVA) followed by Tukey's honestly significant difference (HSD) test using the R language (http://www.r-project.org).

Table 5.3. Potential off-target sequences identified by criterion (i) in medaka genome. Primer sequences for mutation analysis are also shown. Red letters indicate a mutagenized off-target locus

sgRNA	Site	Sequence [5′–3′]	Chromosome position	Forward PCR primer	Reverse PCR primer
No. 1	Target 1	GGCCTCTTCCAAGCTAGTATCGG	chr5: 7,477,613-7,477,591	tgtgactgtagcgggtctga	gtcgcaattgccatcacttt
	OT1-I1a	CGTGTAACCCAAGCTAGTATTGG	chr8: 4,153,407-4,153,385	aaagtttttctggtcccatgt	gtaagggtaaaggggctgct
	OT1-I1b	CGTGTAACCCAAGCTAGTATTGG	chr8: 4,156,178-4,156,156		
	OT1-I2	TAGGTACACCAAGCTAGTATCGG	chr8: 9,508,743-9,508,765	tgccaccaaggattaagaca	cccctgcatgatttcagttt
	OT1-I3	CTATATTACCAAGCTAGTATTGG	chr9: 15,422,034-15,422,012	ctggcttttcaaggcgaata	ggccatcttcttcagtctgg
	OT1-I4	GTTTTGCACCAAGCTAGTATCGG	chr16: 21,913,658-21,913,680	agaaaaagcctggagcaaaa	tacgctcagaccgggtaca
No. 2a	Target 2	CGTCCAGTGCAGCAGAAACGTGG	chr5: 7,477,559-7,477,581	tgtgactgtagcgggtctga	gtcgcaattgccatcacttt
	OT2-I1	CTCCTCCGGCAGCAGAAACGGGG	chr1: 34,070,805-34,070,827	ggcaatcaaggaacagaatga	taaagtcccctcctcccttc
	OT2-I2	AGAGCATCGCAGCAGAAACGAGG	chr1: 38,622,323-38,622,301	ccgcaaactccagtcagtct	cgtgaaattccccagaagtc
	OT2-I3	CTGAAGCTGCAGCAGAAACGGGG	chr4: 6,616,842-6,616,820	ggactggacagtttggagga	tgatgtgaaggtggacatgc
	OT2-I4	AGTCTAGAGCAGCAGAAACGGGG	chr4: 20,089,705-20,089,727	agaaagtcggtggtaacagca	tctagactgcggcatgtgac
	OT2-I5	TAGGAGCAGCAGCAGAAACGAGG	chr5: 24,232,491-24,232,469	agagcagagacgagccagag	aggggatcaacaacaatgga
	OT2-I6	CAAGGACAGCAGCAGAAACGCGG	chr8: 14,070,959-14,070,981	aggcaacaggaggagaaaca	gctgctggaggaggtatctg
	OT2-I7	CAAATGTTGCAGCAGAAACGCGG	chr8: 17,753,755-17,753,733	gcagggtgatacaggatgga	tcaccgatttaccaaatttgaac
	OT2-I8	TGCAGATTGCAGCAGAAACGTGG	chr9: 29,205,714-29,205,692	ggacatttttaaacaccccaaa	gggacatgtgcgcatataaa
	OT2-I9	AGCATGACGCAGCAGAAACGAGG	chr9: 30,256,570-30,256,592	aaggccgataacaagacttcc	cctgtgtgaggaagatgaagg
	OT2-I10	CACTCCCTGCAGCAGAAACGCGG	chr10: 26,433,826-26,433,804	gggattggaggaggttcatc	caggctgaacatcattttgg
	OT2-I11	CATGAGGTGCAGCAGAAACGGGG	chr12: 2,746,166-2,746,144	tgtcatgttccttttgtgtcc	caacacgacctgaaatgtgtg
	OT2-I12	TGATTTGCGCAGCAGAAACGTGG	chr13: 2,841,517-2,841,539	gcgcaattcacatccaaaat	tgtctttaatgtgcagccaaa
	OT2-I13	CTGGAGCCGCAGCAGAAACGTGG	chr13: 19,092,675-19,092,653	gttctctcctcatggcgttg	gccgagttcctttgactgac
	OT2-I14	ATGAAAAAAGCAGCAGAAACGGGG	chr15: 14,490,114-14,490,136	gctgaaatgtaatttggagca	cagccaatgtctaaatgctgtc
	OT2-I15	CTGGAAATGCAGCAGAAACGGGG	chr18: 29,247,728-29,247,706	ggacggtaaacttcgtctgg	ttctgggagtttgagtgaagc
	OT2-I16	TTCTGAGAGCAGCAGAAACGGGG	chr23: 3,690,537-3,690,559	gttctgtcattcccctgagc	caagaaacctgcaggaggag
	OT2-I17	ATTTCTTGGCAGCAGAAACGGGG	chr24: 12,802,667-12,802,645	aagaaatgctggggatgttg	gcaaacacgtttcccaaact
No. 3a	Target 3	CATCTGTCCCGATACTAGCTTGG	chr5: 7,477,583-7,477,605	tgtgactgtagcgggtctga	gtcgcaattgccatcacttt
	OT3-I1	GCTCCAACCCGATACTAGCTTGG	chr8: 9,508,773-9,508,751	cccctgcatgatttcagttt	tgccaccaaggattaagaca
	OT3-I2	GTAGCTGCCCGATACTAGCTAGG	chr10: 8,557,430-8,557,408	cacatgtgttcaaggtgttca	tgtgacacgatctgaacctga
	OT3-I3	GACTCTACCCGATACTAGCTTGG	chr16: 21,913,688-21,913,666	tacgctcagaccgggtaca	agaaaaagcctggagcaaaa
	OT3-I4	TGACCTATCCGATACTAGCTAGG	chr18: 1,045,229-1,045,207	gccttcagccctctgatga	cctttggatccatcaacgtc

Table 5.4. Potential off-target sequences identified by criterion (ii) in medaka genome. Primer sequences for mutation analysis are also shown. Red letters indicate a mutagenized off-target locus

sgRNA	Site	Sequence [5′–3′]	Chromosome position	Forward PCR primer	Reverse PCR primer
No. 1	Target 1	GGCCTCTTCCAAGCTAGTATCGG	chr5: 7,477,613-7,477,591	tgtgactgtagcgggtctga	gtcgcaattgccatcacttt
	OT1-II1	TTTCTCATCCAAGCTAGTATCAG	chr7: 8,868,188-8,868,210	cctcccctgcagacaaatag	ctagctcacagcccctctca
	OT1-II2	TTCCTCGTCCAAGCTGGTATCAG	chr16: 8,282,950-8,282,932	tgccaccaaggattaagaca	cccctgcatgatttcagttt
	OT1-II3	TTCCTCATCCAAGCTAGCATCAG	chr23: 5,103,587-5,103,609	ctggcttttcaaggcgaata	ggccatcttcttcagtctgg
	OT1-II4[a]	TTCCTCATCCAAGCTAGCATCAG	chr15: 20,255,083-20,255,063	tgctctgctccattctgatg acaagttccctgctctgctc	cactagcttacagcccctcaa tttgcactctctcccactagc
No. 2a	Target 2	CGTCCAGTGCAGCAGAAACGTGG	chr5: 7,477,559-7,477,581	tgtgactgtagcgggtctga	gtcgcaattgccatcacttt
	OT2-II1 (OT2-I4)	AGTCTAGAGCAGCAGAAACGGGG	chr4: 20,089,705-20,089,727	agaaagtcggtggtaacagca	tctagactgcggcatgtgac
	OT2-II2	GCTCCAGTGCAGCAGACATGTAG	chr5: 18,780,520-18,780,498	gatgatgtgccagaggaaaaa	tccctgctacaggtcaccat
	OT2-II3	AAACCAGTGCTGCAGAAACGTGG	chr9: 10,268,750-10,268,728	agagtgaagcgtcacacctg	aaagtttgcatggggttctg
	OT2-II4	AATTCAGTGCAACAGAAACGGGG	chr12: 11,210,109-11,210,131	gaaggtagtggccaccagag	ttgctgtggagacgtggtta
	OT2-II5	GCTCCAGGGCAACAGAAACGAAG	chr13: 25,743,533-25,743,555	acctagcagatcggctttca	ggttcaaagtctccccctca
	OT2-II6	CTTCCATTGCAGCAGAAATGCAG	chr15: 17,930,301-17,930,279	agtggattgcaaccaatgaa	tggagacacatcaaatgtattactca
	OT2-II7	ACTCCAGTGCATCAGAAAGGAGG	chr15: 23,412,400-23,412,422	cggtagctccttccacaaac	aacaagccatctgcagtcct
	OT2-II8	TTTCCAGTGCAGCAGGAAGGCAG	chr18: 1,639,052-1,639,030	agagtgttaaaccccgacga	ggtgacaatcctgttatccaca

[a] This off-target site could not be analyzed by heteroduplex mobility assay because of failure to amplify the genomic region using the two pairs of primers.

5.3 Results

Introduction of somatic mutation at the medaka *DJ-1* locus

To produce customized guide RNAs, the pDR274 vector, a T7 polymerase-mediated expression vector for a synthetic sgRNA used in a zebrafish study [104], was used for sgRNA transcription. First, I designed an sgRNA in the second exon of the *DJ-1/park7* gene (Ensembl gene ENSORLG00000004285), successfully disrupted by TALENs in my previous study [81]. A sequence of the form 5′-GG-N_{18}-NGG-3′ was selected for the first target (5′-GGCCTCTTCCAAGCTAGTATCGG-3′; site No. 1) according to a previously described design guideline [104] (Fig.5.1A, B). To induce efficient expression of Cas9 nuclease, a pCS2-based Cas9 nuclease expression vector was used for production of a capped RNA by SP6 RNA polymerase, containing a human codon-optimized *S. pyogenes* Cas9 nuclease fused to a triple FLAG tag and two nuclear localization signal (NLS) in both N- and C-terminals previously used in cultured human cells [94, 113].

To investigate the efficiency of inducing targeted mutations in medaka, the solution containing 25 ng/μL of sgRNA and 100 ng/μL of Cas9 RNA was injected into fertilized eggs of the d-rR medaka strain. Genomic DNA was extracted from each injected embryo at 3 dpf, followed by assessment of the presence of targeted mutations by HMA. Formation of heteroduplexes was observed in all analyzed embryos (Fig. 5.1C), indicating that the RGEN-mediated indels were induced at the target locus. Subsequently, the *DJ-1* gene region containing the target site was PCR-amplified from two representative embryos. The PCR products were subcloned and each clone was sequenced. All the 33 sequenced clones had altered sequences, including 6 types of mutations in embryo #1-1 (17 of 17 sequenced clones; 100%) (Fig. 5.1D) and 7 types of mutations in embryo #1-2 (16 of 16; 100%) (Fig. 5.1E). These results indicate that the RGEN introduced DNA double-strand breaks at the target genomic sequence and thereby induced indels via error-prone nonhomologous end joining repair with high efficiency.

The sgRNAs transcribed by T7 polymerase do not necessarily require the target sites starting with GG

For more flexible targeting by the CRISPR/Cas system, I examined whether GG at the 5′ end of the targeting sequence is required for the sgRNAs transcribed by T7 RNA polymerase. Two genomic sequences (20 bp) followed by a PAM sequence on the second exon of the *DJ-1* gene were selected as additional targets (Fig. 5.2A). Site No. 2 (5′-CGTCCAGTGCAGCAGAAACGTGG-3′) contains CG at the 5′ end and site No. 3 (5′-CATCTGTCCCGATACTAGCTTGG-3′) contains CA at the 5′ end. To design sgRNAs that target these sequences, I employed two strategies as follows: (a) customizing only 18-nts of the sgRNA by replacing mismatches between GG added at the 5′ end and the genomic target sequence; (b) customizing all modifiable 20-nt long sequences of the sgRNA by ignoring the GG added at the 5′ end. The sgRNA No. 2a or 2b for target site No. 2 (Fig. 5.2B) and the sgRNA No. 3a or 3b for site No. 3 (Fig. 5.2C) were designed according to the strategy (a) or (b), respectively. I injected the solution containing 25 ng/μL sgRNA and 100 ng/μL Cas9 RNA. Results of HMA using RGEN-injected embryos showed that all 4 sgRNAs induced mutations at their targeting site (Fig. 5.2D). Subsequent sequence analysis using 2 representative embryos in each sgRNA not only revealed the introduction of indels, but also exhibited that the efficiency of inducing mutation depended on the design of the sgRNA (Fig. 5.2E–H). sgRNA No. 2a (Fig. 5.2E) and 3a (Fig. 5.2G) induced mutations with high efficiencies (28/28; 100% and 24/24; 100%, respectively), whereas sgRNA No. 2b (Fig. 5.2F) and 3b (Fig. 5.2H) induced mutations with relatively lower efficiencies (21/23; 91.3% and 13/29; 44.8%, respectively). These results exhibit that the GG at the 5′end of the target genomic sequence is not essential for DNA cleavage by the sgRNAs transcribed by the T7 promoter. Additionally, these results

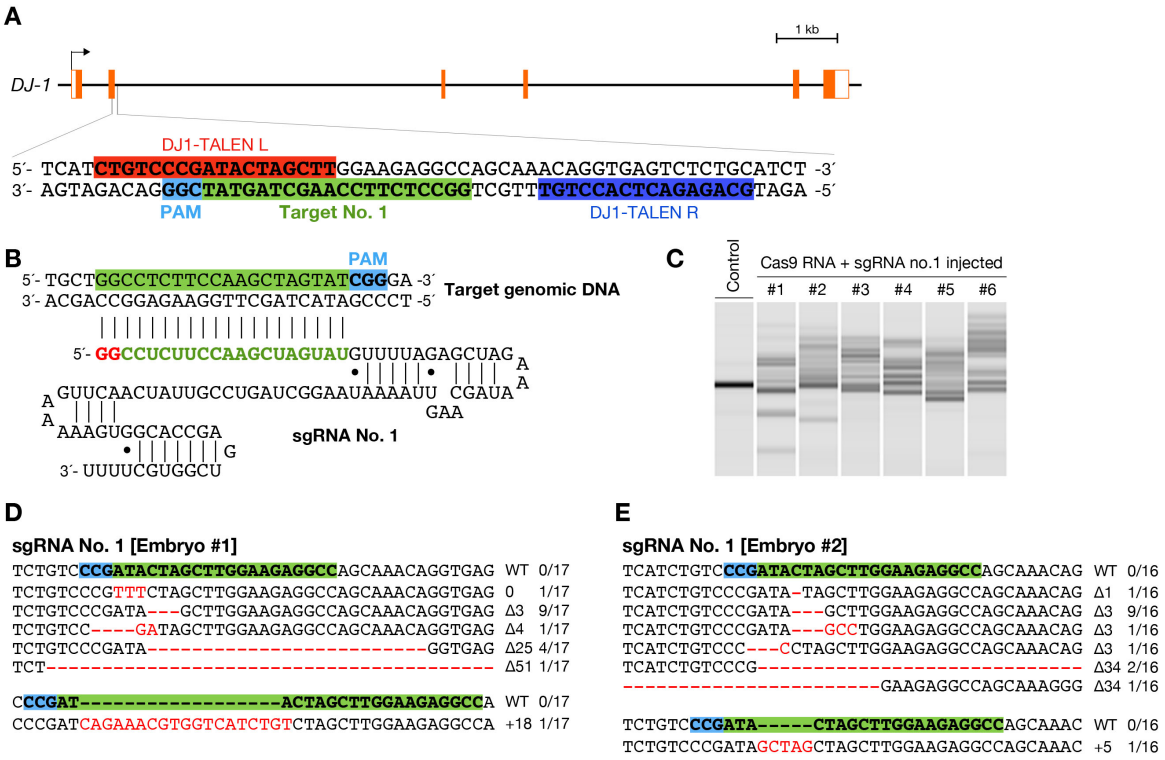

Figure 5.1. Induction of somatic mutations with CRISPR/Cas-mediated RGENs. (A) Schematic representation of the genomic structure of the *DJ-1* gene. Coding and untranslated exon regions are shown as solid and open boxes, respectively. The 20-bp target sequence of sgRNA No. 1 is indicated in green box, adjacent to NGG protospacer adjacent motif (PAM) sequence in light blue box. Red and blue boxes indicate the left and right recognition sequence of previously described TALENs [81]. (B) The sgRNA sequence for target site No. 1. First 20-nts sequence interacts with the complementary strand of the DNA target site. Red and green letters indicate the sequence required by T7 RNA polymerase and the customizable targeting sequence, respectively. (C) Heteroduplex mobility assay (HMA) in embryos injected with a mixture containing 100 ng/μL of Cas9 RNA and 25 ng/μL of sgRNA No. 1. Multiple heteroduplex bands were shown in PCR amplicons from each the RGEN-injected embryo (#1–6), whereas a single band was shown from each "Control" embryo without injection of the RGENs. (D, E) Subcloned sequences observed in the RGEN-injected embryos #1 (D) and #2 (E). Red dashes and letters indicate the identified mutations. The sgRNA targeting sequence and PAM indicate in green and light blue boxes, respectively. The size of deletions and insertions are shown to the right of each mutated sequence (Δ; deletions, +; insertions). Numbers on the right edge indicate the numbers of mutated clones identified from all analyzed clones from each embryo.

indicate that the sgRNAs customized with the 18-nt sequences following the first added GG can induce targeted mutations with higher efficiency.

Both Cas9 RNA and sgRNA induce mutations in a dose-dependent manner

To investigate the dose dependence of RGEN-induced mutation, varying amounts of Cas9 RNA and sgRNA No. 3a were injected because its targeting sequence contains an AluI restriction enzyme site that facilitates restriction fragment length polymorphism (RFLP) analysis (Fig. 5.3A). Most embryos injected with Cas9 RNA and/or the sgRNA developed normally and similar to the untreated embryos (Table 5.5). Genomic DNA was extracted from each surviving embryo at 3 dpf. Subsequently, the PCR amplicon, which included the targeted genomic sequence, was subjected to AluI digestion and

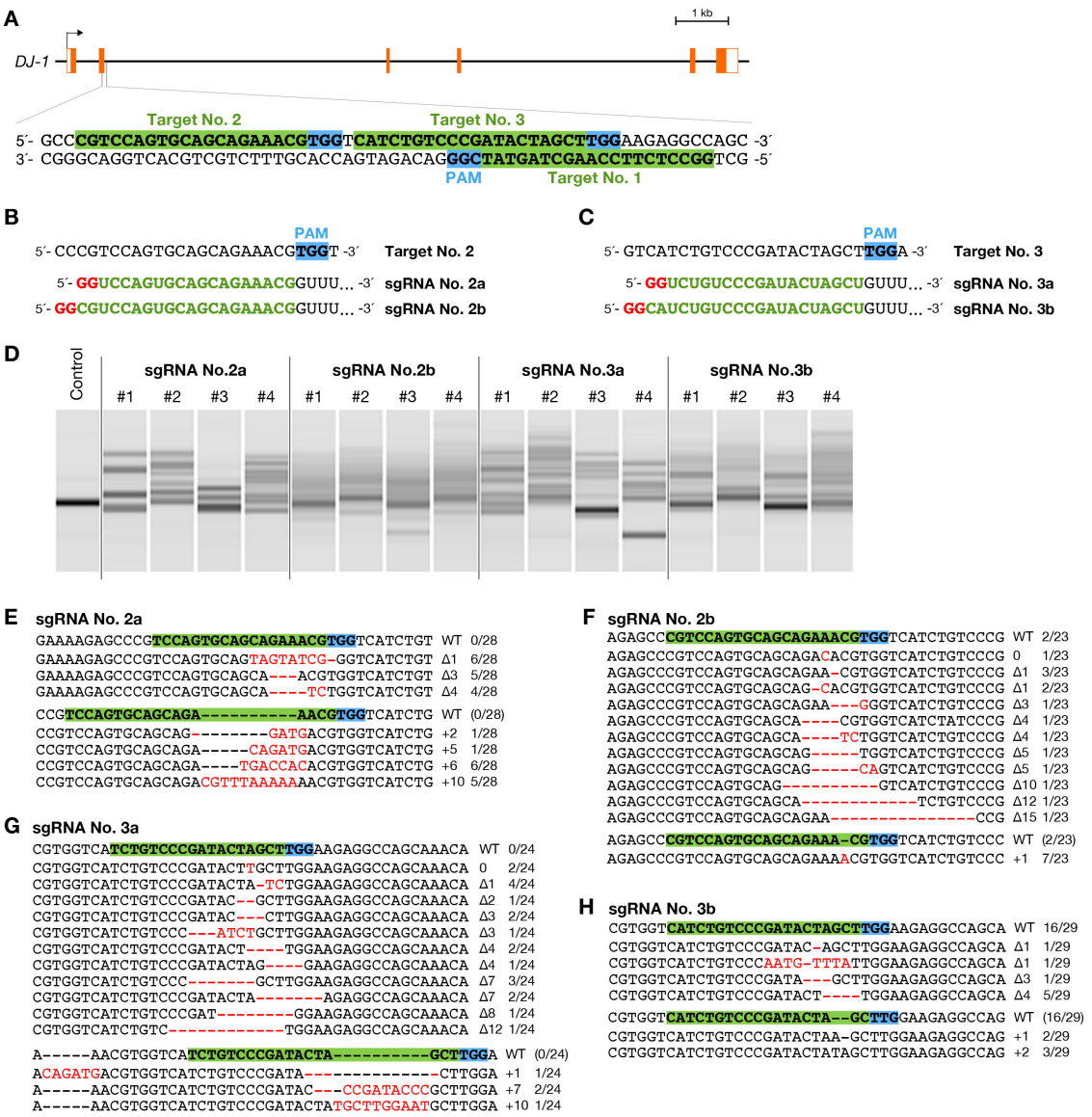

Figure 5.2. Somatic mutations induced at genomic sequences not containing GG at the 5′ ends. (A) Schematic illustration of the additional RGEN targeting sequences on the 2nd exon of *DJ-1* gene. Target site No. 2 and 3 do not contain GG at their 5′ ends, while target site No. 1 starts with the sequence GG. The targeting sequence of sgRNA is indicated in green box, adjacent to NGG protospacer adjacent motif (PAM) sequence in light blue box. (B, C) The sequences of sgRNAs for target site No. 2 (B) and 3 (C). Red and green letters indicate the sequence required by T7 RNA polymerase and the customizable targeting sequence, respectively. Two sgRNAs were designed for each target site. The sgRNA No. 2a and 3a contain the 18-nts sequence complementary to their genomic target site, while the sgRNA No. 2b and 3b contain the 20-nts sequence. These sgRNAs also contain 1- or 2-nt mismatches to their genomic target sequence at 5′ end. (D) Heteroduplex mobility assay (HMA) in embryos injected with a mixture containing 100 ng/μL of Cas9 RNA and 25 ng/μL of sgRNA. Multiple heteroduplex bands were shown in PCR amplicons from each the RGEN-injected embryo, whereas a single band was shown from each "Control" embryo without the injection of the RGENs. (E–H) Subcloned sequences observed in the embryos injected with sgRNA No. 2a (E), 2b (F), 3a (G), or 3b (H). Red dashes and letters indicate the identified mutations. The sgRNA targeting sequence and PAM indicate in green and light blue boxes, respectively. The size of deletions and insertions are shown to the right of each mutated sequence (Δ; deletions, +; insertions). Numbers on the right edge indicate the numbers of mutated clones identified from all analyzed clones from each embryo.

Table 5.5. Survival of embryos injected with varying amounts of Cas9 RNA and/or sgRNA

sgRNA No.	Cas9 (ng/μL)	sgRNA (ng/μL)	Injected	Survival at 1 dpf	Survival at 3 dpf
Control	100	0	18	18	16
1	100	25	22	21	19
2a	100	5	16	16	16
	100	10	21	21	21
	100	25	20	20	20
2b	100	25	20	20	20
3a	100	1	22	21	21
	100	10	21	21	20
	100	25	20	20	19
	0	25	22	21	20
	10	25	21	21	21
	30	25	22	22	22
3b	100	25	12	12	11

analyzed by the MultiNA system. All samples that were injected with both Cas9 RNA and sgRNA showed the undigested fragment (a+b, Fig. 5.3B) while control samples without Cas9 RNA and/or sgRNA showed no undigested fragment but two AluI-digested fragment (a and b, Fig. 5.3B). Then, I calculated the disrupting activity of the RGEN at each concentration using the quantities of digested and undigested fragments. Serial dilutions of the Cas9 RNA exhibited that 10 ng/μL Cas9 RNA induced mutations with significantly lower efficiency (81.2±2.9%) as compared to 30 and 100 ng/μL (92.4±1.8% and 95.7±2.5%, respectively) (Fig. 5.3C). Similar results were obtained with sgRNA, as exhibited by a significantly low efficiency of mutation with 1 ng/μL sgRNA (46.4±6.6%) as compared to 10 and 25 ng/μL (96.5±1.3% and 95.7±2.5%, respectively) (Fig. 5.3D). These results indicate that the efficiency of both Cas9 RNA and sgRNA in inducing mutations is dose dependent.

Off-target alterations with the RGENs in the medaka genome

To assess the possibility of induction of off-target mutagenesis by RGEN, candidate off-target sequences that could potentially be targeted by the 3 sgRNAs (No. 1, 2a, and 3a) for the *DJ-1* gene were searched in medaka genome. Previous *in vitro* studies [92] and in bacteria [114] and human cells [94] have shown that cleavage by Cas9 can be abolished by single mismatches in the "seed" sequence, a 10–12-bp sequence located in the 3′ end of the 20-bp targeting region. I therefore searched the medaka genome for candidate sites that perfectly match the 12-bp sequence at the 3′ ends of the 20-bp targeting sequence and the NGG PAM sequence, referred to as criterion (i), (see "Off-target analysis" in Materials and Methods). I identified 4, 17, and 4 candidate sites for the sgRNA No. 1, 2a, and 3a, respectively (Table 5.3). Efficient alterations were identified in the embryos injected with the sgRNA No. 2a at a genomic locus (OT2-I4: 5′-**A**GTC**T**A**G**AGCAGCAGAAACGGGG-3′) harboring 3-bp mismatches (Fig. 5.4A) with HMA, while no alteration was detected at other candidate sites (Fig. 5.5).

Recently, Fu and colleagues revealed that one or more mismatches located in the 3′ half of the sgRNA targeting region are tolerated [95], and Hsu and colleagues also revealed that *S. pyogenes* Cas9 can cleave targets with a NAG PAM [96]. Therefore, I investigated potential off-target sites identified by another criterion. Based on my data described in the section "The sgRNAs transcribed by T7 polymerase do not necessarily require the target sites starting with GG", which suggests that the 2-nt sequence at the 5′ end of the sgRNAs is not crucial to targeting sequence recognition of the

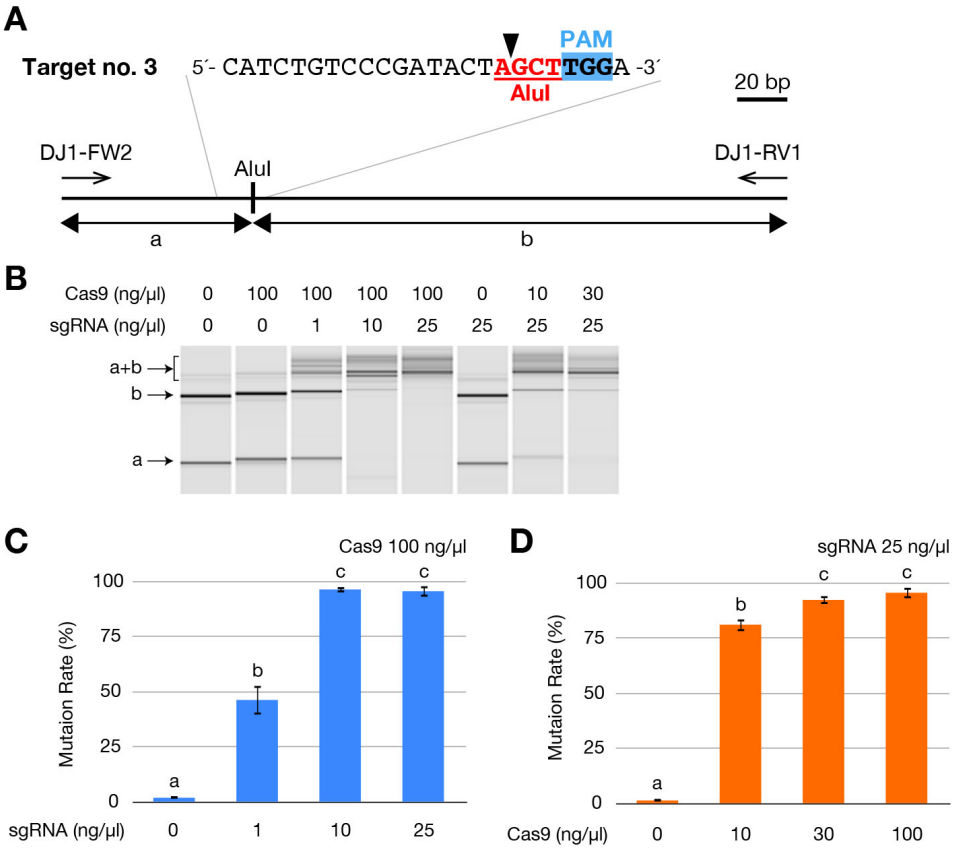

Figure 5.3. Dose-dependent mutagenesis by the RGENs. (A) Schematic illustration of restriction fragment length polymorphism (RFLP) analysis to calculate mutation frequencies. The sgRNA No. 3a contatin an AluI restriction enzyme site (Red letters with underline) on the potential cleavage site indicated by an arrowhead. A 285 bp fragment amplified using primers DJ1-FW2 and DJ1-RV1 produces both 75 bp (a) and 210 bp fragments by AluI digestion in wild type. (B) Gel image of AluI-digested fragments analyzed in MultiNA system. The RGEN-injected embryos exhibited undigested fragments (a+b). Images from a representative embryo injected with varying amounts of Cas9 RNA and sgRNA No. 3a are shown. (C, D) Mutation rates at each injected Cas9 RNA concentration with 25 ng/μL of sgRNA (C) and at each injected sgRNA concentration with 100 ng/μL of Cas9 RNA (D). The mutation rate was calculated as the molar concentration of the undigested fragment (a+b) with AluI as a percentage of the sum of molar concentrations of the undigested fragment (a+b) and the larger digested fragment (b). The molar concentration of each fragment was quantified using the MultiNA Viewer software. Columns and error bars represent mean ± s.e.m. (n = 12). The different letters at the top of the columns indicate significant differences ($P < 0.05$; one-way ANOVA followed by Tukey's HSD test).

RGENs, I searched the genome for candidate sites that match with the 18-bp sequence at the 3′ ends of the targeting sequence harboring up to 2-bp mismatches adjacent to either NGG or NAG PAM sequence, referred to as criterion (ii). I identified 4 and 8 additional candidate sites for the target site No. 1 and 2a, respectively (Table 5.4), including the OT2-I4 meeting the first criterion (Table 5.3), and then detected alterations in the embryos injected with the sgRNA No. 2a at a locus (OT2-II4: 5′-AATTCAGTGCAACAGAAACGGGG-3′) (Fig. 5.4B). DNA sequencing confirmed that mutations were induced with high efficiency at the OT2-I4 (11/11; 100%) (Fig. 5.4C) and low efficiency at the OT2-II4 (1/10; 10%) (Fig. 5.4D). These results showed that the RGENs have the potential to induce off-target mutations *in vivo*.

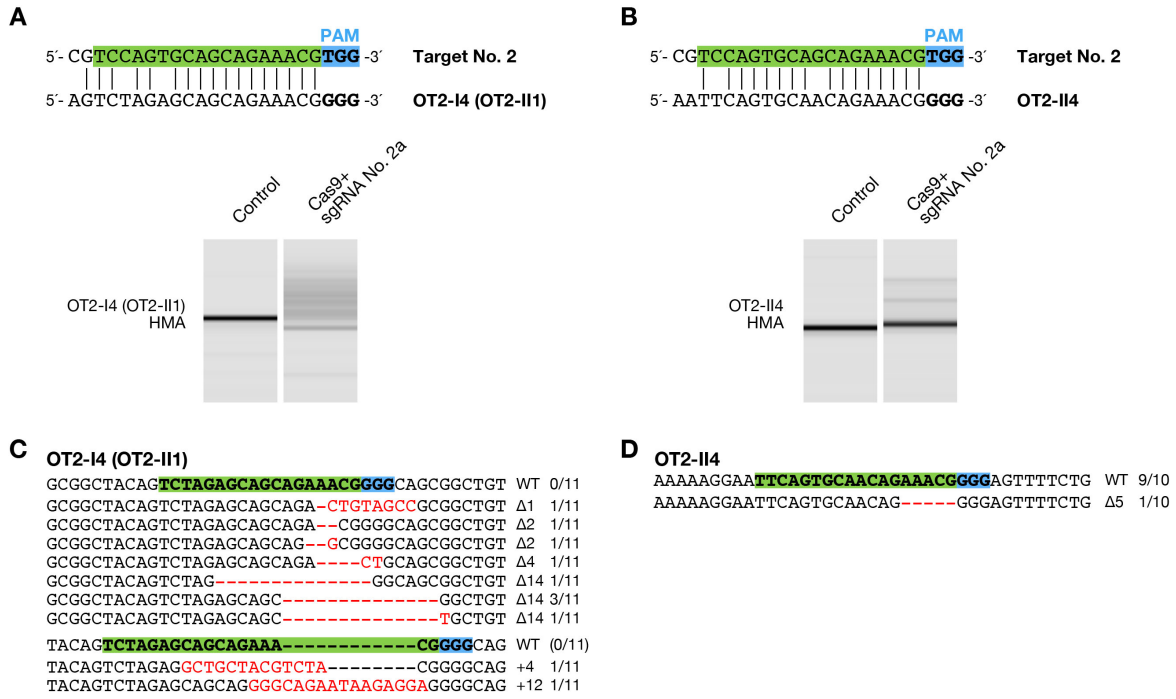

Figure 5.4. Analysis of off-target mutagenesis. (A,B) Heteroduplex mobility assay (HMA) of the mutagenized off-target loci OT2-I4 (OT2-II1) (A) and OT2-II4 (B). The upper panel shows the alignment of the off-target sites with the targeting sequence No. 2. The targeting sequence of sgRNA is indicated in green box, adjacent to NGG protospacer adjacent motif (PAM) sequence in light blue box. The lower panel shows HMA of the off-target loci using genomic DNA mixtures of the 12 embryos. Multiple heteroduplex bands were shown in PCR amplicons from embryos injected with 100 ng/μL of Cas9 RNA and 25 ng/μL of sgRNA No. 2a, whereas a single band was shown from "Control" embryos without injection of the RGENs. (C, D) Subcloned sequences of off-target alterations at OT2-I4 (OT2-II1) (C) and OT2-II4 (D) were identified in the RGEN-injected embryos. Red dashes and letters indicate the identified mutations. The sgRNA targeting sequence and PAM indicate in green and light blue boxes, respectively. The size of deletions and insertions are shown to the right of each mutated sequence (Δ; deletions, +; insertions). Numbers on the right edge indicate the numbers of mutated clones identified from all analyzed clones from each genomic DNA mixture.

Furthermore, I investigated the dose effect of sgRNA on off-target alterations using sgRNA No. 2a. Cas9 RNA (100 ng/μL) was injected with 5 or 10 ng/μL of sgRNA No. 2a and then I analyzed the *DJ-1* target locus and two off-target loci (OT2-I4 and OT2-II4), which were mutated in the previous experiment, using genomic DNA mixture from 12 embryos at 3 dpf. At the *DJ-1* locus, the lower doses of the sgRNA, 10 ng/μL (12/12; 100%) (Fig. 5.6B) and 5 ng/μL (8/12; 66.7%) (Fig. 5.6C), induced mutations as efficiently as 25 ng/μL (28/28; 100%) (Fig. 5.2E). On the other hand, at the off-target loci OT2-I4 and OT2-II4, the lower doses of the sgRNA, 10 ng/μL (5/11; 45.5% and 0/12; 0%, respectively) (Fig. 5.6D, F) and 5 ng/μL (1/12; 8.3% and 0/9; 0%, respectively) (Fig. 5.6E, G), dramatically reduced mutation frequencies compared to 25 ng/μL (11/11; 100% and 1/10; 10%, respectively) (Fig. 5.4C, D). These results showed that the sgRNA No. 2a induced mutations more efficiently at the on-target locus than the off-target loci. These also suggest that lower dosage of sgRNA is likely to reduce off-target effects by the RGENs.

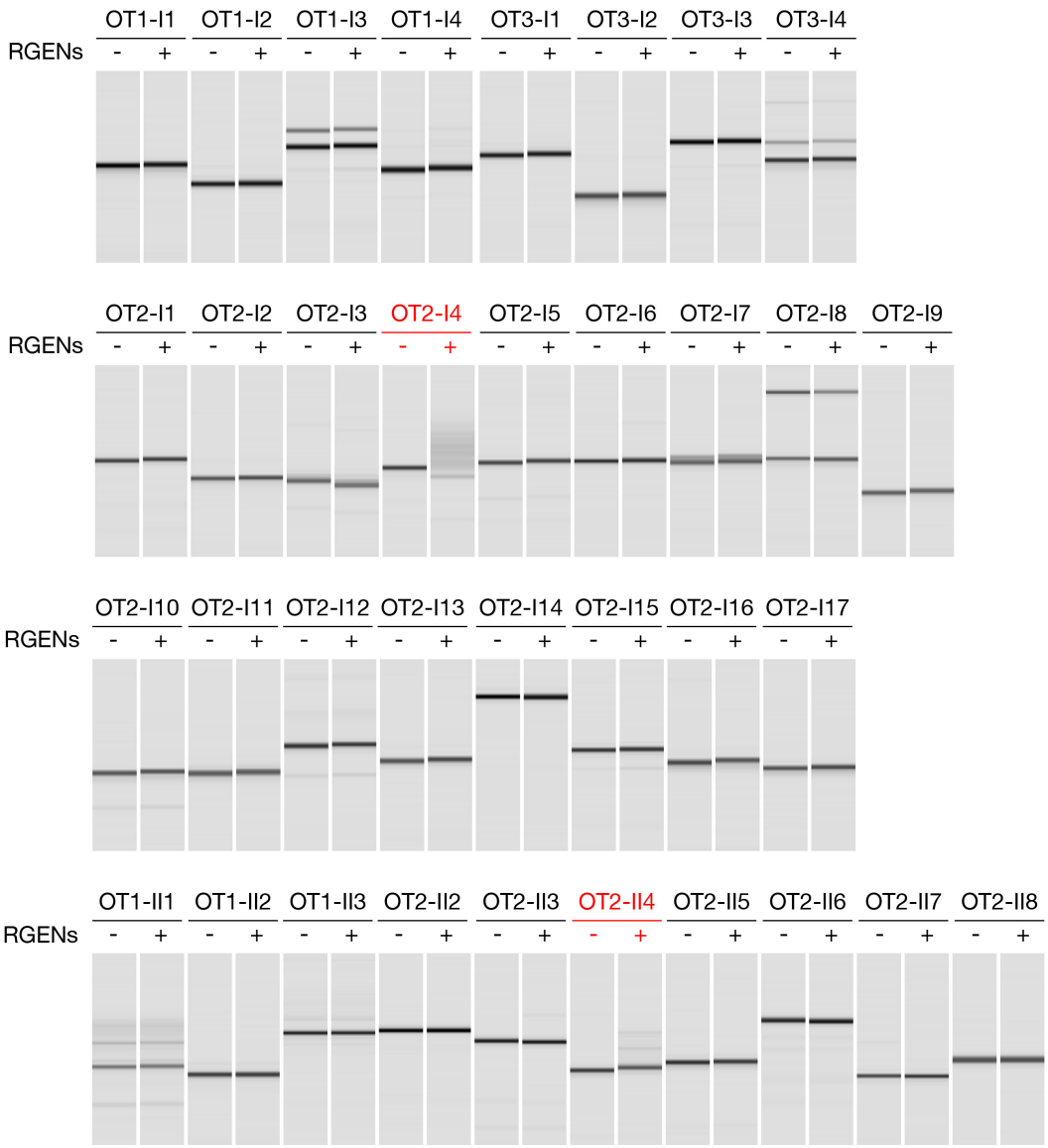

Figure 5.5. Analysis of off-target mutagenesis. (A,B) Heteroduplex mobility assay (HMA) of the mutagenized off-target loci OT2-I4 (OT2-II1) (A) and OT2-II4 (B). The upper panel shows the alignment of the off-target sites with the targeting sequence No. 2. The targeting sequence of sgRNA is indicated in green box, adjacent to NGG protospacer adjacent motif (PAM) sequence in light blue box. The lower panel shows HMA of the off-target loci using genomic DNA mixtures of the 12 embryos. Multiple heteroduplex bands were shown in PCR amplicons from embryos injected with 100 ng/μL of Cas9 RNA and 25 ng/μL of sgRNA No. 2a, whereas a single band was shown from "Control" embryos without injection of the RGENs. (C, D) Subcloned sequences of off-target alterations at OT2-I4 (OT2-II1) (C) and OT2-II4 (D) were identified in the RGEN-injected embryos. Red dashes and letters indicate the identified mutations. The sgRNA targeting sequence and PAM indicate in green and light blue boxes, respectively. The size of deletions and insertions are shown to the right of each mutated sequence (Δ; deletions, +; insertions). Numbers on the right edge indicate the numbers of mutated clones identified from all analyzed clones from each genomic DNA mixture.

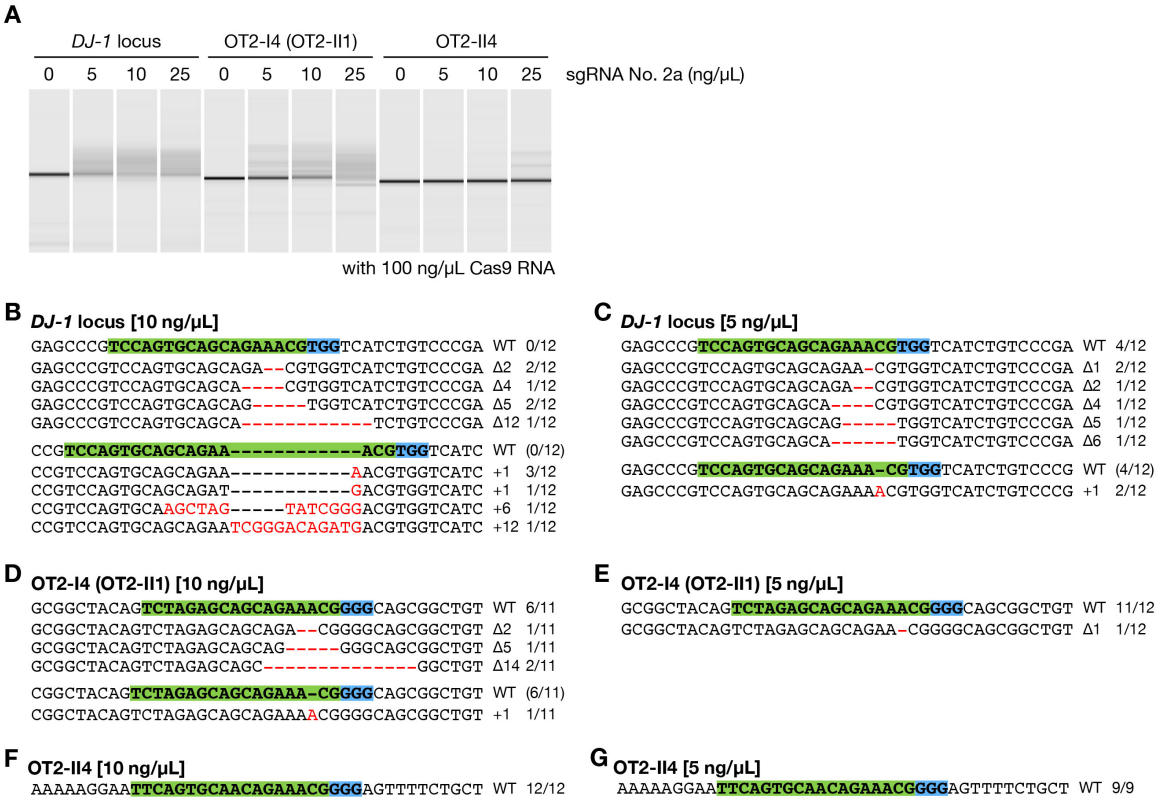

Figure 5.6. Dose-dependency of off-target alterations by the RGEN. Both the *DJ-1* targeting locus and two disrupted off-target loci were analyzed using genomic DNA mixture of the 12 embryos that were injected with dilution series of sgRNA No. 2a and 100 ng/μL Cas9 RNA. (A) Heteroduplex mobility assay (HMA). Each analyzed locus and concentration of the injected sgRNA was shown in the upper side of the panel. (B, C) Subcloned sequence of the targeting locus observed in the embryos injected with either 10 ng/μL (B) or 5 ng/μL (C) of sgRNA No. 2a. (D–G) Subcloned sequence of the off-target locus OT2-I4 (OT2-II1) (D, E) or OT2-II4 (F, G) observed in the embryos injected with either 1 ng/μL (D, F) or 5 ng/μL (E, G) of sgRNA No. 2a. (B–G) Red dashes and letters indicate the identified mutations. The sgRNA targeting sequence and PAM indicate in green and light blue boxes, respectively. The size of deletions and insertions are shown to the right of each mutated sequence (Δ; deletions, +; insertions). Numbers on the right edge indicate the numbers of mutated clones identified from all analyzed clones from each genomic DNA mixture.

Evaluation of RGEN-induced germ line mutations

To test whether RGENs can induce heritable mutations, I raised the RGEN-injected fish to sexual maturity and analyzed their progeny. Of the 40 eggs injected with 100 ng/μL Cas9 RNA and 25 ng/μL sgRNA No. 1, 32 (80%) hatched normally. Five G0 fish were mated with wild-type fish of the d-rR strain, and their F1 embryos were genotyped by HMA. I identified that all 5 G0 fish transmitted the RGEN-induced mutations to their progeny. The germ line transmission rates of the mutations in each G0 fish ranged from 42.9% (12 of 28; #1–4) to 100% (27 of 27; #1–3, 23 of 23; #1–5) (Fig. 5.7). The mutation pattern found in the germ cells of each G0 founder varied from 1 (#1–4) to 6 (#1–2). All mutations identified in F1 embryos are shown in Fig. 5.7. These results indicate that the RGENs induced heritable mutations with high efficiency.

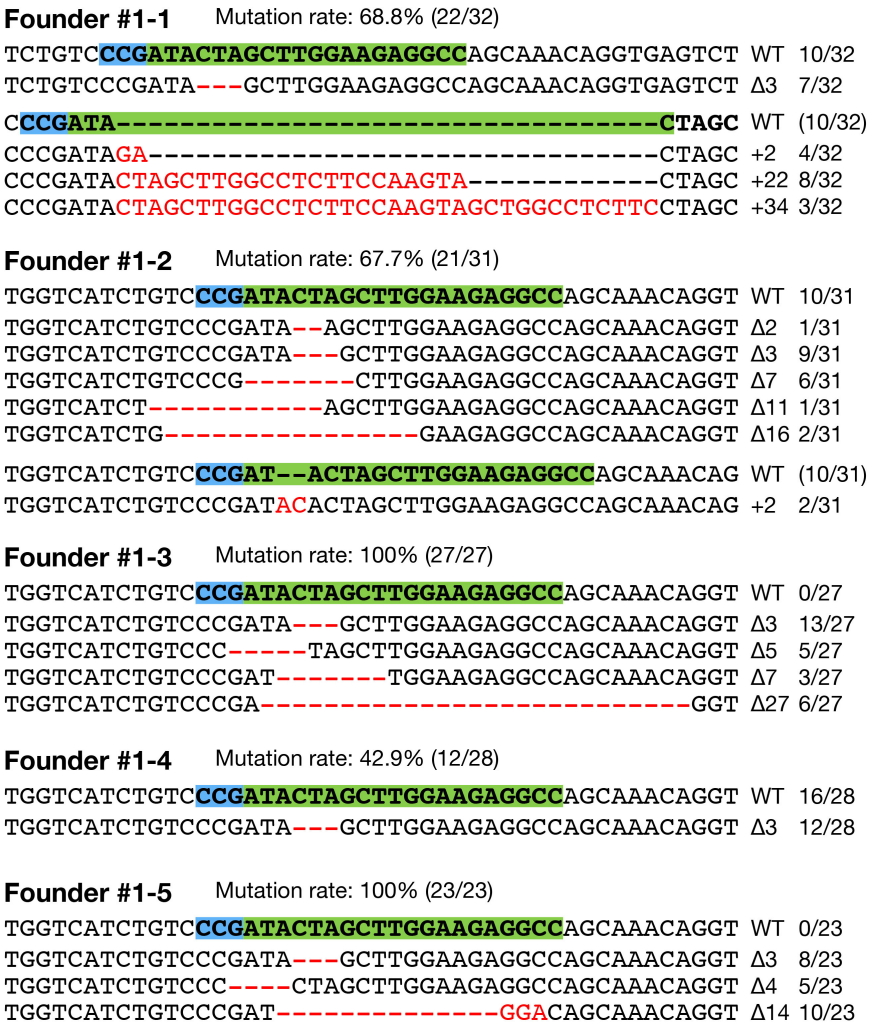

Figure 5.7. Germ line transmission of the RGEN-induced mutations. Each G0 founder that was injected with 100 ng/μL of Cas9 RNA and 25 ng/μL of sgRNA No. 1 was mated with wild-type fish to screen heritable mutations. Mutation sequences identified in each F1 embryo of them by heteroduplex mobility assay (HMA) and subsequent direct sequencing were shown. Red dashes and letters indicate the identified mutations. The sgRNA targeting sequence and protospacer adjacent motif (PAM) indicate in green and light blue boxes, respectively. The size of deletions and insertions are shown to the right of each mutated sequence (Δ; deletions, +; insertions). Numbers on the right edge indicate the numbers of mutated embryos identified from all analyzed embryos. The frequencies of mutations in each founder are indicated on the top of mutation sequences.

5.4 Discussion

In this chapter, I described a simple and efficient approach for targeted mutagenesis in medaka by using the CRISPR/Cas-mediated RGENs. The RGENs can induce targeted genomic cleavage when injected with only capped RNA encoding a Cas9 endonuclease and a sgRNA guiding the nuclease to the complementary genomic sequence. All the designed sgRNAs induced targeted somatic mutations with high efficiency (44.8–100%; average, 86.8%). G0 founders that were injected with the RGENs carried mutations in their germ cells with high efficiency. These efficiencies are as high as those in my

Table 5.6. A proposed guideline for design of efficient sgRNAs transcribed by the T7 promoter

Guideline	Sequence [5′–3′]
Target genomic sequence	N18-NGG
Transcribed sgRNA sequence	GG-N18-GUUUAG...
Sence oligonucleotide sequence for pDR274	TAGG-N_{18}
Anti-sence oligonucleotide sequence for pDR274	AAAC-N_{18}[a]

[a] This N_{18} sequence should be reverse and complement.

mutagenesis study using TALENs in medaka [81]. These results mean that the RGENs function as an efficient engineered nuclease system in medaka.

The previously designed guidelines for an sgRNA transcribed by T7 RNA polymerase requires any sequence of the form 5′-GG-N_{18}-NGG-3′ that occurs once in every 128 bp of a random DNA sequence [104]. Efficient induction of mutations by the sgRNAs designed for the target site No. 2 and 3 has revealed that mismatches between the 2-nt sequence at the 5′ ends of the sgRNAs and the target genomic sequence are tolerated. It was also reported that double mismatches at the 5′ ends are tolerated in zebrafish [103], suggesting that the RGEN can target any sequence only adjacent to a NGG PAM sequence that occurs once in every 8 bp. In this study, the sgRNAs starting with the sequence 5′-GG-N_{18}-3′ (No. 2a and 3a) induced mutations more efficiently as compared to the sequence 5′-GG-N_{20}-3′ (No. 2b and 3b). From the results, a guideline is proposed for design of sgRNAs that can efficiently disrupt target genomic sequences in medaka (Table 5.6). On the other hand, one of the 3 examined sgRNA with the sequence 5′-GG-N_{20}-3′ more efficiently induced mutations as compared to the sequence 5′-GG-N18-3′ in the zebrafish study [104]. Since the effects of the 5′ ends of sgRNAs on cleaving activities were investigated in only a few examples, more comprehensive investigations will be required to generalize the effectiveness of the 5′ structures to other targeting sites.

Previous *in vivo* works defined a 12-bp sequence adjacent to a PAM as a seed sequence and counted the genomic sequences that perfectly matched the seed sequence as potential off-target sites [98–101]. However, the study in human cells revealed that one or more mismatches located in the 12-bp sequences are tolerated [95, 109, 110], suggesting that some *in vivo* off-target alterations are likely to be missed in these works. In fact, although one of the two mutagenized off-target loci (OT2-I4, Fig. 5.4) meets this criterion (called "criterion (i)" in this study), the other locus (OT2-II4, Fig. 5.4), harboring a single mismatch in the 12-bp sequence of a seed sequence, does not meet this criterion. Both these mutagenized off-target loci meet the criterion (ii), matching 16 to 18 of 18-bp sequence at the 3′ end of the targeting sequence followed by a NRG (either the NGG or NAG) PAM.

It was reported that potential off-targets meeting the criterion (ii) were efficiently disrupted in cultured human cells [95, 96, 109, 110] and zebrafish [105]. Altogether, I propose that potential off-target loci identified by the criterion (ii), harboring 2- or fewer bp mismatches in the 18-bp targeting sequence followed by a NRG PAM, should be analyzed for screening unwanted mutagenesis. However, Cho and colleagues showed that some RGENs can distinguish on-target sites from off-target sites that differ by at least two bases [109]. Both this report and my limited analysis suggest that further investigations (e.g. genome-wide or deep-sequencing analysis) will be required to determine the generalized criteria for searching the off-target sites in medaka and other organisms.

Significant induction of *in vivo* off-target alterations indicates that the potentially confounding effects of off-target mutations should be considered in analysis using the RGEN-mediated genome-edited organisms. Also, since my approach for searching of potential off-target sites is based on similarities to the targeting sequences, I may miss some off-target effects in this study. However, in this study,

fish injected with the RGENs developed normally (Table 5.5), suggesting that their off-target effects are not crucial for viability and have little non-specific toxicity unlike found in the fish injected with ZFNs [71]. Additionally, each sgRNA that was designed in this study has unique profile of off-target activities and only the two loci for sgRNA No. 2 were mutagenized (Figs. 5.4 and 5.5). These suggest that validating the phenotypes with at least two independent lines generated by different sgRNAs is important to eliminate the off-target effects, in addition to cleaning the background mutations by repeated outcrossing and rescue experiments. Furthermore, I found that 5 or 10 ng/μL of sgRNA No. 2a induced off-target alterations with significantly lower efficiencies than did 25 ng/μL of the sgRNA (Fig. 5.6). This indicates that injection with lower dosage of sgRNAs will also become an effective way to reduce the off-target effects.

At present, ZFNs, TALENs, and CRISPR/Cas-mediated RGENs are three successful options for targeted genome editing in medaka [71, 80, 81]. Both the TALEN and the CRISPR/Cas systems allow for the construction of highly efficient nucleases that target desired sequences more easily than the ZFN system. Compared to the TALENs, the CRISPR/Cas system has some advantageous characteristics for efficient genome editing. Firstly, determination of DNA cleavage specificity by guide RNA sequences allows the customizing of the RGENs only by modification of the 5′ end of the sgRNA using annealed oligonucleotides, while the customizing of TALENs requires preparation of multiple vectors (at least 35 vectors, as described earlier [68, 81]) and complex assembly processes. Secondly, the RGENs can efficiently cleave DNA targets containing CpG methylation sites [96], while TALENs are sensitive to methylation [115]. Finally, Cas9 nickases can be simply engineered by the introduction of a point mutation into Cas9 nuclease (e.g. D10A) [92], which are likely to efficiently induce precise genome engineering via homology-directed repair without the effects of indel mutations induced via non-homologous end joining pathway [94]. These indicate that the CRISPR/Cas-mediated RGENs have the potential to be developed as an alternative technology for targeted genome editing in medaka and other organisms.

Chapter 6

Effects of chronic fluoxetine administration on anxiety-related and social behaviors in medaka

6.1 Introduction

The assessment of behavioral changes caused by genetic, pharmacological, or toxicological manipulations is an important way to understand the gene functions or the *in vivo* effects of drugs and toxic compounds. However, since animal behaviors are sensitive to a variety of environmental factors, the behavioral phenotyping is generally a laborious work. In rodent models, some test batteries, consisting of different well-established and reproducible behavioral paradigms, have been developed for multitiered behavioral phenotyping [116–118]. These batteries can minimize the risk of both false positive and false negative results and therefore enable accurate interpretations of the phenotypes.

Teleost fishes are the largest group among vertebrate classes [119] and they exhibit remarkable diversity in their morphology, physiology, and behaviors for adaptation to the diverse habitat. Recently, small laboratory fishes, especially zebrafish, have become popular models in neurobehavioral and neuropsychiatric research, which has been used for analysis of complex brain disorders (e.g., depression, autism, drug abuse, and cognitive defilicts) and screening of neuropsychiatric drugs [120, 121]. For the comparative assessment between mammals and zebrafish, some behavioral paradigms established in the mouse model have been transferred into the zebrafish [121], and in fact, combinations of a number of behavioral paradigms characterized significant behavioral changes induced by administration of a hallucinogenic drug [122] and a single gene *fgfr1a* mutation [123].

Medaka, a small fish model for genetics, have also become a neurobehavioral model that particularly exhibits complex social and/or visually-evoked behaviors, such as shoaling/schooling [124–126], aggressive behaviors [127], mating preference [46, 128], mate-guarding behaviors [129], social learning [130], mirror approaching [131], predation [132], and startle response [133]. These studies and my previous demonstration of targeted mutagenesis in using targetable nuclease systems [71, 81, 112, 134] indicates that medaka will become a useful model for understanding of behavioral and brain functions of genes; however, in medaka, there have been few studies that comprehensively evaluated the behavioral effects of genetic manipulations by the multitiered phenotyping strategies.

In this chapter, I aimed to establish a behavioral testing system for assessment of the behavioral alterations in medaka by the multitiered strategy. I demonstrated the usability of the system by characterizing the behavioral alterations in medaka adult fish induced by chronic administration of fluoxetine, a selective serotonin reuptake inhibitor (SSRI) class of anti-depressant, that block serotonin reuptake into the presynaptic cells by serotonin transporter and therefore effectively increases the extracellular

serotonin levels in the synaptic clefts [135]. Previous studies showed that fluoxetine affected adult complex behaviors in teleost fish species, such as aggressive behavior in the bluehead wrasse (*Thalassoma bifasciatum*) [136], the Siamese fighting fish (*Betta splendens*) [137], and the Gulf toadfish (*Opsanus beta*) [138], locomotor behavior in Chinook salmon (*Oncorhynchus tshawtscha*) [139] and sheepshead minnow (*Cyprinodon variegates*) [140], and anxiety-related behavior in the zebrafish [141–143] and fathead minnow (*Pimephales promelas*) [144]. However, there is few studies on the behavioral effects of fluoxetine in medaka except to a report about altered photomotor response in hatching larvae [145], whereas previous reports using medaka have investigated the effects of fluoxetine on embryonic development, reproduction, and estradiol level [146, 147] and the uptake and bioaccumulation [148, 149] in terms of toxicological research. Therefore, the behavioral effects of chronic fluoxetine treatment in medaka, especially on the anxiety-related and social behaviors, were examined by five behavioral test paradigms including diving test, open-filed test, light–dark transition test, mirror approaching test, and social interaction test that are regarded as effective paradigms to evaluate locomotor activities, anxiety-related behaviors, and social behaviors in teleost [131, 141, 150–152]. The behavioral data of testing fish was acquired and analyzed by an automated behavioral testing system consisting of a video tracking software and test chambers for automated quantification of the medaka behavior.

6.2 Materials and Methods

Fish and housing conditions

The d-rR strain medaka fish [66] is maintained as a closed colony with little polymorphisms among the individuals and is a parental strain of a inbred strain Hd-rR whose whole genome was sequenced [3], which is used for a standard laboratory strain in a wide range of scientific research. I used this strain in this study to evaluate the pharmacological effects with minimal effects of both genetic and environmental backgrounds.

Embryos were raised in embryo culture medium (0.1% NaCl, 0.003% KCl, 0.004% $CaCl_2{\cdot}2H_2O$, and $MgSO_4{\cdot}7H_2O$) on a 14/10 h light/dark cycle at 26 ℃. Hatched fish were raised in groups of 8–10 fish per 2-L tank with recirculating filtered water at 27 ℃. The fish tanks were illuminated by white fluorescent tube on a 14/10 h light/dark cycle. The fish were fed newly hatched *Artemia* nauplii and commercial powdered foods (for larval fish: Sweetfish Super Gold #0, Oriental Yeast; for juvenile and adult fish: Otohime B2, Marubeni Nisshin Feed, for juvenile and adult fish) once or twice a day. The 4 month-old fish were subjected to the following pharmacological manipulation and the behavioral testing. The standard length of the examined male or female fish was 20.03 ± 1.20 or 20.22 ± 1.69 mm, respectively (n = 24 each). After the experimentation, all tested fish were sacrificed by deep anesthesia using MS-222 (Sigma–Aldrich). This work was conducted using the protocols approved by the Animal Experimentation Committee of Kyoto University (permission number: 26-71).

Pharmacological manipulations

Stock solutions of 1 mg/mL fluoxetine hydroxychloride (F132, Sigma–Aldrich) was prepared in distilled water and kept at 4 ℃ until use. The stock solution was diluted to 100 ng/mL with conditioned water (0.003% Red Sea Salt, Red Sea Aquatics, Houston, TX; 0.05% Tetra Vital, Tetra; 0.05% Tetra AquaSafe, Tetra; 0.025% Tetra ContraChlorine, Tetra). Two groups of 12 fish per tank (including both male and female) were exposed to 2 L of fluoxetine-containing water for 10 days with tank water changes every 2 days. Their respective controls were kept in conditioned water without fluoxetine but in otherwise identical conditions.

Behavioral testing

Apparatuses and software All apparatuses for behavioral testing were set up in a wooden cube (36 cm height $*$ 36 cm width $*$ 38 cm depth) with a door to stabilize the testing condition. Video images of the test fish were recorded using a USB webcam (DC-NCR300UY, Hanwha) from front of the testing tank (diving and light–dark transition test) or above the tank (open-field, mirror biting, and social interaction test). The testing tanks for the diving and light–dark transition test were illuminated using an LED panel light (300 lx) attached to the top panel, and the tanks for other paradigms were illuminated four light bars (550 lx) attached to each side panel at 75 mm height from the bottom panel. Behavioral data were acquired and analyzed by custom-made software with OpenCV computer vision library. Images were captured every 100 msec. Captured images were subtracted background image and binarized. The calculated gravity points of binarized fish objects were used as fish position. All behavioral parameters used in this study including swimming distance and velocity were calculated by the time course of fish position.

Test procedures Behavioral testing including five paradigms (open-field, diving, light–dark transition, mirror biting, and social interaction) was performed over five days. Each fish was subjected to open-field and diving test at the first and second days, to light–dark transition and mirror biting test at the third and forth days, and to social interaction test at the fifth day. Before introducing test fish into the test tank, they were individually introduced in a 1-L pre-treatment tank by a fishnet. The sex of each test fish was determined by anal fin shape, and then was transferred to the tank for the behavioral testing.

Diving test Diving test is a well-established paradigm to quantify stress responses and anxiety-related behaviors in zebrafish [141]. The test was conducted using a rectangular tank (200 mm length $*$ 50 mm width $*$ 150 mm height) consisting of white acrylic panels except a transparent acrylic panel at the front face and filled with the conditioned water to a height of 120 mm (Fig. 6.1A). The tank was divided into five virtual horizontal areas (24 mm height each) (Fig. 6.1B). Fish were individually introduced into the test tank, and their behaviors were recorded for 10 min to calculate distance traveled (mm), freezing duration (s), the time spent in the top area (s), latency to enter the top (s), the number of entries into the top, and the time spent in the bottom area (s).

Open-field test Open field test is a behavioral paradigm to assess anxiety levels and locomotor activity in zebrafish [150]. The test was performed in a white acrylic tank (200 mm length $*$ 200 mm width $*$ 75 mm height) filled with the conditioned water to a height of 20 mm (Fig. 6.2A). The bottom of the tank was virtually divided into center (120 mm $*$ 120 mm, 60% of length and width) and peripheral (the area within 80 mm from the walls) areas (Fig. 6.2B). Fish were individually introduced into the center of the tank, and their trajectories were recorded for 15 min. Distance traveled (mm), freezing duration (s), the time spent in center area (s), and the numbers of entries into center area was calculated for each group.

Light–dark transition test The light–dark transition test is widely used to quantify anxiety-related behavior of teleost species [152]. A rectangular acrylic tank (200 mm length $*$ 50 mm width $*$ 100 mm height) was divided equally into two compartments, left-half dark and right-half light (100 mm length each) (Figs. 6.3A and B). The light compartment consisted of white walls and bottom and was illuminated by the LED panel, while the dark one consisted of black walls and bottom and was shielded from light with an opaque lid. The front face of the tank consisted of a transparent acrylic panel for the camera recording. The tank was filled with the conditioned water to a height of 30 mm (Fig. 6.3A). Fish were individually introduced into the light compartment, and their behaviors were recorded for 10 min to calculate distance traveled (mm), the time spent in the light area (s), the time spent in the dark area (s), latency to entry into the dark (s), and the number of transitions between two compartments.

Mirror biting test Mirror approaching behavior is defined as a model of the social behavior in medaka [131]. The mirror-biting test apparatus consisted of white acrylic rectangular tank (200 mm length $*$ 90 mm width $*$ 70 mm height) with a transparent acrylic bar (5 mm square $*$ 90 mm height) in each four corner to attach a mirror (90 mm width $*$ 70 mm height) to the tank (Fig, 6.4A). The tank was filled with the conditioned water to a height of 20 mm. The bottom of the tank was virtually divided into 20 areas (10 mm length $*$ 90 mm width each), and stay in an area closet to the mirror was defined as the "mirror-biting" behavior (Fig. 6.4B). Fish were individually introduced into the center of tank, and their trajectories were recorded for 10 min to calculate the time of mirror biting (s), latency to enter the mirror biting area (s), the number of mirror biting, and distance traveled (mm).

Social interaction test Social interaction test is used to evaluate interactions between two fish in an open-field. The test was conducted using the same apparatus as the open-field test filled with the conditioned water to a height of 20 mm (Fig. 6.2A). A pair of two congeneric fish was introduced into the tank and their trajectories were recorded for 10 min. The frames at which two individuals were detected as a fish object were defined as the "contact" frames to calculate latency to the first contact (s), the time of contact (s), and the number of contact. Average distances between the two fish (mm) were also calculated using the XY coordinate data read out from the behavioral analysis software.

Data analysis

All statistical analysis were performed using GraphPad Prism 6 for Windows (GraphPad Software). Differences between treatments over time were analyzed using two-way repeated measured (RM) analysis of variance (ANOVA) followed by Sidak's multiple comparison test. Differences between treatments were analyzed using Welch's *t*-test, except latency outcomes were analyzed using survival curves and log-rank (Mantel-Cox) test [153, 154].

All data were presented as mean $\pm$ S.E.M. Three-dimensional reconstructions of spatiotemporal traces of fish were generated using Python 2.7 with the packages NumPy and Matplotlib. The X-, Y-coordinate, and time (frame count) that were obtained from XY coordinate output files from the behavioral analysis software were plotted on the X-, Y-, and Z-axis, respectively.

6.3 Results

Detailed results of statistical analysis in behavioral testing were described in the Appendix section.

In the diving test, the fluoxetine treatment did not affect distance traveled in the 10-min test in both male and female (Fig. 6.1E–G). Total duration of freezing was not affected in both male and female (Fig. 6.1J), while freezing during the first 1 min significantly decreased in both male (Fig. 6.1H) and female (Fig. 6.1I). Fluoxetine-treated fish exhibited more time spent in the top area (Fig. 6.1K–M), lower latency to enter the top area (Fig. 6.1N, O), increasing number of entries into the top area (Fig. 6.1P), and less time spent in the bottom area (Fig. 6.1Q). These behavioral alterations were clearly demonstrated by three-dimensional reconstructions of representative traces (Fig. 6.1C, D).

In the open-field test, three-dimensional reconstructions of representative fish traces are shown in Fig 6.2C, D. Fluoxetine-treated fish showed significantly decreasing distance traveled in the 15-min test in both male (Fig. 6.2E, G) and female (Fig. 6.2F, G) and shorter freezing duration in the first 1 min of the 15-min test (Fig. 6.2H, I) but not in the total 15-min test (Fig. 6.2J). Fluoxetine-treated fish spent significantly more time in the center area of the tank (Fig. 6.2M), especially during the first 2 or 3 min in both male (Fig. 6.2K) and female (Fig. 6.2L), respectively. Total number of entries into the center area was not affected in both male and female (Fig. 6.2P) but number of entries into the center during 2–3 min was significantly increasing in female (Fig. 6.2O).

In the light–dark transition test, fluoxetine-treated fish showed significantly decreasing distance traveled in the 10-min test (Fig. 6.3C). However, time spent in the light (Fig. 6.3D) and the dark area (Fig.

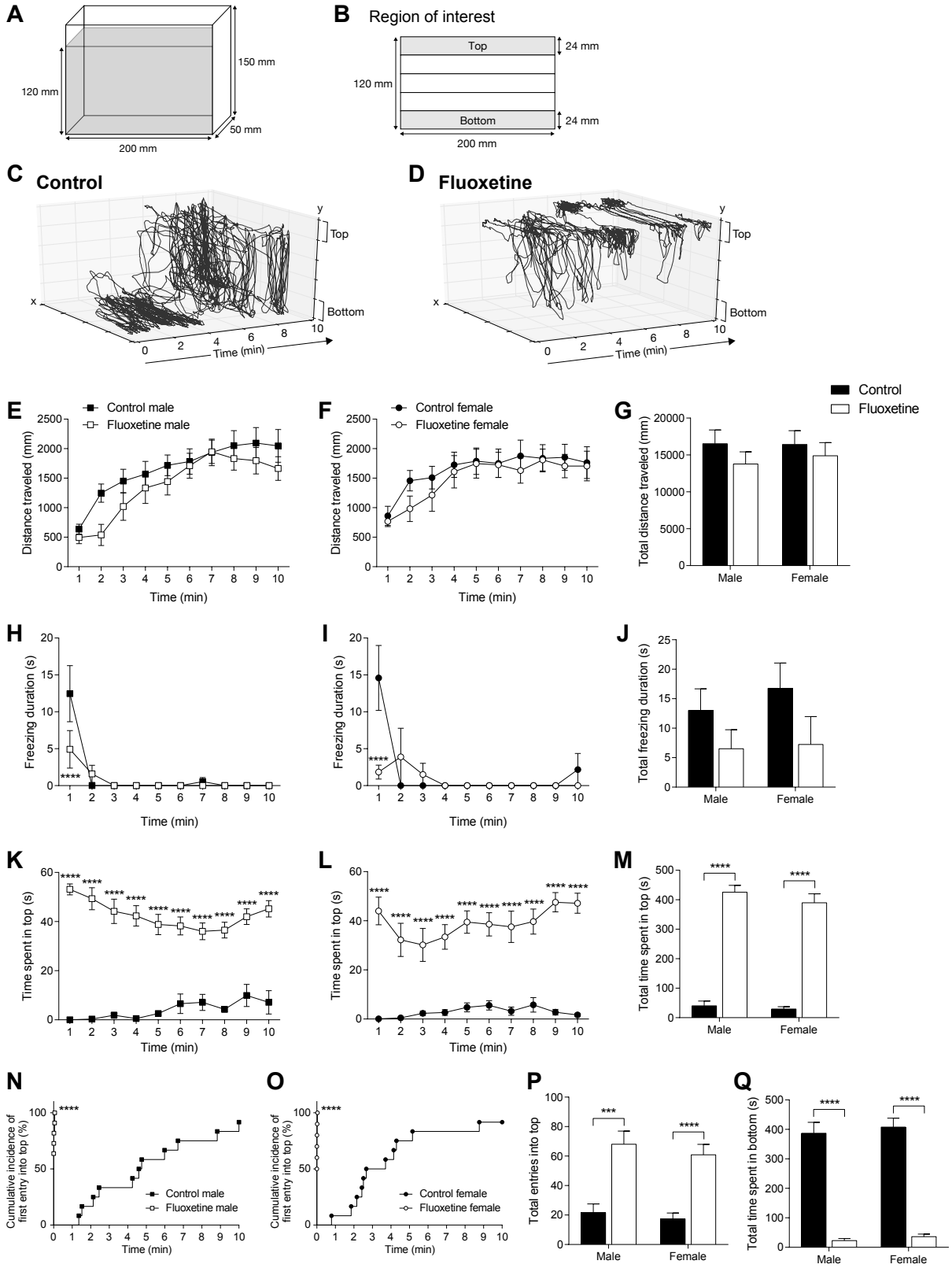

Figure 6.1. (Continued on the following page.)

Figure 6.1. Diving test. (A) An illustration of the test tank. The tank is filled with 1200 mL (120 mm depth) of conditioned water. (B) A region of interest (200 mm width $*$ 120 mm height) is vertically divided into five areas (200 mm width $*$ 24 mm height each) including "top" and "bottom" area. (C, D) Representative traces of control (C) and fluoxetine-treated (D) fish. The three-dimensional traces were generated by plotting coordinate data of fish traces across the time of the test. (E–P) Behavioral effect of fluoxetine treatment on medaka tested in the diving test. (E–G) Distance (mm) traveled for 1 min bins in male (E) and female (F) fish, and total distance (mm) traveled for 10 min (G). (H–J) Duration (s) of freezing behavior for 1 min bins in male (H) and female (I) fish, and total duration (s) of freezing for 10 min (J). (K-M) Time spent (s) in the top area for 1 min bins in male (K) and female (L) fish, and total time spent (s) in the top area for 10 min (M). (N, O) Cumulative incidence of the first entry into the top area in male (N) and female (O). (P) Total number of entries into the top area. (Q) Total time spent (s) in the bottom area. Control male, n = 12; Control female, n =12; Fluoxetine male, n = 11; Fluoxetine female, n = 10. Data are shown as mean $\pm$ S.E.M. Differences between treatments over time were analyzed by two-way repeated measured ANOVA and Sidak's multiple comparison test; differences between treatments were calculated by Welch's t-test. Symbols indicate significant differences compared to controls. Cumulative incidence of the first entry into the top area was analyzed using survival curves and log-rank (Mantel-Cox) test. $*P < 0.05$; $**P < 0.01$; $***P < 0.001$; $****P < 0.0001$.

6.3E), and latency to enter the dark area (Fig. 6.3F, G) were unaffected by the fluoxetine treatment. The fluoxetine treatment also produced significantly decreasing number of transitions between the areas in both male and female (Fig. 6.3J). In female, the number of transitions during 2–4 min were significantly decreased (Fig. 6.3I).

In the mirror-biting test, the fluoxetine treatment produced significantly less time of mirror biting (Fig. 6.4G), especially during the anterior half of the 10-min test in both male (Fig. 6.4E) and female (Fig. 6.4F). This behavioral alteration was also clearly demonstrated in three-dimensional reconstructions of representative fish (Fig. 6.4C, D). The fluoxetine administration did not affect latency to the first mirror biting (Fig. 6.4H, I) and number of mirror biting (Fig. 6.4J). However, distance traveled in the 10-min test was significantly decreasing in the fluoxetine-treated fish (Fig. 6.4K).

In the two-fish social interaction test, average distance between two fish was not affected by the fluoxetine treatment (Fig. 6.5A). The fluoxetine treatment produced significantly longer latency to the first contact (Fig. 6.5B, C). Fluoxetine-treated fish did not show any significant difference in total contact time (Fig. 6.5F) but only the female fish showed significantly decreasing contact time during the 2–3 min of the 10-min test (Fig. 6.5E). Number of contact was significantly reduced in the male fish (Fig. 6.5G, I) but not in the female (Fig. 6.5H, I).

6.4 Discussion

Here, I successfully detected significant behavioral alterations in medaka adult fish induced by chronic fluoxetine administration using a newly developed behavioral testing system with the five paradigms. Because medaka serves as an excellent model for toxicology, previous studies on the effects of fluoxetine using medaka were mainly focused on toxicological viewpoints such as reproduction, larval toxicity, uptake, accumulation and depuration [146–149]. Although Chrffre *et al.* reported the behavioral effects of fluoxetine on medaka, they evaluated only locomotion induced by changes in light intensities using the larval fish [145]. This is the first report to assess the effects of chronic fluoxetine treatment on the anxiety-related and social behaviors in medaka adult fish by combining with a number of paradigms. These results indicate that medaka and the behavioral testing system for assessing their anxiety-related and social behaviors is enough sensitive to assess and screen the pharmaceutical effects and toxicity of not only SSRIs but also other pharmacological agents from the aspect of animal behaviors.

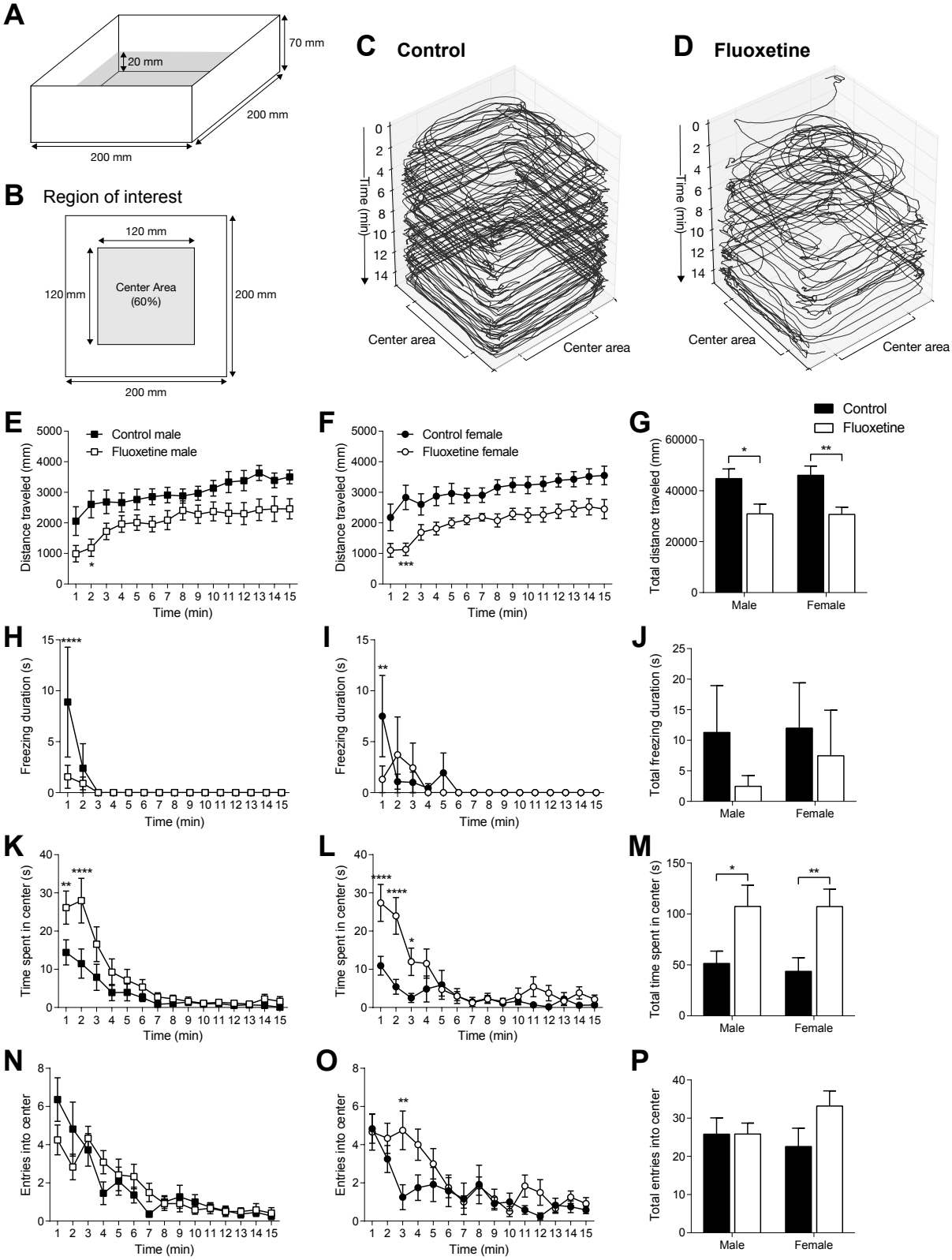

Figure 6.2. (Continued on the following page.)

Figure 6.2. Open-field test. (A) An illustration of the test tank. The tank is filled with 800 mL (20 mm depth) of conditioned water. (B) A region of interest (200 mm $*$ 200 mm) contains a 60 % center area (120 mm $*$ 120 mm). (C, D) Representative traces of control (C) and fluoxetine-treated (D) fish. The three-dimensional traces were generated by plotting coordinate data of fish traces across the time of the test. (E–P) Behavioral effect of fluoxetine treatment on medaka tested in the open-field test. (E–G) Distance (mm) traveled for 1 min bins in male (E) and female (F) fish, and total distance (mm) traveled for 15 min (G). (H–J) Duration (s) of freezing behavior for 1 min bins in male (H) and female (I) fish, and total duration (s) of freezing for 15 min (J). (K–M) Time spent (s) in the center area for 1 min bins in male (K) and female (L) fish, and total time spent (s) in the center area for 15 min (M). (N–P) Number of entries into the center area for 1 min bins in male (N) and female (O) fish, and total number of entries into the center area for 15 min (P). Control male, n = 11; Control female, n =12; Fluoxetine male, n = 12; Fluoxetine female, n = 12. Data are shown as mean $\pm$ S.E.M. Differences between treatments over time were analyzed by two-way repeated measured ANOVA and Sidak's multiple comparison test; differences between treatments were calculated by Welch's t-test. Symbols indicate significant differences compared to controls. $*P < 0.05$; $**P < 0.01$; $***P < 0.001$; $****P < 0.0001$.

SSRIs are typically used as first-line pharmacotherapy in anxiety disorders [155] and have also been demonstrated to have anxiolytic effects in rodent models [156]. In teleost fish, the diving test is one of the most well established paradigms for assessing anxiety-like behavioral responses and chronic fluoxetine treatment has been reported to induce anxiolytic responses [141, 143, 144]. Chronic treatment with fluoxetine in medaka induced behavioral changes such as an overall increase time spent in the top area, shorter latency to the first entry into the top area, a larger number of top transitions (Fig. 6.1), similar to previous reports in zebrafish. These results indicate that the diving test in medaka has successfully detected anxiolytic responses induced by chronic fluoxetine treatment and would become a robust model of anxiety-like behavior as well as zebrafish.

The open-field test is a popular paradigm to assess anxiety-like behavior in rodents [157]. Medaka with chronic fluoxetine treatment exhibited an increase time spent in the center area of the open-field, especially during the first a few minutes of the test (Fig. 6.2K–M), which is in agreement with anxiolytic effects found in juvenile Chinook salmon [139] and BALB/c mice [156] treated chronically with fluoxetine. These alterations of the place preferences in the open-field were also considered as an anxiolytic responce in zebrafish, which was found in fish treated with α-fluoromethylhistidine, the inhibitor of histamine production [150]. In fact, histamine administration decreased the activity of serotonergic neurons in rat hypothalamus [157], suggesting that α-fluoromethylhistidine may have the same effect as fluoxetine on behaviors regulated by serotonergic neurons. These findings indicate that an increase time spent in the center area would be an anxiolytic response in medaka and the place preference in the open-field might be useful indicator of anxiety in medaka. Additionally, in both the diving and open-field test, fluoxetine-treated fish significantly reduced duration of freezing during the first 1 minute. Anxiogenic treatments in zebrafish, such as administration of the alarm substance and mutation of the glucocorticoid receptor, increased durations of the freezing with decreased expression of a serotonin transporter gene *slc6a4a* [158, 159] and the responses were attenuated by fluoxetine administration [159, 160]. These facts support that the shorter freezing duration could be considered as one of the anxiolytic responses in medaka.

The light–dark preference has been already established as an anxiety model in rodents, based on the innate aversion to brightly illuminated areas and spontaneous exploratory behavior in response to mild stressors [161]. A wide range of teleost species also have the innate aversion to the illuminated environment [162, 163], which was used to evaluate anxiolytic effects such as chronic fluoxetine and buspirone as an increase time spent in the lighted compartment [142]. However, in this study, medaka spent more time in the bright area than the dark with or without chronic fluoxetine treatment (Fig. 6.3D, E). This result shows that the innate aversion of the bright areas in medaka, at least the d-rR

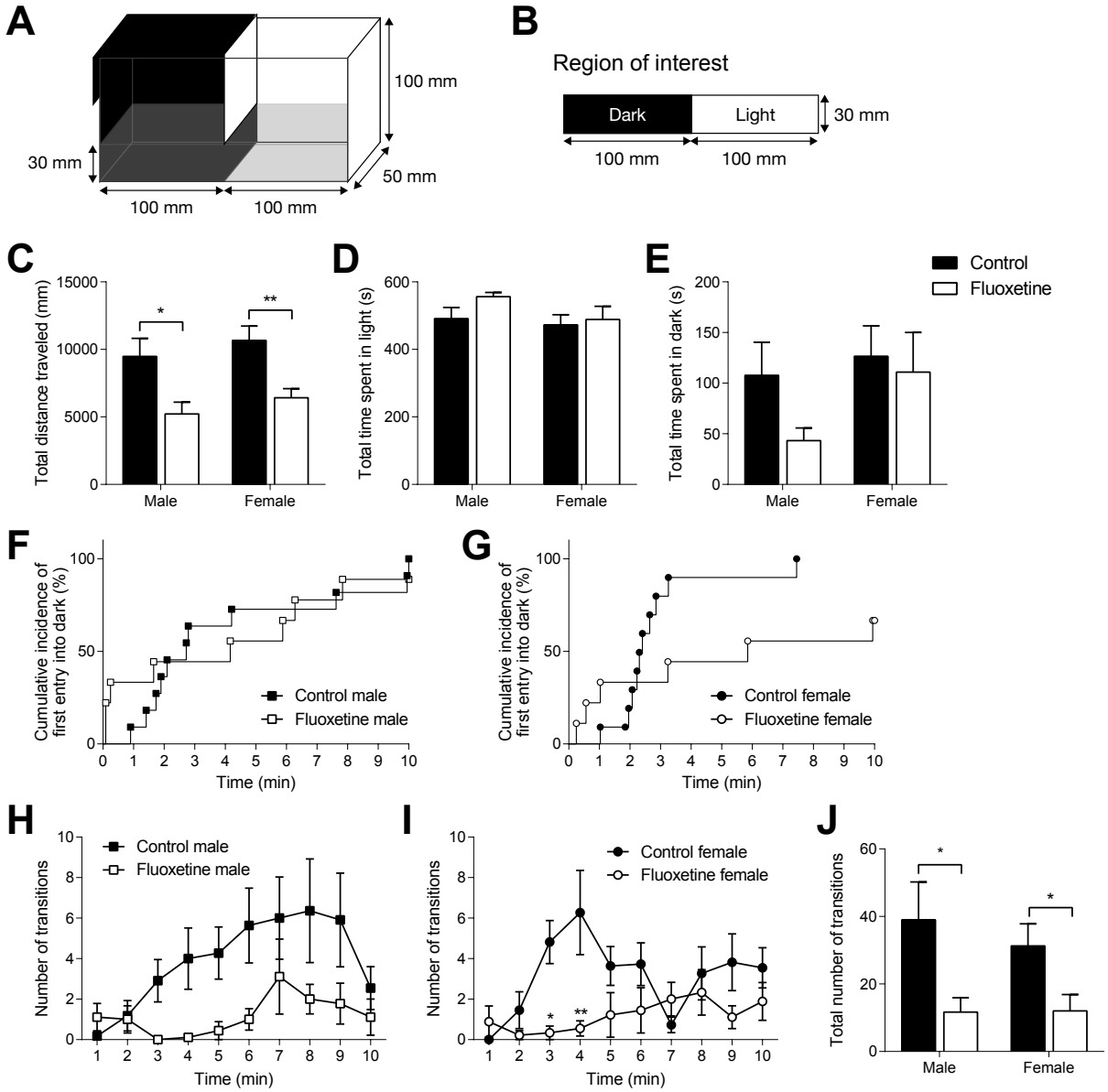

Figure 6.3. Light/dark transition test. (A) An illustration of the test tank. The tank is filled with 600 mL (30 mm depth) of conditioned water. (B) A region of interest (200 mm width $*$ 30 mm height) is divided into the "dark" and the "light" areas (100 mm width $*$ 30 mm height each). (C–I) Behavioral effect of fluoxetine treatment on medaka tested in the light/dark transition test. (C) Total distance (mm) traveled for 10 min. (D, E) Total time spent (s) in the light (D) and dark (E) area. (F, G) Cumulative incidence of the first entry into the dark area in male (F) and female (G). (H–J) Number of transitions between the areas for 1 min bins in male (H) and female (I) fish, and total number of transitions between the areas for 10 min (J). Control male, n = 11; Control female, n =11; Fluoxetine male, n = 9; Fluoxetine female, n = 9. Data are shown as mean $\pm$ S.E.M. Differences between treatments over time were analyzed by two-way repeated measured ANOVA and Sidak's multiple comparison test; differences between treatments were calculated by Welch's t-test. Symbols indicate significant differences compared to controls. Cumulative incidence of the first entry into the dark area was analyzed using survival curves and log-rank (Mantel-Cox) test. $*P < 0.05$; $**P < 0.01$; $***P < 0.001$; $****P < 0.0001$.

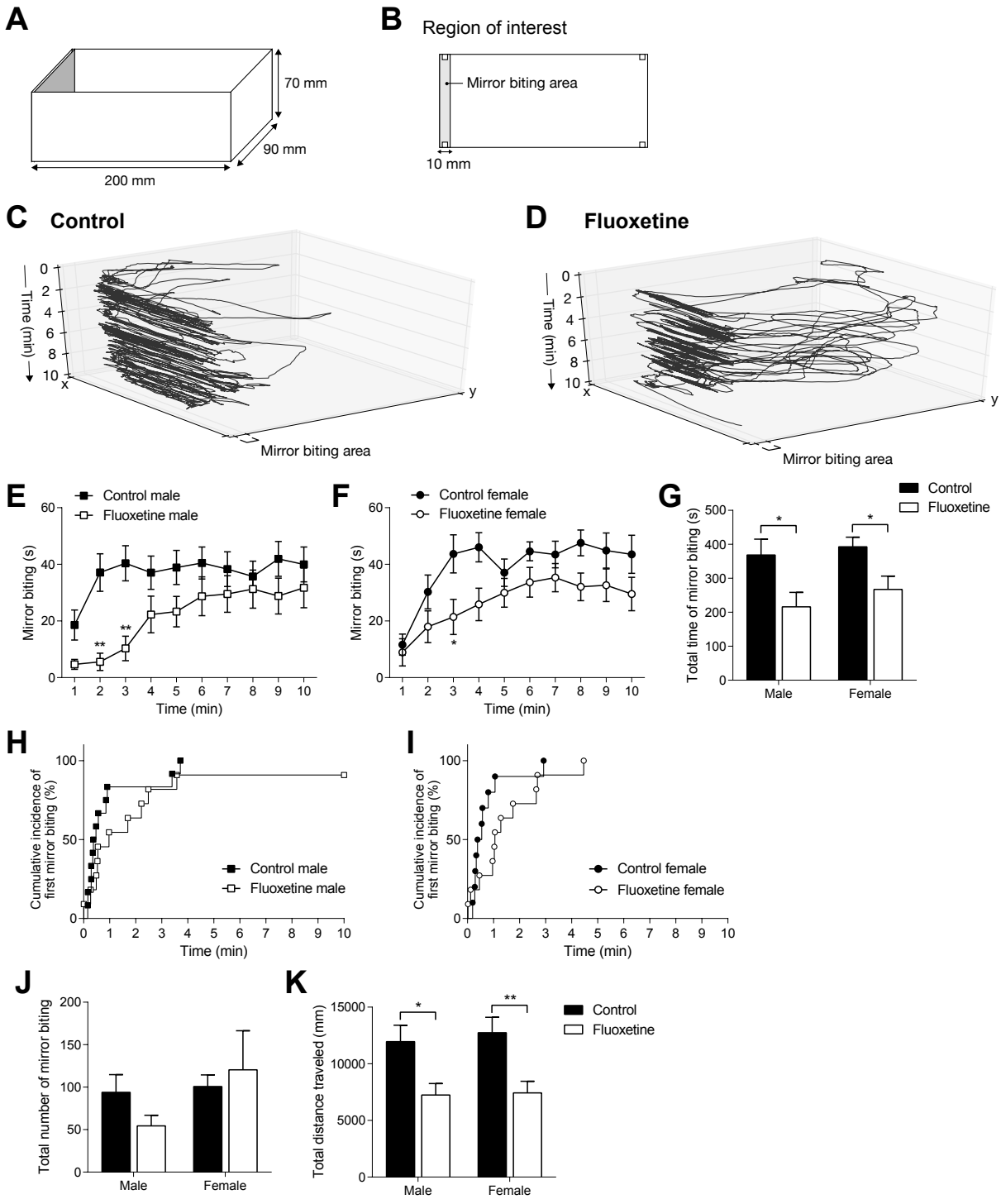

Figure 6.4. (Continued on the following page.)

Figure 6.4. Mirror-biting test. (A) An illustration of the test tank. A mirror is attached to the inner side wall of the tank. The tank is filled with 360 mL (20 mm depth) of conditioned water. (B) An area closest to the mirror (10 mm width $*$ 90 mm height) is defined as the mirror biting area in a region of interest (200 mm width $*$ 90 mm height). (C, D) Representative traces of control (C) and fluoxetine-treated (D) fish. The three-dimensional traces were generated by plotting coordinate data of fish traces across the time of the test. (E–J) Behavioral effect of fluoxetine treatment on medaka tested in the mirror-biting test. (E–G) Time spent (s) in the mirror biting area for 1 min bins in male (E) and female (F) fish, and total time spent (s) in the mirror biting area for 10 min (G). (H, I) Cumulative incidence of the first mirror biting in male (H) and female (I). (J) Total number of entries into the mirror biting area for 10 min. (K) Total distance (mm) traveled for 10 min. Control male, $n = 12$; Control female, $n = 10$; Fluoxetine male, $n = 11$; Fluoxetine female, $n = 11$. Data are shown as mean $\pm$ S.E.M. Differences between treatments over time were analyzed by two-way repeated measured ANOVA and Sidak's multiple comparison test; differences between treatments were calculated by Welch's t-test. Symbols indicate significant differences compared to controls. Cumulative incidence of the first mirror biting was analyzed using survival curves and log-rank (Mantel-Cox) test. $*P < 0.05$; $**P < 0.01$; $***P < 0.001$; $****P < 0.0001$.

strain, could be not affected by fluoxetine but also be lost congenetically. In fact, it has been reported that the eastern mosquitofish (*Gambusia holbrooki*) did not present a preference for the dark environments, contrary to other poeciliidae species such as the guppy (*Poecilia reticulata*) and the swordtail (*Xiphophorus helleri*) [152], and medaka also has polymorphisms among strains or populations in some behavioral traits [133, 164]. These indicate the need for a more careful discussion in medaka about the innate aversion of illuminated environments and the usability of the light–dark transition paradigm to assess their anxiety.

Fluoxetine is known to affect social behaviors including social anxiety [165] and impulsive aggression [166], and previous studies have been reported that fluoxetine also altered aggressive behavior in teleost [136–138]. In this study, to assess the effects of chronic fluoxetine treatment on the social behaviors, I performed two behavioral paradigms: the mirror-biting test and the social interaction test. The mirror approaching behavior in medaka is considered as a simple and robust model of socially induced anxiety [131]. The mirror biting time was significantly decreased by chronic treatment of fluoxetine in both sexes (Fig. 6.4E–G). This effect is consistent with the behavioral alteration induced by administration of an anxiolytic agent diazepam [131] that decreases the stress response as measured by cortisol level as well as fluoxetine in zebrafish [167]. These indicate that fluoxetine decreased the socially induced anxiety in medaka as well as the previous reports in humans and rodents.

The social interaction test was used to investigate the effects on direct interactive behaviors between two congeneric individuals (male-to-male or female-to-female). Chronic fluoxetine treatment in medaka induced longer latency to the first contact (Fig. 6.5B, C), a shorter contact time in female (Fig. 6.5E), and a decrease number of contact in male (Fig. 6.5G, I). This result suggests that chronic treatment with fluoxetine induces a decrease in social interactions, which could agree with a decreased territorial aggression by chronic fluoxetine treatment in male bluehead warasses [136]. However, as I defined all encounters between the tested two fish as the "contact" to quantify the behaviors automatically, the social interaction in this paradigm includes a wide range of social behaviors such as aggression, defense, and sociability. This indicates that manual observation and categorization of the social behaviors as previously reported in aggressive behavior of medaka [127] will be required for a more detailed consideration of the effects of chronic fluoxetine treatment on the social behaviors.

I also found that fish chronically treated with fluoxetine showed a significantly short distance traveled in the open-field test (Fig. 6.2E–G), the light–dark transition test (Fig. 6.3C), and the mirror-biting test (Fig. 6.4K) but not in the diving test (Fig. 6.1E–G). Since all 3 paradigms that were found the significant differences use the shallow test tanks (20-30 mm depth of water) contrary to the deepwater tank in the diving test (120 mm depth), chronic fluoxetine treatment reduces horizontal locomotor ac-

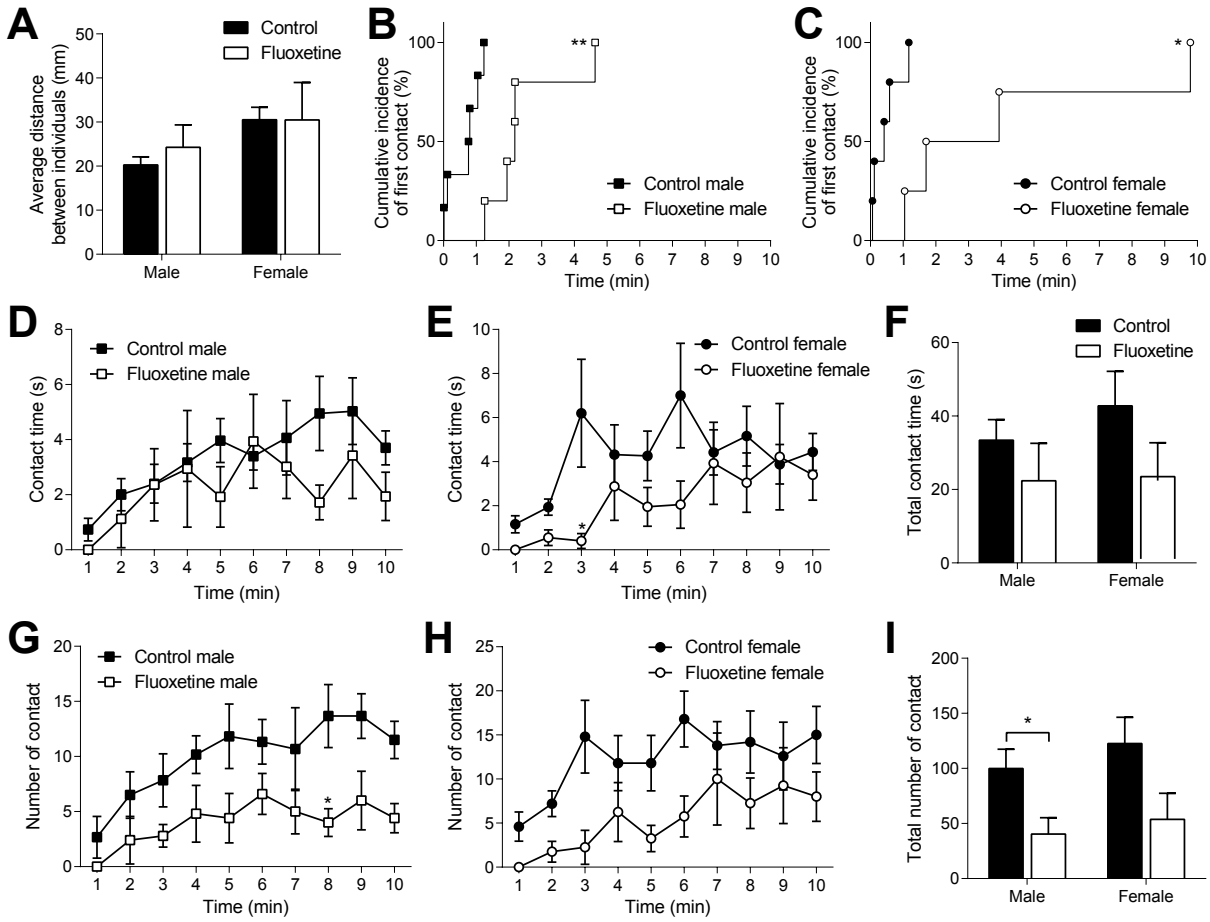

Figure 6.5. Two-fish social interaction test. (A) Average distance (mm) between the test individuals for 10 min. (B, C) Cumulative incidence of the first contact between fish in male (B) and female (C). (D–F) Time (s) of contacts between fish for 1 min bins in male (D) and female (E), and total time (s) of contacts for 10 min (F). (G–I) Number of contacts between fish for 1 min bins in male (G) and female (H), and total number of contacts for 10 min (I). Control male, $n = 6$; Control female, $n = 5$; Fluoxetine male, $n = 5$; Fluoxetine female, $n = 4$. Data are shown as mean $\pm$ S.E.M. Differences between treatments over time were analyzed by two-way repeated measured ANOVA and Sidak's multiple comparison test; differences between treatments were calculated by Welch's *t*-test. Symbols indicate significant differences compared to controls. Cumulative incidence of the first social interaction was analyzed using survival curves and log-rank (Mantel-Cox) test. $^{*}P < 0.05$; $^{**}P < 0.01$; $^{***}P < 0.001$; $^{****}P < 0.0001$.

tivity but not vertical activity. Given these different effects between horizontal and vertical locomotor, a decreased horizontal activity could be caused by alterations of exploration behavior and/or place preference in the shallow tanks rather than impairment of motor functions. Decreased horizontal activities induced by chronic fluoxetine treatment were also observed in the juvenile Chinook salmon [139] and the sheepshead minnow [140], indicating that this effect would be common to a wide range of teleost species. However, identifying a specific cause for the effects will require some additional tests to assess motor function correspond to rotarod and footprint analysis in rodents [168].

Previous studies reported that fluoxetine exhibited the effects that was significantly different between male and female on the efficacy in depressed patients [169], on the behaviors in mice [170], and on neuroplasticity and pharmacokinetics in mice [171]. Since medaka shows sexually dimorphic expressions of *tph1* and *tph2* genes involved in serotonin synthesis in the brain [172], fluoxetine may

also have sexually different effects on the behaviors of teleost fish species; however, there was little evidence for the different effects. In this study, both male and female fish were subjected to all five paradigms, revealing that there was no significant difference in most behavioral parameters, but I found differences in increased center entries of female in the open-field test (Fig. 6.2O) and decreased contact time of female (Fig. 6.5E) and decreased contact numbers of male (Fig. 6.5G) in the social interaction test. Although further detailed considerations, especially at the cellular and/or tissue levels, will be required to discuss the significance of these different parameters, my results emphasize the importance of behavioral assessment using both sexes for further understanding of the pharmaceutical effects in teleost fish.

The behavioral characterization of medaka using the behavioral testing system will allow us to assess the behavioral effects of not only the pharmacological treatments but also genetic manipulations. Recently, the advanced molecular genetic techniques such as targeted genome editing with targetable nuclease systems [81, 112, 134] and spatiotemporal control of transgenes by Cre/loxP system [173] has been available in medaka. In combination with these techniques, the testing system will become a powerful tool for showing function of specific genes and neural circuits in complex behaviors of adult fish. Furthermore, medaka also provides unique genetic resources such as a many highly inbred strains and closely related species native to different habitats [174]. Behavioral characterization of these strains and/or species with the testing system could contribute to an understanding of genetic control of the anxiety-related and social behaviors.

Chapter 7

Behavioral phenotyping of tph2-deficient mutant fish generated by TALENs

7.1 Introduction

Comprehensive behavioral analysis of knockout mice generated by homologous recombination in ES cells is one of the most successful strategies to identify the functional roles of many genes in the brain and dissect the genetic basis of animal complex behaviors [175]. Recently, medaka have become a neurobehavioral model fish because they exhibit complex social and/or visually-evoked behaviors; however, there have been few studies in medaka that comprehensively evaluated the behavioral effects of genetic manipulations by the multitiered phenotyping strategies. Therefore, in the last chapters, I demonstrated an automated behavioral testing system for small laboratory fish by assessing the behavioral alterations casued by the chronic fluoxetine treatment, whose results indicates that the system will enable us to analyze the phenotypes of mutant strains for understanding of gene functions in the brains and the behaviors. Also, I described efficient and simple methods for targeted mutagenesis in medaka using targetable nuclease systems, which allow us to easily generate mutant strains harboring the mutantion(s) of genes of interest. These suggests that a combination of the behavioral testing system and the targeted mutagenesis will make a significant contribution to the reverse genetical understanding of the gene functions in terms of the behaviors.

In this chapter, to show the utility of the established techniques to understand the behavioral functions of genes, I demonstrated the neurobehavioral phenotyping of a medaka mutant that had a frameshifted deletion in the *tph2* gene induced by transcription activator-like (TAL) effector nucleases (TALENs). The *tph2* gene encodes a tryptophan hydroxylase, an enzyme involved in the synthesis of serotonin (5-hydroxytryptamine; 5-HT). 5-HT is a bioactive monoamine that acts a neurotransmitter the central nervous system (CNS) as well as a hormone in the peripheral organ systems including cardiovascular, pulmonary, gastrointestinal, and genitourinary systems [176]. Teleost fishes generally have two major sites for serotonergic neurons (neurons containing 5-HT as a neurotransmitter) — the raphe nuclei in the brain stem and posterior tuberculum/hypothalamic populations [177–181]. Previous works in zebrafish and medaka reported that the *tph2* gene is expressed by serotonergic neurons of the raphe nuclei [172, 182]. In zebrafish, the serotonergic neurons in the raphe nuclei send axonal projections to a number of brain regions including telencephalon, diencephalon, and mesencephalon [183]. This indicates that those neurons involve in a wide range of behaviors in teleost fishes because the raphe serotonergic neurons in mammals, which innervate much of the rest of the CNS by diffuse projections [176], regulate a variety of behaviors, such as circadian rhythm, sleep–wake cycle, appetite,

aggression, sexual behavior, sensorimotor reactivity, and learning [184]. In fact, some pharmacological reports exhibited that 5-HT plays an important role in modulating various behaviors in teleost fishes, such as locomotion [185–188], aggression [136,189,190], and fear/anxiety [141,154]. However, there are few report on the genetic dissection of serotonergic functions and therefore the serotonergic functions in behaviors of teleost fishes have remain largely unknown. Here, behavioral alterations resulting from the 5-HT deficiency in the raphe nuclei of the *tph2* mutant fish were analyzed by five behavioral paradigms (diving, open-field, light–dark transition, mirror approaching, and social interaction) for the assessment of locomotor activities, anxiety-related behaviors, and social behaviors.

7.2 Materials and Methods

Fish and housing conditions

The d-rR strain (closed colony) [66] of medaka was used in this study. Embryos were raised in embryo culture medium (0.1% NaCl, 0.003% KCl, 0.004% $CaCl_2{\cdot}2H_2O$, and $MgSO_4{\cdot}7H_2O$) on a 14/10 h light/dark cycle at 26 ℃. Hatched fish were raised in groups of 8–10 fish per 2-L tank with recirculating filtered water at 27 ℃. The fish tanks were illuminated by white fluorescent tube on a 14/10 h light/dark cycle. The fish were fed newly hatched *Artemia* nauplii and commercial powdered foods (for larval fish: Sweetfish Super Gold #0, Oriental Yeast; for juvenile and adult fish: Otohime B2, Marubeni Nisshin Feed, for juvenile and adult fish) once or twice a day. This work was conducted using the protocols approved by the Animal Experimentation Committee of Kyoto University (permission number: 26-71).

Targeted gene disruption using TALENs

Potential TALEN target sites in the sixth exon of *tph2* gene (ENSORLT00000000279.1) were searched using the TALEN Targeter program (https://tale-nt.cac.cornell.edu/node/add/talen) [67]. TAL repeats were assembled by a modified Golden Gate assembly method as described previously [81]. Capped RNA encoding each TALEN was transcribed using the mMessage mMachine SP6 kit (Life Technologies) followed by purifying with the RNeasy mini kit (QIAGEN). A pair of TALENs (150 ng/μL) was injected into the fertilized eggs of the d-rR strain by a microinjection method [39].

The *tph2* mutant were genotyped by a HMA–MultiNA method [112] using PCR primers 5′-TGACCCATACTCCCCACAGT-3′ and 5′-GCCACAGTGTTTGGTGAGAA-3′. Sequences of the identified mutant alleles were determined by direct sequencing of PCR product amplified using primers 5′-AGGGTTTCAAGGACGAGGTT-3′ and 5′-TCTCGAGGAGACAGGTAGCC-3′.

Immunohistochemistry

For whole-mount staining of embryos, embryos whose chorion were removed using the hatching enzyme were fixed with 4% paraformaldehyde (PFA) in phosphate buffered saline (PBS) at 4 ℃ overnight. Fixed embryos were rinsed in PBS containing 0.005% Tween-20 (PBST) and then dehydrated in a graded methanol series (25, 50, 75, and 100%). The embryos were rehydrated in a reverse methanol series, rinsed in water, permeabilized by cold acetone at -20 ℃ for 20 min, re-rinsed in water, and rinsed in PBST. The embryos were then blocked at 4 ℃ for overnight in PBS with 0.3% Triton X-100, 1% dimethylsulfoxide (DMSO), 2% normal goat serum (NGS), and 0.1% bovine serum albumin (BSA). The blocked embryos were incubated in a primary antiserum containing a serotonin rabbit antibody (ImmunoStar, #20080, 1:500) at 4 ℃ for orvernight, washed with PBST, and then incubated in a secondary antiserum containing a donkey anti-rabbit IgG (H+L) secondary antibody, Alexa Fluor 488 conjugate (Life Technologies, Carlsbad, CA, #R37118, 1:500) at 4 ℃ for overnight. The embryos were washed with PBST and cleared in a glycerol series (30, 70, and 100%). The fluorescent images were captured using a fluorescence stereomicroscope MZFLIII with GFP2 filter set

(Leica Microsystems) with a digital CCD camera VB-7010 (KEYENCE).

For adult brains, heads of fish anesthetized deeply with MS-222 (Sigma, St. Louis, MO) were fixed with Bouin's solution for a day at room temperature (RT), dehydrated with a series of the Tissue Dehydration Solution A (Wako Pure Chemical Industries, Osaka, Japan) (50, 70, and 100%), and embedded in paraffin. Serial coronal sections of 10 μm thickness were cut throughout the brain. The paraffin sections were deparraffinized with xylen and Tissue Dehydration Solution A and then rehydrated with PBS. The sections were blocked in PBS with 0.25% Triton X-100 (PBSTx) containing 2% NGS for an hour at RT, incubated in a primary antiserum containing a serotonin rabbit antibody (ImmunoStar, #20080, 1:2000) for an hour at RT, washed with PBSTx, then incubated in a secondary antiserum containing an anti-rabbit IgG, alkaline phospatase (AP)-linked antibody (Cell Signaling Technology, Danvers, MA, 1:1000). Signals were developed using nitroblue tetrazolium and 5-bromo-4-chloro-3-indolyl phosphatate in the NTMT buffer containing 100 mM NaCl, 100 mM Tris-HCl (pH9.5), 50 mM $MgCl_2$, and 0.1% Tween-20. The sections were imaged using a light transmission microscope (BX51, OLYMPUS) with a digital CCD camera (DP72, OLYMPUS).

Neurochemical assessment by liquid chromatography with tandem mass spectrometry (LC-MS/MS)

Each brain was dissected from adult fish anesthetized deeply with MS-222 and immediately stored at -80 ℃ until the following extraction step. The brain was homogenized in 100 μL of the ice-cold extraction buffer containing 4% $HClO_4$, 0.2% EDTA, and 0.05% $NaHSO_3$ followed by centrifugation at 20,000 x g, for 20 min. The pellet was solubilized in 100 μL of 0.5 N NaOH at 60 ℃ for 20 min and the protein content was quantified using Micro BCA Protein Assay Kit (Thermo Scientific, Rockford, IL). The supernatant was subjected to the neurochemical quantification. LC-MS/MS analysis was performed using a high performance liquid chromatograph Prominence system (Shimadzu) coupled with a triple quadrupole mass spectrometer LCMS-8040 with an ESI interface (Shimadzu). The neurochemicals were separated on a reverse-phase porous ODS column Unison UK-C18 (particle size: 3 μm, internal diameter: 2.0 mm, length: 150 mm, Imtakt) at 40 ℃ with a binary gradient elution using 0.1% formic acid (solvent A) and 80% acetonitrile (solvent B) at a flow rate of 0.2 mL/min. The gradient profile was as follows: 0–15 min, 0–25% B; 15–20 min, 25–100% B; 20–25 min, 100% B; 25–25.01 min, 100–0% B; and 25.01–40 min, 0% B. Serotonin (5-HT), 5-hydroxytruptophan (5-HTP), tryptophan (Trp), and dopamine (DA) were detected from each brain homogenate by the multireaction monitoring (MRM) whose conditions were optimized using the standard chemicals obtained from Nacalai Tesque. The total ion current of three fragment ions resulting from each neurochemical (5-HT: m/z 115.10, 117.10, and 132.10 from 177.20; 5-HTP: m/z 162.00, 134.10, and 77.05 from 221.20; Trp: m/z 146.05, 118.10, and 91.10 from 205.25; DA: m/z 91.05, 65.05, and 119.05 from 154.20). The amount of each neurochemical was calibrated using a standard curve plotted for four different amount of the standard chemical (0.5, 0.1, 0.05, 0.01 ng).

Behavioral testing

The body length of each fish at 8 weeks post hatching (wph) was measured by capturing images of fish with a ruler using a digital camera (CX2, Ricoh) and quantifying the numbers of pixels using ImageJ software (National Institutes of Health; http://imagej.nih.gov/ij/). Subsequently, each fish was subjected to 5 behavioral paradigms (diving, open-field, light–dark, mirror, and social interaction) according to procedures and apparatuses that have been previously described [191].

Statistical analysis

All graphing data are presented as mean ± S.E.M. Statistical analysis were performed using GraphPad Prism 6 for Windows (GraphPad Software). Differences between treatments over time were analyzed using two-way repeated measured (RM) analysis of variance (ANOVA) followed by Sidak's multiple

comparison test. Differences between treatments were analyzed using Welch's *t*-test, except latency outcomes were analyzed using survival curves and log-rank (Mantel-Cox) test.

7.3 Results

Targeted disruption of *tph2* gene using TALENs

By searching a medaka genome database, we found at least three genes encoding tryptophan hydroxylase, *tph1a* (Ensembl gene number ENSORLG00000005962), *tph1b* (ENSORLG00000015541) and *tph2* (ENSORLG00000000223), in the genome. Kawabata et al. previously showed that the *tph2* gene is an ortholog of the human *TPH2* and is expressed in the raphe nuclei of the brain stem, dorsal posterior nucleus in the thalamus, and the anterior part of the medulla oblongata [172]. To disrupt the tph2 function, we designed a pair of TALENs that can recognize and cleave a target site on the sixth exon (Fig. 7.1A) and injected with capped RNAs encoding these TALENs into the fertilized eggs. Each injected fish was mated with a wild-type fish, and then fish harboring a 13 bp deletion ($tph2^{\Delta 13}$) on the target exon were identified in the F1 generation (Fig. 7.1B). This deletion causes a frame-shift and results in a premature stop codon with additional 4 residues of an altered sequence (Fig.7.1B) that would be expected to truncate the tryptophan hydroxylase lacking part of the catalytic domain (Biopterin_H, NCBI accession number pfam00351) (Fig. 7.1C). By intercrossing between F1 fish that heterozygously carries the deletion ($tph2^{+/\Delta 13}$), I obtained a F2 family containing homozygous mutant fish ($tph2^{\Delta 13/\Delta 13}$) and found that the homozygous mutant fish are viable and fertile (data not shown).

Deficiency of 5-HT synthesis in the raphe nuclei of $tph2^{\Delta 13/\Delta 13}$ fish

To evaluate the enzymatic activity of the truncated tph2 protein, 5-HT in the serotonergic neurons of the brain were detected in both $tph2^{+/+}$ and $tph2^{\Delta 13/\Delta 13}$ fish by immunohistochemistry using an anti-5-HT antibody. Whole-mount immunostaining in 4-dpf embryos showed that the $tph2^{\Delta 13/\Delta 13}$ embryos lost a 5-HT-positive population in the raphe nuclei of the brain stem but not in the pineal gland (Fig. 7.2). For further consideration of 5-HT distribution in the brain, the coronal sections of the adult brains were immunohistochemically stained. While the $tph2^{+/+}$ brain exhibited the 5-HT positive signals in the neuronal cells of the raphe nuclei (Fig. 7.3A), the $tph2^{\Delta 13/\Delta 13}$ brain lost the signals (Fig. 7.3B). Additionally, a number of 5-HT-positive axons were found in the telencephalon of the $tph2^{+/+}$ brain (Fig. 7.3C) but not of the $tph2^{\Delta 13/\Delta 13}$ brain (Fig. 7.3D). On the other hand, there were no differences in the 5-HT-positive populations in the pineal gland (Fig. 7.3E, F), the pituitary gland (Fig. 7.3G, H), and the hypothalamus such as the posterior parvocellular preoptic nucleus (PPp) (Fig. 7.3I, J) and the posterior recess nucleus (NRP) (Fig. 7.3K, L), where other tryptophan hydroxylase genes (*tph1a* and/or *tph1b*) express [172, 192].

Subsequently, for the quantitative assessment of the tph2 enzymatic activity, two metabolites (5-HTP and 5-HT) and a substrate (tryptophan) of the tryptophan hydroxylase were quantified in each wild-type or mutant brain using the LC-MS/MS with a MRM method. The $tph2^{\Delta 13/\Delta 13}$ fish showed significant reductions of the metabolites 5-HT (male: $t = 7.855$, $df = 9.479$, $P < 0.0001$; female: $t = 5.530$, $df = 7.845$, $P = 0.0006$; Fig. 7.4A) and 5-HTP (male: $t = 2.872$, $df = 9.933$, $P = 0.0167$; female: $t = 3.639$, $df = 9.979$, $P = 0.0046$; Fig. 7.4B). On the other hand, the amount of tryptophan was significantly increased in the $tph2^{\Delta 13/\Delta 13}$ brain (male: $t = 4.080$, $df = 9.969$, $P = 0.0022$; female: $t = 2.292$, $df = 9.737$, $P = 0.0455$; Fig. 7.4C). The dopamine levels in the brain were not affected by the *tph2* mutation (male: $t = 2.002$, $df = 8.552$, $P = 0.0781$; female: $t = 0.3051$, $df = 9.864$, $P = 0.7666$; Fig. 7.4D). These results indicate that the enzymatic activity is lost in the truncated tph2 protein translated from the $tph2^{\Delta 13}$ allele.

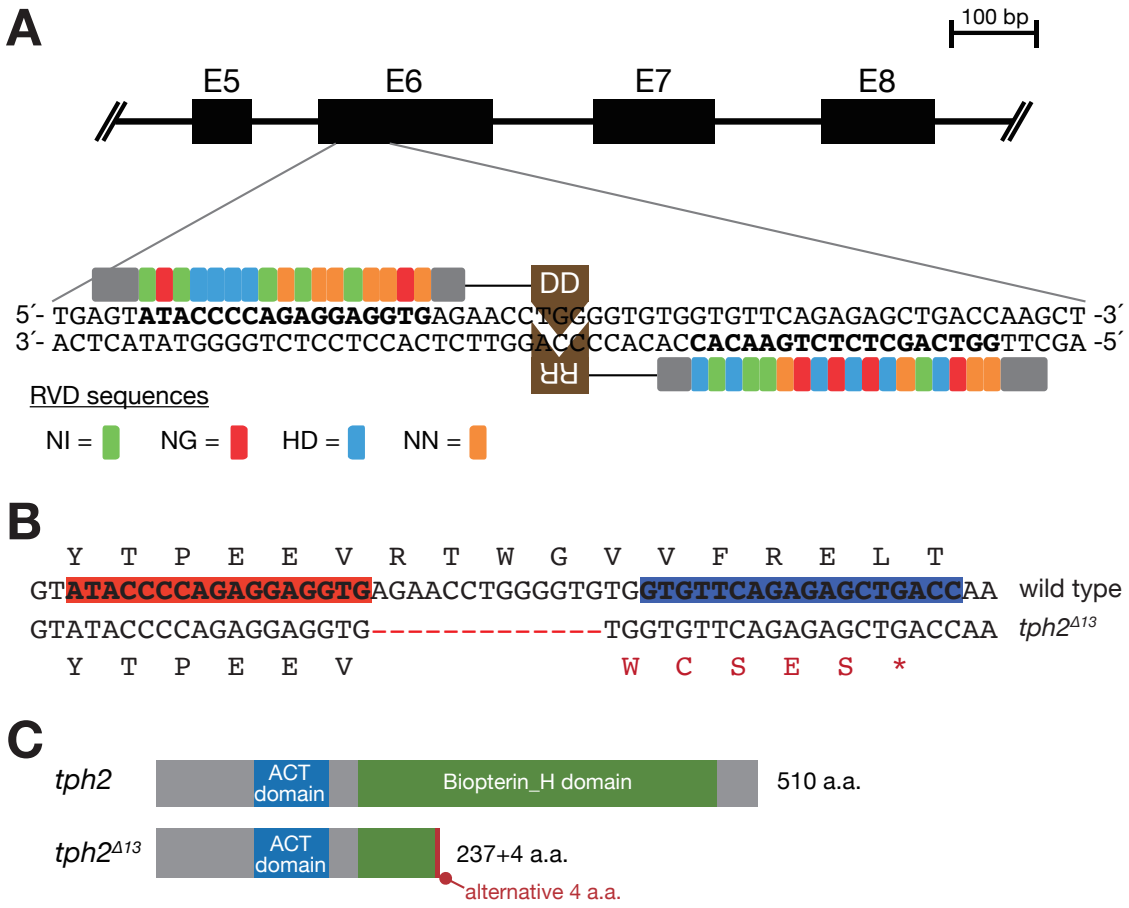

Figure 7.1. Generation of a medaka strain deficient in tryptophan hydroxylase 2 (*tph2*). (A) Schematic illustration of mutagenesis mediated by transcription activator-like (TAL) effector nucleases (TALENs) in the sixth exon (E6) of the *tph2* gene. The amino acid sequence of each repeat variable di-residues (RVD) is indicated by the color of each box; green for NI, red for NG, blue for HD, and orange for NN. (B) Nucleotide sequence and translated amino acid sequence from wild-type and a mutant tph2 allele ($tph2^{\Delta 13}$). Red or blue box indicates the left or right recognition sites of the TALENs, respectively. Red dashes indicate the TALEN-induced deletion. The mutant allele produces an additional region of altered translation, which is indicated by green letters. (C) The predicted protein structures were translated from the wild type (*tph2*) and the frame-shifted ($tph2^{\Delta 13}$) allele. The frame-shifted allele could produce a truncated protein (237 amino acids with an alternative 4 amino acids sequence) harboring a partial loss of the Biopterin_H domain whereas the wild-type allele could produce a 510 a.a. protein.

Behavioral phenotyping of the $tph2^{\Delta 13/\Delta 13}$ fish

For the behavioral phenotyping, $tph2^{+/+}$ or $tph2^{\Delta 13/\Delta 13}$ fish were obtained by mating between F2 $tph2^{+/+}$ or $tph2^{\Delta 13/\Delta 13}$ fish, respectively, and two genotypes of the hatched larvae were separately reared for 8 weeks under the same conditions. There were no significant differences between genotypes in the body length of both male ($tph2^{+/+}$: 21.59 mm $\pm$ 0.2060, n = 36; $tph2^{\Delta 13/\Delta 13}$: 21.72 mm $\pm$ 0.3175, n = 31; t = 0.3294, df = 52.59, P = 0.7432) and female ($tph2^{+/+}$: 21.83 mm $\pm$ 0.2124, n = 30; $tph2^{\Delta 13/\Delta 13}$: 21.81 mm $\pm$ 0.3408, n = 27; t = 0.06154, df = 44.15, P = 0.9512). Therefore, these fish were subjected to the following behavioral testing.

Detailed results of statistical analysis in behavioral testing were described in the Appendix section.

The diving test is a well-established paradigm that quantify the diving response of each tested fish

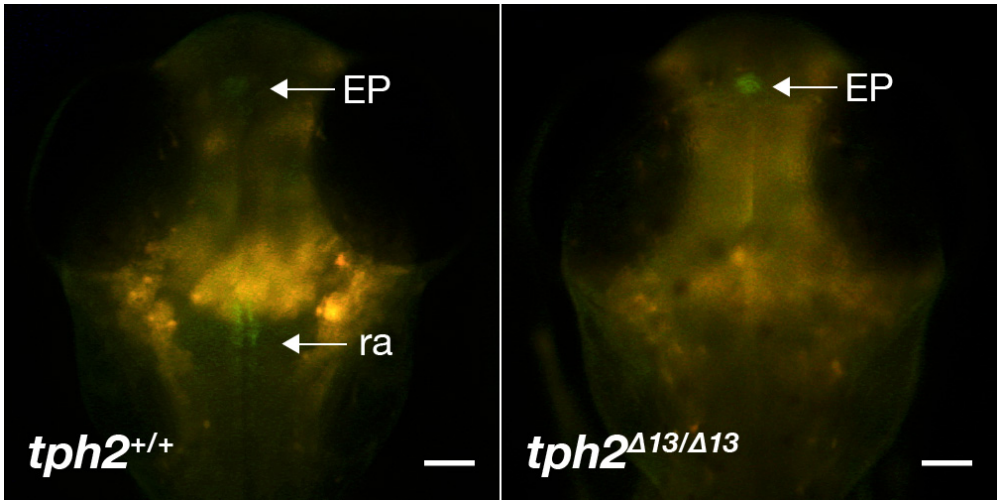

Figure 7.2. Dorsal views of 4 days post-fertilization (dpf) embryos that were immunostained by anti-serotonin (5-HT) antibody. The wild-type embryo ($tph2^{+/+}$) shows the green immunofluorescent signals in both the raphe nuclei of the brain stem (ra) and the pineal gland (EP). On the other hand, the homozygous mutant embryo ($tph2^{\Delta 13/\Delta 13}$) exhibits the signals only in the pineal gland but not in the raphe nuclei. Scale bars: 100 μm.

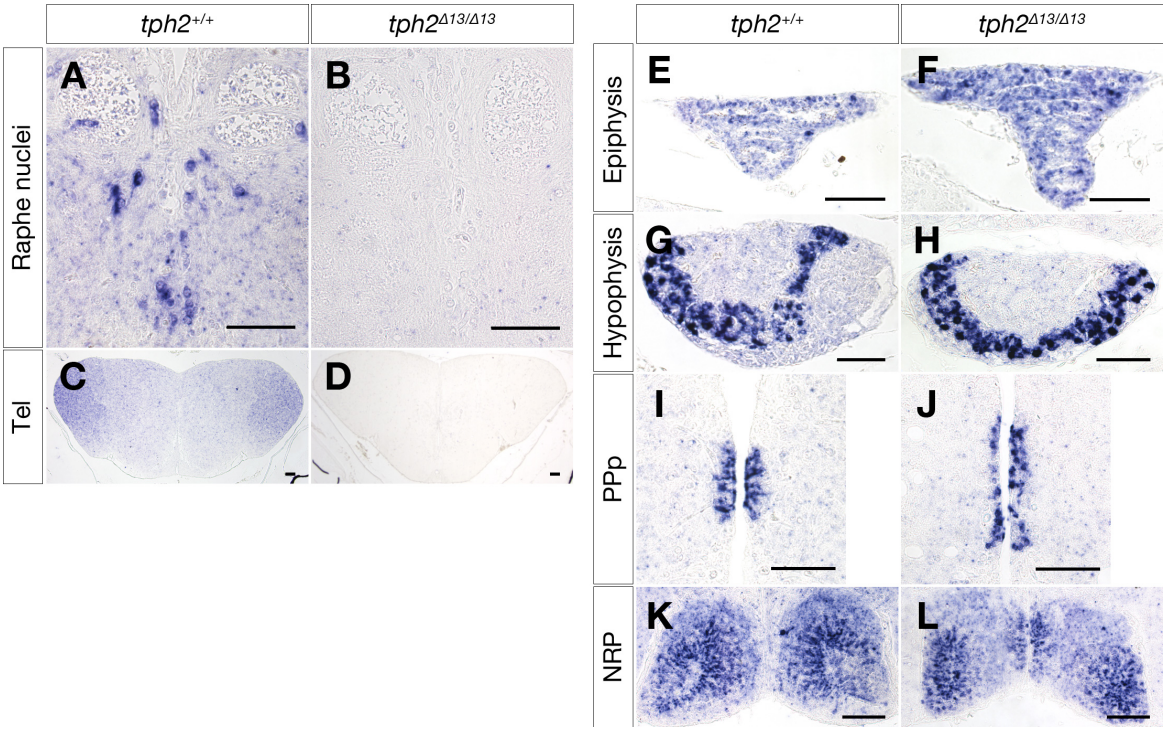

Figure 7.3. Immunohistochemical staining of serotonin (5-HT) in the brain of the wild-type ($tph2^{+/+}$) and the mutant fish ($tph2^{\Delta 13/\Delta 13}$). The $tph2^{\Delta 13/\Delta 13}$ brain shows 5-HT deficiency in the raphe nuclei (A, B) and the axons located in telencephalon (tel) (C, D), while there is no differences between $tph2^{+/+}$ and $tph2^{\Delta 13/\Delta 13}$ in pineal gland (epiphysis) (E, F), pituitary gland (hypophysis) (G, H), posterior parvocellular preoptic nucleus (PPp) (I, J), and posterior recess nucleus (NRP) (K, L). Scale bars: 50 μm.

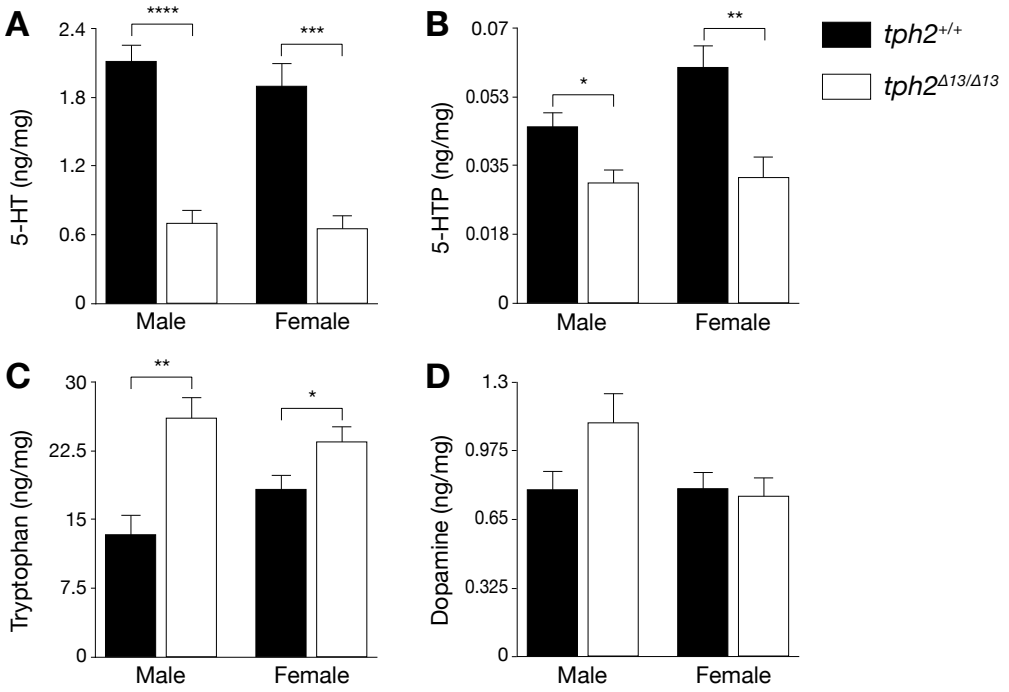

Figure 7.4. Quantification of neurochemicals by liquid chromatography with tandem mass spectrometry (LC-MS/MS) in the whole brain of wild type ($tph2^{+/+}$) and tph2-deficient ($tph2^{\Delta 13/\Delta 13}$) fish. Serotonin (5-HT) (A), its precursors, 5-hydroxytryptophan (5-HTP) (B) and tryptophan (C), and another monoamine (dopamine) (D) are quantified by a multireaction monitoring (MRM) method. All values are presented as mean of the amount (ng) $\pm$ S.E.M. per protein (mg) measured by a bicinchoninic acid (BCA) protein assay method. Differences between genotypes were calculated by Welch's *t*-test. $^{*}P < 0.05$, $^{**}P < 0.01$, $^{***}P < 0.001$, $^{****}P < 0.0001$, tph2-deficient fish compared to the congeneric wild type fish. $n = 6$ for each group.

to assess stress, fear, and anxiety-related behaviors of teleost fishes [141]. The $tph2^{\Delta 13/\Delta 13}$ fish showed a decreased distance traveled in both male (Fig. 7.5A, C) and female (Fig. 7.5B, C). The duration of freezing behavior was significantly increased by the mutation in both male (Fig. 7.5D, F) and female (Fig. 7.5E, F). Time spent in the bottom area was significantly increased in the muntat female (Fig. 7.5H, I) but not in the mutant male (Fig. 7.5G, I). Number of entries into the top area was significantly decreased by the mutation in both the male (Fig. 7.5J, L) and the female (Fig. 7.5K, L). The latency to the first entry into the top area was not affected by the mutation (Fig. 7.5M, N).

The open-field test is a paradigm that assesses the horizontal locomotor in a shallow test tank to evaluate the locomotor activity and the anxiety [150]. No significant differences between two genotypes in distance traveled in the 15-min test were found in both male and female (Fig. 7.6A–C). The durations of freezing behavior were significantly increased by the mutaion during the first 1 or 2 min in both male (Fig. 7.6D) and female (Fig. 7.6E) while the total duration of the freezing was significantly increased in the mutant female but not in the mutant male (Fig. 7.6F). Total time spent in the center area was not altered by the genotype (Fig. 7.6I) but the center time during 1–2 min of the 15-min test was significantly increased only in the $tph2^{\Delta 13/\Delta 13}$ female (Fig. 7.6H). Total number of entries into the center area was not affected by the mutaion (Fig. 7.6L) but was significantly decreased during the first 1 min of the 15-min test only in the mutant female (Fig. 7.6K).

The light–dark transition test is a behavioral paradigm to assess anxiety in both rodents and teleost fishes, which is based on the innate aversion to brightly illuminated environment and spontaneous exploratory behavior [161–163]. The *tph2* genotype unaffected the time spent in both light (Fig. 7.7A)

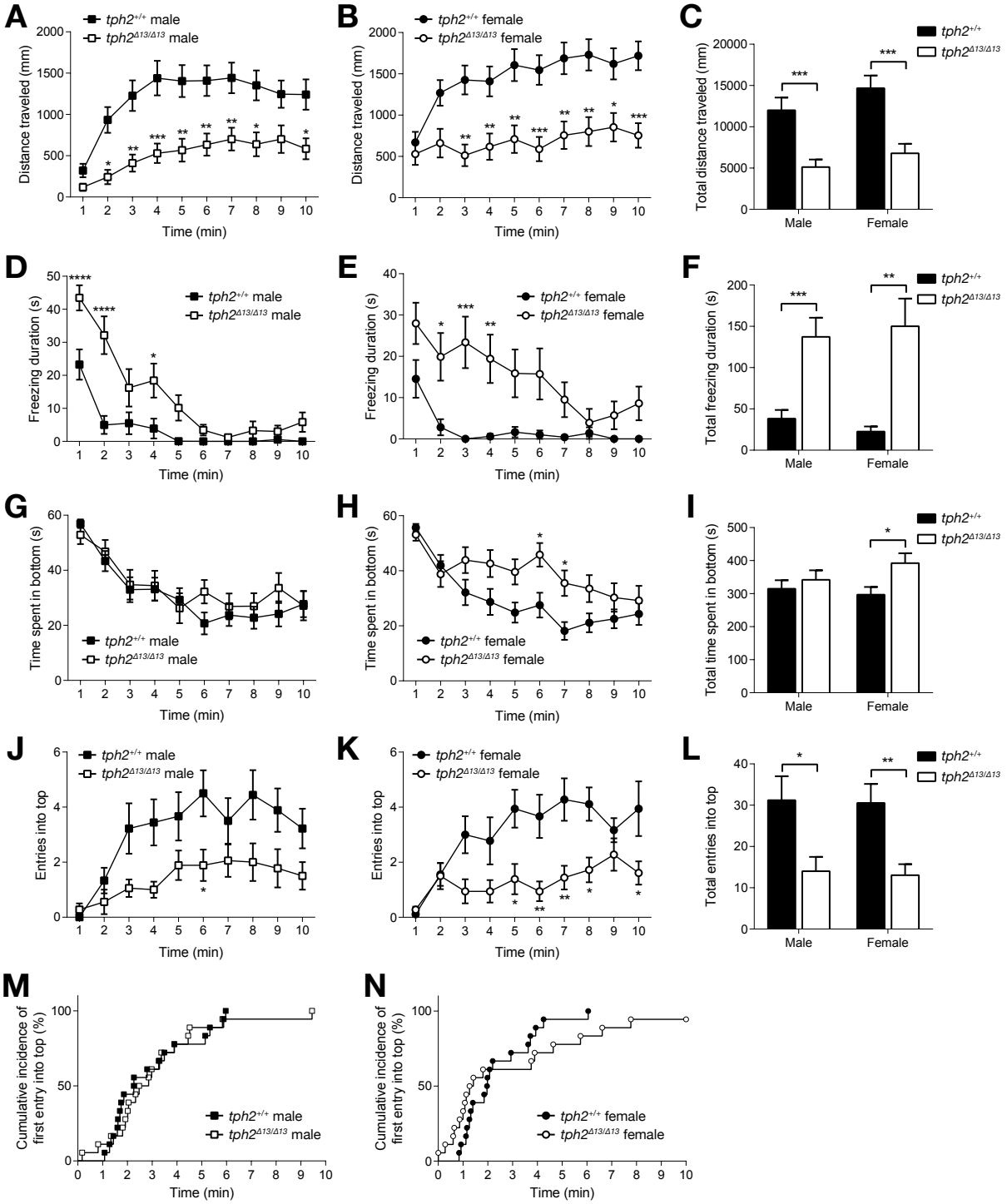

Figure 7.5. (Continued on the following page.)

Figure 7.5. Behavioral phenotypes of *tph2*$^{\Delta 13/\Delta 13}$ fish tested in the diving test. (A–C) Distance (mm) traveled for 1 min bins in male (A) and female (B) fish, and total distance (mm) traveled for 10 min (C). (D–F) Duration (s) of freezing behavior for 1 min bins in male (D) and female (E) fish, and total duration (s) of freezing for 10 min (F). (G–I) Time spent (s) in the bottom area for 1 min bins in male (G) and female (H) fish, and total time spent (s) in the bottom area for 10 min (I). (J–L) Number of entries into the top area for 1 min bins in male (J) and female (K), and total number of entries into the top area (L). (M, N) Cumulative incidence of the first entry into the top area in male (M) and female (N). $n = 18$ in each group. Data are shown as mean $\pm$ S.E.M. Differences between treatments over time were analyzed by two-way repeated measured ANOVA and Sidak's multiple comparison test; differences between treatments were calculated by Welch's *t*-test. Symbols indicate significant differences compared to controls. Cumulative incidence of the first entry into the top area was analyzed using survival curves and log-rank (Mantel-Cox) test. $*P < 0.05$; $**P < 0.01$; $***P < 0.001$; $****P < 0.0001$.

and dark (Fig. 7.7B) areas. Total number of the transitions between both areas (Fig. 7.7C), latency to the first entry into the dark area (Fig. 7.7D, E), and total distance of traveled in the 10-min test were also unaffected by the genotype. Total duration of freezing behavior for the 10-min test was significantly increased in *tph2*$^{\Delta 13/\Delta 13}$ male but not in the female(Fig. 7.7I). The freezing duration during the first 1 min was significantly increased in both the male (Fig. 7.7G) and the female (Fig. 7.7H).

The mirror biting behavior is a well-established model of the social behavior, including socially-induced anxiety, in medaka [131]. The *tph2*$^{\Delta 13/\Delta 13}$ fish did not exhibit any significant changes in time of mirror biting for the 10-min test in both male and female (Fig. 7.8A–C) and latency to the first mirror biting (Fig. 7.8K, L). The number of mirror biting was significantly decreased by the mutation in male (Fig. 7.8D, F) but not in female (Fig. 7.8E, F). The *tph2*$^{\Delta 13/\Delta 13}$ fish significantly increased the duration of freezing behavior in both male (Fig. 7.8G, I) and female (Fig. 7.8H). Total distance traveled was unaffected by the genotype (Fig. 7.8J).

The two-fish social interaction test is a behavioral paradigm to evaluate direct social interactions between two congeneric fish (male-to-male or female-to-female). The *tph2* genotype did not affect the average distance between individuals for the 10-min test (Fig. 7.9A) and latency to the first contact (Fig. 7.9B, C). The contact time was significantly increased by the mutation in female (Fig. 7.9E, F) but not in male (Fig. 7.9D, F). The number of contacts was unaffected by the mutation in both male and female (Fig. 7.9G–I).

7.4 Discussion

Here, I generated a *tph2*-deficient strain of medaka by targeted mutagenesis mediated by TALENs and identified the significant alterations of behaviors caused by the mutation using five behavioral paradigms. Because this mutant lost 5-HT in the serotonergic neurons projected from the raphe nuclei of the brain stem, these behavioral alterations result from the impairment of serotonergic neurotransmission from the raphe nuclei, which will reveal functions of the raphe serotonergic systems in medaka behaviors. These results suggest that a combination of the genome editing technology established in the previous chapters and the behavioral testing system that was newly developed in the last chapter is an effective technique for understanding of gene functions in complex behaviors of medaka and other teleost fishes. Although previous studies in teleost fishes demonstrated the behavioral effects of the serotonergic dysfunction caused by pharmacological manipulations, such as with a tryptophan hydroxylase inhibitor *p*-chlorophenylalanine (PCPA) or the 5-HT$_{1A}$ receptor antagonist WAY 100,635 [154, 189, 190], there is no report to genetically disrupt the serotonergic functions in teleost fishes. Therefore, this study is the first report on generating the mutant of seronotergic genes and assessment of the behavioral phenotypes in teleost fishes.

TPH2 gene encodes a brain-specific isozyme of tryptophan hydroxylase in mammals [193], and

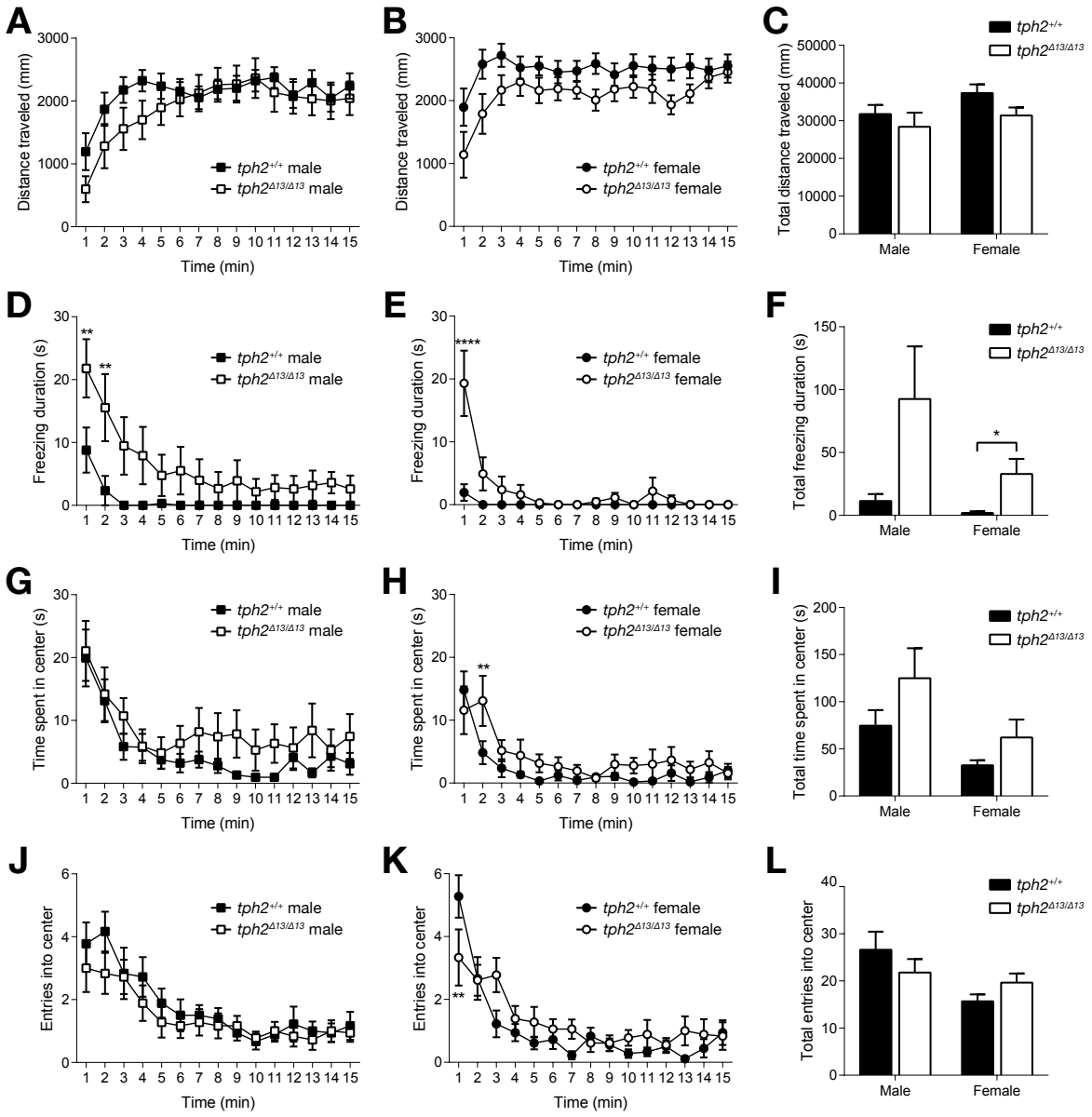

Figure 7.6. Behavioral phenotypes of *tph2*$^{\Delta 13/\Delta 13}$ fish tested in the open-field test. (A–C) Distance (mm) traveled for 1 min bins in male (A) and female (B) fish, and total distance (mm) traveled for 15 min (C). (D–F) Duration (s) of freezing behavior for 1 min bins in male (D) and female (E) fish, and total duration (s) of freezing for 15 min (F). (G–I) Time spent (s) in the center area for 1 min bins in male (G) and female (H) fish, and total time spent (s) in the center area for 15 min (I). (J–L) Number of entries into the center area for 1 min bins in male (J) and female (K) fish, and total number of entries into the center area for 15 min (L). $n = 18$ in each group. Data are shown as mean $\pm$ S.E.M. Differences between treatments over time were analyzed by two-way repeated measured ANOVA and Sidak's multiple comparison test; differences between treatments were calculated by Welch's *t*-test. Symbols indicate significant differences compared to controls. $^{*}P < 0.05$; $^{**}P < 0.01$; $^{***}P < 0.001$; $^{****}P < 0.0001$.

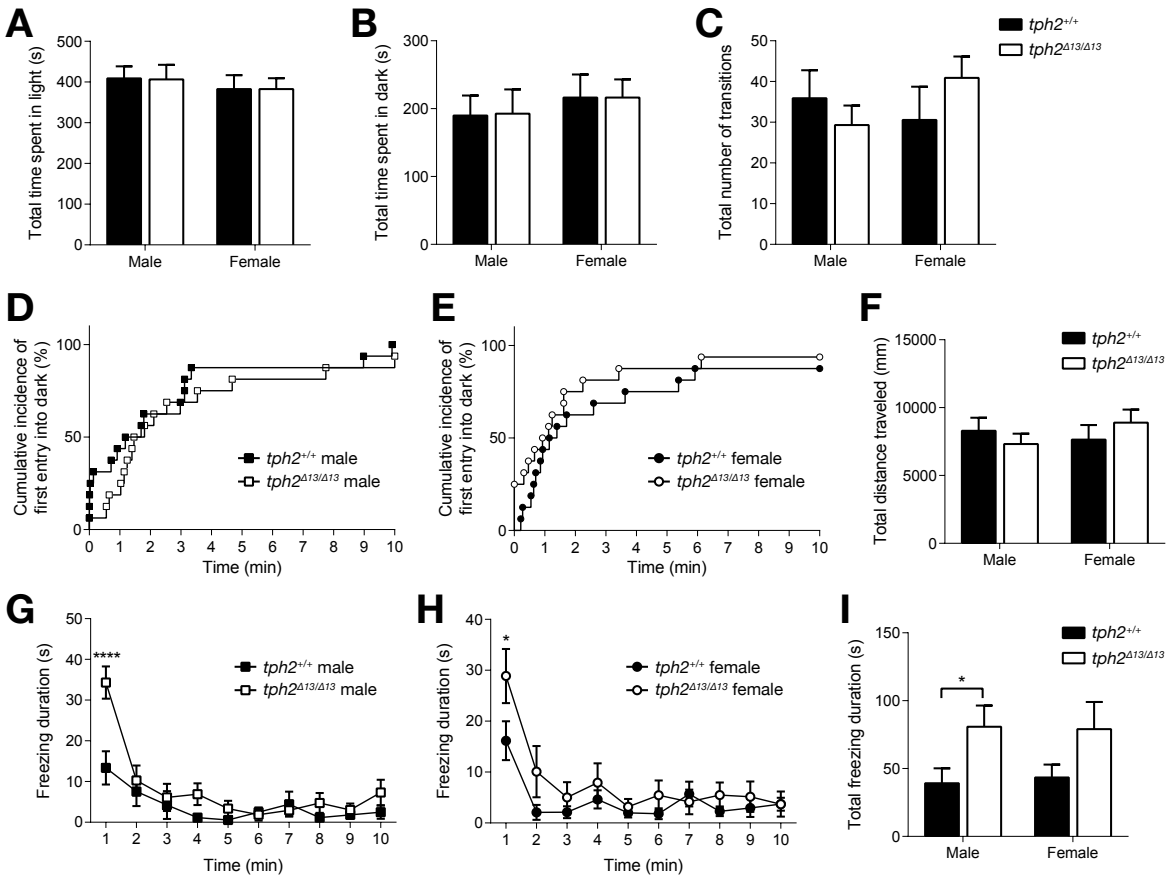

Figure 7.7. Behavioral phenotypes of *tph2*$^{\Delta 13/\Delta 13}$ fish tested in the light–dark transition test. (A, B) Total time spent (s) in the light (A) and dark (B) area. (C) Total number of transitions between the areas for 10 min. (D, E) Cumulative incidence of the first entry into the dark area in male (D) and female (E). (F) Total distance (mm) traveled for 10 min. (G–I) Duration (s) of freezing behavior for 1 min bins in male (G) and female (H) fish, and total duration (s) of freezing for 10 min (I). $n = 16$ in each group. Data are shown as mean $\pm$ S.E.M. Differences between treatments over time were analyzed by two-way repeated measured ANOVA and Sidak's multiple comparison test; differences between treatments were calculated by Welch's *t*-test. Symbols indicate significant differences compared to controls. Cumulative incidence of the first entry into the dark area was analyzed using survival curves and log-rank (Mantel-Cox) test. $^*P < 0.05$; $^{**}P < 0.01$; $^{***}P < 0.001$; $^{****}P < 0.0001$.

therefore *Tph2* knockout mice drastically decreased the 5-HT content in the brain (less than 10%) [194, 195]. The *tph2*$^{\Delta 13/\Delta 13}$ fish exhibited a decreased 5-HT content in the brain but the residual content (approximately 30% of the wild-type) is higher than the knockout mice (Fig. 7.4A). This residual 5-HT in the *tph2*$^{\Delta 13/\Delta 13}$ brain would be mainly derived from the posterior tuberculum and the hypothalamic populations of serotonergic neurons widely found in vertebrates except eutherian mammals, which express *tph1a* gene for the 5-HT synthesis in zebrafish [182] and medaka [172]. In fact, immunohistochemical staining of 5-HT in the *tph2*$^{\Delta 13/\Delta 13}$ brain showed the 5-HT-positive neurons in the posterior tuberculum and hypothalamus such as PPp and NRP. However, as well as the raphe neurons, the 5-HT-positive signals in the telencephalon were largely lost in the *tph2*$^{\Delta 13/\Delta 13}$ fish. In zebrafish, the serotonergic neurons in the raphe nuclei send the axonal projection to a wide range of the brain region including the telencephalon [183] similar to mammals [176]. The telencephalon of teleost fishes contains some regions that are considered as homologous regions of mammalian limbic systems including amygdala, hippocampus, nucleus accumbens, and stiatum, which would be involved

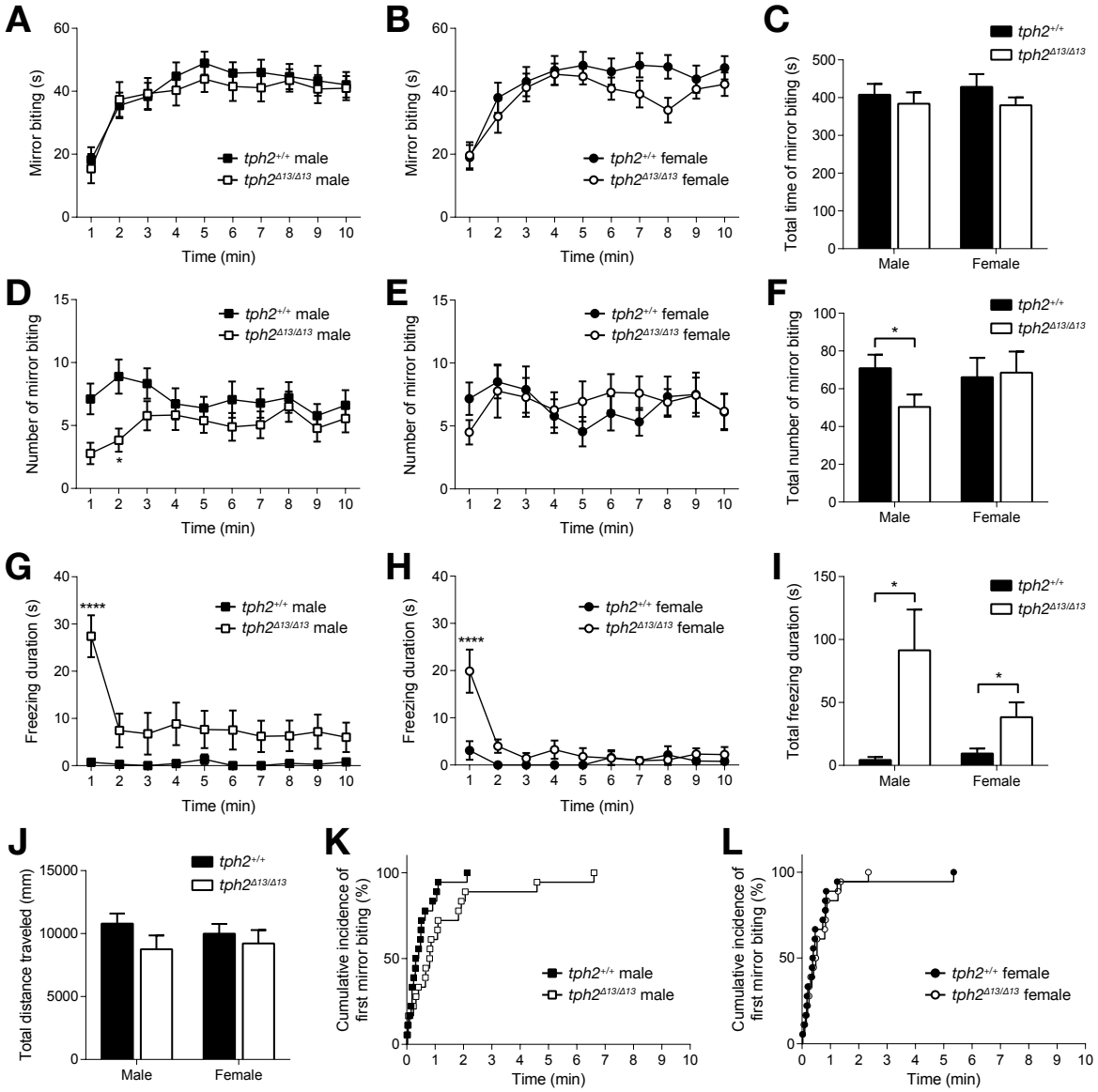

Figure 7.8. Behavioral phenotypes of *tph2*$^{\Delta 13/\Delta 13}$ fish tested in the mirror-biting test. (A–C) Time (s) spent in the mirror biting area for 1 min bins in male (A) and female (B) fish, and total time spent (s) in the mirror biting area for 10 min (C). (D–F) Number of entries into the mirror biting area for 1 min bins in male (D) and female (E) fish, and total number of entries into the mirror biting area for 10 min (F). (G–I) Duration (s) of freezing behavior for 1 min bins in male (G) and female (H) fish, and total duration (s) of freezing for 10 min (I). (J) Total distance (mm) traveled for 10 min. (K, L) Cumulative incidence of the first mirror biting in male (K) and female (L). $n = 18$ in each group. Data are shown as mean $\pm$ S.E.M. Differences between treatments over time were analyzed by two-way repeated measured ANOVA and Sidak's multiple comparison test; differences between treatments were calculated by Welch's *t*-test. Symbols indicate significant differences compared to controls. Cumulative incidence of the first mirror biting was analyzed using survival curves and log-rank (Mantel-Cox) test. $^{*}P < 0.05$; $^{**}P < 0.01$; $^{***}P < 0.001$; $^{****}P < 0.0001$.

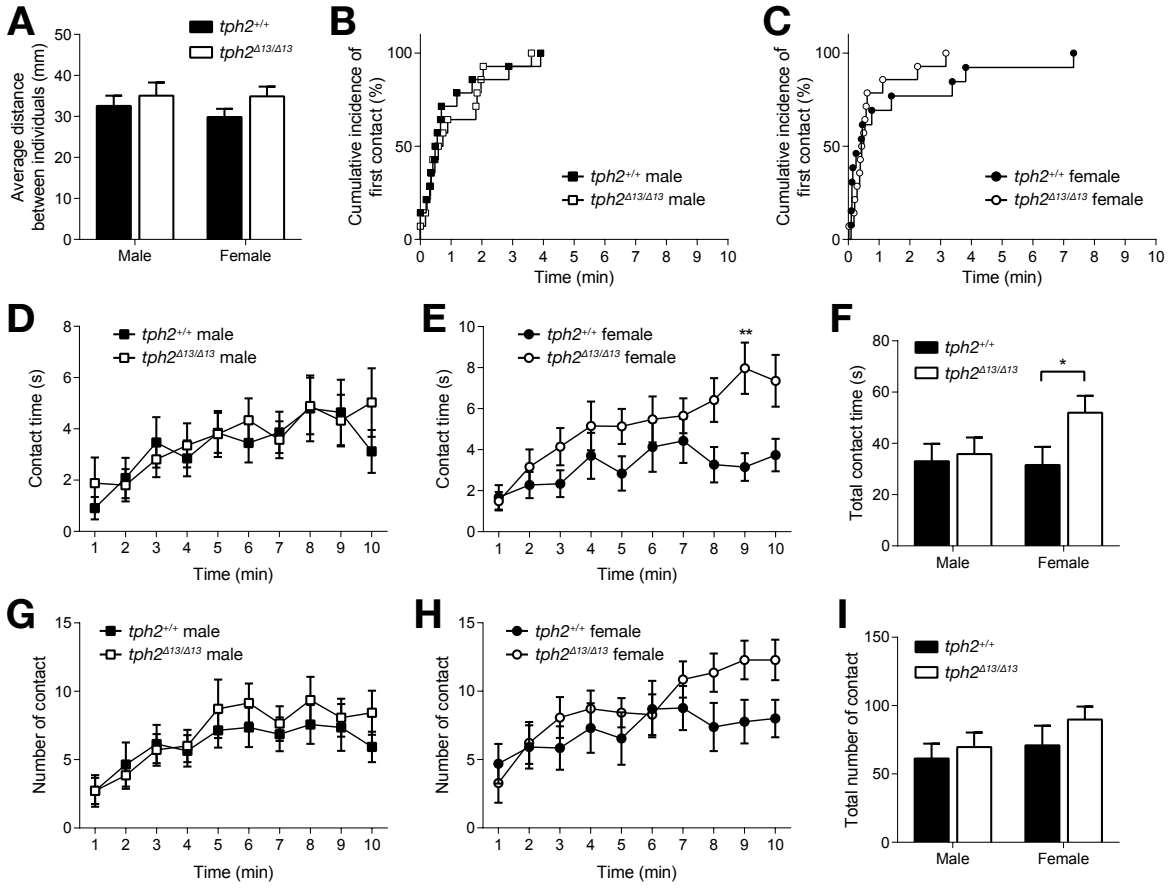

Figure 7.9. Behavioral phenotypes of *tph2*$^{\Delta 13/\Delta 13}$ fish tested in the two-fish social interaction test. (A) Average distance (mm) between the test individuals for 10 min. (B, C) Cumulative incidence of the first contact between fish in male (B) and female (C). (D–F) Time (s) of contacts between fish for 1 min bins in male (D) and female (E), and total time (s) of contacts for 10 min (F). (G–I) Number of contacts between fish for 1 min bins in male (G) and female (H), and total number of contacts for 10 min (I). $n = 14$ in each group except $n = 13$ in the *tph2*$^{\Delta 13/\Delta 13}$ female. Data are shown as mean $\pm$ S.E.M. Differences between treatments over time were analyzed by two-way repeated measured ANOVA and Sidak's multiple comparison test; differences between treatments were calculated by Welch's *t*-test. Symbols indicate significant differences compared to controls. Cumulative incidence of the first social interaction was analyzed using survival curves and log-rank (Mantel-Cox) test. $^{*}P < 0.05$; $^{**}P < 0.01$; $^{***}P < 0.001$; $^{****}P < 0.0001$.

in adult complex behaviors such as learning, aggression, and reproduction [196]. These suggest that deficiency of the 5-HT neurotransmission to the telencephalon in the *tph2*$^{\Delta 13/\Delta 13}$ fish will affect the broad range of behaviors.

The behavioral testing showed that the *tph2*$^{\Delta 13/\Delta 13}$ fish significantly increased the freezing duration, especially during the first minutes of each test, in all paradigms except the social interaction test that does not measure the freezing duration of each fish (Figs. 7.5D–F, 7.6D–F, 7.7G–I, 7.8G–I). Freezing is thought to be one of the indicators of heightened anxiety in behavioral analysis of zebrafish [141, 197]. Increased freezing duration in zebrafish was found when a mutant of the glucocorticoid receptor was placed into a novel environment [159] and was caused by exposure of conspecific alarm substance [158, 160]. These manipulations causing the longer freezing were accompanied with a decreased expression of a 5-HT transporter gene *slc6a4a* in the raphe nuclei [158, 159] and/or of a transcription factor gene *pet1* [158] involved in differentiation of the raphe serotonergic neurons [182].

Additionally, they also showed that the increased freezing duration was attenuated by administration of fluoxetine, a selective serotonin reuptake inhibitor (SSRI) class of anti-depressant [159, 160]. Also, in medaka, I showed that chronic administration of fluoxetine decreased the freezing duration in the first few minutes of the behavioral paradigms [191]. These facts suggest that the raphe serotonergic neurons inhibit the anxiogenic responces, especially freezing, and therefore the impairment of the raphe serotonergic function resulted in the elevated anxiogenic behaviors.

The elevated anxiety level in the *tph2*$^{\Delta 13/\Delta 13}$ fish is also supported by the diving test. An increased diving (or bottom-dwelling) behavior, one of the most reliable indices of elevated anxiety in teleost fishes including medaka and zebrafish [141], was shown as the longer time spent in the bottom area in the *tph2*$^{\Delta 13/\Delta 13}$ female (Fig. 7.5H, I) and the decreased number of entries into the top area (Fig. 7.5J–L). However, thigmotaxis (tendency to remain close the walls) in the open-field test, an anxiety index decreased by chronic fluoxetine treatment in medaka [191], was not affected by the deficiency of tph2 protein in the male (Fig. 7.6G) or tended to be increased in the female (Fig. 7.6H). These alterations were consisted with those of zebrafish treated with a tryptophan hydroxylase inhibitor PCPA, which showed an increased diving behavior and a decreased thigmotaxis [154].

Previous studies have suggested that 5-HT has a dual role on the control of anxiety and defensive behaviors, increasing anxiety-like behavior mediated by amygdala or inhibiting fear-like behavior mediated by periaqueductal gray [154, 198]. Serotonergic drugs produced different results among some anxiety indices including bottom-dwelling, thigmotaxis, and dark/light preference in zebrafish [154]. The different effects of deficiency of tph2 protein were also observed in *tph2* knockout mice that exhibited both anxiolytic, such as longer time spent in open arms in the elevated plus maze test [199] and longer time spent in light compartment in the light/dark box test [200], and anxiogenic responses, such as increased immobility and a decreased entries in the center in open-field test [201]. Additionally, the *tph2* knockout mice exhibited an enhanced acquisition and retention of fear memory [201]. These indicate the different effects of *tph2* mutation on anxiety-related behaviors (freezing, bottom-dwelling, and thigmotaxis) could reflect the dual role of 5-HT in medaka; however, further considerations in the brain regions involved in neural circuits for anxiety and fear and axonal projection patterns of serotonergic neurons to the regions will be required for understanding of the role of 5-HT on the control of anxiety and fear in medaka and other teleost fish species.

Previous studies in human and mice suggested that polymorphisms of *tph2* and other serotonergic genes are associated with alterations of social behaviors such as aggression [202–204] and autism [205–207]. The *tph2* knockout mice showed increased aggressive behaviors [194, 199, 200] and autism spectrum disorders-like behaviors (social impairments, communication deficits, and repetitive behaviors) [208]. In this study, *tph2*$^{\Delta 13/\Delta 13}$ fish exhibited altered social behaviors, such as decreased numbers of mirror biting in the male in the mirror-biting test (Fig. 7.8D, F) and increased duration of contact between individuals in female in the social interaction test (Fig. 7.9E, F). Because the decreased number of mirror biting was unaccompanied by a decreased time spent in the mirror biting area, the female fish showed longer durations of each mirror biting. The mirror approaching behavior in medaka is considered as a model of socially induced anxiety [131], and therefore, the behavioral alteration in the *tph2*$^{\Delta 13/\Delta 13}$ male suggests the raphe serotonergic neurons could negatively regurate anxiety induced by isolation. On the other hand, the increased duration of contact in the social interaction test indicates an elevated "social interaction" between two *tph2*$^{\Delta 13/\Delta 13}$ female individuals; however, the "social interaction" is defined only in terms of the distances of the two individuals and therefore will contain a broad range of behaviors including aggression and shoaling. Further direct observations and characterization of the interactive behaviors, as performed to characterize the aggressive behaviors [127], will be required to make a detailed interpretation of the altered social interaction.

In this study, both male and female fish were subjected to the behavioral testing, which revealed that there were sexual differences in the behaviors affected by the *tph2* mutation, such as a decreased number of mirror biting only in male (Fig. 7.8D, F) or an increased time spent in the bottom (Fig.

7.5H, I), an increased time spent in the center (Fig. 7.6H), and an increased contact time (Fig. 7.9F) only in female. The *tph2* gene showed a sexual difference in the expression in dorsal posterior nucleus (thalamus) (DP) but not in the raphe nuclei of medaka brain [172], and therefore, the *tph2*-expressing neurons in DP may be involved in the sexual dimorphic effects. The sexual differences in the behavioral effects of the tph2 deficiency were also reported in the *tph2* knockout mice [201]. A plasma testosterone level was increased in the *tph2* knockout male but not in female mice [200], indicating the differences at least partly were caused by changes of sex steroid levels. Additionally, it has been reported that enhancing serotonergic neurotransmission by fluoxetine administration causes low expression of arginine vasotocin (AVT) in the bluehead warasse (*Thalassoma bifasciatum*) [209]. Previous study showed that the AVT system in the medaka brain is involved in aggression and sexual behaviors [127, 129] and the *avt* expression shows sexual differences in some brain regions [172]. These facts suggest that the sexual differences in the behavioral effects can be partly explained by sexually-dimorphic dysregulation of AVT and other hormones that are controlled by the serotonergic neurons.

Chapter 8

General Discussion

In this study, I demonstrated the successful targeted mutagenesis in medaka using targetable nuclease systems—ZFNs, TALENs, and CRISPR/Cas system. All three systems were introduced as RNA sequences into each fertilized egg of medaka by the microinjection method, thereby inducing small insertions and deletions on the target DNA sequence with high efficiency. The mutation events were occurred at the germ cells of the injected fish and therefore were efficiently transmitted to next generations. Subsequently, I showed that the frame-shifted mutation on the *tph2* gene by TALENs caused impairment of the 5-HT synthesis in the raphe nuclei of the brain stem, resulting in alterations of anxiety-related and social behaviors that were assessed with a newly developed behavioral testing system for small laboratory fish. These facts indicate that targeted mutagenesis using the targetable nuclease systems has become a powerful technology to elucidate gene functions within organisms, especially in adult phenotypes including complex behaviors, by reverse genetics approaches in medaka and other teleost fish species.

As mentioned above, three nuclease systems are now available to induce the site-specific DNA cleavage in medaka. TALENs and CRISPR/Cas system are two feasible options for efficient targeted mutagenesis whereas ZFNs are not suitable because of their difficulty of customization of the DNA recognition domains and higher cytotoxicity. Characteristics of the two systems are summarized at Table 8.1. Customization of target sequence in the CRISPR/Cas system is simpler only by modification of the 5′ end of sgRNA, while customization of TALENs requires preparation and maintenance of a library of 34 vectors for the golden gate assembly. Recently, some studies showed that the Cas9 nuclease can be guided by complex of chemically-synthesized short RNAs (crRNA and tracrRNA) [210, 211], suggesting that target sequences in the CRISPR/Cas system can be easily customized only by ordering synthesized crRNA as ordering oligonucleotides for PCR primers. Target sequence can flexibly selected in both systems without some previous restrictions, including the 5′ end of T in TALENs [56] and the 5′ GG in CRISPR/Cas system [104] as demonstrated in this study. Additionally, a large part of TALENs and sgRNA that were designed for any target sequences could successfully disrupt the target genes. However, the target specificity of CRISPR/Cas system is relatively low and therefore off-target alterations are sometimes induced while there are less potential off-target sites in TALENs because of their longer recognition sequences. Finally, CRISPR/Cas system has advantages in multiplex gene editing because a nuclease can target a number of genes by introduction of a number of guide RNAs. Based on these features, we need to consider which system is more suitable for the experiment and then decide which to adopt.

Medaka has been used as a vertebrate model in genetics since the early 1900s [212]. There are several advantageous characteristics to using the medaka in genetics and genomics research, such as availability of a high-quality draft genome sequence [3] (also released a “nearly-complete” version; http://utgenome.org/medaka_v2/) and of a broad range of genetic resources including laboratory standard strains, highly polymorphic inbred strains, wild populations, and the *Oryzias* genus of related

Table 8.1. Characteristics of TALENs and CRISPR/Cas system as genome editing tools

	TALENs	CRISPR/Cas system
Customization	Relatively complex	Simple
Design	Very flexible	Flexible
Success rate	High	High
Specificity	Relatively high	Relatively low
Multiplex editing	Unsuitable	Suitable

species [174, 213, 214]. Reverse genetics in medaka had been conducted by the TILLING [16, 215]; however, the saturated mutant library was constructed using a Kyoto-Cab strain [16] and therefore the other strains cannot be subjected to this approach. On the other hand, the targetable nuclease systems can disrupt the targeted genes in any strains whose fertilized eggs are available, such as the strain from a wild population [112] and a related species *O. dancena* [216]. The combination of targetable nuclease systems and these resources will make it possible to fully examine the relationship among the targeted gene function, the genetic backgrounds, and environmental factors.

Reverse genetics in medaka has also become a powerful tool in biomedical research. Although zebrafish has already been one of the canonical models for studying human disease, medaka is used for the complementarity argument for gene functions that were diversified the teleost whole-genome duplication followed by subfunction partitioning or subfunctionalization [217]. Medaka strains harboring mutations in genes involved in human diseases have already been established using the TILLING method [16, 218–221]. Targeted mutagenesis using TALENs or CRISPR/Cas system is rapid, less laborious, and cost-effective technology compared to the TILLING method, which will facilitate loss-of-function analysis of human disease-related genes in medaka. Furthermore, medaka is a widely used model for aquatic (eco)toxicology [222]. The targeted mutagenesis technology will also help examine the genetic basis of biological responses to toxicological compounds.

Breeding of aquacultured fish driven by reverse genetics is currently in progress in fugu using a TILLING approach [17]; however, the adoption of this approach in other teleost fishes has been hindered because the approach requires much effort to construct, maintain, and screen the mutagenized library and long time to analyze homozygous phenotypes (at least 3 generations for homozygous mutants). On the other hand, the targetable nuclease systems can adopt any teleost fish species whose fertilized eggs are available for the microinjection experiment and often produce homozygous phenotypes in the injected generation as described in this study, which indicates targeted mutagenesis using the nuclease systems will become an effective approach for molecular breeding of aquacultured fish. The nuclease systems have already been adopted in some farmed fish species, such as yellow catfish (*Tachysurus fulvidraco*) [223,224], rainbow trout (*Oncorhynchus mykiss*) [225,226], Nile tilapia (*Oreochromis niloticus*) [227, 228], and Atlantic salmon (*Salmo salar*) [229]. The experimental methods for targeted mutagenesis using the targeted nucleases in medaka, including an efficient genotyping method using HMA–MultiNA, were optimized for RNA microinjection into the fertilized eggs and the following step for identification and segregation of germ-line mutations. Therefore, rapid and effective mutagenesis with higher mutation efficiencies compared to other cultured fishes [223–229] has been achieved by these methods. Application of the mutagenesis methods established in this study to farmed fishes can facilitate the molecular breeding of cultured fish, especially driven by the reverse genetics approaches, such as targeted mutagenesis using the CRISPR/Cas system in fugu and red sea bream (*Pagrus major*) by our research group (Kuroyanagi and Kishimoto *et al.* in preparation; Kishimoto *et al.* unpublished). Addittionally, there is limited knowledge in teleost fishes about genes responsible for economic traits such as growth, feeding, stress responses, and sexual maturation. Targeted

mutagenesis in medaka will also help to understand molecular mechanisms of the economic traits and effectiveness of genes that were reported to be involved in the traits in limited teleost species or other vertebrates to the breeding in a broad range of fishes.

Genome editing using targetable nuclease systems allows not only for targeted mutagenesis by small insertions and deletions but also for targeted integration of DNA fragments and precise modification of small regions including single nucleotide polymorphisms (SNPs) [18–20]. Indeed, targeted integration of reporter/driver genes by non-homologous end joining [230, 231] or homology-directed repair [232–234] and targeted correction of a point mutation [235] have already been reported in zebrafish and medaka. These techniques enable advanced genome engineering such as expression of genes of interest driven by endogenous regulatory elements and precise amino acid replacement; however, the success rates are not as high as those of targeted mutagenesis and therefore those technologies have not become popular in the fish research community. Thus, refinement of factors affecting the efficiency, such as genomic DNA cleavage efficiency by the nucleases and donor DNA structure, will be required to establish efficient methods for the advanced genome engineering. Knowledge about efficient targeted mutagenesis in medaka is certain to serve as a basis for this refinement.

Summary

Chapter 1. General Introduction
Genetics is the study to know the relationships between genes and phenotypic traits in living organisms. Recent advances in DNA sequencing technologies have increased the importance of reverse genetics for understanding of functions of individual genes found in the sequenced genome. Of course, a number of genomes have been sequenced in teleost fish species including both models for basic research fields and fishes for aquaculture and the fishing industry. However, available techniques for genetic manipulation in teleost fishes, especially loss-of-function approaches, has been restricted, and thus, understanding of each gene function identified in the genome sequencing projects by the reverse genetics approach has been hindered. In this study, I intended to establish the efficient analytical techniques for gene functions by the reverse genetics approach in medaka (*Oryzias latipes*), a small fish model suitable for genetics, which could be easily applied to a wide range of teleost fish species. I focused on genome editing using targetable nuclease systems that has become a powerful tool for approaches involving reverse genetics in a wide range of organisms. These systems efficiently induce site-specific DNA double-strand breaks (DSBs), resulting in targeted gene disruptions by insertions and deletions (indels) or targeted gene integrations by homologous recombination. Firstly, I demonstrated targeted mutagenesis by small insertions and deletions (indels) in medaka using three classes of targetable nuclease systems: zinc-finger nucleases (ZFNs), transcription activator-like (TAL) effector nucleases (TALENs), and clustered regularly interspaced short palindromic repeats (CRISPR)/CRISPR-associated (Cas) system-based RNA-guided endonucleases (RGENs). Subsequently, to assess the usefulness of targeted mutagenesis using the nucleases in loss-of-function analysis, I also demonstrated targeted disruption of medaka *tph2* gene that is involved in serotonin synthesis in the brain stem and examined the neurobehavioral phenotypes in the homozygous mutant by a newly developed behavioral testing system for medaka.

Chapter 2. Targeted mutagenesis using zinc-finger nucleases
ZFNs are artificial nucleases consisting of engineered zinc fingers fused to the nuclease domain of FokI. In this chapter, I demonstrated successful gene disruption in somatic and germ cells of medaka using ZFN to target exogenous *EGFP* genes. Embryos that were injected with an RNA sequence pair coding for ZFNs showed mosaic loss of green fluorescent protein fluorescence in skeletal muscle. A number of mutations that included both deletions and insertions were identified within the ZFN target site in each embryo, whereas no mutations were found at the non-targeted sites. Additionally, ZFN-induced mutations were introduced in germ cells and efficiently transmitted to the next generation. The mutation frequency varied (6–100%) in the germ cells from each founder, and a founder carried more than two types of mutation in germ cells.

Chapter 3. Targeted mutagenesis using custom-designed transcription activator-like effector nucleases
TALENs consist of a fusion between a FokI nuclease domain and a transcription activator-like (TAL) effector DNA recognition domain found in plant pathogenic bacteria. In this chapter, I demonstrated efficient targeted mutagenesis in medaka using TALENs. I designed and constructed a pair of TALENs

targeting the medaka *DJ-1* gene, a homolog of human *DJ-1/PARK7*. These TALENs induced a number of insertions and deletions in the injected embryos with extremely high efficiency. This induction of mutations occurred in a dose-dependent manner. All screened G0 fish injected with the TALENs transmitted the TALEN-induced mutations to the next generation with high efficiency (44–100%). These TALENs induced site-specific mutations because none of the mutations were found at potential off-target sites. Additionally, the DJ-1 protein was lost in *DJ-1*$^{\Delta 7/\Delta 7}$ fish that carried a TALEN-induced frameshift mutation in both alleles. I also investigated the effect of the N- and C-terminal regions of the TAL effector domain on the gene-disrupting activity of DJ1-TALENs and found that 287 amino acids at the N terminus and 63 amino acids at the C terminus of the TAL domain exhibited the highest disrupting activity in the injected embryos. These results suggest that TALENs enable us to rapidly and efficiently establish knockout medaka strains.

Chapter 4. Design, evaluation, and screening methods for efficient targeted mutagenesis with TALENs

In this chapter, I have described efficient detection methods for TALEN-induced mutations at endogenous loci and presented guidelines of TALEN design for efficient targeted mutagenesis in medaka. I performed a heteroduplex mobility assay (HMA) using an automated microchip electrophoresis system, which is a simple and high-throughput method for evaluation of in vivo activity of TALENs and for genotyping mutant fish of F1 or later generations. I found that a specific pattern of mutations is dominant for TALENs harboring several base pairs of homologous sequences in target sequence. Furthermore, I found that a 5′ T, upstream of each TALEN-binding sequence, is not essential for genomic DNA cleavage. These findings provide information that expands the potential of TALENs and other engineered nucleases as tools for targeted genome editing in a wide range of organisms including medaka and other teleost fishes.

Chapter 5. Targeted mutagenesis using CRISPR/Cas system

CRISPR/Cas system-based RGEN, consisting of the endonuclease Cas9 protein and small guide RNA to program the recognition specificity of the Cas9, has recently emerged as a simple and efficient tool for targeted genome editing. In this chapter, I showed successful targeted mutagenesis using RGENs in medaka. Somatic and heritable mutations were induced with high efficiency at the targeted genomic sequence on the *DJ-1* gene in embryos that had been injected with the single guide RNA (sgRNA) transcribed by a T7 promoter and capped RNA encoding a Cas9 nuclease. The sgRNAs that were designed for the target genomic sequences without the 5′ end of GG required by the T7 promoter induced the targeted mutations. This suggests that the RGEN can target any sequence adjacent to an NGG protospacer adjacent motif (PAM) sequence, which would occur once every 8 bp. The off-target alterations at two genomic loci harboring double mismatches in the 18-bp targeting sequences were induced in the RGEN-injected embryos. However, I also found that the off-target effects could be reduced by lower dosages of sgRNA. Taken together, these results suggest that CRISPR/Cas-mediated RGENs may be an efficient and flexible tool for genome editing in medaka.

Chapter 6. Effects of chronic fluoxetine administration on anxiety-related and social behaviors in medaka

Medaka have used as a model in neurobehavioral research because of their complex social and/or visually-evoked behaviors; however, there have been few studies that comprehensively evaluated the behavioral effects of genetic manipulations by the multitiered phenotyping strategies that are used behavioral phenotyping of knockout mice. In this chapter, I established a behavioral testing system for assessment of the behavioral alterations in medaka by the multitiered strategy. To demonstrate the usability of the system, the behavioral alterations in medaka adult fish chronically administrated fluoxetine, a selective serotonin reuptake inhibitor (SSRI) class of anti-depressant, were assessed using five

behavioral paradigms (diving, open-field, light-dark transition, mirror-biting, and social interaction) as indicators of anxiety-related and social behaviors. Fish chronically treated with fluoxetine exhibited anxiolytic responses such as an overall increased time spent in the top area in the diving test and an increased time spent in center area in the open-field test. Analysis of socially evoked behavior showed that chronic fluoxetine administration decreased the number of mirror biting times in the mirror-biting test and increased latency to first contact in the social interaction test. Additionally, chronic fluoxetine administration reduced the horizontal locomotor activity in the open-field test but not the vertical activity in the diving test. These investigations are mostly consistent with previous reports in the other teleost species and rodent models. These results indicate that behavioral assessment in medaka adult fish will become useful for not only pharmaceutical and toxicological screening but also understanding the gene function in animal behaviors.

Chapter 7. Behavioral phenotyping of tph2-deficient mutant fish generated by TALENs
In this chapter, to show the utility of the established techniques to understand the behavioral functions of genes, I demonstrated the neurobehavioral phenotyping of a medaka mutant that had a frame-shifted deletion in the *tph2* gene, encoding a tryptophan hydroxylase involved in the synthesis of serotonin (5-hydroxytryptamine; 5-HT), induced by TALENs. At first, I showed that the mutant fish were deficient in 5-HT of the raphe nuclei in the brain stem by immunohistochemical and mass spectrometric analysis. Subsequently, the behavioral alterations in the mutant fish were assessed using five behavioral paradigms (diving, open-field, light-dark transition, mirror approaching, and social interaction). The *tph2* mutant fish exhibited decreased locomotor activity and reduced the number of entries to the top area in the diving test. The *tph2* mutant female also showed a decreased mirror biting time in the mirror biting test and an increased contact number in social interaction test. In addition, the *tph2* mutant fish exhibited longer duration of freezing for the first several minutes of each test in all examined paradigms. These results indicate that the *tph2* gene will be involved in modulation of anxiety/fear responses and social behaviors in medaka. These facts also suggest that a combination of the genome editing technology established in the previous chapters and the behavioral testing system that was newly developed in the last chapter is an effective technique for understanding of gene functions in complex behaviors of medaka and other teleost fishes.

Chapter 8. General Discussion
In this study, I demonstrated the successful targeted mutagenesis in medaka using targetable nuclease systems–ZFNs, TALENs, and CRISPR/Cas system. All three systems were introduced as RNA sequences into each fertilized egg of medaka by the microinjection method, thereby inducing small insertions and deletions on the target DNA sequence with high efficiency. The mutation events were occurred at the germ cells of the injected fish and therefore were efficiently transmitted to next generations. Subsequently, I showed that the frame-shifted mutation on the *tph2* gene by TALENs caused impairment of the 5-HT synthesis in the raphe nuclei of the brain stem, resulting in alterations of anxiety-related and social behaviors that were assessed with a newly developed behavioral testing system for small laboratory fish. These facts indicate that targeted mutagenesis using the targetable nuclease systems has become a powerful technology to elucidate gene functions within organisms, especially in adult phenotypes including complex behaviors, by reverse genetics approaches in medaka and other teleost fish species. These techniques will make a significant contribution in a broad range of studies including basic biology, biomedical research, toxicology, and aquaculture/fisheries.

Acknowledgement

I would like to express the deepest appreciation to Dr. Masato Kinoshita, Division of Applied Biosciences, Graduate School of Agriculture, Kyoto University, for his advice and guidance on a whole extent of research project in this thesis, from the basis of molecular biology experiment and fish breeding to design and conceiving of all experiments. Without his warm and generous support, I would not work on this project with very few precedent in our laboratory.

I would like to show my great gratitude to Dr. Kenji Sato, Division of Applied Biosciences, Graduate School of Agriculture, Kyoto University, for his supervision for the last 2 years of my Ph.D. work, giving insightful comments on this thesis, and kind technical support on the LC-MS/MS experiment. I am also grateful to Dr. Haruhiko Toyohara, Division of Applied Biosciences, Graduate School of Agriculture, Kyoto University, for his supervision for the anterior half of my Ph.D. work and giving suggestive comment in the laboratory seminar.

I would like to express my appreciation to the examination committee members Dr. Shigeki Sawayama and Dr. Masatomo Tagawa, Division of Applied Biosciences, Graduate School of Agriculture, Kyoto University, for their critical reading of this thesis. I also would like to thank Dr. Tagawa for his support on histological analysis.

I would be deeply grateful to Dr. Hiroshi Hosokawa, Department of Intelligence Science and Technology, Graduate School of Informatics, Kyoto University, for development of the software for automated behavioral testing, detailed advice on development of the behavioral testing apparutuses and immunohistochemistry, and extensive discussion on neurobehavioral analysis. I also would like to thank Dr. Shingo Maegawa, Department of Intelligence Science and Technology, Graduate School of Informatics, Kyoto University, for his support and encouragement on behavioral analysis and immunohistochemistry and constructive discussion. Additionally, I am grateful to them to have been introduced that the world around us is not what it seems.

I sincerely thank my current and former colleagues in Laboratory of Marine Biological Function, Division of Applied Biosciences, Graduate School of Agriculture, Kyoto University, for their kind help and wide-ranging discussion. Especially, I would like to offer my special thanks to Dr. Youhei Washio for technical support on immunohistochemistry and advise on fish biology/fisheries and to all members of the Kinoshita group for their continuing support on fish care and other experiments. Additionally, I am grateful to members of Laboratory of Biological Information, Department of Intelligence Science and Technology, Graduate School of Informatics, Kyoto University, for their help during the behavioral testing.

I would be grateful to Dr. Takashi Yamamoto, Dr. Hiroshi Ochiai, and Dr. Tetsushi Sakuma, Department of Mathematical and Life Sciences, Graduate School of Science, Hiroshima University, for helpful advice on the engineered nucleases and providing plasmid vectors for EGFP-ZFNs and the 6-modules assembly of TAL repeats. Also, I am grateful to members of Molecular Genetics Laboratory, Department of Mathematical and Life Sciences, Graduate School of Science, Hiroshima University, for their help during my stay for a month to learn construction of TALENs in October, 2011.

I would like to thank Dr. Takeshi Kitano, Graduate School of Science and Technology, Kumamoto University, for sharing the information on EGFP-ZFNs in medaka, Dr. Yasuhiro Kamei, Spectrography and Bioimaging Facility, National Institute for Basic Biology, for his support on the melting

curve analysis, Dr. Ryosuke Takahashi and Dr. Norihito Uemura, Department of Neurology, Graduate School of Medicine, Kyoto University, for constructive suggestions and help on the *DJ-1* and *snca* experiment, Dr. Hiroyoshi Ariga, Graduate School of Pharmaceutical Sciences, Hokkaido University, for providing the medaka DJ-1 antibody, Dr. Keiji Inohaya, Department of Biological Information, Tokyo Institute of Technology, for useful suggestion and providing plasmids on TALENs for *notch1b* and *tbx6*, and Dr. Yasutoshi Yoshiura, National Research Institute of Fisheries and Enhancement of Inland Sea, Fisheries Research Agency, and Dr. Manfred Schartl, Department Physiological Chemistry, Biocenter, University of Würzburg, for sharing information on TALENs for *mc4r*.

I also would like to thank Dr. Daniel Voytas, University of Minnesota, for providing the Golden Gate TALEN and TAL Effector Kit, Dr. Kazuyuki Hoshijima and Dr. David Grunwald, University of Utah, for providing the pCS2TAL3DD and the pCS2TAL3RR vectors, Dr. Keith Joung, Massachusetts General Hospital and Harvard Medical School, for providing the pDR274 vector, Dr. Feng Zhang, Broad Institute and Massachusetts Institute of Technology, for providing pX330 vector and allowing for a wide distribution of the modified vector pCS2+hSpCas9, and Addgene, the nonprofit global plasmid repository, for providing many plasmids and a wide distribution of my plasmid pCS2+hSpCas9.

I thank NBRP medaka for developing the off-target analysis tools and providing hatching enzyme. I am also grateful to many fish researchers including my collaborators for considerable encouragement on this work.

This work was in part supported by Grant-in-Aid for JSPS Fellows Grant Number 25-1682.

Finally, I appreciate my family, especially my parents, for supporting me throughout my Ph.D. years and my life in general.

References

[1] Capecchi MR. (2005) Gene targeting in mice: functional analysis of the mammalian genome for the twenty-first century. *Nat. Rev. Genet.* **6**, 507–512.

[2] Howe K, Clark MD, Torroja CF, Torrance J, Berthelot C, Muffato M, et al. (2013) The zebrafish reference genome sequence and its relationship to the human genome. *Nature* **496**, 498–503.

[3] Kasahara M, Naruse K, Sasaki S, Nakatani Y, Qu W, Ahsan B, et al. (2007) The medaka draft genome and insights into vertebrate genome evolution. *Nature* **447**, 714–749.

[4] Jones FC, Grabherr MG, Chan YF, Russell P, Mauceli E, Johnson J, et al. (2012) The genomic basis of adaptive evolution in threespine sticklebacks. *Nature* **484**, 55–61.

[5] Schartl M, Walter RB, Shen Y, Garcia T, Catchen J, Amores A, et al. (2013) The genome of the platyfish, Xiphophorus maculatus, provides insights into evolutionary adaptation and several complex traits. *Nat. Genet.* **45**, 567–572.

[6] Brawand D, Wagner CE, Li YI, Malinsky M, Keller I, Fan S, et al. (2014) The genomic substrate for adaptive radiation in African cichlid fish. *Nature* **513**, 375–381.

[7] Aparicio S, Chapman J, Stupka E, Putnam N, Chia JM, Dehal P, et al. (2002) Whole-genome shotgun assembly and analysis of the genome of Fugu rubripes. *Science* **297**, 1301–1310.

[8] Star B, Nederbragt AJ, Jentoft S, Grimholt U, Malmstrøm M, Gregers TF, et al. (2011) The genome sequence of Atlantic cod reveals a unique immune system. *Nature* **477**, 207–210.

[9] Berthelot C, Brunet F, Chalopin D, Juanchich A, Bernard M, Noël B, et al. (2014) The rainbow trout genome provides novel insights into evolution after whole-genome duplication in vertebrates. *Nat. Commun.* **5**, 3657.

[10] Davidson WS, Koop BF, Jones SJM, Iturra P, Vidal R, Maass A, et al. (2010) Sequencing the genome of the Atlantic salmon (Salmo salar). *Genome Biol.* **11**, 403.

[11] Chen S, Zhang G, Shao C, Huang Q, Liu G, Zhang P, et al. (2014) Whole-genome sequence of a flatfish provides insights into ZW sex chromosome evolution and adaptation to a benthic lifestyle. *Nat. Genet.* **46**, 253–260.

[12] Nakamura Y, Mori K, Saitoh K, Oshima K, Mekuchi M, Sugaya T, et al. (2013) Evolutionary changes of multiple visual pigment genes in the complete genome of Pacific bluefin tuna. *Proc. Natl. Acad. Sci. U. S. A.* **110**, 11061–11066.

[13] Nasevicius A, & Ekker SC. (2000) Effective targeted gene knockdown in zebrafish. *Nat. Genet.* **26**, 216–220.

[14] Wienholds E, Schulte-Merker S, Walderich B, & Plasterk RHA. (2002) Target-selected inactivation of the zebrafish rag1 gene. *Science* **297**, 99–102.

[15] Wienholds E. (2003) Efficient target-selected mutagenesis in zebrafish. *Genome Res.* **13**, 2700–2707.

[16] Taniguchi Y, Takeda S, Furutani-Seiki M, Kamei Y, Todo T, Sasado T, et al. (2006) Generation of medaka gene knockout models by target-selected mutagenesis. *Genome Biol.* **7**, R116.

[17] Kuroyanagi M, Katayama T, Imai T, Yamamoto Y, Chisada SI, Yoshiura Y, et al. (2013) New approach for fish breeding by chemical mutagenesis: establishment of TILLING method in fugu (Takifugu rubripes) with ENU mutagenesis. *BMC Genomics* **14**, 786.

[18] Carroll D. (2014) Genome engineering with targetable nucleases. *Annu. Rev. Biochem.* **83**,

409–439.
[19] Sakuma T, & Woltjen K. (2014) Nuclease-mediated genome editing: At the front-line of functional genomics technology. *Dev. Growth Differ.* **56**, 2–13.
[20] Urnov FD, Rebar EJ, Holmes MC, Zhang HS, & Gregory PD. (2010) Genome editing with engineered zinc finger nucleases. *Nat. Rev. Genet.* **11**, 636–646.
[21] Bibikova M, Golic M, Golic KG, & Carroll D. (2002) Targeted chromosomal cleavage and mutagenesis in Drosophila using zinc-finger nucleases. *Genetics* **161**, 1169–1175.
[22] Beumer KJ, Trautman JK, Bozas A, Liu JL, Rutter J, Gall JG, et al. (2008) Efficient gene targeting in Drosophila by direct embryo injection with zinc-finger nucleases. *Proc. Natl. Acad. Sci. U. S. A.* **105**, 19821–19826.
[23] Ochiai H, Fujita K, Suzuki Ki, Nishikawa M, Shibata T, Sakamoto N, et al. (2010) Targeted mutagenesis in the sea urchin embryo using zinc-finger nucleases. *Genes Cells* **15**, 875–885.
[24] Young JJ, Cherone JM, Doyon Y, Ankoudinova I, Faraji FM, Lee AH, et al. (2011) Efficient targeted gene disruption in the soma and germ line of the frog Xenopus tropicalis using engineered zinc-finger nucleases. *Proc. Natl. Acad. Sci. U. S. A.* **108**, 7052–7057.
[25] Geurts AM, Cost GJ, Freyvert Y, Zeitler B, Miller JC, Choi VM, et al. (2009) Knockout rats via embryo microinjection of zinc-finger nucleases. *Science* **325**, 433.
[26] Mashimo T, Takizawa A, Voigt B, Yoshimi K, Hiai H, Kuramoto T, et al. (2010) Generation of knockout rats with X-linked severe combined immunodeficiency (X-SCID) using zinc-finger nucleases. *PLoS One* **5**, e8870.
[27] Cui X, Ji D, Fisher Da, Wu Y, Briner DM, & Weinstein EJ. (2011) Targeted integration in rat and mouse embryos with zinc-finger nucleases. *Nat. Biotechnol.* **29**, 64–67.
[28] Doyon Y, McCammon JM, Miller JC, Faraji F, Ngo C, Katibah GE, et al. (2008) Heritable targeted gene disruption in zebrafish using designed zinc-finger nucleases. *Nat. Biotechnol.* **26**, 702–708.
[29] Meng X, Noyes MB, Zhu LJ, Lawson ND, & Wolfe SA. (2008) Targeted gene inactivation in zebrafish using engineered zinc-finger nucleases. *Nat. Biotechnol.* **26**, 695–701.
[30] Foley JE, Yeh JRJ, Maeder ML, Reyon D, Sander JD, Peterson RT, et al. (2009) Rapid mutation of endogenous zebrafish genes using zinc finger nucleases made by Oligomerized Pool ENgineering (OPEN). *PLoS One* **4**, e4348.
[31] Takeda H, & Shimada A. (2010) The art of medaka genetics and genomics: what makes them so unique? *Annu. Rev. Genet.* **44**, 217–241.
[32] Ozato K, Kondoh H, Inohara H, Iwamatsu T, Wakamatsu Y, & Okada T. (1986) Production of transgenic fish: introduction and expression of chicken δ-crystallin gene in medaka embryos. *Cell Differ.* **19**, 237–244.
[33] Kinoshita M, Murata K, Naruse K, & Tanaka M. (2009) *Medaka*. (John Wiley & Sons, Ltd., Ames, Iowa, USA), p. 445.
[34] Kim YG, Cha J, & Chandrasegaran S. (1996) Hybrid restriction enzymes: zinc finger fusions to Fok I cleavage domain. *Proc. Natl. Acad. Sci. U. S. A.* **93**, 1156–1160.
[35] Pabo CO, Peisach E, & Grant RA. (2001) Design and selection of novel Cys2His2 zinc finger proteins. *Annu. Rev. Biochem.* **70**, 313–340.
[36] Watanabe T, Ochiai H, Sakuma T, Horch HW, Hamaguchi N, Nakamura T, et al. (2012) Non-transgenic genome modifications in a hemimetabolous insect using zinc-finger and TAL effector nucleases. *Nat. Commun.* **3**, 1017.
[37] Suehiro Y, Kinoshita M, Okuyama T, Shimada A, Naruse K, Takeda H, et al. (2010) Transient and permanent gene transfer into the brain of the teleost fish medaka (Oryzias latipes) using human adenovirus and the Cre-loxP system. *FEBS Lett.* **584**, 3545–3549.
[38] Yusa K, Rad R, Takeda J, & Bradley A. (2009) Generation of transgene-free induced pluripotent mouse stem cells by the piggyBac transposon. *Nat. Methods* **6**, 363–369.

[39] Kinoshita M, Kani S, Ozato K, & Wakamatsu Y. (2000) Activity of the medaka translation elongation factor 1alpha-A promoter examined using the GFP gene as a reporter. *Dev. Growth Differ.* **42**, 469–478.

[40] Tanaka M, Kinoshita M, Kobayashi D, & Nagahama Y. (2001) Establishment of medaka (Oryzias latipes) transgenic lines with the expression of green fluorescent protein fluorescence exclusively in germ cells: a useful model to monitor germ cells in a live vertebrate. *Proc. Natl. Acad. Sci. U. S. A.* **98**, 2544–2549.

[41] Guo J, Gaj T, & Barbas CF. (2010) Directed evolution of an enhanced and highly efficient FokI cleavage domain for zinc finger nucleases. *J. Mol. Biol.* **400**, 96–107.

[42] Knaut H, Steinbeisser H, Schwarz H, & Nüsslein-Volhard C. (2002) An evolutionary conserved region in the vasa 3'UTR targets RNA translation to the germ cells in the zebrafish. *Curr. Biol.* **12**, 454–466.

[43] Kurokawa H, Aoki Y, Nakamura S, Ebe Y, Kobayashi D, & Tanaka M. (2006) Time-lapse analysis reveals different modes of primordial germ cell migration in the medaka Oryzias latipes. *Dev. Growth Differ.* **48**, 209–221.

[44] Pruett-Miller SM, Connelly JP, Maeder ML, Joung JK, & Porteus MH. (2008) Comparison of zinc finger nucleases for use in gene targeting in mammalian cells. *Mol. Ther.* **16**, 707–717.

[45] Kinoshita M. (2004) Transgenic medaka with brilliant fluorescence in skeletal muscle under normal light. *Fish. Sci.* **70**, 645–649.

[46] Fukamachi S, Yada T, Meyer A, & Kinoshita M. (2009) Effects of constitutive expression of somatolactin alpha on skin pigmentation in medaka. *Gene* **442**, 81–87.

[47] Qiu P, Shandilya H, D'Alessio JM, O'Connor K, Durocher J, & Gerard GF. (2004) Mutation detection using Surveyor nuclease. *Biotechniques* **36**, 702–707.

[48] Miller JC, Holmes MC, Wang J, Guschin DY, Lee YL, Rupniewski I, et al. (2007) An improved zinc-finger nuclease architecture for highly specific genome editing. *Nat. Biotechnol.* **25**, 778–785.

[49] Carl M, Loosli F, & Wittbrodt J. (2002) Six3 inactivation reveals its essential role for the formation and patterning of the vertebrate eye. *Development* **129**, 4057–4063.

[50] Dorn S, Aghaallaei N, Jung G, Bajoghli B, Werner B, Bock H, et al. (2012) Side chain modified peptide nucleic acids (PNA) for knock-down of six3 in medaka embryos. *BMC Biotechnol.* **12**, 50.

[51] Bogdanove AJ, & Voytas DF. (2011) TAL effectors: customizable proteins for DNA targeting. *Science* **333**, 1843–1846.

[52] Christian M, Cermak T, Doyle EL, Schmidt C, Zhang F, Hummel A, et al. (2010) Targeting DNA double-strand breaks with TAL effector nucleases. *Genetics* **186**, 757–761.

[53] Miller JC, Tan S, Qiao G, Barlow Ka, Wang J, Xia DF, et al. (2011) A TALE nuclease architecture for efficient genome editing. *Nat. Biotechnol.* **29**, 143–148.

[54] Boch J, Scholze H, Schornack S, Landgraf A, Hahn S, Kay S, et al. (2009) Breaking the code of DNA binding specificity of TAL-type III effectors. *Science* **326**, 1509–1512.

[55] Moscou MJ, & Bogdanove AJ. (2009) A simple cipher governs DNA recognition by TAL effectors. *Science* **326**, 1501.

[56] Cermak T, Doyle EL, Christian M, Wang L, Zhang Y, Schmidt C, et al. (2011) Efficient design and assembly of custom TALEN and other TAL effector-based constructs for DNA targeting. *Nucleic Acids Res.* **39**, e82.

[57] Reyon D, Tsai SQ, Khayter C, Foden JA, Sander JD, & Joung JK. (2012) FLASH assembly of TALENs for high-throughput genome editing. *Nat. Biotechnol.* **30**, 460–465.

[58] Sanjana NE, Cong L, Zhou Y, Cunniff MM, Feng G, & Zhang F. (2012) A transcription activator-like effector toolbox for genome engineering. *Nat. Protoc.* **7**, 171–192.

[59] Huang P, Xiao A, Zhou M, Zhu Z, Lin S, & Zhang B. (2011) Heritable gene targeting in

zebrafish using customized TALENs. *Nat. Biotechnol.* **29**, 699–700.
[60] Sander JD, Cade L, Khayter C, Reyon D, Peterson RT, Joung JK, et al. (2011) Targeted gene disruption in somatic zebrafish cells using engineered TALENs. *Nat. Biotechnol.* **29**, 697–698.
[61] Tesson L, Usal C, Ménoret S, Leung E, Niles BJ, Remy S, et al. (2011) Knockout rats generated by embryo microinjection of TALENs. *Nat. Biotechnol.* **29**, 695–696.
[62] Lei Y, Guo X, Liu Y, Cao Y, Deng Y, Chen X, et al. (2012) Efficient targeted gene disruption in Xenopus embryos using engineered transcription activator-like effector nucleases (TALENs). *Proc. Natl. Acad. Sci. U. S. A.* **109**, 17484–17489.
[63] Liu J, Li C, Yu Z, Huang P, Wu H, Wei C, et al. (2012) Efficient and specific modifications of the Drosophila genome by means of an easy TALEN strategy. *J. Genet. Genomics* **39**, 209–215.
[64] Ma S, Zhang S, Wang F, Liu Y, Liu Y, Xu H, et al. (2012) Highly efficient and specific genome editing in silkworm using custom TALENs. *PLoS One* **7**, e45035.
[65] Bonifati V, Rizzu P, Baren van MJ, Schaap O, Breedveld GJ, Krieger E, et al. (2003) Mutations in the DJ-1 gene associated with autosomal recessive early-onset parkinsonism. *Science* **299**, 256–259.
[66] Yamamoto TO. (1953) Artificially induced sex-reversal in genotypic males of the medaka (Oryzias latipes). *J. Exp. Zool.* **123**, 571–594.
[67] Doyle EL, Booher NJ, Standage DS, Voytas DF, Brendel VP, VanDyk JK, et al. (2012) TAL Effector-Nucleotide Targeter (TALE-NT) 2.0: tools for TAL effector design and target prediction. *Nucleic Acids Res.* **40**, W117–W122.
[68] Sakuma T, Hosoi S, Woltjen K, Suzuki KI, Kashiwagi K, Wada H, et al. (2013) Efficient TALEN construction and evaluation methods for human cell and animal applications. *Genes to Cells* **18**, 315–326.
[69] Dahlem TJ, Hoshijima K, Jurynec MJ, Gunther D, Starker CG, Locke AS, et al. (2012) Simple Methods for Generating and Detecting Locus-Specific Mutations Induced with TALENs in the Zebrafish Genome. *PLoS Genet.* **8**, e1002861.
[70] Li HM, Taira T, Maita C, Ariga H, & Iguchi-Ariga SM. (2006) Protection against nonylphenol-induced cell death by DJ-1 in cultured Japanese medaka (Oryzias latipes) cells. *Toxicology* **228**, 229–238.
[71] Ansai S, Ochiai H, Kanie Y, Kamei Y, Gou Y, Kitano T, et al. (2012) Targeted disruption of exogenous EGFP gene in medaka using zinc-finger nucleases. *Dev. Growth Differ.* **54**, 546–556.
[72] Mussolino C, Morbitzer R, Lutge F, Dannemann N, Lahaye T, & Cathomen T. (2011) A novel TALE nuclease scaffold enables high genome editing activity in combination with low toxicity. *Nucleic Acids Res.* **39**, 9283–9293.
[73] Bedell VM, Wang Y, Campbell JM, Poshusta TL, Starker CG, Krug II RG, et al. (2012) In vivo genome editing using a high-efficiency TALEN system. *Nature* **491**, 114–118.
[74] Cade L, Reyon D, Hwang WY, Tsai SQ, Patel S, Khayter C, et al. (2012) Highly efficient generation of heritable zebrafish gene mutations using homo- and heterodimeric TALENs. *Nucleic Acids Res.* **40**, 8001–8010.
[75] Kim RH, Smith PD, Aleyasin H, Hayley S, Mount MP, Pownall S, et al. (2005) Hypersensitivity of DJ-1-deficient mice to 1-methyl-4-phenyl-1,2,3,6-tetrahydropyrindine (MPTP) and oxidative stress. *Proc. Natl. Acad. Sci. U. S. A.* **102**, 5215–5220.
[76] Bretaud S, Allen C, Ingham PW, & Bandmann O. (2007) p53-dependent neuronal cell death in a DJ-1-deficient zebrafish model of Parkinson's disease. *J. Neurochem.* **100**, 1626–1635.
[77] Szurek B, Rossier O, Hause G, & Bonas U. (2002) Type III-dependent translocation of the Xanthomonas AvrBs3 protein into the plant cell. *Mol. Microbiol.* **46**, 13–23.
[78] Carroll D. (2011) Genome engineering with zinc-finger nucleases. *Genetics* **188**, 773–782.
[79] Joung JK, & Sander JD. (2013) TALENs: a widely applicable technology for targeted genome editing. *Nat. Rev. Mol. Cell Biol.* **14**, 49–55.

[80] Chen J, Zhang X, Wang T, Li Z, Guan G, & Hong Y. (2012) Efficient detection, quantification and enrichment of subtle allelic alterations. *DNA Res.* **19**, 423–433.
[81] Ansai S, Sakuma T, Yamamoto T, Ariga H, Uemura N, Takahashi R, et al. (2013) Efficient Targeted Mutagenesis in Medaka Using Custom-Designed Transcription Activator-Like Effector Nucleases. *Genetics* **193**, 739–749.
[82] Hisano Y, Ota S, Arakawa K, Muraki M, Kono N, Oshita K, et al. (2013) Quantitative assay for TALEN activity at endogenous genomic loci. *Biol. Open* **2**, 363–367.
[83] Ota S, Hisano Y, Muraki M, Hoshijima K, Dahlem TJ, Grunwald DJ, et al. (2013) Efficient identification of TALEN-mediated genome modifications using heteroduplex mobility assays. *Genes to Cells* **18**, 450–458.
[84] Furutani-Seiki M, Sasado T, Morinaga C, Suwa H, Niwa K, Yoda H, et al. (2004) A systematic genome-wide screen for mutations affecting organogenesis in Medaka, Oryzias latipes. *Mech. Dev.* **121**, 647–658.
[85] Fukamachi S, Shimada A, & Shima A. (2001) Mutations in the gene encoding B, a novel transporter protein, reduce melanin content in medaka. *Nat. Genet.* **28**, 381–385.
[86] Fukamachi S, Kinoshita M, Tsujimura T, Shimada A, Oda S, Shima A, et al. (2008) Rescue from oculocutaneous albinism type 4 using medaka slc45a2 cDNA driven by its own promoter. *Genetics* **178**, 761–769.
[87] McVey M, & Lee SE. (2008) MMEJ repair of double-strand breaks (director ' s cut): deleted sequences and alternative endings. *Trends Genet.* **24**, 529–538.
[88] Mak ANS, Bradley P, Cernadas RA, Bogdanove AJ, & Stoddard BL. (2012) The crystal structure of TAL effector PthXo1 bound to its DNA target. *Science* **335**, 716–719.
[89] Römer P, Recht S, Strauß T, Elsaesser J, Schornack S, Boch J, et al. (2010) Promoter elements of rice susceptibility genes are bound and activated by specific TAL effectors from the bacterial blight pathogen, Xanthomonas oryzae pv. oryzae. *New Phytol.* **187**, 1048–1057.
[90] Wiedenheft B, Sternberg SH, & Doudna JA. (2012) RNA-guided genetic silencing systems in bacteria and archaea. *Nature* **482**, 331–338.
[91] Gasiunas G, Barrangou R, Horvath P, & Siksnys V. (2012) Cas9-crRNA ribonucleoprotein complex mediates specific DNA cleavage for adaptive immunity in bacteria. *Proc. Natl. Acad. Sci. U. S. A.* **109**, E2579–E2586.
[92] Jinek M, Chylinski K, Fonfara I, Hauer M, Doudna JA, & Charpentier E. (2012) A programmable dual-RNA-guided DNA endonuclease in adaptive bacterial immunity. *Science* **337**, 816–821.
[93] Cho SW, Kim S, Kim JM, & Kim JS. (2013) Targeted genome engineering in human cells with the Cas9 RNA-guided endonuclease. *Nat. Biotechnol.* **31**, 230–232.
[94] Cong L, Ran FA, Cox D, Lin S, Barretto R, Habib N, et al. (2013) Multiplex genome engineering using CRISPR/Cas systems. *Science* **339**, 819–823.
[95] Fu Y, Foden JA, Khayter C, Maeder ML, Reyon D, Joung JK, et al. (2013) High-frequency off-target mutagenesis induced by CRISPR-Cas nucleases in human cells. *Nat. Biotechnol.* **31**, 822–826.
[96] Hsu PD, Scott DA, Weinstein JA, Ran FA, Konermann S, Agarwala V, et al. (2013) DNA targeting specificity of RNA-guided Cas9 nucleases. *Nat. Biotechnol.* **31**, 827–832.
[97] Mali P, Yang L, Esvelt KM, Aach J, Guell M, DiCarlo JE, et al. (2013) RNA-guided human genome engineering via Cas9. *Science* **339**, 823–826.
[98] Wang H, Yang H, Shivalila CS, Dawlaty MM, Cheng AW, Zhang F, et al. (2013) One-step generation of mice carrying mutations in multiple genes by CRISPR/cas-mediated genome engineering. *Cell* **153**, 910–918.
[99] Bassett AR, Tibbit C, Ponting CP, & Liu JL. (2013) Highly efficient targeted mutagenesis of drosophila with the CRISPR/Cas9 system. *Cell Rep.* **4**, 220–228.

[100] Gratz SJ, Cummings AM, Nguyen JN, Hamm DC, Donohue LK, Harrison MM, et al. (2013) Genome engineering of Drosophila with the CRISPR RNA-guided Cas9 nuclease. *Genetics* **194**, 1029–1035.
[101] Friedland AE, Tzur YB, Esvelt KM, Colaiácovo MP, Church GM, & Calarco JA. (2013) Heritable genome editing in C. elegans via a CRISPR-Cas9 system. *Nat. Methods* **10**, 741–743.
[102] Chang N, Sun C, Gao L, Zhu D, Xu X, Zhu X, et al. (2013) Genome editing with RNA-guided Cas9 nuclease in Zebrafish embryos. *Cell Res.* **23**, 465–472.
[103] Hwang WY, Fu Y, Reyon D, Maeder ML, Kaini P, Sander JD, et al. (2013) Heritable and precise zebrafish genome editing using a CRISPR-Cas system. *PLoS One* **8**, e68708.
[104] Hwang WY, Fu Y, Reyon D, Maeder ML, Tsai SQ, Sander JD, et al. (2013) Efficient genome editing in zebrafish using a CRISPR-Cas system. *Nat. Biotechnol.* **31**, 227–229.
[105] Jao LE, Wente SR, & Chen W. (2013) Efficient multiplex biallelic zebrafish genome editing using a CRISPR nuclease system. *Proc. Natl. Acad. Sci. U. S. A.* **110**, 13904–13909.
[106] Xiao A, Wang Z, Hu Y, Wu Y, Luo Z, Yang Z, et al. (2013) Chromosomal deletions and inversions mediated by TALENs and CRISPR/Cas in zebrafish. *Nucleic Acids Res.* **41**, e141.
[107] Mussolino C, & Cathomen T. (2013) RNA guides genome engineering. *Nat. Biotechnol.* **31**, 208–209.
[108] Ran FA, Hsu PD, Lin CY, Gootenberg JS, Konermann S, Trevino AE, et al. (2013) Double nicking by RNA-guided CRISPR Cas9 for enhanced genome editing specificity. *Cell* **154**, 1380–1389.
[109] Cho SW, Kim S, Kim Y, Kweon J, Kim HS, Bae S, et al. (2014) Analysis of off-target effects of CRISPR/Cas-derived RNA-guided endonucleases and nickases. *Genome Res.* **24**, 132–141.
[110] Wang T, Wei JJ, Sabatini DM, & Lander ES. (2014) Genetic screens in human cells using the CRISPR-Cas9 system. *Science* **343**, 80–84.
[111] Turner DL, & Weintraub H. (1994) Expression of achaete-scute homolog 3 in Xenopus embryos converts ectodermal cells to a neural fate. *Genes Dev.* **8**, 1434–1447.
[112] Ansai S, Inohaya K, Yoshiura Y, Schartl M, Uemura N, Takahashi R, et al. (2014) Design, evaluation, and screening methods for efficient targeted mutagenesis with transcription activator-like effector nucleases in medaka. *Dev. Growth Differ.* **56**, 98–107.
[113] Ran FA, Hsu PD, Wright J, Agarwala V, Scott DA, & Zhang F. (2013) Genome engineering using the CRISPR-Cas9 system. *Nat. Protoc.* **8**, 2281–2308.
[114] Jiang W, Bikard D, Cox D, Zhang F, & Marraffini LA. (2013) RNA-guided editing of bacterial genomes using CRISPR-Cas systems. *Nat. Biotechnol.* **31**, 233–239.
[115] Valton J, Dupuy A, Daboussi F, Thomas S, Marechal A, Macmaster R, et al. (2012) Overcoming transcription activator-like effector (TALE) DNA binding domain sensitivity to cytosine methylation. *J. Biol. Chem.* **287**, 38427–38432.
[116] Crawley JN. (1999) Behavioral phenotyping of transgenic and knockout mice: experimental design and evaluation of general health, sensory functions, motor abilities, and specific behavioral tests. *Brain Res.* **835**, 18–26.
[117] Crawley JN, & Paylor R. (1997) A Proposed Test Battery and Constellations of Specific Behavioral Paradigms to Investigate the Behavioral Phenotypes of Transgenic and Knockout Mice. *Horm. Behav.* **31**, 197–211.
[118] Karl T, Pabst R, & Hörsten von S. (2003) Behavioral phenotyping of mice in pharmacological and toxicological research. *Exp. Toxicol. Pathol.* **55**, 69–83.
[119] Nelson JS. (2006) *Fishes of the World, 4th Edition*. Vol. 7, p. 624.
[120] Stewart AM, Braubach O, Spitsbergen J, Gerlai R, & Kalueff AV. (2014) Zebrafish models for translational neuroscience research: from tank to bedside. *Trends Neurosci.* **37**, 264–278.
[121] Kalueff AV, Stewart AM, & Gerlai R. (2014) Zebrafish as an emerging model for studying complex brain disorders. *Trends Pharmacol. Sci.* **35**, 63–75.

[122] Grossman L, Utterback E, Stewart A, Gaikwad S, Chung KM, Suciu C, et al. (2010) Characterization of behavioral and endocrine effects of LSD on zebrafish. *Behav. Brain Res.* **214**, 277–284.
[123] Norton WHJW, Stumpenhorst K, Faus-Kessler T, Folchert A, Rohner N, Harris MPM, et al. (2011) Modulation of Fgfr1a signaling in zebrafish reveals a genetic basis for the aggression-boldness syndrome. *J. Neurosci.* **31**, 13796–13807.
[124] Imada H, Hoki M, Suehiro Y, Okuyama T, Kurabayashi D, Shimada A, et al. (2010) Coordinated and cohesive movement of two small conspecific fish induced by eliciting a simultaneous optomotor response. *PLoS One* **5**, e11248.
[125] Nakayama K, Oshima Y, Hiramatsu K, Shimasaki Y, & Honjo T. (2005) Effects of polychlorinated biphenyls on the schooling behavior of Japanese medaka (Oryzias latipes). *Environ. Toxicol. Chem.* **24**, 2588–2593.
[126] Nakayasu T, & Watanabe E. (2014) Biological motion stimuli are attractive to medaka fish. *Anim. Cogn.* **17**, 559–575.
[127] Kagawa N. (2013) Social rank-dependent expression of arginine vasotocin in distinct preoptic regions in male Oryzias latipes. *J. Fish Biol.* **82**, 354–363.
[128] Okuyama T, Yokoi S, Abe H, Isoe Y, Suehiro Y, Imada H, et al. (2014) A neural mechanism underlying mating preferences for familiar individuals in medaka fish. *Science* **343**, 91–94.
[129] Yokoi S, Okuyama T, Kamei Y, Naruse K, Taniguchi Y, Ansai S, et al. (2015) An essential role of the arginine vasotocin system in mate-guarding behaviors in triadic relationships of medaka fish (Oryzias latipes). *PLoS Genet.* **11**, e1005009.
[130] Ochiai T, Suehiro Y, Nishinari K, Kubo T, & Takeuchi H. (2013) A new data-mining method to search for behavioral properties that induce alignment and their involvement in social learning in medaka fish (Oryzias latipes). *PLoS One* **8**, e71685.
[131] Tsubokawa T, Saito K, Kawano H, Kawamura K, Shinozuka K, & Watanabe S. (2009) Pharmacological effects on mirror approaching behavior and neurochemical aspects of the telencephalon in the fish, medaka (Oryzias latipes). *Soc. Neurosci.* **4**, 276–286.
[132] Matsunaga W, & Watanabe E. (2012) Visual motion with pink noise induces predation behaviour. *Sci. Rep.* **2**, 1–7.
[133] Tsuboko S, Kimura T, Shinya M, Suehiro Y, Okuyama T, Shimada A, et al. (2014) Genetic control of startle behavior in medaka fish. *PLoS One* **9**, e112527.
[134] Ansai S, & Kinoshita M. (2014) Targeted mutagenesis using CRISPR/Cas system in medaka. *Biol. Open* **3**, 362–371.
[135] Malagie I, Trillat AC, Jacquot C, & Gardier AM. (1995) Effects of acute fluoxetine on extracellular serotonin levels in the raphe: An in vivo microdialysis study. *Eur. J. Pharmacol.* **286**, 213–217.
[136] Perreault H, Semsar K, & Godwin J. (2003) Fluoxetine treatment decreases territorial aggression in a coral reef fish. *Physiol. Behav.* **79**, 719–724.
[137] Lynn SE, Egar JM, Walker BG, Sperry TS, & Ramenofsky M. (2007) Fish on Prozac: a simple, noninvasive physiology laboratory investigating the mechanisms of aggressive behavior in Betta splendens. *AJP Adv. Physiol. Educ.* **31**, 358–363.
[138] McDonald MD, Gonzalez A, & Sloman KA. (2011) Higher levels of aggression are observed in socially dominant toadfish treated with the selective serotonin reuptake inhibitor, fluoxetine. *Comp. Biochem. Physiol. Part C Toxicol. Pharmacol.* **153**, 107–112.
[139] Clements S, & Schreck CB. (2007) Chronic administration of fluoxetine alters locomotor behavior, but does not potentiate the locomotor stimulating effects of CRH in juvenile Chinook salmon (Oncorhynchus tshawytscha). *Comp. Biochem. Physiol. - A Mol. Integr. Physiol.* **147**, 43–49.
[140] Winder VL, Pennington PL, Hurd MW, & Wirth EF. (2012) Fluoxetine effects on sheepshead

minnow (Cyprinodon variegatus) locomotor activity. *J. Environ. Sci. Heal. Part B* **47**, 51–58.
[141] Egan RJ, Bergner CL, Hart PC, Cachat JM, Canavello PR, Elegante MF, et al. (2009) Understanding behavioral and physiological phenotypes of stress and anxiety in zebrafish. *Behav. Brain Res.* **205**, 38–44.
[142] Maximino C, Silva da AWB, Gouveia A, & Herculano AM. (2011) Pharmacological analysis of zebrafish (Danio rerio) scototaxis. *Prog. Neuropsychopharmacol. Biol. Psychiatry* **35**, 624–631.
[143] Wong RY, Oxendine SE, & Godwin J. (2013) Behavioral and neurogenomic transcriptome changes in wild-derived zebrafish with fluoxetine treatment. *BMC Genomics* **14**, 348.
[144] Margiotta-Casaluci L, Owen SF, Cumming RI, Polo de A, Winter MJ, Panter GH, et al. (2014) Quantitative cross-species extrapolation between humans and fish: the case of the antidepressant fluoxetine. *PLoS One* **9**, e110467.
[145] Chiffre A, Clérandeau C, Dwoinikoff C, Le Bihanic F, Budzinski H, Geret F, et al. (2014) Psychotropic drugs in mixture alter swimming behaviour of Japanese medaka (Oryzias latipes) larvae above environmental concentrations. *Environ. Sci. Pollut. Res.*
[146] Brooks BW, Foran CM, Richards SM, Weston J, Turner PK, Stanley JK, et al. (2003) Aquatic ecotoxicology of fluoxetine. *Toxicol. Lett.* **142**, 169–183.
[147] Foran CM, Weston J, Slattery M, Brooks BW, & Huggett DB. (2004) Reproductive assessment of Japanese medaka (Oryzias latipes) following a four-week fluoxetine (SSRI) exposure. *Arch. Environ. Contam. Toxicol.* **46**, 511–517.
[148] Nakamura Y, Yamamoto H, Sekizawa J, Kondo T, Hirai N, & Tatarazako N. (2008) The effects of pH on fluoxetine in Japanese medaka (Oryzias latipes): Acute toxicity in fish larvae and bioaccumulation in juvenile fish. *Chemosphere* **70**, 865–873.
[149] Paterson G, & Metcalfe CD. (2008) Uptake and depuration of the anti-depressant fluoxetine by the Japanese medaka (Oryzias latipes). *Chemosphere* **74**, 125–130.
[150] Peitsaro N, Kaslin J, Anichtchik OV, & Panula P. (2003) Modulation of the histaminergic system and behaviour by alpha-fluoromethylhistidine in zebrafish. *J. Neurochem.* **86**, 432–441.
[151] Matsunaga W, & Watanabe E. (2010) Habituation of medaka (Oryzias latipes) demonstrated by open-field testing. *Behav. Processes* **85**, 142–150.
[152] Maximino C, Marques de Brito T, Dias CAGDM, Gouveia A, & Morato S. (2010) Scototaxis as anxiety-like behavior in fish. *Nat. Protoc.* **5**, 209–216.
[153] Jahn-Eimermacher A, Lasarzik I, & Raber J. (2011) Statistical analysis of latency outcomes in behavioral experiments. *Behav. Brain Res.* **221**, 271–275.
[154] Maximino C, Puty B, Benzecry R, Araújo J, Lima MG, de Jesus Oliveira Batista E, et al. (2013) Role of serotonin in zebrafish (Danio rerio) anxiety: relationship with serotonin levels and effect of buspirone, WAY 100635, SB 224289, fluoxetine and para-chlorophenylalanine (pCPA) in two behavioral models. *Neuropharmacology* **71**, 83–97.
[155] Hoffman EJ, & Mathew SJ. (2008) Anxiety disorders: a comprehensive review of pharmacotherapies. *Mt. Sinai J. Med.* **75**, 248–262.
[156] Dulawa SC, Holick KA, Gundersen B, & Hen R. (2004) Effects of chronic fluoxetine in animal models of anxiety and depression. *Neuropsychopharmacology* **29**, 1321–1330.
[157] Prut L, & Belzung C. (2003) The open field as a paradigm to measure the effects of drugs on anxiety-like behaviors: A review. *Eur. J. Pharmacol.* **463**, 3–33.
[158] Ogawa S, Nathan FM, & Parhar IS. (2014) Habenular kisspeptin modulates fear in the zebrafish. *Proc. Natl. Acad. Sci. U. S. A.* **111**, 3841–3846.
[159] Ziv L, Muto A, Schoonheim PJ, Meijsing SH, Strasser D, Ingraham HA, et al. (2013) An affective disorder in zebrafish with mutation of the glucocorticoid receptor. *Mol. Psychiatry* **18**, 681–691.
[160] Maximino C, Lima MG, Costa CC, Guedes IML, & Herculano AM. (2014) Fluoxetine and WAY 100,635 dissociate increases in scototaxis and analgesia induced by conspecific alarm substance

in zebrafish (Danio rerio Hamilton 1822). *Pharmacol. Biochem. Behav.* **124**, 425–433.
[161] Bourin M, & Hascoët M. (2003) The mouse light/dark box test. *Eur. J. Pharmacol.* **463**, 55–65.
[162] Yoshida M, Nagamine M, & Uematsu K. (2005) Comparison of behavioral responses to a novel environment between three teleosts, bluegill Lepomis macrochirus, crucian carp Carassius langsdorfii, and goldfish Carassius auratus. *Fish. Sci.* **71**, 314–319.
[163] Maximino C, Marques T, & Dias F. (2007) A comparative analysis of the preference for dark environments in five teleosts. *Int. J. Comp. Psychol.* **20**, 351–367.
[164] Kagawa N. (2014) Comparison of aggressive behaviors between two wild populations of Japanese medaka, Oryzias latipes and O. sakaizumii. *Zoolog. Sci.* **31**, 116–121.
[165] Canton J, Scott KM, & Glue P. (2012) Optimal treatment of social phobia: Systematic review and meta-analysis. *Neuropsychiatr. Dis. Treat.* **8**, 203–215.
[166] Coccaro EF, & Kavoussi RJ. (1997) Fluoxetine and impulsive aggressive behavior in personality-disordered subjects. *Arch. Gen. Psychiatry* **54**, 1081–1088.
[167] De Abreu MS, Koakoski G, Ferreira D, Acosta Oliveira T, Santos Da Rosa JG, Gusso D, et al. (2014) Diazepam and fluoxetine decrease the stress response in zebrafish. *PLoS One* **9**, 1–5.
[168] Brooks SP, & Dunnett SB. (2009) Tests to assess motor phenotype in mice: a user's guide. *Nat. Rev. Neurosci.* **10**, 519–529.
[169] Marténvi F, Dossenbach M, Mraz K, & Metcalfe S. (2001) Gender differences in the efficacy of fluoxetine and maprotiline in depressed patients: A double-blind trial of antidepressants with serotonergic or norepinephrinergic reuptake inhibition profile. *Eur. Neuropsychopharmacol.* **11**, 227–232.
[170] Monleón S, Urquiza A, Carmen Arenas M, Vinader-Caerols C, & Parra A. (2002) Chronic administration of fluoxetine impairs inhibitory avoidance in male but not female mice. *Behav. Brain Res.* **136**, 483–488.
[171] Hodes GE, Hill-Smith TE, Suckow RF, Cooper TB, & Lucki I. (2010) Sex-specific effects of chronic fluoxetine treatment on neuroplasticity and pharmacokinetics in mice. *J. Pharmacol. Exp. Ther.* **332**, 266–273.
[172] Kawabata Y, Hiraki T, Takeuchi A, & Okubo K. (2012) Sex differences in the expression of vasotocin/isotocin, gonadotropin-releasing hormone, and tyrosine and tryptophan hydroxylase family genes in the medaka brain. *Neuroscience* **218**, 65–77.
[173] Okuyama T, Isoe Y, Hoki M, Suehiro Y, Yamagishi G, Naruse K, et al. (2013) Controlled Cre/loxP site-specific recombination in the developing brain in medaka fish, Oryzias latipes. *PLoS One* **8**, e66597.
[174] Kirchmaier S, Naruse K, Wittbrodt J, & Loosli F. (2015) The genomic and genetic toolbox of the teleost medaka (Oryzias latipes). *Genetics* **199**, 905–918.
[175] Crawley JN. (2008) Behavioral phenotyping strategies for mutant mice. *Neuron* **57**, 809–818.
[176] Berger M, Gray JA, & Roth BL. (2009) The expanded biology of serotonin. *Annu. Rev. Med.* **60**, 355–366.
[177] Kah O, & Chambolle P. (1983) Serotonin in the brain of the goldfish, Carassius auratus. An immunocytochemical study. *Cell Tissue Res.* **234**, 319–333.
[178] Ekström P, & Van Veen T. (1984) Distribution of 5-hydroxytryptamine (serotonin) in the brain of the teleost Gasterosteus aculeatus L. *J. Comp. Neurol.* **226**, 307–320.
[179] Frankenhuis-van den Heuvel THM, & Nieuwenhuys R. (1984) Distribution of serotonin-immunoreactivity in the diencephalon and mesencephalon of the trout, Salmo gairdneri. *Anat. Embryol. (Berl).* **169**, 193–204.
[180] Batten TF, Berry PA, Maqbool A, Moons L, & Vandesande F. (1993) Immunolocalization of catecholamine enzymes, serotonin, dopamine and L-dopa in the brain of Dicentrarchus labrax (Teleostei). *Brain Res. Bull.* **31**, 233–252.
[181] Kaslin J, & Panula P. (2001) Comparative anatomy of the histaminergic and other aminergic

systems in zebrafish (Danio rerio). *J. Comp. Neurol.* **440**, 342–377.
[182] Lillesaar C, Tannhäuser B, Stigloher C, Kremmer E, & Bally-Cuif L. (2007) The serotonergic phenotype is acquired by converging genetic mechanisms within the zebrafish central nervous system. *Dev. Dyn.* **236**, 1072–1084.
[183] Lillesaar C, Stigloher C, Tannhäuser B, Wullimann MF, & Bally-Cuif L. (2009) Axonal projections originating from raphe serotonergic neurons in the developing and adult zebrafish, Danio rerio, using transgenics to visualize raphe-specific pet1 expression. *J. Comp. Neurol.* **512**, 158–182.
[184] Lucki I. (1998) The spectrum of behaviors influenced by serotonin. *Biol. Psychiatry* **44**, 151–162.
[185] Clements S, Moore FL, & Schreck CB. (2003) Evidence that acute serotonergic activation potentiates the locomotor-stimulating effects of corticotropin-releasing hormone in juvenile chinook salmon (Oncorhynchus tshawytscha). *Horm. Behav.* **43**, 214–221.
[186] Genot G, Conan GY, Barthelemy L, & Peyraud C. (1984) Effects of 5-HT serotonin on spontaneous locomotor activity of eels. *Comp. Biochem. Physiol. C.* **79**, 189–192.
[187] Gabriel JP, Mahmood R, Kyriakatos A, Söll I, Hauptmann G, Calabrese RL, et al. (2009) Serotonergic modulation of locomotion in zebrafish: endogenous release and synaptic mechanisms. *J. Neurosci.* **29**, 10387–10395.
[188] Koutoku T, Zhang R, Tachibana T, Oshima Y, & Furuse M. (2003) Effect of acute L-tryptophan exposure on the brain serotonergic system and behavior in the male medaka. *Zoolog. Sci.* **20**, 121–124.
[189] Adams CF, Liley NR, & Gorzalka BB. (1996) PCPA increases aggression in male firemouth cichlids. *Pharmacology* **53**, 328–330.
[190] Clotfelter ED, O'Hare EP, McNitt MM, Carpenter RE, & Summers CH. (2007) Serotonin decreases aggression via 5-HT1A receptors in the fighting fish Betta splendens. *Pharmacol. Biochem. Behav.* **87**, 222–231.
[191] Ansai S, Hosokawa H, Maegawa S, & Kinoshita M. (2016) Chronic fluoxetine treatment induces anxiolytic responses and altered social behaviors in medaka, Oryzias latipes. *Behav. Brain Res.* **303**, 126–136.
[192] Lillesaar C. (2011) The serotonergic system in fish. *J. Chem. Neuroanat.* **41**, 294–308.
[193] Walther DJ, Peter JU, Bashammakh S, Hörtnagl H, Voits M, Fink H, et al. (2003) Synthesis of serotonin by a second tryptophan hydroxylase isoform. *Science* **299**, 76.
[194] Alenina N, Kikic D, Todiras M, Mosienko V, Qadri F, Plehm R, et al. (2009) Growth retardation and altered autonomic control in mice lacking brain serotonin. *Proc. Natl. Acad. Sci. U. S. A.* **106**, 10332–10337.
[195] Savelieva KV, Zhao S, Pogorelov VM, Rajan I, Yang Q, Cullinan E, et al. (2008) Genetic Disruption of Both Tryptophan Hydroxylase Genes Dramatically Reduces Serotonin and Affects Behavior in Models Sensitive to Antidepressants. *PLoS One* **3**, e3301.
[196] O'Connell LA, & Hofmann HA. (2011) The Vertebrate mesolimbic reward system and social behavior network: A comparative synthesis. *J. Comp. Neurol.* **519**, 3599–3639.
[197] Blaser RE, Chadwick L, & McGinnis GC. (2010) Behavioral measures of anxiety in zebrafish (Danio rerio). *Behav. Brain Res.* **208**, 56–62.
[198] Graeff FG, Viana MB, & Mora PO. (1997) Dual role of 5-HT in defense and anxiety. *Neurosci. Biobehav. Rev.* **21**, 791–799.
[199] Mosienko V, Bert B, Beis D, Matthes S, Fink H, Bader M, et al. (2012) Exaggerated aggression and decreased anxiety in mice deficient in brain serotonin. *Transl. Psychiatry* **2**, e122.
[200] Angoa-Pérez M, Kane MJ, Briggs DI, Sykes CE, Shah MM, Francescutti DM, et al. (2012) Genetic depletion of brain 5HT reveals a common molecular pathway mediating compulsivity and impulsivity. *J. Neurochem.* **121**, 974–984.

[201] Gutknecht L, Popp S, Waider J, Sommerlandt FMJ, Göppner C, Post A, et al. (2015) Interaction of brain 5-HT synthesis deficiency, chronic stress and sex differentially impact emotional behavior in Tph2 knockout mice. *Psychopharmacology (Berl).* pp. 2429–2441.
[202] Craig IW, & Halton KE. (2009) Genetics of human aggressive behaviour. *Hum. Genet.* **126**, 101–113.
[203] Kulikov AV, Osipova DV, Naumenko VS, & Popova NK. (2005) Association between Tph2 gene polymorphism, brain tryptophan hydroxylase activity and aggressiveness in mouse strains. *Genes, Brain Behav.* **4**, 482–485.
[204] Osipova DV, Kulikov AV, & Popova NK. (2009) C1473G polymorphism in mouse tph2 gene is linked to tryptophan hydroxylase-2 activity in the brain, intermale aggression, and depressive-like behavior in the forced swim test. *J. Neurosci. Res.* **87**, 1168–1174.
[205] Cook EH, & Leventhal BL. (1996) The serotonin system in autism.
[206] Chugani DC. (2002) Role of altered brain serotonin mechanisms in autism. *Mol. Psychiatry* **7**, S16–S17.
[207] Coon HH, Dunn D, Lainhart JE, Miller J, Hamil C, Battaglia A, et al. (2005) Possible association between autism and variants in the brain-expressed tryptophan hydroxylase gene (TPH2). *Am. J. Med. Genet. B. Neuropsychiatr. Genet.* **135B**, 42–46.
[208] Kane MJ, Angoa-Peréz M, Briggs DI, Sykes CE, Francescutti DM, Rosenberg DR, et al. (2012) Mice genetically depleted of brain serotonin display social impairments, communication deficits and repetitive behaviors: possible relevance to autism. *PLoS One* **7**, e48975.
[209] Semsar K, Perreault HaN, & Godwin J. (2004) Fluoxetine-treated male wrasses exhibit low AVT expression. *Brain Res.* **1029**, 141–147.
[210] Kotani H, Taimatsu K, Ohga R, Ota S, & Kawahara A. (2015) Efficient multiple genome modifications induced by the crRNAs, tracrRNA and Cas9 Protein complex in zebrafish. *PLoS One* **10**, e0128319.
[211] Aida T, Chiyo K, Usami T, Ishikubo H, Imahashi R, Wada Y, et al. (2015) Cloning-free CRISPR/Cas system facilitates functional cassette knock-in in mice. *Genome Biol.* **16**, 87.
[212] Aida T. (1921) On the inheritance of color in a fresh-water fish, APLOCHEILUS LATIPES Temmick and Schlegel, with special reference to sex-Linked inheritance. *Genetics* **6**, 554–573.
[213] Naruse K, Hori H, Shimizu N, Kohara Y, & Takeda H. (2004) Medaka genomics: a bridge between mutant phenotype and gene function. *Mech. Dev.* **121**, 619–628.
[214] Spivakov M, Auer TO, Peravali R, Dunham I, Dolle D, Fujiyama A, et al. (2014) Genomic and phenotypic characterization of a wild medaka population: towards the establishment of an isogenic population genetic resource in fish. *G3 (Bethesda).* **4**, 433–445.
[215] Ishikawa T, Kamei Y, Otozai S, Kim J, Sato A, Kuwahara Y, et al. (2010) High-resolution melting curve analysis for rapid detection of mutations in a Medaka TILLING library. *BMC Mol. Biol.* **11**, 70.
[216] Takehana Y, Matsuda M, Myosho T, Suster ML, Kawakami K, Shin-I T, et al. (2014) Co-option of Sox3 as the male-determining factor on the Y chromosome in the fish Oryzias dancena. *Nat. Commun.* **5**, 4157.
[217] Schartl M. (2014) Beyond the zebrafish: diverse fish species for modeling human disease. *Dis. Model. Mech.* **7**, 181–192.
[218] Matsui H, Taniguchi Y, Inoue H, Kobayashi Y, Sakaki Y, Toyoda A, et al. (2010) Loss of PINK1 in medaka fish (Oryzias latipes) causes late-onset decrease in spontaneous movement. *Neurosci. Res.* **66**, 151–161.
[219] Matsui H, Gavinio R, Asano T, Uemura N, Ito H, Taniguchi Y, et al. (2013) PINK1 and parkin complementarily protect dopaminergic neurons in vertebrates. *Hum. Mol. Genet.* **22**, 2423–2434.
[220] Uemura N, Koike M, Ansai S, Kinoshita M, Ishikawa-Fujiwara T, Matsui H, et al. (2015) Viable

neuronopathic Gaucher disease model in Medaka (Oryzias latipes) displays axonal accumulation of alpha-synuclein. *PLoS Genet.* **11**, e1005065.

[221] Morita A, Nakahira K, Hasegawa T, Uchida K, Taniguchi Y, Takeda S, et al. (2012) Establishment and characterization of Roberts syndrome and SC phocomelia model medaka (Oryzias latipes). *Dev. Growth Differ.* **54**, 588–604.

[222] Padilla S, Cowden J, Hinton DE, Yuen B, Law S, Kullman SW, et al. (2009) Use of medaka in toxicity testing. *Curr. Protoc. Toxicol.* **1**.

[223] Dong Z, Ge J, Li K, Xu Z, Liang D, Li J, et al. (2011) Heritable targeted inactivation of myostatin gene in yellow catfish (Pelteobagrus fulvidraco) using engineered zinc finger nucleases. *PLoS One* **6**, e28897.

[224] Dong Z, Ge J, Xu Z, Dong X, Cao S, Pan J, et al. (2014) Generation of myostatin B knockout yellow catfish (Tachysurus fulvidraco) using transcription activator-like effector nucleases. *Zebrafish* **11**, 265–74.

[225] Yano A, Guyomard R, Nicol B, Jouanno E, Quillet E, Klopp C, et al. (2012) An immune-related gene evolved into the master sex-determining gene in rainbow trout, Oncorhynchus mykiss. *Curr. Biol.* **22**, 1423–1428.

[226] Yano A, Nicol B, Jouanno E, & Guiguen Y. (2014) Heritable targeted inactivation of the rainbow trout (Oncorhynchus mykiss) master sex-determining gene using zinc-finger nucleases. *Mar. Biotechnol. (NY).* **16**, 243–250.

[227] Li MH, Yang HH, Li MR, Sun YL, Jiang XL, Xie QP, et al. (2013) Antagonistic roles of Dmrt1 and Foxl2 in sex differentiation via estrogen production in tilapia as demonstrated by TALENs. *Endocrinology* **154**, 4814–4825.

[228] Li M, Yang H, Zhao J, Fang L, Shi H, Li M, et al. (2014) Efficient and heritable gene targeting in tilapia by CRISPR/Cas9. *Genetics* **197**, 591–599.

[229] Edvardsen RB, Leininger S, Kleppe L, Skaftnesmo KO, & Wargelius A. (2014) Targeted mutagenesis in Atlantic salmon (Salmo salar L.) using the CRISPR/Cas9 system induces complete knockout individuals in the F0 generation. *PLoS One* **9**, e108622.

[230] Auer TO, Duroure K, Cian AD, Concordet JP, & Del Bene F. (2014) Highly efficient CRISPR / Cas9-mediated knock-in in zebrafish by homology-independent DNA repair. *Genome Res.* **24**, 142–153.

[231] Kimura Y, Hisano Y, Kawahara A, & Higashijima SI. (2014) Efficient generation of knock-in transgenic zebrafish carrying reporter/driver genes by CRISPR/Cas9-mediated genome engineering. *Sci. Rep.* **4**, 6545.

[232] Zu Y, Tong X, Wang Z, Liu D, Pan R, Li Z, et al. (2013) TALEN-mediated precise genome modification by homologous recombination in zebrafish. *Nat. Methods* **10**, 329–331.

[233] Hisano Y, Sakuma T, Nakade S, Ohga R, Ota S, Okamoto H, et al. (2015) Precise in-frame integration of exogenous DNA mediated by CRISPR/Cas9 system in zebrafish. *Sci. Rep.* **5**, 8841.

[234] Stemmer M, Thumberger T, Del Sol Keyer M, Wittbrodt J, & Mateo JL. (2015) CCTop: an intuitive, flexible and reliable CRISPR/Cas9 target prediction tool. *PLoS One* **10**, e0124633.

[235] Irion U, Krauss J, & Nusslein-Volhard C. (2014) Precise and efficient genome editing in zebrafish using the CRISPR/Cas9 system. *Development* **141**, 4827–4830.

Appendix

Statistical results of behavioral effects of chronic fluoxetine administration

Diving test

The fluoxetine treatment did not affect distance traveled in the 10-min test in both male (two-way RM ANOVA: treatment, $F_{[1,21]} = 1.205, P = 0.2848$; time, $F_{[9,189]} = 1.205, P < 0.0001$; interaction, $F_{[9,189]} = 1.205, P = 0.1952$; Fig. 6.1E and Welch's t-test: $t = 1.106, P = 0.2812$, Fig. 6.1G) and female (two-way RM ANOVA: treatment, $F_{[1,20]} = 0.3423, P = 0.5650$; time, $F_{[9,180]} = 12.36, P < 0.0001$; interaction, $F_{[9,180]} = 1.205, P = 0.6018$; Fig. 6.1F and Welch's t-test: $t = 0.5928, P = 0.5600$, Fig. 6.1G). Total duration of freezing was not affected in both male (two-way RM ANOVA: treatment, $F_{[1,21]} = 0.5098, P = 0.2028$; time, $F_{[9,189]} = 32.27, P < 0.0001$; interaction, $F_{[9,189]} = 6.712, P = 0.0063$; Fig. 6.1H and Welch's t-test: $t = 1.325, P = 0.1995$, Fig. 6.1J) and female (two-way RM ANOVA: treatment, $F_{[1,20]} = 0.6773, P = 0.1507$; time, $F_{[9,180]} = 17.50, P < 0.0001$; interaction, $F_{[9,180]} = 13.11, P < 0.0001$; Fig. 6.1I and Welch's t-test: $t = 1.493, P = 0.1516$, Fig. 6.1J), while freezing during the first 1 min significantly decreased in both male ($t = 4.940, P < 0.0001$, Fig. 6.1H) and female ($t = 6.061, P < 0.0001$, Fig. 6.1I). Fluoxetine-treated fish exhibited more time spent in the top area (male: two-way RM ANOVA, treatment, $F_{[1,21]} = 187.7, P < 0.0001$; time, $F_{[9,189]} = 1.577, P = 0.1247$; interaction, $F_{[9,189]} = 4.459, P < 0.0001$; Fig. 6.1K; Welch's t-test, $t = 13.51, P < 0.0001$, Fig. 6.1M; female: two-way RM ANOVA, treatment, $F_{[1,20]} = 154.1, P < 0.0001$; time, $F_{[9,180]} = 1.963, P = 0.0460$; interaction, $F_{[9,180]} = 1.984, P = 0.0435$; Fig. 6.1L; Welch's t-test, $t = 11.44, P < 0.0001$, Fig. 6.1M), lower latency to enter the top area (male: $\chi^2 = 26.92, P < 0.0001$, Fig. 6.1N and female: $\chi^2 = 26.11, P < 0.0001$, Fig. 6.1O), increasing number of entries into the top area (male: $t = 4.320, P = 0.0004$ and female: $t = 5.356, P < 0.0001$; Fig. 6.1P), and less time spent in the bottom area (male: $t = 9.657, P < 0.0001$ and female: $t = 11.84, P < 0.0001$; Fig. 6.1Q).

Open-field test

Fluoxetine-treated fish showed significantly decreasing distance traveled in the 15-min test in both male (two-way RM ANOVA: treatment, $F_{[1,21]} = 6.512, P = 0.0186$; time, $F_{[14,294]} = 10.16, P < 0.0001$; interaction, $F_{[14,294]} = 0.7912, P = 0.6786$; Fig. 6.2E and Welch's t-test: $t = 2.557, P = 0.0184$, Fig. 6.2G) and female (two-way RM ANOVA: treatment, $F_{[1,22]} = 10.89, P = 0.0033$; time, $F_{[14,308]} = 14.25, P < 0.0001$; interaction, $F_{[14,308]} = 1.047, P = 0.4066$; Fig. 6.2F and Welch's t-test: $t = 3.299, P = 0.0035$, Fig. 6.2G) and shorter freezing duration in the first 1 min of the 15-min test (male: $t = 4.898, P < 0.0001$, Fig. 6.2H; female: $t = 3.664, P = 0.0043$, Fig. 6.2I) but not in the total 15-min test (male: $t = 1.123, P = 0.2852$; female: $t = 0.4310, P = 0.6707$; Fig. 6.2J). Fluoxetine-treated fish spent significantly more time in the center area of the tank (male: $t = 2.314, P = 0.0331$; female: $t = 2.939, P = 0.0079$; Fig. 6.2M), especially during the first 2 or 3 min in both male (two-way RM ANOVA: treatment, $F_{[1,21]} = 5.103, P = 0.0346$; time, $F_{[14,294]} = 21.28, P < 0.0001$; interaction, $F_{[14,294]} = 2.777, P = 0.0007$; Sidak's multiple comparison test: 0–1 min, $t = 3.584, P = 0.0059$; 1–2 min, $t = 5.038, P < 0.0001$; Fig. 6.2K) and female (two-way RM ANOVA: treatment, $F_{[1,22]} = 8.637, P = 0.0076$; time, $F_{[14,308]} = 13.58, P < 0.0001$; interaction, $F_{[14,308]} = 4.530, P < 0.0001$; Sidak's multiple comparison test: 0–1 min, $t = 5.231, P < 0.0001$; 1–2

min, $t = 5.903, P < 0.0001$; 2–3 min, $t = 3.006, P = 0.0419$; Fig. 6.2L), respectively. Total number of entries into the center area was not affected in both male ($t = 0.002943, P = 0.9977$, Fig. 6.2P) and female ($t = 1.695, P = 0.1047$, Fig. 6.2P) but number of entries into the center during 2–3 min was significantly increasing in female (two-way RM ANOVA: treatment, $F_{[1,22]} = 2.872, P = 0.1043$; time, $F_{[14,308]} = 9.713, P < 0.0001$; interaction, $F_{[14,308]} = 1.785, P = 0.0399$; Sidak's multiple comparison test: 2–3 min, $t = 3.976, P = 0.0013$; Fig. 6.2O).

Light-dark transition test

Fluoxetine-treated fish showed significantly decreasing distance traveled in the 10-min test (male: $t = 2.688$, $P = 0.0158$; female: $t = 3.380$, $P = 0.0037$; Fig. 6.3C). However, time spent in the light (male: $t = 1.850$, $P = 0.0876$; female: $t = 0.3226$, $P = 0.7512$; Fig. 6.3D) and the dark area (male: $t = 1.852$, $P = 0.0873$; female: $t = 0.3160$, $P = 0.7561$; Fig. 6.3E), and latency to enter the dark area (male: $\chi^2 = 0.03330$, $P = 0.8552$, Fig. 6.3F; female: $\chi^2 = 3.284$, $P = 0.0699$, Fig. 6.3G) were unaffected by the fluoxetine treatment. The fluoxetine treatment also produced significantly decreasing number of transitions between the areas in both male ($t = 2.277$, $P = 0.0407$, Fig. 6.3J) and female ($t = 2.364$, $P = 0.0299$, Fig. 6.3J). In female, the number of transitions during 24 min were significantly decreased (two-way RM ANOVA: treatment, $F_{[1,18]} = 5.168$, $P = 0.0355$; time, $F_{[9,162]} = 2.285$, $P = 0.0194$; interaction, $F_{[9,162]} = 2.918$, $P = 0.0031$; Sidak's multiple comparison test: 2–3 min, $t = 3.063$, $P = 0.0250$; 3–4 min, $t = 3.905$, $P = 0.0013$; Fig. 6.3I).

Mirror-biting test

The fluoxetine treatment produced significantly less time of mirror biting (male: $t = 2.418, P = 0.0248$; female: $t = 2.601, P = 0.0182$; Fig. 6.4G), especially during the anterior half of the 10-min test in both male (two-way RM ANOVA: treatment, $F_{[1,21]} = 5.773, P = 0.0256$; time, $F_{[9,189]} = 7.606, P < 0.0001$; interaction, $F_{[9,189]} = 2.492, P = 0.0103$; Sidak's multiple comparison test: 1–2 min, $t = 3.804, P = 0.0019$; 2–3 min, $t = 3.629, P = 0.0036$; Fig. 6.4E) and female (two-way RM ANOVA: treatment, $F_{[1,19]} = 6.526, P = 0.0194$; time, $F_{[9,171]} = 9.091, P < 0.0001$; interaction, $F_{[9,171]} = 0.9139, P = 0.5145$; Sidak's multiple comparison test: 2–3 min, $t = 2.917, P = 0.0389$; Fig. 6.4F). The fluoxetine administration did not affect latency to the first mirror biting (male: $\chi^2 = 1.319, P = 0.2507$, Fig. 6.4H; female: $\chi^2 = 2.000, P = 0.1573$, Fig. 6.4I) and number of mirror biting (male: $t = 1.624, P = 0.1219$; female: $t = 0.4097, P = 0.6894$; Fig. 6.4J). However, distance traveled in the 10-min test was significantly decreasing in the fluoxetine-treated fish (male: $t = 2.654, P = 0.0155$; female: $t = 3.107, P = 0.0064$; Fig. 6.4K).

Two-fish social interaction test

Average distance between two fish was not affected by the fluoxetine treatment (male: $t = 0.7341, P = 0.4956$; female: $t = 0.005327, P = 0.9960$; Fig. 6.5A). The fluoxetine treatment produced significantly longer latency to the first contact (male: $\chi^2 = 10.26, P = 0.0014$, Fig. 6.5B; female: $\chi^2 = 5.693, P = 0.0170$; Fig. 6.5C). Fluoxetine-treated fish did not show any significant difference in total contact time (male: $t = 0.9480, P = 0.3780$; female: $t = 1.462, P = 0.1894$; Fig. 6.5F) but only the female fish showed significantly decreasing contact time during the 2–3 min of the 10-min test (two-way RM ANOVA: treatment, $F_{[1,7]} = 2.127, P = 0.1880$; time, $F_{[9,63]} = 3.381, P = 0.0019$; interaction, $F_{[9,63]} = 1.806, P = 0.0847$; Sidak's multiple comparison test: 2–3 min, $t = 2.978, P = 0.0391$; Fig. 6.5E). Number of contact was significantly reduced in the male fish (two-way RM ANOVA: treatment, $F_{[1,9]} = 6.339, P = 0.0329$; time, $F_{[9,81]} = 5.332, P < 0.0001$; interaction, $F_{[9,81]} = 0.8301, P = 0.5904$; Sidak's multiple comparison test: 7–8 min, $t = 3.048, P = 0.0298$; Fig. 6.5G; Welch's t-test: $t = 2.582, P = 0.0296$, Fig. 6.5I) but not in the female (two-way RM ANOVA: treatment, $F_{[1,7]} = 4.081, P = 0.0831$; time, $F_{[9,63]} = 5.047, P < 0.0001$; interaction, $F_{[9,63]} = 1.119, P = 0.3630$; Fig. 6.5H; Welch's t-test: $t = 2.052, P = 0.0801$, Fig. 6.5I).

Statistical results of behavioral alterations in tph2-deficient fish

Diving test

The *tph2*$^{\Delta 13/\Delta 13}$ fish showed a decreased distance traveled in both male (two-way RM ANOVA: genotype, $F_{[1,34]} = 15.05, P = 0.0005$; time, $F_{[9,306]} = 16.80, P < 0.0001$; interaction, $F_{[9,306]} = 2.400, P = 0.0122$; Fig. 7.5A; Welch's *t*-test, $t = 3.880$, $df = 28.03$, $P = 0.0006$, Fig. 7.5C) and female (two-way RM ANOVA: genotype, $F_{[1,34]} = 16.99, P = 0.0002$; time, $F_{[9,306]} = 7.654, P < 0.0001$; interaction, $F_{[9,306]} = 2.989, P = 0.0020$; Fig. 7.5B; Welch's *t*-test, $t = 4.122$, $df = 31.64$, $P = 0.0003$, Fig. 7.5C). The duration of freezing behavior was significantly increased by the mutation in both male (two-way RM ANOVA: genotype, $F_{[1,34]} = 15.16, P = 0.0004$; time, $F_{[9,306]} = 30.57, P < 0.0001$; interaction, $F_{[9,306]} = 5.165, P < 0.0001$; Fig. 7.5D; Welch's *t*-test, $t = 3.894$, $df = 23.70$, $P = 0.0007$, Fig. 7.5F) and female (two-way RM ANOVA: genotype, $F_{[1,34]} = 13.95, P = 0.0007$; time, $F_{[9,306]} = 6.446, P < 0.0001$; interaction, $F_{[9,306]} = 2.070, P = 0.0320$, Fig. 7.5E; Welch's *t*-test, $t = 3.734$, $df = 18.20$, $P = 0.0015$, Fig. 7.5F). Time spent in the bottom area was significantly increased in the mutant female (two-way RM ANOVA: genotype, $F_{[1,34]} = 6.339, P = 0.0167$; time, $F_{[9,306]} = 12.93, P < 0.0001$; interaction, $F_{[9,306]} = 2.483, P = 0.0095$, Fig. 7.5H; Welch's *t*-test, $t = 2.518$, $df = 32.01$, $P = 0.0170$, Fig. 7.5I) but not in the mutant male (two-way RM ANOVA: genotype, $F_{[1,34]} = 0.4932, P = 0.4873$; time, $F_{[9,306]} = 13.90, P < 0.0001$; interaction, $F_{[9,306]} = 0.8677, P = 0.5545$, Fig. 7.5G; Welch's *t*-test, $t = 0.7023$, $df = 33.71$, $P = 0.4873$, Fig. 7.5I). Number of entries into the top area was significantly decreased by the mutation in both the male (two-way RM ANOVA: genotype, $F_{[1,34]} = 6.515, P < 0.0001$; time, $F_{[9,306]} = 9.191, P < 0.0001$; interaction, $F_{[9,306]} = 1.843, P = 0.0602$, Fig. 7.5J; Welch's *t*-test, $t = 2.552$, $df = 27.87$, $P = 0.0165$, Fig. 7.5L) and the female (two-way RM ANOVA: genotype, $F_{[1,34]} = 10.79, P = 0.0024$; time, $F_{[9,306]} = 6.981, P < 0.0001$; interaction, $F_{[9,306]} = 2.963, P = 0.0022$, Fig. 7.5K; Welch's *t*-test, $t = 3.286$, $df = 27.27$, $P = 0.0028$, Fig. 7.5L). The latency to the first entry into the top area was not affected by the mutation (male: $\chi^2 = 0.06380$, $P = 0.8006$, Fig. 7.5M; female: $\chi^2 = 0.8050$, $P = 0.3696$, Fig. 7.5N).

Open-field test

No significant differences between two genotypes in distance traveled in the 15-min test were found in both male (two-way RM ANOVA: genotype, $F_{[1,34]} = 0.5700, P = 0.4554$; time, $F_{[14,476]} = 12.97, P < 0.0001$; interaction, $F_{[14,476]} = 1.849, P = 0.0297$; Fig. 7.6A; Welch's *t*-test, $t = 0.7550$, $df = 28.93$, $P = 0.4563$, Fig. 7.6C) and female (two-way RM ANOVA: genotype, $F_{[1,34]} = 3.717, P = 0.0622$; time, $F_{[14,476]} = 4.945, P < 0.0001$; interaction, $F_{[14,476]} = 1.065, P = 0.3872$; Fig. 7.6B; Welch's *t*-test, $t = 1.928$, $df = 33.83$, $P = 0.0623$, Fig. 7.6C). The durations of freezing behavior were significantly increased by the mutation during the first 1 or 2 min in both male (two-way RM ANOVA: genotype, $F_{[1,34]} = 3.669, P = 0.0639$; time, $F_{[14,476]} = 11.78, P < 0.0001$; interaction, $F_{[14,476]} = 2.764, P = 0.0006$; Sidak's multiple comparison test: 0–1 min, $t = 3.651, P = 0.0043$; 1–2 min, $t = 3.710, P = 0.0034$; Fig. 7.6D) and female (two-way RM ANOVA: genotype, $F_{[1,34]} = 2.668, P = 0.0144$; time, $F_{[14,476]} = 10.45, P < 0.0001$; interaction, $F_{[14,476]} = 7.079, P < 0.0001$; Sidak's multiple comparison test: 0–1 min, $t = 9.639, P < 0.0001$; Fig. 7.6E) while the total duration of the freezing was significantly increased in the mutant female ($t = 2.579$, $df = 17.42$, $P = 0.0193$, Fig. 7.6F) but not in the mutant male ($t = 1.915$, $df = 17.58$, $P = 0.0719$, Fig. 7.6F). Total time spent in the center area was not altered by the genotype (male: $t = 1.403$, $df = 25.62$, $P = 0.1727$; female: $t = 1.491$, $df = 19.80$, $P = 0.1516$; Fig. 7.6I) but the center time during 1–2 min of the 15-min test was significantly increased only in the *tph2*$^{\Delta 13/\Delta 13}$ female (two-way RM ANOVA: genotype, $F_{[1,34]} = 2.224, P = 0.1451$; time, $F_{[14,476]} = 11.28, P < 0.0001$; interaction, $F_{[14,476]} = 1.414, P = 0.1419$; Sidak's multiple comparison test: 1–2 min, $t = 3.498, P = 0.0076$; Fig. 7.6H). Total number of entries

into the center area was not affected by the mutaion (male: $t = 1.010$, $df = 31.56$, $P = 0.3202$; female: $t = 1.643$, $df = 32.06$, $P = 0.1102$; Fig. 7.6L) but was significantly decreased during the first 1 min of the 15-min test only in the mutant female (two-way RM ANOVA: genotype, $F_{[1,34]} = 2.699, P = 0.1096$; time, $F_{[14,476]} = 14.09, P < 0.0001$; interaction, $F_{[14,476]} = 1.865, P = 0.0280$; Sidak's multiple comparison test: 0–1 min, $t = 3.440, P = 0.0094$; Fig. 7.6K).

Light-dark transition test

The *tph2* genotype unaffected the time spent in both light (male: $t = 0.05737$, $df = 28.94$, $P = 0.9546$; female: $t = 0.002024$, $df = 28.46$, $P = 0.9984$; Fig. 7.7A) and dark (male: $t = 0.06031$, $df = 28.94$, $P = 0.9523$; female: $t = 0.002027$, $df = 28.46$, $P = 0.9984$; Fig. 7.7B) areas. Total number of the transitions between both areas (male: $t = 0.7832$, $df = 26.78$, $P = 0.4404$; female: $t = 1.061$, $df = 25.68$, $P = 0.2986$; Fig. 7.7C), latency to the first entry into the dark area (male: $\chi^2 = 0.9656, P = 0.3258$, Fig. 7.7D; female: $\chi^2 = 0.8650, P = 0.3523$, Fig. 7.7E), and total distance of traveled (male: $t = 0.7986$, $df = 28.36$, $P = 0.4311$; female: $t = 0.8632$, $df = 29.62$, $P = 0.3950$; Fig. 7.7F) in the 10-min test were also unaffected by the genotype. Total duration of freezing behavior for the 10-min test was significantly increased in $tph2^{\Delta 13/\Delta 13}$ male ($t = 2.173$, $df = 26.89$, $P = 0.0388$; Fig. 7.7I) but not in the female($t = 1.606$, $df = 21.39$, $P = 0.1229$; Fig. 7.7I). The freezing duration during the first 1 min was significantly increased in both the male (two-way RM ANOVA: genotype, $F_{[1,30]} = 4.722, P = 0.0378$; time, $F_{[9,270]} = 16.63, P < 0.0001$; interaction, $F_{[9,270]} = 3.802, P = 0.0002$; Sidak's multiple comparison test: 0–1 min, $t = 5.792, P < 0.0001$; Fig. 7.7G) and the female (two-way RM ANOVA: genotype, $F_{[1,30]} = 2.580, P = 0.1187$; time, $F_{[9,270]} = 12.36, P < 0.0001$; interaction, $F_{[9,270]} = 1.495, P = 0.1494$; Sidak's multiple comparison test: 0–1 min, $t = 3.286, P = 0.0113$; Fig. 7.7H).

Mirror-biting test

The $tph2^{\Delta 13/\Delta 13}$ fish did not exhibit any significant changes in time of mirror biting for the 10-min test in both male (two-way RM ANOVA: genotype, $F_{[1,34]} = 0.3184, P = 0.5763$; time, $F_{[9,306]} = 13.09, P < 0.0001$; interaction, $F_{[9,306]} = 0.2699, P = 0.9823$; Fig. 7.8A; Welch's: $t = 0.5642$, $df = 33.96$, $P = 0.5763$; Fig. 7.8C) and female (two-way RM ANOVA: genotype, $F_{[1,34]} = 1.510, P = 0.2276$; time, $F_{[9,306]} = 13.80, P < 0.0001$; interaction, $F_{[9,306]} = 0.9177, P = 0.5099$; Fig. 7.8B; Welch's$t = 1.229$, $df = 28.14$, $P = 0.2293$; Fig. 7.8C) and latency to the first mirror biting (male: $\chi^2 = 3.674, P = 0.0553$, Fig. 7.8K; female: $\chi^2 = 0.2653, P = 0.6065$, Fig. 7.8L). The number of mirror biting was significantly decreased by the mutation in male (two-way RM ANOVA: genotype, $F_{[1,34]} = 4.435, P = 0.0427$; time, $F_{[9,306]} = 0.9071, P = 0.5192$; interaction, $F_{[9,306]} = 1.288, P = 0.2426$; Sidak's multiple comparison test: 1–2 min, $t = 3.152, P = 0.0175$; Fig. 7.8D; Welch's *t*-test, $t = 2.106$, $df = 33.77$, $P = 0.0427$, Fig. 7.8F) but not in female (two-way RM ANOVA: genotype, $F_{[1,34]} = 0.02501, P = 0.8753$; time, $F_{[9,306]} = 1.286, P = 0.2438$; interaction, $F_{[9,306]} = 1.137, P = 0.3358$; Fig. 7.8E; Welch's *t*-test, $t = 0.1581$, $df = 33.75$, $P = 0.8753$, Fig. 7.8F). The $tph2^{\Delta 13/\Delta 13}$ fish significantly increased the duration of freezing behavior in both male (two-way RM ANOVA: genotype, $F_{[1,34]} = 7.183, P = 0.0113$; time, $F_{[9,306]} = 8.458, P < 0.0001$; interaction, $F_{[9,306]} = 7.941, P < 0.0001$; Fig. 7.8G; Welch's *t*-test, $t = 2.680$, $df = 17.17$, $P = 0.0157$, Fig. 7.8I) and female (two-way RM ANOVA: genotype, $F_{[1,34]} = 5.409, P = 0.0261$; time, $F_{[9,306]} = 10.92, P < 0.0001$; interaction, $F_{[9,306]} = 6.878, P < 0.0001$; Fig. 7.8H; Welch's *t*-test, $t = 2.326$, $df = 20.95$, $P = 0.0302$, Fig. 7.8I). Total distance traveled was unaffected by the genotype (male: $t = 1.498$, $df = 30.91$, $P = 0.1444$; female: $t = 0.5856$, $df = 31.25$, $P = 0.5624$; Fig. 7.8J).

Two-fish social interaction test

The *tph2* genotype did not affect the average distance between individuals for the 10-min test (male: $t = 0.6153$, $df = 24.49$, $P = 0.5440$; female: $t = 1.620$, $df = 24.57$, $P = 0.1179$; Fig. 7.9A) and latency

to the first contact (male: $\chi^2 = 0.04152, P = 0.8385$, Fig. 7.9B; female: $\chi^2 = 0.5151, P = 0.4730$, Fig. 7.9C). The contact time was significantly increased by the mutation in female (two-way RM ANOVA: genotype, $F_{[1,26]} = 4.463, P = 0.0448$; time, $F_{[9,234]} = 7.026, P < 0.0001$; interaction, $F_{[9,234]} = 2.233, P = 0.0209$; Sidak's multiple comparison test: 8–9 min, $t = 3.590, P = 0.0040$; Fig. 7.9E; Welch's t-test, $t = 2.110$, $df = 24.68$, $P = 0.0452$, Fig. 7.9F) but not in male (two-way RM ANOVA: genotype, $F_{[1,26]} = 0.08711, P = 0.7702$; time, $F_{[9,234]} = 5.301, P < 0.0001$; interaction, $F_{[9,234]} = 0.7039, P = 0.7051$; Fig. 7.9D; Welch's t-test, $t = 0.2951$, $df = 25.96$, $P = 0.7702$, Fig. 7.9F). The number of contacts was unaffected by the mutation in both male (two-way RM ANOVA: genotype, $F_{[1,26]} = 0.2958, P = 0.5912$; time, $F_{[9,234]} = 8.115, P < 0.0001$; interaction, $F_{[9,234]} = 0.6602, P = 0.7444$; Fig. 7.9G; Welch's t-test, $t = 0.5439$, $df = 26.00$, $P = 0.5912$, Fig. 7.9I) and female (two-way RM ANOVA: genotype, $F_{[1,25]} = 1.235, P = 0.2770$; time, $F_{[9,225]} = 7.508, P < 0.0001$; interaction, $F_{[9,225]} = 1.919, P = 0.0503$; Fig. 7.9H; Welch's t-test, $t = 1.096$, $df = 21.09$, $P = 0.2854$, Fig. 7.9I).